Environment and Lake Systems Across Africa: Understanding the Relationship between Environments, Lakes, and Hominins

Dissertation

der Mathematisch-Naturwissenschaftlichen Fakultät

der Eberhard Karls Universität Tübingen

zur Erlangung des Grades eines

Doktors der Naturwissenschaften

(Dr. rer. nat.)

vorgelegt von

Elena Lynn Robakiewicz

aus Worcester, USA

Tübingen

2023

Gedruckt mit Genehmigung der Mathematisch-Naturwissenschaftlichen Fakultät der Eberhard Karls Universität Tübingen.

Tag der mündlichen Qualifikation:	21.06.2023
Dekan:	Prof. Dr. Thilo Stehle
1. Berichterstatter/-in:	Prof. Dr. Lisa Park Boush
2. Berichterstatter/-in:	Dr. Annett Junginger

ACKNOWLEDGEMENTS

I would like to thank my advisors, Dr. Lisa Park Boush and Dr. Annett Junginger, for their support and willingness to help see my collaboration goals through. Thank you to the rest of my advisory committee, Dr. Ran Feng, Dr. Michael Hren, and Dr. Christian Tryon, for their help with planning and oversight of these projects. I would like to thank my coauthors from my published (Chapter 4) and submitted (Chapter 2) papers, Dr. Jeffery Stone, Dr. Bernie Owen, Dr. Carolina Rosca, Dr. Alan Deino, Dr. Yannick Garcin, Dr. Martin Trauth, and Dr. Simon Kübler, for their edits and support for those publications. Thank you to Veronika Schöttle whose Master's work was instrumental in the work for Chapter 2. Thank you to Dr. Nicholas Conard for his support in teaching a geologist archaeologists' tricks. I would like to thank my collaborator and navigator, Dr. Daniela de Matos, for all the work she put in to make Angola field work possible. I would like to thank our collaborators and team members in Angola including the Department of Geology and Mining at the Instituto Superior Politécnico da Huíla-Universidade Mandume Ya Ndemufayo in Lubango for their support and assistance in the field. A special thank you to my family and dearest friends for their support and trust throughout this process. And of course the biggest thanks to my partner who is the greatest gift to come out of this dissertation – thank you for joining and supporting me on this journey.

My work within these projects was funded through support through UConn's Outstanding Fellows Program, the Geological Society of America, the Explorer's Club, and the Fulbright Foundation.

Table of Contents

CHAPTER 1: INTRODUCTION

1.1. BACKGROUND AND SIGNIFICANCE

As everyday impacts of anthropogenic climate change are increasingly felt throughout the world, the conversation about how humans have altered the planet, climate, and environments has become ubiquitous. The impacts, however, are not unidirectional. Climate change has always shaped, and will continue to shape, how organisms evolve and change (e.g., Matthew & Colbert, 1939; Axelrod, 1948; Darlington, 1959; Gienapp et al., 2008; Gillespie & Roderick, 2014). As such, humans have evolved, migrated, and adapted/structured societies in response to changing temperatures and humidities that influence subsistence and livelihood (e.g., Vrba, 1980; deMenocal, 1995; Potts, 1998; Wynn, 2004; Fagan, 2008; van der Leeuw, 2008; Evans et al., 2018; Rosenzweig & Marston, 2018).

The impact of climate on humans is clearest in our dependence on water. From earliest life, to our early ancestors, to modern societies, water is a necessity. We need water – not just to sustain ourselves, but also for countless economic tasks such as food preparation, agriculture and livestock, washing, fishing, transport, energy, etc. (Lapworth et al., 2017). Water's pivotal role in sustaining life has resulted in water/humidity argued as an important mechanism to explain changes in hominin evolution, migration, and technological innovation (e.g., Vrba, 1995; Potts, 1998; deMenocal, 2004; Carto et al., 2009; Trauth et al., 2009; Blome et al., 2012; Ziegler et al., 2013; Castañeda et al., 2016; d'Errico et al., 2017; Schaebitz et al., 2021; Foerster et al., 2022). Therefore, in order to better understand humans' past and future connection with climate, understanding water's role within and response to climate, or hydroclimate, is pertinent.

1.1.1. Lakes as a Key to Understanding Environments

The hydrosphere consists of the interaction between dynamic reservoirs including oceans, lakes, rivers, groundwater, the cryosphere, and the atmosphere (Eby, 2016).

Throughout the hydrological cycle, energy, nutrients, and mass are moved between reservoirs. The atmosphere, the most dynamic reservoir containing less than 0.001% of all water on Earth (Kump et al., 1999), hosts the evaporation, condensation, and precipitation of water. Changes in the atmosphere, such as temperature, have a consequential impact on how water moves across the planet. For many places on earth, particularly tropical ones, changes to atmospheric dynamics and hydroclimate quickly and profoundly impact ecological habitats and environments. The movement of water between reservoirs of the hydrosphere erodes regolith and rock, transports solutes and sediments, and deposits materials, creating the sediment routing system and distributing proxies into basins (Fig. 1; Robertson et al., 2022).

Geological basins are important proxy reservoirs to understand geologic history and the climatological past. Over hominin timescales (i.e., within the last 8 Ma), ocean and lake basins provide the most complete climate records, with other records, such as Quade et al. (1992), providing glimpses into climate through less common records such as carbon isotopes of paleosols and tooth enamel. Marine records have a longer scientific history beginning in 1966 with the Deep Sea Drilling Project (which has become other organization through time) compared to the International Continental Drilling Program which began in 1996 (IODP, 2023), resulting in fewer long-term lacustrine versus marine records. Compared to continental basin records, however, marine basin records have lower resolution due

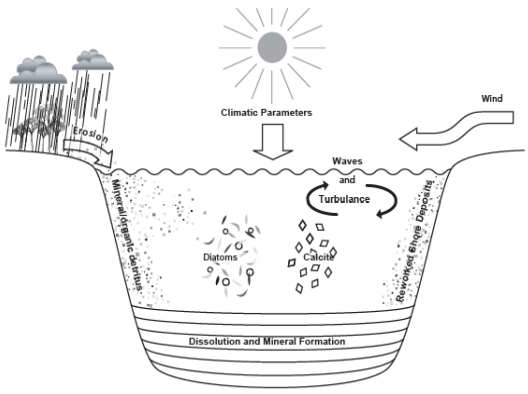

Figure 1: Schematic from Brauer (2004) on how proxies like diatoms deposit into lake basins as layers.

To greater time-averaging and require more interpretation because oceans are large and represent depositional inputs from a greater area (deMenocal, 1995; Levin, 2015). In addition, if the research goal is to better understand terrestrial climate's impact on hominins, such reservoirs are far removed from the African interior where much of the early paleontological record derives with many of the earliest Eastern African archaeological and paleoanthropological finds associated with past water bodies (Gregory, 1921; Leakey, 1931). Lacustrine records, in comparison, provide more localized records that can indicate the complex patchwork of landscapes and often provide higher resolution environmental records. Data from lakes allows us to determine environmental response to global climate phenomenon. Closed basins, though often fragmented, are particularly responsive to climate change and contain diverse sedimentary records (Trauth et al., 2010). With a modern understanding of the mechanisms that control lake deposition and regional climate, we can use past archives from these basins to understand how hydroclimate has changed through time.

1.1.2. Grand Challenges

The motivating questions of this dissertation come from these grand challenges: **(a)** How can we use geochemical and micropaleontological lake proxies to better understand current and past climate change? **(b)** What are the time scales and rates of environmental change across global climate phenomena at different times in Africa? **(c)** Which mechanisms of global climate change influence African environments? **(d)** How do changes in hydroclimate impact hominin evolution and innovation across Africa? While these questions cannot be answered within this dissertation, the case studies to be presented use these questions as a focal point to better provide context for understanding the complex, uncertain, and highly debated relationships between global climate, regional African hydroclimates, and hominin evolution and innovation.

1.2. THEORETICAL FRAMEWORKS

1.2.1. Human Evolution, Migration, and Innovation in Africa

Since the Plio-Pleistocene, African lake basins and their sediments have preserved evidence of hominin migration, evolution (e.g., Brown et al., 1985; Prat et al., 2005; Spoor et al., 2007; Caley et al., 2018; Sanchez Goñi, 2020, Gosling et al 2022), and technological adaptation (e.g., Leakey, 1931; Robertshaw, 1984; Robbins, 2006; Tryon et al., 2014; Brooks et al., 2018) (Fig. 2). While evidence supports a relationship between climate change and migration out of Africa (Carto et al., 2009; Carotenuto et al., 2016; deMenocal & Springer, 2016; Hosfield & Cole, 2018), overly simplified models do not reflect the complex environmental change across Africa during the Pleistocene (Scerri et al., 2019) and require further data. Numerous studies relating paleoanthropological and paleoenvironmental evidence suggest causal links between climates, environments, and hominin evolution. Two

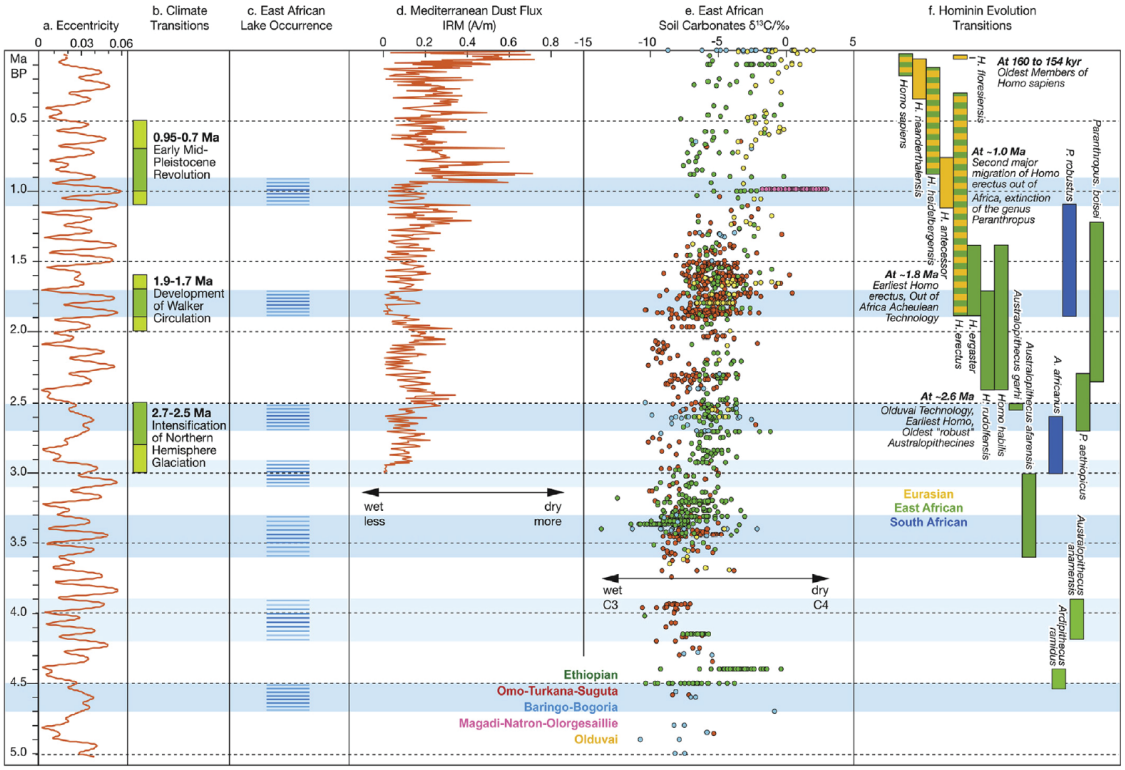

Figure 2: Taken from Maslin et al. (2014) showing the relationship between changes in **a.** eccentricity (Berger & Loutre, 1991), **b.** known global climate transitions, **c.** lacustrine phases in Eastern Africa (Trauth et al., 2005, 2007; Shultz & Maslin, 2013), **d.** Mediterranean dust flux (Larrasoaña et al., 2003), **e.** Eastern African soil carbonate d13C levels, and **f.** hominin evolution, migration, and technological innovation (Shultz et al., 2012).

frameworks dominate current discussions on climate change and hominin evolution: **(1)** turnover pulse (Vrba, 1980; Vrba, 1995; deMenocal, 2004; Bonnefille, 2010; DiMaggio et al., 2015; Joordens et al., 2019; Lupien et al., 2020) and **(2)** variable selection (Potts, 1998; Potts & Faith, 2015; Potts et al., 2020), including the related pulsed climate variable selection (Maslin & Trauth 2009; Trauth et al., 2010; Maslin et al., 2014). **(1)** The turnover pulse hypothesis states that the extinction, replacement, and migration of species is a result of major, global climate change. As climate changes, environments are disrupted, forcing generalists and specialists to compete, resulting in speciation (Vrba, 1995). The main driver proposed for hominin evolution is the intensification of Northern Hemisphere Glaciation ~2.8 Ma, resulting in aridity in Africa, although the evidence for such intensification controlling hominin evolution has been scrutinized (Behrensmeyer et al., 1997; Larrasoaña et al., 2003; Trauth et al., 2007; deMenocal, 2011; Bibi & Kiessling, 2015; Trauth et al., 2021). **(2)** The variable selection hypothesis states that hominin adaptations evolved due to increased climatic variability, creating dynamic environments that influenced speciation and population spread (Potts, 1998). Pulsed climate variable selection highlights that wet and variable climates occur in “pulses” along eccentricity timescales (Trauth et al., 2010; Maslin et al., 2015). Both variable selection arguments have been called into question in a recent macroevolutionary study (Cohen et al., 2022). Like the evolutionary record, the relationship between climate and technological innovation is complicated, due to difficulties comparing sporadic and localized archaeological evidence with continuous, regional climatological and environmental records (Faith et al., 2021). Complex relationships between technological changes and mosaic African environments since the Pleistocene (Roberts et al., 2016) result in diverse results as to whether or not hominin technological advances are related to environmental change (e.g., Blome et al., 2012; Mackay et al., 2014; Tryon et al., 2014; Conard & Will, 2015; Wilkins et al., 2017; Will et al., 2019; Potts et al., 2020; Mackay et al., 2022; Carr et al., 2023).

Overall, long-term, high-resolution lacustrine records can help constrain environmental variability to begin to resolve some of these discussions.

1.2.2. Quaternary Climate Variability in Africa

Global, long-term climate is driven by changes in solar insolation (Ruddiman, 2001). Most changes in insolation and its distribution across the planet over long timescales are determined by the astronomical Milankovitch cycles including **(a)** eccentricity (the shape of Earth's orbit); **(b)** obliquity (the axial tilt relative to Earth's plane of orbit around the sun); and **(c)** precession (Earth's wobble as it spins on its axis)(Milankovitch, 1941). These cycles have periodicities of 100,000, 41,000, and 23,000 years, respectively, that influence global climatic trends. Eccentricity changes the amount of insolation to reach the planet, impacting general warming and cooling trends. Obliquity determines seasonality and creates periodic glacial/interglacial cycles at high latitudes which in turn affect global climate, sea level, and sea surface temperatures (SST) (Imbrie & Imbrie, 1980). Eccentricity amplifies the effect of the precession cycle by creating low latitude forcing called "eccentricity-modulated precession" which is responsible for variations in tropical monsoon intensity and timing (Bergner & Loutre, 1991; Trauth et al., 2009). Eccentricity-modulated precession affects the intensity of monsoons along the equator and is responsible for periods of "Green Sahara" (Kutzbach et al., 1997; Liu et al., 2004). Different cycles along different time scales affect locations uniquely (Lupien et al., 2022), requiring investigation as to how these cycles impact regional African climates.

Small-scale climate signals are entangled within the fluctuating Milankovitch cycles, adding spatial complexity at each location which experiences large-scale signals uniquely based on local changes in the hydrological cycle (Peixóto & Oort, 1984). These local signals include **(a)** ocean currents and SST; **(b)** air masses; and **(c)** monsoons.

(a) The major currents around Africa, including the Benguela in the southwest, the Agulhas in the southeast, the Antarctic Circumpolar in the south, and the

Canary in the northwest, dictate rainfall patterns along African coastlines by affecting air mass boundaries and moisture availability/transport (Tyson, 1986; Tyson & Preston-Whyte, 2000). Generally, colder currents inhibit precipitation whereas warmer currents promote precipitation. Global SST are also important in their role in atmospheric moisture transport (Paeth & Friederichs, 2004), including the El Niño Southern Oscillation (ENSO) and the Indian Ocean Dipole (IOD) (Koroly & Vincent, 1998). Positive ENSO years result in warm waters in the eastern Pacific and cool waters in the western Pacific, increasing rainfall in Eastern Africa and decreasing rainfall in the southwest (Ntale & Gan, 2004; Nicholson, 2017). Walker Circulation weakens during positive IOD years due to SST warming in the western Indian Ocean and cooling in the eastern Indian Ocean, resulting in wetter conditions in Eastern Africa two to three times higher than long-term means (Marchant et al., 2007; Hirons & Turner, 2018; Lüdecke et al., 2021; Palmer et al., 2023). The teleconnection between global SST and African rainfall is an incredibly active realm of research, with other global SST phenomenon like North Atlantic Oscillation and Atlantic Multidecadal Oscillation, considered less important or understood (Lüdecke et al., 2021).

(b) The mid-latitude Westerlies in northern and southern Africa and the Intertropical Convergence Zone (ITCZ, which is related to the moist tropical rainbelt) near the equator are responsible for the movement of moist air across Africa (Tyson, 1986; Koroly & Vincent, 1998; Tyson & Preston-Whyte, 2000). The Westerlies are frontal boundaries where cool, dry polar air collides with warm, moist tropical air (Tyson & Preston-Whyte, 2000), causing instability, convection, and precipitation (Tyson, 1986). During globally warm periods, the Westerlies strengthen and move poleward, decreasing precipitation in the extreme northern and southern regions of Africa and increasing rainfall in the interior, whereas during cold periods, they weaken,

move equatorward, increasing rainfall at the extremes and decreasing rainfall in the interior (Tyson, 1986; Toggweiler & Russell, 2008; Figure 3). The ITCZ reflects the amount of solar insolation received by Earth's atmosphere and surface, creating a low-pressure zone that draws in moisture and creates heavy rainfall between the ITCZ and equator (Tyson, 1986; Tyson & Preston-Whyte, 1998). Throughout the year, the ITCZ moves between the Tropics of Cancer and Capricorn, but also fluctuates on longer timescales due to eccentricity-modulated precession with periodicity of 19-23,000 years (Gasse et al., 2008). Another important air mass is the Congo Air Boundary (CAB) which is the area of convergence between the Atlantic and Indian Ocean airstreams which, like the ITCZ, brings significant rain and annually oscillates north and south (Nicholson, 2000; Tyson & Preston-Whyte, 2000). Changing insolation over thousands of years has resulted in the CAB's movement, including north-eastward expansions (Junginger et al., 2014).

(c) The West African and Indian Monsoons are most influential on African climate. Summer differential heating between the land and ocean causes air over the land to rise, creates an area of low pressure, draws in moist air from

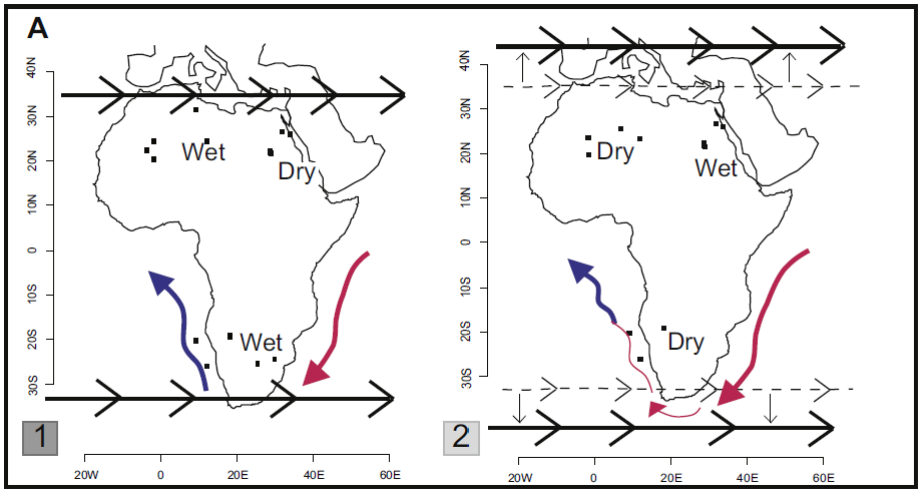

Figure 3: Taken from Blome et al. (2012) showing the theoretical movement of the westerlies (black arrows) and that theoretical movement's impact on rainfall in the African interior. Schematic 1 represents equator-ward movement of the Westerlies bringing precipitation to North and South Africa, and cutting off Agulhas current around the continent and schematic 2 represents the Westerlies more pole-ward, with the opposite effect.

over the ocean, and produces monsoonal rainfall on land (Liu et al., 2004). The West African Monsoon impacts latitudes between 9-20° N, with decreasing strength eastward but impacts regions as east as Ethiopia and South Sudan (Nicholson, 2017). The Indian Monsoon impacts the moisture availability for northern and eastern Africa where stronger Indian Monsoons result in drier conditions during the monsoon season (July to September and December to February), but wetter conditions off-season (Nicholson, 2017). The strength of monsoons through time is dependent on the location of the ITCZ and therefore related to changes in precession (e.g., Sikka & Gadgil, 1980; Fleitmann et al., 2007; Geen et al., 2020).

1.2.3. Chemistry as Climate Proxy

Chemistry within lake basins is dependent upon various factors such as lithology, climate, productivity/biological activity, catchment processes, pollution/human activities, etc. (Boyle et al., 2001; Eby, 2016). How exactly these components impact one another and influence lake chemistry depends on the physical and chemical weathering processes within the basin. Physical weathering is the breakdown of materials through atmospheric conditions including heat, water, ice, and pressure (Macheyeti et al., 2020). Physical weathering occurs as a result of temperature, pressure, or biota, like freeze-thaw cycles, endolithic microbial action, and plant roots. Physical weathering does not include any chemical change, but instead, most often, abrasion, or the diminution of original material. Chemical weathering is the process of atmospheric, hydrospheric, and biologic agents reacting with the mineral constituents of rocks (Loughnan, 1969). Chemical weathering occurs when minerals dissolve and/or alter due to exposure to precipitation; acidic soils from bacteria, fungi, and plant root discharge; or gaseous oxygen and carbon dioxide (Loughnan, 1969; Kump et al., 1999). The chemical weathering rate is influenced by precipitation, temperature, topography, and parent material (Loughnan, 1969). Chemical weathering is often gradual and results in the formation of secondary

minerals through oxidation and hydrolysis (Macheyeti et al., 2020). Weathered material is transported into reservoirs through wind, landslides, and, most often, water through rivers, groundwater, and surface runoff. Water leading into basins acts as an effective transporter of suspended inorganic matter (Al, Fe, Si, Ca, K, Mg, Na, P), dissolved major species (HCO_3^-, Ca^{2+}, SO_4^{2-}, H_4SiO_4, Cl^-, Na^+, Mg^{2+}, and K^+), dissolved nutrient elements (N and P), suspended and dissolved organic matter, and suspended and dissolved trace metals (Berner, 1996). Other chemical components within lake basins are authigenic, forming within the basin, and include the alteration or precipitation of minerals. With an understanding of how components are brought into, altered within, and precipitated out of systems, workers use grain size and sedimentation; certain elements and elemental ratios; stable isotopes; and other geochemical parameters like loss on ignition, total organic carbon, etc. to reconstruct past climates and environments from lake sediments.

1.2.4. Diatoms as Environmental Proxy

Diatoms, which are most thoroughly described by Round et al. (1990), are unicellular eukaryotes, most of which vary in size from 5-200 μm. Diatoms create siliceous, ornamented cell walls called frustules that are extremely diverse in size and shape. It is estimated that there are well over a million species that can live in the plankton/benthos of oceanic, coastal, or freshwaters and even surfaces of moist habitats like soils or mosses (Falkowski & Knoll, 2007), making them incredibly well-dispersed. Diatoms have been used to reconstruct lake chemistry and water quality in historic and modern contexts: whether to reconstruct past changes in hydroclimate (e.g., Gasse et al., 1995; Gasse et al., 1997; Battarbee et al., 2001; Fritz et al., 2010) or to monitor modern pollution cheaply and reliably (e.g., Lange-Bertalot, 1979; Sladecek, 1996). Diatoms, like other primary producers, require sufficient light, inorganic nitrogen, phosphorus, and trace elements to survive, with each diatom taxon responding to certain biological requirements which allows for reconstruction of certain controlling variables. Diatoms provide information on their various

ecologies; each taxon has a specific preference for certain physical (temperature, light, turbulence, etc.) and chemical (pH, dissolved organic carbon, nutrients, salinity, etc.) parameters (Battarbee et al., 2001). Diatoms are preferable indicators due to their **(1)** sensitivity to changes in water chemistry, **(2)** abundance in both past and modern sediments, **(3)** siliceous frustules which can withstand some dissolution post-deposition, and **(4)** large geographic (cosmopolitan) ranges (Gasse et al., 1995). Despite concerns that cosmopolitan diatom ecological preferences may not be universal (Vanormelingen et al., 2008; Soinenen & Teittinen, 2019), when used with other proxies, diatoms provide information about water's physical and chemical controls within a basin. Through statistical techniques, including but not limited to transfer functions, Canonical Correspondence Analysis, hierarchical cluster analysis, and weighted averaging regression (e.g., Gasse et al., 1995; Bergner & Trauth, 2004, Birks et al., 2010; Juggins, 2013; Owen et al., 2014), paleoclimatologists can create quantitative reconstructions of past conditions, providing valuable insights into past ecologies and hydroclimates.

1.3. DISSERTATION OVERVIEW

1.3.1. Chapter 2: Hydrochemistry and Diatom Assemblages on the Humpata Plateau, Southwestern Angola

The second chapter, published in *Geosciences*, is a modern study of hydrochemistry on the Humpata Plateau in southwestern Angola in southwestern Africa (Robakiewicz et al., 2021). Diatoms are effective and inexpensive paleoclimate and pollution indicators for modern water systems. They have been used in northern, eastern, and southern Africa as such because of their well-documented ecologies in those regions, but, with a large gap of modern assemblage studies in Angola, this inexpensive method for water quality studies is less reliable. To close this gap, modern diatoms were sampled across four water bodies on the Humpata Plateau in southwestern Angola in the dry season of July 2019, with in-situ measurements of pH, conductivity, and total dissolved solids and laboratory analysis

of cations and anions to better understand modern diatom assemblages in southwestern Angola, the hydrochemical variables determining their communities, and potential human impact on local water. It was found that bedrock determines local hydrochemistry and that diatoms in southwestern Angola can provide insight into relative conductivities and trophic levels. Limited data hinder interpretations of diatom ecological preferences for pH, temperature, alkalinity, ions, and pollution, requiring further analyses. This research is beneficial for both African diatomists interested in using accurate transfer functions across Africa to reconstruct paleoclimates as well as local communities and hydrologists interested in understanding water chemistry and pollution, given that these studied sites are vital water resources for local communities on the Humpata Plateau. As such, this project involves the active participation and communication with local officials and community leaders to engage in dialogue to address concerns related to local hydrology. In addition, monitoring of diatom communities will allow for comparison in the future to better understand how anthropogenic climate change is impacting the hydrochemistry on the Humpata Plateau.

1.3.2. Chapter 3: Hydroclimate Cycles over 35,000 years as Lake Nakuru, Kenya

The third chapter, to be submitted to *Quaternary Science Reviews*, looks at Lake Nakuru, a shallow, highly alkaline lake in the Central Kenyan Rift, over the last 35,000 years, encompassing both the Last Glacial Maximum (LGM) and the African Humid Period (AHP). While general trends about environments of the LGM and AHP are understood in Eastern Africa, the rate of environmental transition in and out of these phases and environmental variability within them is not well understood. Amplifier lakes (lakes that amplify climate signals like Lake Nakuru) are vital to understand the rate of environmental change in response to larger scale global climate change. This record includes high-resolution sampling from the upper ~11.5 meters of two duplicate, 17-meter drill cores taken by the Lake Naivasha Coring

Project in 2004 with a chronology based on a newly developed age model and aims to answer a) how variable is chemistry, depth, and rate of change of Lake Nakuru across the LGM and into the AHP? and b) which aspects of global climate is Lake Nakuru responding to across this time period? Using lithological, geochemical, and micropaleontological techniques, it was found that Lake Nakuru underwent phases of oxic/anoxic conditions that may be related to changes in climate and/or volcanic activity. With evidence of long-term impacts from volcanic activity absent, such changes are hypothesized to be related to millennial-scale changes during the Late Pleistocene including the Dansgaard-Oeschger cycles and Heinrich Events. By reconstructing the paleolimnology of Lake Nakuru across dynamic global phases, this research aims to contribute to increased understanding of how large-scale systems impact small-scale systems. Reconstruction of the hydroclimate at Lake Nakuru can therefore be used as a relevant regional environmental reconstruction by archaeologists interested in technological transitions and population migrations from the Late Stone Age to the Neolithic

1.3.3. Chapter 4: Hydroclimate reconstructions in the Suguta Valley, northern Kenya, during the Early-Middle Pleistocene Transition

The fourth chapter of this dissertation, which has been accepted in *Palaeogeography, Palaeoclimatology, Palaeoecology,* explores lake levels at Paleolake Suguta located in the Northern Kenyan Rift across the Early/Mid-Pleistocene Transition (EMPT) (Robakiewicz et al., 2023). The EMPT from 1,200–700 ka represents a major global climate transition from glacial cycles dominated by 41,000- to 100,000-year cycles, yet the mechanisms that caused this transition and how African lakes responded to it are not well understood. At Paleolake Suguta, a flood basalt has preserved rare lacustrine EMPT-aged sediments, preserving valuable paleoenvironmental proxies. This research presents a reconstruction of hydrological changes during the EMPT from a 41-m outcrop using diatom morphologies, sedimentology, and X-Ray Fluorescence data in order to answer how

variable EMPT hydroclimate is from ~931-831 ka. From these data, Paleolake Suguta appears to be fairly stable from ~931-905 ka followed by a period of dry conditions leading into a more variable stage from ~885-831 ka. During this volatile phase, paleolake Suguta ranged from a deep stratified lake, to a shallow, well-mixed lake, to a completely desiccated lake playa with incredibly rapid transitions. After ~831 ka, the basin becomes drier with evidence for periods of a swampier floodplain. This record displays the intricacies of environmental and lake level change across the EMPT and will help provide context for understanding how the EMPT impacted regional environments as well as for potential hominin discoveries within these well-preserved Middle Pleistocene Suguta strata in the future.

1.4. BROADER IMPACTS AND GOALS

This dissertation provides an overview into how shifts in large scale climate can cause variability in lake levels and chemistry. Reconstructing paleolake dynamics offers insight into variable environments, especially in response to changes in global climate. These changes impact flora and fauna, from diatoms to humans and our hominin ancestors. By understanding limnological variability in the past, future workers can better understand how archaeological sites and paleolakes are related, potentially extrapolating on how hominins may have migrated throughout the landscape or why there may have been transitions in past cultures. In addition, by understanding modern changes in hydrochemistry, we can help prepare vulnerable communities to modern climate change to ensure the livelihood and safety of individuals. By understanding past and present limnological systems, we can better understand the planet, our history, and the climatological future.

1.5. REFERENCES

Axelrod, D. I. 1948. "Climate and Evolution in Western North America during Middle Pliocene Time." *Evolution* 2 (2): 127-144. doi:10.1111/j.1558-5646.1948.tb02736.x.

Battarbee, R. W., V. J. Jones, R. J. Flower, N. G. Cameron, H. Bennion, L. Carvalho, and S. Juggins. 2001. "Diatoms." In *Tracking Environmental Change using Lake Sediments. Volume 3: Terrestrial, Algal, and Siliceous Indicators*, edited by J. P. Smol, H. J. B. Birks and W. M. Last, 155-202: Kluwer Academic Publishers.

Behrensmeyer, A. K., R. Potts, T. Plummer, L. Tauxe, N. Opdyke, and T. Jorstad. 1995. "The Pleistocene Locality of Kanjera, Western Kenya: Stratigraphy, Chronology and Paleoenvironments." *Journal of Human Evolution* 29 (3): 247-274.

Bergner, A. G. N. and M. H. Trauth. 2004. "Comparison of the Hydrological and Hydrochemical Evolution of Lake Naivasha (Kenya) during Three Highstands between 175 and 60 Kyr BP." *Palaeogeography, Palaeoclimatology, Palaeoecology* 215 (1): 17-36. doi:10.1016/j.palaeo.2004.07.033.

Berner, E. K. 1996. *Global Environment: Water, Air, and Geochemical Cycles*, edited by Robert A. Berner. Upper Saddle River, N.J.: Upper Saddle River, N.J.: Prentice Hall.

Bibi, F. and W. Kiessling. 2015. "Continuous Evolutionary Change in Plio-Pleistocene Mammals of Eastern Africa." *Proceedings of the National Academy of Sciences* 112 (34): 10623-10628.

Birks, H. J. B., O. Heiri, H. Seppä, and A. E. Bjune. 2010. "Strengths and Weaknesses of Quantitative Climate Reconstructions Based on Late-Quaternary Biological Proxies." *Quaternary International* 279-280: 52. doi:10.1016/j.quaint.2012.07.228.

Blome, M. W., A. S. Cohen, C. A. Tryon, A. S. Brooks, and J. Russell. 2012. "The Environmental Context for the Origins of Modern Human Diversity: A Synthesis of Regional Variability in African Climate 150,000–30,000 Years Ago." *Journal of Human Evolution* 62 (5): 563-592. doi:10.1016/j.jhevol.2012.01.011.

Bonnefille, R.. 2010. "Cenozoic Vegetation, Climate Changes and Hominid Evolution in Tropical Africa." *Global and Planetary Change* 72 (4): 390-411. doi:10.1016/j.gloplacha.2010.01.015.

Boyle, J. F., R. C. Chiverrell, and D. Schillereff. 2015. "Inorganic Geochemical Methods in Palaeolimnology." In *Micro-XRF Studies of Sediment Cores*, edited by I. W. Croudace and R. G. Rothwell, 83-141. Dordrecht: Springer Netherlands.

Brooks, A. S., J. E. Yellen, R. Potts, A. K. Behrensmeyer, A. L. Deino, D. E. Leslie, S. H. Ambrose, et al. 2018. "Long-Distance Stone Transport and Pigment use in the Earliest Middle Stone Age." *Science* (New York, N.Y.) 360 (6384): 90. doi:10.1126/science.aao2646.

Brown, F., J. Harris, R. Leakey, and A. Walker. 1985. "Early Homo Erectus Skeleton from West Lake Turkana, Kenya." *Nature* 316 (6031): 788-792. doi:10.1038/316788a0.

Caley, T., T. Extier, J. A. Collins, E. Schefuß, L. Dupont, B. Malaizé, L. Rossignol, et al. 2018. "A Two-Million-Year-Long Hydroclimatic Context for Hominin Evolution in Southeastern Africa." *Nature* 560 (7716): 76-79. doi:10.1038/s41586-018-0309-6.

Carotenuto, F., N. Tsikaridze, L. Rook, D. Lordkipanidze, L. Longo, S. Condemi, and P. Raia. 2016. "Venturing Out Safely: The Biogeography of Homo Erectus Dispersal Out of Africa." *Journal of Human Evolution* 95: 1-12. doi:10.1016/j.jhevol.2016.02.005.

Carr, A. S., B. M. Chase, S. J. Birkinshaw, P. J. Holmes, M. Rabumbulu, and B. A. Stewart. 2023. "Paleolakes and Socioecological Implications of Last Glacial "Greening" of the South African Interior." *Proceedings of the National Academy of Sciences* 120 (21): e2221082120. doi:10.1073/pnas.2221082120.

Carto, S. L., A. J. Weaver, R. Hetherington, Y. Lam, and E. C. Wiebe. 2009. "Out of Africa and into an Ice Age: On the Role of Global Climate Change in the Late Pleistocene Migration of Early Modern Humans Out of Africa." *Journal of Human Evolution* 56 (2): 139-151. doi:10.1016/j.jhevol.2008.09.004.

Castañeda, I. S., T. Caley, L. Dupont, J.-H. Kim, B. Malaizé, and S. Schouten. 2016. "Middle to Late Pleistocene Vegetation and Climate Change in Subtropical Southern East Africa." *Earth and Planetary Science Letters* 450: 306-316. doi:10.1016/j.epsl.2016.06.049.

Cohen, A. S., A. Du, J. Rowan, C. L. Yost, A. L. Billingsley, C. J. Campisano, E. T. Brown, et al. 2022. "Plio-Pleistocene Environmental Variability in Africa and its Implications for Mammalian Evolution." *Proceedings of the National Academy of Sciences* 119 (16): e2107393119. doi:10.1073/pnas.2107393119.

Conard, N. J. and M. Will. 2015. "Examining the Causes and Consequences of Short-Term Behavioral Change during the Middle Stone Age at Sibudu, South Africa." *PLoS One* 10 (6): e0130001. doi:10.1371/journal.pone.0130001.

Darlington, P. J. 1959. "Area, Climate, and Evolution." *Evolution* 13 (4): 488-510. doi:10.1111/j.1558-5646.1959.tb03038.x.

deMenocal, P. B. 2004. "African Climate Change and Faunal Evolution during the Pliocene-Pleistocene." *Earth and Planetary Science Letters* 220 (1): 3-24. doi:10.1016/S0012-821X(04)00003-2.

deMenocal, P. B. 2011. "Climate and Human Evolution." *Science* 331 (6017): 540-542. doi:10.1126/science.1190683.

deMenocal, P. B. 1995. "Plio-Pleistocene African Climate." *Science* 270 (5233): 53-59. doi:10.1126/science.270.5233.53.

deMenocal, P. B. and C. Stringer. 2016. "Human Migration: Climate and the Peopling of the World." *Nature* 538 (7623). doi:10.1038/nature19471.

D'Errico, F., W. E. Banks, D. L. Warren, G. Sgubin, K. van Niekerk, C. Henshilwood, A.-L. Daniau, and M. F. Sánchez Goñi. 2017. "Identifying Early Modern Human Ecological Niche Expansions and Associated Cultural Dynamics in the South African Middle Stone Age." *Proceedings of the National Academy of Sciences of the United States of America*. doi:10.1073/pnas.1620752114.

DiMaggio, E. N., C. J. Campisano, J. Rowan, G. Dupont-Nivet, A. L. Deino, F. Bibi, M. E. Lewis, et al. 2015. "Late Pliocene Fossiliferous Sedimentary Record and the Environmental Context of Early Homo from Afar, Ethiopia." *Science* 347 (6228): 1355-1359. doi:10.1126/science.aaa1415.

Eby, G. N. 2016. "The Continental Environment." In *Principles of Environmental Geochemistry*, edited by G. N. Eby, 313-386.

Evans, N. P., T. K. Bauska, F. Gázquez-Sánchez, M. Brenner, J. H. Curtis, and D. A. Hodell. 2018. "Quantification of Drought during the Collapse of the Classic Maya Civilization." *Science* 361 (6401): 498-501. doi:10.1126/science.aas9871.

Fagan, B. 2008. *The Great Warming: Climate Change and the Rise and Fall of Civilizations* Bloomsbury Publishing USA.

Faith, J. T., A. Du, A. K. Behrensmeyer, B. Davies, D. B. Patterson, J. Rowan, and B. Wood. 2021. "Rethinking the Ecological Drivers of Hominin Evolution." *Trends in Ecology & Evolution* (Amsterdam) 36 (9): 797-807. doi:10.1016/j.tree.2021.04.011.

Falkowski, P. G. and A. H. Knoll. 2007. *Evolution of Primary Producers in the Sea*. Amsterdam; Boston: Elsevier Academic Press.

Fleitmann, D., H. Cheng, S. Badertscher, R. L. Edwards, M. Mudelsee, O. M. Göktürk, A. Fankhauser, et al. 2009. "Timing and Climatic Impact of Greenland Interstadials Recorded in Stalagmites from Northern Turkey." *Geophysical Research Letters* 36 (19). doi:10.1029/2009GL040050.

Foerster, V., A. Asrat, C. B. Ramsey, E. T. Brown, M. S. Chapot, A. Deino, W. Duesing, M. Grove, A. Hahn, and A. Junginger. 2022. "Pleistocene Climate Variability in Eastern Africa Influenced Hominin Evolution." *Nature Geoscience* 15 (10): 805-811.

Fritz, S. C., B. F. Cumming, F. Gasse, and K. R. Laird. 2010. "Diatoms as Indicators of Hydrologic and Climatic Change in Saline Lakes." In *Hydrologic and climatic change in saline lakes*, 186-208: Cambridge University Press. doi:10.1017/CBO9780511763175.011.

Gasse, F., S. Juggins, and L. B. Khelifa. 1995. "Diatom-Based Transfer Functions for Inferring Past Hydrochemical Characteristics of African Lakes." *Palaeogeography, Palaeoclimatology, Palaeoecology* 117 (1): 31-54. doi:10.1016/0031-0182(94)00122-O.

Gasse, F., P. Barker, P. A. Gell, S. C. Fritz, and F. Chalie. 1997. "Diatom-Inferred Salinity in Palaeolakes: An Indirect Tracer of Climate Change." *Quaternary Science Reviews* 16 (6): 547-563. doi:10.1016/S0277-3791(96)00081-9.

Gasse, F., F. Chalié, A. Vincens, M. A. J. Williams, and D. Williamson. 2008. "Climatic Patterns in Equatorial and Southern Africa from 30,000 to 10,000 Years Ago Reconstructed from Terrestrial and Near-Shore Proxy Data." *Quaternary Science Reviews* 27 (25): 2316-2340. doi:10.1016/j.quascirev.2008.08.027.

Geen, R., S. Bordoni, D. S. Battisti, and K. Hui. 2020. "Monsoons, ITCZs, and the Concept of the Global Monsoon." *Reviews of Geophysics (1985)* 58 (4): doi:10.1029/2020RG000700.

Gienapp, P., C. Teplitsky, J. S. Alho, J. A. Mills, and J. Merila. 2008. "Climate Change and Evolution: Disentangling Environmental and Genetic Responses." *Molecular Ecology* 17 (1): 167-178. doi:10.1111/j.1365-294X.2007.03413.x.

Gillespie, R. G. and G. K. Roderick. 2014. "Evolution: Geology and Climate Drive Diversification." *Nature (London)* 509 (7500): 297-298. doi:10.1038/509297a.

Gosling, W. D., E. M. L. Scerri, and S. Kaboth-Bahr. 2022. "The Climate and Vegetation Backdrop to Hominin Evolution in Africa." *Philosophical Transactions of the Royal Society of London. Series B. Biological Sciences* 377 (1849): 20200483. doi:10.1098/rstb.2020.0483.

Gregory, J. W. 1921. *The Rift Valleys and Geology of East Africa; an Account of the Origin & History of the Rift Valleys of East Africa & their Relation to the Contemporary Earth-Movements which Transformed the Geography of the World. with some Account of the Prehistoric Stone Implements, Soils, Water Supply, & Mineral Resources of the Kenya Colony.* England: Seely, Service & Co. Limited.

Hirons, L. and A. Turner. 2018. "The Impact of Indian Ocean Mean-State Biases in Climate Models on the Representation of the East African Short Rains." *Journal of Climate* 31 (16): 6611-6631. doi:10.1175/JCLI-D-17-0804.1.

Hosfield, R. and J. Cole. 2018. "Early Hominins in North-West Europe: A Punctuated Long Chronology?" *Quaternary Science Reviews* 190: 148-160. doi:10.1016/j.quascirev.2018.04.026.

Imbrie, J. and J. Z. Imbrie. 1980. "Modeling the Climatic Response to Orbital Variations." *Science (New York, N.Y.)* 207 (4434): 943. doi:10.1126/science.207.4434.943.

IODP. 2023. “History.” IODP. https://www.iodp.org/about-iodp/history

Joordens, J. C. A., H. B. Vonhof, C. S. Feibel, L. J. Lourens, G. Dupont-Nivet, van der Lubbe, Jeroen H. J. L, M. J. Sier, G. R. Davies, and D. Kroon. 2011. "An Astronomically-Tuned Climate Framework for Hominins in the Turkana Basin." *Earth and Planetary Science Letters* 307 (1): 1-8. doi:10.1016/j.epsl.2011.05.005.

Juggins, S. 2013. "Quantitative Reconstructions in Palaeolimnology: New Paradigm Or Sick Science?" *Quaternary Science Reviews* 64: 20-32. doi:10.1016/j.quascirev.2012.12.014.

Junginger, A., S. Roller, L. A. Olaka, and M. H. Trauth. 2014. "The Effects of Solar Irradiation Changes on the Migration of the Congo Air Boundary and Water Levels of Paleo-Lake Suguta, Northern Kenya Rift, during the African Humid Period (15–5 Ka BP)." *Palaeogeography, Palaeoclimatology, Palaeoecology* 396: 1-16. doi:10.1016/j.palaeo.2013.12.007.

Koroly, D. J. and D. G. Vincent 1998. *Meteorology of the Southern Hemisphere*. Boston, Mass.: American Meteorological Society.

Kump, L. R., J. Kasting, and R. G. Crane. 1999. "The Atmospheric Circulation System." In *The Earth System*, edited by J. F. Kasting and R. G. Crane. Upper Saddle River, N.J.: Prentice Hall.

Kutzbach, J. E. and Z. Liu. 1997. "Response of the African Monsoon to Orbital Forcing and Ocean Feedbacks in the Middle Holocene." *Science* 278 (5337): 440-443. doi:10.1126/science.278.5337.440.

Lange-Bertalot, H. 1979. "Pollution Tolerance of Diatoms as a Criterion for Water Quality Estimation." *Nova Hedwigia Beiheft* 64: 285-304.

Lapworth, D. J., D. C. W. Nkhuwa, J. Okotto-Okotto, S. Pedley, M. E. Stuart, M. N. Tijani, and J. Wright. 2017. "Urban Groundwater Quality in Sub-Saharan Africa: Current Status and Implications for Water Security and Public Health." *Hydrogeology Journal* 25 (4): 1093-1116. doi:10.1007/s10040-016-1516-6.

Larrasoaña, J., A. Roberts, E. Rohling, M. Winklhofer, and R. Wehausen. 2003. "Three Million Years of Monsoon Variability Over the Northern Sahara." *Climate Dynamics* 21 (7): 689-698. doi:10.1007/s00382-003-0355-z.

Leakey, L. S. B. 1931. "East African Lakes." *The Geographical Journal* 77 (6): 497-508. doi:10.2307/1785041.

Leakey, L. S. B. 1931. *The Stone Age Cultures of Kenya Colony*. Cambridge England: The University Press.

Levin, N. E. 2015. *Environment and Climate of Early Human Evolution*. Vol. 43. Palo Alto, Calif. :. doi:10.1146/annurev-earth-060614-105310.

Liu, Z., S. Harrison, J. Kutzbach, and B. Otto-Bliesner. 2004. "Global Monsoons in the Mid-Holocene and Oceanic Feedback." *Climate Dynamics* 22 (2): 157-182. doi:10.1007/s00382-003-0372-y.

Loughnan, F. C. 1969. *Chemical Weathering of the Silicate Minerals*. New York: New York, American Elsevier Pub. Co.

Lüdecke, H.-J., G. Müller-Plath, M. G. Wallace, and S. Lüning. 2021. "Decadal and Multidecadal Natural Variability of African Rainfall." *Journal of Hydrology Regional Studies* 34: 100795. doi:10.1016/j.ejrh.2021.100795.

Lupien, R. L., J. M. Russell, M. Grove, C. C. Beck, C. S. Feibel, and A. S. Cohen. 2020. "Abrupt Climate Change and its Influences on Hominin Evolution during the Early Pleistocene in the Turkana Basin, Kenya." *Quaternary Science Reviews* 245: 106531. doi:10.1016/j.quascirev.2020.106531.

Macheyeki, A. S., X. Li, D. P. Kafumu, and F. Yuan. 2020. "Chapter 1 - Elements of Exploration Geochemistry." In *Applied Geochemistry*, edited by A. S. Macheyeki, X. Li, D. P. Kafumu and F. Yuan, 1-43: Elsevier. doi:10.1016/B978-0-12-819495-9.00001-3.

Mackay, A., S. J. Armitage, E. M. Niespolo, W. D. Sharp, M. C. Stahlschmidt, A. F. Blackwood, K. C. Boyd, et al. 2022. "Environmental Influences on Human Innovation and Behavioural Diversity in Southern Africa 92-80 Thousand Years Ago." *Nature Ecology & Evolution* 6 (4): 361-369. doi:10.1038/s41559-022-01667-5.

Mackay, A., B. A. Stewart, and B. M. Chase. 2014. "Coalescence and Fragmentation in the Late Pleistocene Archaeology of Southernmost Africa." *Journal of Human Evolution* 72: 26-51. doi:10.1016/j.jhevol.2014.03.003.

Marchant, R., C. Mumbi, S. Behera, and T. Yamagata. 2007. "The Indian Ocean Dipole the Unsung Driver of Climatic Variability in East Africa." *African Journal of Ecology* 45 (1): 4-16. doi:10.1111/j.1365-2028.2006.00707.x.

Maslin, M. A., C. M. Brierley, A. M. Milner, S. Shultz, M. H. Trauth, and K. E. Wilson. 2014. "East African Climate Pulses and Early Human Evolution." *Quaternary Science Reviews* 101: 1-17. doi:10.1016/j.quascirev.2014.06.012.

Maslin, M. A. and M. H. Trauth. 2009. *"*Plio-Pleistocene East African Pulsed Climate Variability and its Influence on Early Human Evolution." *The First Humans – Origin and Early Evolution of the Genus Homo* Dordrecht: Springer Netherlands. 151-158.

Matthew, W. D. and E. H. Colbert. 1939. *Climate and Evolution*. 2nd ed. New York Academy of Sciences.

Milankovitch, M. M. 1941. "Canon of Insolation and the Iceage Problem." *Koniglich Serbische Akademice Beograd Special Publication* 132.

Nicholson, S. E. 2000. "The Nature of Rainfall Variability Over Africa on Time Scales of Decades to Millenia." *Global and Planetary Change* 26 (1): 137-158. doi:10.1016/S0921-8181(00)00040-0.

———. 1996. "A Review of Climate Dynamics and Climate Variability in Eastern Africa." In *The Limnology, Climatology and Paleoclimatology of the East African Lakes.,* edited by T. C. Johnson, E. O. Odada, and K. T. Whittaker. Amsterdam, The Netherlands, Gordon and Breach Science Publishers: 25-56.

Owen, R. B., R. W. Renaut, A. K. Behrensmeyer, and R. Potts. 2014. "Quaternary Geochemical Stratigraphy of the Kedong–Olorgesailie Section of the Southern Kenya Rift Valley." *Palaeogeography, Palaeoclimatology, Palaeoecology* 396: 194-212. doi:10.1016/j.palaeo.2014.01.011.

Paeth, H. and P. Friederichs. 2004. "Seasonality and Time Scales in the Relationship between Global SST and African Rainfall." *Climate Dynamics* 23 (7): 815-837. doi:10.1007/s00382-004-0466-1.

Palmer, P. I., C. M. Wainwright, B. Dong, R. I. Maidment, K. G. Wheeler, N. Gedney, J. E. Hickman, et al. 2023. "Drivers and Impacts of Eastern African Rainfall Variability." *Nature Reviews. Earth & Environment* 4 (4): 254-270. doi:10.1038/s43017-023-00397-x.

Peixóto, J. P. and A. H. Oort. 1984. "Physics of Climate." *Reviews of Modern Physics* 56 (3): 365-429. doi:10.1103/RevModPhys.56.365.

Potts, R. 1998. "Environmental Hypotheses of Hominin Evolution." *American Journal of Physical Anthropology* 107 (27): 93-136. doi:10.1002/(SICI)1096-8644(1998)107:27+3.0.CO;2-X.

Potts, R., R. Dommain, J. W. Moerman, A. K. Behrensmeyer, A. L. Deino, S. Riedl, E. J. Beverly, et al. 2020. "Increased Ecological Resource Variability during a Critical Transition in Hominin Evolution." *Science Advances* 6 (43): eabc8975. doi:10.1126/sciadv.abc8975.

Potts, R. and J. T. Faith. 2015. "Alternating High and Low Climate Variability: The Context of Natural Selection and Speciation in Plio-Pleistocene Hominin Evolution." *Journal of Human Evolution* 87: 5-20. doi:10.1016/j.jhevol.2015.06.014.

Prat, S., J.-P. Brugal, J.-J. Tiercelin, J.-A. Barrat, M. Bohn, A. Delagnes, S. Harmand, et al. 2005. "First Occurrence of Early Homo in the Nachukui Formation (West Turkana, Kenya) at 2.3-2.4Myr." *Journal of Human Evolution* 49 (2): 230-240. doi:10.1016/j.jhevol.2005.03.009.

Quade, Jay, Thure E. Cerling, John C. Barry, Michele E. Morgan, David R. Pilbeam, Allan R. Chivas, Julia A. Lee-Thorp, and Nikolaas J. van der Merwe. 1992. "A 16-Ma Record of Paleodiet using Carbon and Oxygen Isotopes in Fossil Teeth from Pakistan." Chemical Geology 94 (3): 183-192. doi:10.1016/S0009-2541(10)80003-8. https://www.sciencedirect.com/science/article/pii/S0009254110800038.

Robakiewicz, E., D. de Matos, J. R. Stone, and A. Junginger. 2021. “Hydrochemistry and Diatom Assemblages on the Humpata Plateau, Southwestern Angola.” *Geosciences*. 11, 359. https://doi.org/10.3390/geosciences11090359

Robakiewicz, E., R. B. Owen, C. Rosca, A. Deino, Y. Garcin, M. T. Trauth, S. Kübler, and A. Junginger, accepted 2023, “Hydroclimate reconstructions in the Suguta Valley, northern Kenya, during the Early-Middle Pleistocene Transition.” *Palaeogeography, Palaeoclimatology, Palaeoecology.*

Robbins, L. H. 2006. "Lake Turkana Archaeology : The Holocene: Lake Rudolf (Turkana) as Colonial Icon in East Africa." *Ethnohistory* 53 (1): 67-93.

Robertshaw, P. 1984. "Archaeology in Eastern Africa: Recent Developments and More Dates." *The Journal of African History* 25 (4): 369-393. doi:10.1017/S0021853700028449.

Robertson, D. M., H. A. Perlman, and T. N. Narisimhan. 2022. *Hydrological Cycle and Water Budgets*. doi:10.1016/B978-0-12-819166-8.00008-6.

Rosenzweig, M. S. and J. M. Marston. 2018. "Archaeologies of Empire and Environment." *Journal of Anthropological Archaeology* 52: 87-102. doi:10.1016/j.jaa.2018.08.004.

Round, F. E., R. M. Crawford, and D. G. Mann. 1990. *Diatoms: Biology and Morphology of the Genera* Cambridge University Press.

Ruddiman, W. F. 2001. *Earth's Climate; Past and Future*. New York, NY, United States: W. H. Freeman and Company.

Sánchez Goñi, M. F. 2020. "Regional Impacts of Climate Change and its Relevance to Human Evolution." *Evolutionary Human Sciences* 2. doi:10.1017/ehs.2020.56.

Scerri, E. M. L., Lounès Chikhi, and M. G. Thomas. 2019. "Beyond Multiregional and Simple Out-of-Africa Models of Human Evolution." *Nature Ecology & Evolution* 3 (10): 1370-1372. doi:10.1038/s41559-019-0992-1.

Schaebitz, F., A. Asrat, H. F. Lamb, A. S. Cohen, V. Foerster, W. Duesing, S. Kaboth-Bahr, et al. 2021. "Hydroclimate Changes in Eastern Africa Over the Past 200,000 Years may have Influenced Early Human Dispersal." *Communications Earth & Environment* 2 (1). doi:10.1038/s43247-021-00195-7.

Sikka, D. R. and S. Gadgil. 1980. "On the Maximum Cloud Zone and the ITCZ Over Indian Longitudes during the Southwest Monsoon." *Monthly Weather Review* 108 (11): 1840-1853.

Sladecek, V. 1986. "Diatoms as Indicators of Organic Pollution." *Acta Hydrochimica Et Hydrobiologica* 14 (5): 555-566. doi:10.1002/aheh.19860140519.

Soininen, J. and A. Teittinen. 2019. "Fifteen Important Questions in the Spatial Ecology of Diatoms." *Freshwater Biology* 64 (11): 2071-2083. doi:10.1111/fwb.13384.

Spoor, F., S. Antón C., P. N. Gathogo, M. G. Leakey, I. McDougall, F. H. Brown, C. Kiarie, L. N. Leakey, and F. K. Manthi. 2007. "Implications of New Early Homo Fossils from Ileret, East of Lake Turkana, Kenya." *Nature* 448 (7154): 688-691. doi:10.1038/nature05986.

Toggweiler, J. R. and J. Russell. 2008. "Ocean Circulation in a Warming Climate." *Nature* 451 (7176): 286-288. doi:10.1038/nature06590.

Trauth, M. H., J. C. Larrasoana, and M. Mudelsee. 2009. *Trends, Rhythms and Events in Plio-Pleistocene African Climate*. Vol. 11. Katlenburg-Lindau: Katlenburg-Lindau, Germany: Copernicus GmbH on behalf of the European Geosciences Union (EGU).

Trauth, M. H., A. Asrat, Na. Berner, F. Bibi, V. Foerster, M. Grove, S. Kaboth-Bahr, M. A. Maslin, M. Mudelsee, and F. Schäbitz. 2021. "Northern Hemisphere Glaciation, African Climate and Human Evolution." *Quaternary Science Reviews* 268: 107095. doi:10.1016/j.quascirev.2021.107095.

Trauth, M. H., M. A. Maslin, A. L. Deino, A. Junginger, M. Lesoloyia, E. O. Odada, D. O. Olago, L. A. Olaka, M. R. Strecker, and R. Tiedemann. 2010. "Human Evolution in a Variable Environment: The Amplifier Lakes of Eastern Africa." *Quaternary Science Reviews* 29 (23): 2981-2988. doi:10.1016/j.quascirev.2010.07.007.

Trauth, M. H., M. A. Maslin, A. L. Deino, M. R. Strecker, A. G. N. Bergner, and M. Dühnforth. 2007. "High- and Low-Latitude Forcing of Plio-Pleistocene East African Climate and Human Evolution." *Journal of Human Evolution* 53 (5): 475-486. doi:10.1016/j.jhevol.2006.12.009.

Tryon, C. A., J. T. Faith, D. J. Peppe, W. F. Keegan, K. N. Keegan, K. H. Jenkins, S. Nightingale, et al. 2014. "Sites on the Landscape: Paleoenvironmental Context of Late Pleistocene Archaeological Sites from the Lake Victoria Basin, Equatorial East Africa." *Quaternary International* 331: 20-30. doi:10.1016/j.quaint.2013.05.038.

Tyson, P. D. and R. A. Preston-Whyte. 2000. *The Weather and Climate of Southern Africa*, edited by A. Attwell. 2nd ed. Cape Town: Oxford University Press Southern Africa.

Tyson, P. D. 1986. *Climatic Change and Variability in Southern Africa*. Cape Town: Oxford University Press.

van der Leeuw, S. E. 2008. "Climate and Society: Lessons from the Past 10000 Years." *Ambio* 37: 476-482. doi:10.1579/0044-7447-37.sp14.476.

Vanormelingen, P., E. Verleyen, and W. Vyverman. 2008. "The Diversity and Distribution of Diatoms: From Cosmopolitanism to Narrow Endemism." *Biodiversity and Conservation* 17 (2): 393-405. doi:10.1007/s10531-007-9257-4.

Vrba, E. S. 1980. "Evolution, Species and Fossils: How does Life Evolve?" *South African Journal of Science* 76 (2): 61-84.

Vrba, E. S. 1995. "On the Connections between Paleoclimate and Evolution." In *Paleoclimate and Evolution, with Emphasis on Human Origins*, 24-43: Yale University.

Wilkins, J., K. S. Brown, S. Oestmo, T. Pereira, K. L. Ranhorn, B. J. Schoville, and C. W. Marean. 2017. "Lithic Technological Responses to Late Pleistocene Glacial Cycling at Pinnacle Point Site 5-6, South Africa." *PLoS One* 12 (3): e0174051. doi:10.1371/journal.pone.0174051.

Will, M., N. J. Conard, and C. A. Tryon. 2019. "Timing and Trajectory of Cultural Evolution on the African Continent 200,000-30,000 Years Ago." *Modern Human Origins and Dispersal*: 25-72.

Wynn, J. G. 2004. "Influence of Plio-Pleistocene Aridification on Human Evolution: Evidence from Paleosols of the Turkana Basin, Kenya." *American Journal of Physical Anthropology* 123 (2): 106-118. doi:10.1002/ajpa.10317.

Ziegler, M., M. H. Simon, I. R. Hall, S. Barker, C. Stringer, and R. Zahn. 2013. "Development of Middle Stone Age Innovation Linked to Rapid Climate Change." *Nature Communications* 4. doi:10.1038/ncomms2897.

CHAPTER 2: Hydrochemistry and Diatom Assemblages on the Humpata Plateau, Southwestern Angola [1]

2.1. INTRODUCTION

Water is a valuable resource, particularly for populations in the dry subhumid Humpata Plateau in southwestern Angola. Beyond consumption and food preparation, daily economic tasks depend on water, including excremental waste management, agriculture, livestock production, washing, fishing, and other economic activities [1]. The use of water for these activities can lead to pollution, which reduces individuals' access to clean, fresh water [2]. Although in recent years Angola has established policies to decrease water pollution (whether from heavy metals, agriculture, industry, or excremental waste) and increase water quality [2], in much of the country, little is known about local water chemistry, particularly beyond urban areas [1,3]. Studies of rural water sources are limited because many techniques used to manage and analyze water are time consuming and access to collection sites is limited due to a lack of roads in many rural communities across the country [4]. This emphasizes the importance for communities to have in-depth knowledge about their local water supplies and adopt practices that support community-based monitoring to keep waters clean [5].

In environments with variable annual precipitation such as the Humpata Plateau, water access is even more crucial. Most accessible and potable water comes from small, cold-water springs fed by groundwater during the rainy season. Because of climate change, drastic changes in annual African rainfall threaten many of these rural communities that depend on the replenishment of springs during the rainy season [6]. To begin to solve some issues that accompany limited access to fresh, clean water (poverty, malnourishment, water-borne disease, etc.), it is necessary to begin to record and analyze the water quality of rural water to empower local communities to retain high water quality [5]. This project combines water chemistry data and diatom assemblage analysis to understand water quality and pollution on

[1] ROBAKIEWICZ, E.; DE MATOS, D.; STONE, J.R.; & JUNGINGER, A., 2021. Hydrochemistry and Diatom Assemblages on the Humpata Plateau, Southwestern Angola: *Geosciences. 11, 359.* https://doi.org/10.3390/geosciences11090359

the Humpata Plateau in an effective and simple manner that can embolden communities to protect their water resources.

Diatoms are siliceous microalga frequently used to identify and reconstruct changes in lake chemistry and water quality related to climate change or anthropogenic pollution [7–10]. Diatom ecology provides environmental information because each taxon has specific preferences for certain physical (temperature, light, turbulence, etc.) and chemical (pH, dissolved organic carbon, nutrients, salinity, etc.) parameters [8]. Physical parameters are often difficult to deduce as they impact chemical parameters and cannot be dissociated from other variables [8,11,12]. Diatom analyses, therefore, focus on the reconstruction and interpretation of chemical parameters (particularly pH, conductivity, and pollutants), which are more readily discernible. Diatoms are strong water-quality indicators because of (1) their sensitivity to changes in water chemistry, (2) their numerical abundance in both past and modern sediments, (3) their siliceous frustules, which can withstand some dissolution post-deposition, (4) their rapid response to changing variables as primary producers, and (5) the large geographic ranges of some taxa, although recent studies show that many species may not be as cosmopolitan as previously suspected and instead represent similar morphotypes [13–15]. Therefore, collecting diatoms with relevant water chemistry data can be extremely valuable in discerning water quality and environmental change.

This research focuses on determining diatom taxa on the Humpata Plateau in southwestern Angola to understand how they relate to local hydrochemistry and anthropogenic pollution from agricultural and excremental waste. It aims to act as a guide for future studies in rural regions of Africa where resources are scarce, and travel is difficult, to continually monitor chemical changes. Specifically, the objectives of this study are to:

1. Record modern diatom assemblages at five sites in southwestern Angola.
2. Determine which hydrochemical variables diatom communities can estimate for local water bodies.
3. Identify potential human impact on water through differences in water quality and diatom assemblages.

2.2. GEOLOGICAL AND CLIMATIC SETTING

2.2.1. Geography and Geology

As Africa's seventh largest country, Angola, located in southwestern Africa (Figure 1A), displays drastically varied geologies, landscapes, and climates [16]. In southwestern Angola, the dry subhumid Humpata Plateau extends over 300 km east and west and reaches an elevation of 2,300 m [3,17] (Figure 1B). The Province of Huíla, where the Humpata Plateau is located, has an area of 78,879 km^2 with a population of around 2.6 million people, with the majority of the population surrounding the province's capital city, Lubango [18]. The Plateau is made of a Proterozoic craton overlain by the Chela Group, a 600 m thick volcanic sedimentary sequence deposited between 1.947 and 1.810 Ga (Figure 1C) [17–21]. The top layer of the Chela Group, called the Leba Formation, is composed of layers of greyish-blue dolomitic limestone scattered with stromatolites, argillites (lightly metamorphosed mudstone), and chert (Figure 1D) [18]. The Leba Formation unconformably lies over the Cangalongue Formation, which is composed of interbedded red sandstones, red shales, limestones, and siltstones [21]. The calcite-rich bedrock contains karst features including caves and springs which have been associated with paleontological and archaeological finds [22]. The soils on the Humpata Plateau consist mainly of leptosols (shallow, gravelly soils) and ferralsols (heavily weathered and iron and aluminum rich red/yellow soils), both of which have low fertility [16].

2.2.2. Seasonality and Climate

The seasons in southwestern Angola are dominated by yearly fluctuations in precipitation rather than temperature, with a warmer/rainy season from the end of September until May and a cooler/dry season from the end of May until September [3]. Ninety-five percent of annual rainfall across Angola occurs during the wet season [23]. From the Humpata weather gauge located at 15.069° S and 13.251° E at an altitude of 1880 m, average monthly temperatures from 2015 to 2018 range, inclusively, from a dry season average of 15.5°C to a wet season average of 18.2°C, with a four-year annual average of 17.3°C [24]. In contrast, precipitation varies, inclusively, from a dry season average of 0.35 mm of rain per month to a wet season average of 136 mm of rain per month [24]. Annual precipitation varies slightly across the sampled sites. Based on data from the Climate Change Knowledge Portal,

across the sampling sites, average annual precipitation from 1910 to 1998 varies from Cascatinha da Zootécnica at 570 mm/year to Nandimba Tchivinguiro at 498 mm/year [25]. Since the 1930s, this area has seen a decrease in rainfall, although data is fragmented [6,25]. The decadal averages for Cascatinha da Zootécnica and Nandimba Tchivinguiro from the 1930s to 1970s range from 609–812 mm/yr and 523–680 mm/yr, respectively [25]. In contrast, the average for Cascatinha da Zootécnica and Nandimba Tchivinguiro, respectively, were 477 and 407 mm/yr in the 1980s and 446 and 395 mm/yr in the 1990s [25]. Unfortunately, scarce data since 1998 reduce the ability to further analyze how current rainfall patterns differ, although local communities stress that water availability has decreased in recent memory [Personal Communication, Field Season 2019].

Rainfall in southwestern Angola is controlled by sea surface temperatures, specifically the Benguela Current, and air masses including high- and low-pressure systems that move seasonally over southern Africa. The cold Benguela Current, which moves northward along the western coast of southern Africa to about 15° S (shifting seasonally between 14° S and 16° S), dictates rainfall patterns along Angola's coast by decreasing moisture availability and transport [26]. High-pressure systems lead to fair weather conditions and include the South Atlantic Anticyclone and the South Indian Anticyclone, which make landfall during the austral winter [27]. Low-pressure systems that create wet conditions include the Angola Low and Tropical Temperate Trough and develop over southern Angola during the austral summer. Larger low-pressure systems that affect southwestern Angolan rainfall include the Intertropical Convergence Zone and the Congo Air Boundary [26]. The Intertropical Convergence Zone reflects the amount of solar insolation received by the atmosphere and Earth's surface, leading to a band of low pressure near the equator, which draws in moisture and rainfall [27]. The Congo Air Boundary is the area of convergence of airmasses derived from the South and the Congo Air Boundary [26]. The Intertropical Convergence Zone reflects the amount of solar insolation received by the atmosphere and Earth's surface, leading to a band of low pressure near the equator, which draws in moisture and rainfall [27]. The Congo Air Boundary is the area of convergence of airmasses derived from the South Atlantic and Indian Oceans, bringing moisture over southern Africa and resulting in rainfall [27]. Larger global phenomenon including the Atlantic Walker Cell and El Niño

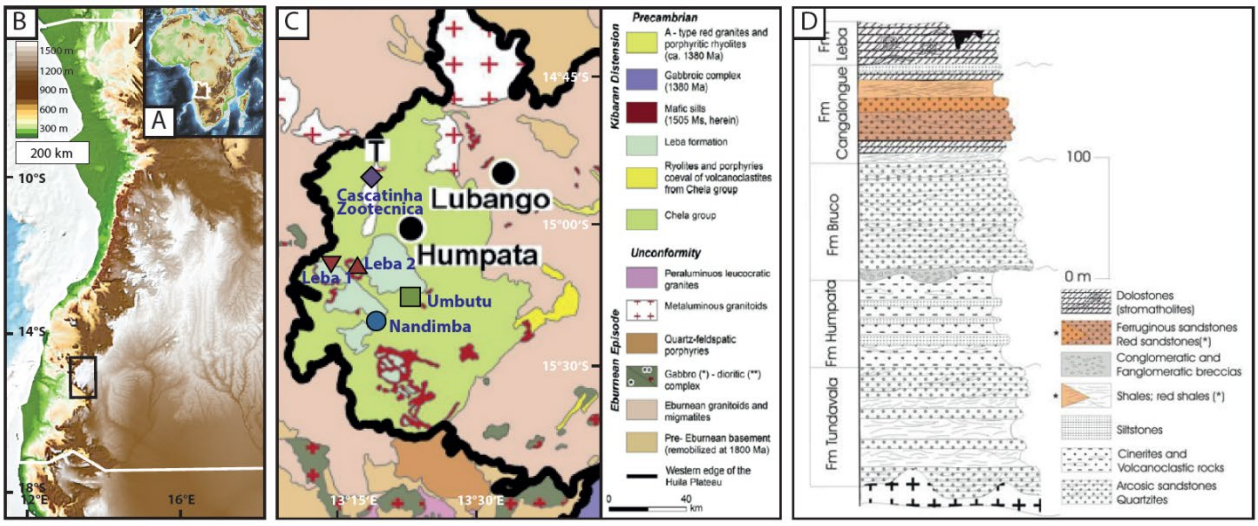

Figure 1. (**A**) Topographic map of Africa with Angola outlined in white. (**B**) Topographic map of western Angola with the study area outlined with a black box. (**C**) A close-up of the bedrock at the edge of the Humpata Plateau (Modified from Lopes et al., 2019) [18]. Sites from this study are added to the map and are located on the Leba Formation, Chela Group, or metaluminous granitoid. (**D**) A cross-section of the Chela Group, including the Leba and Cangalongue Formations on the Humpata Plateau (From Pereira et al., 2011) [21]. Asterisks (*) denote the shading for red shales and red sandstones.

events likely contribute to Angolan rainfall through time, although their impacts are not well understood [28].

2.2.3. Hydrological Setting

The southwestern part of the Humpata Plateau is located within the Cunene (or Kunene) Basin. The Cunene River represents the confluence of water within the basin. The Cunene River starts within the highlands near Huambo at 12.8° S, 15.7° E, creates the border between Angola and Namibia, and dr into the Atlantic Ocean at Foz da Cunene where discharge is about 15 km³/yr [29]. Mean annual runoff of the Cunene Basin is 5500 million m^3/yr [30]. With 60% of Angolan territory located at an altitude between 1000 and 2000 m [23], Angola acts as the “water tower” of southern and central Africa [16]. The Cunene Basin is located next to the Okavango Basin in the east and the Cuvelai Basin in the south, which both feed into two of Africa’s largest wetlands, the Kalahari and Etosha, respectively [16]. The current barrier between the Cunene and Cuvelai Basins is only a few meters in elevation, but sufficient to prevent Cunene flooding from flowing into the Cuvelai System [31,32]. Nonetheless, the three basins are likely connected hydraulically underground [31]. International disagreements related to use and control of the

Cunene River's water have resulted because these systems provide access to potable water for populations throughout the region [29].

2.3. MATERIALS AND METHODS

2.3.1. Sample Collection

Samples were collected during the dry season in July 2019 from four water bodies including
cold springs (Umbutu and Nandimba Tchivinguiro), a river (Leba), and a waterfall pool (Cascatinha da Zootécnica) (Figure 2). Sites for sampling were found by searching for bodies of water on Google Earth and communicating with local people about small springs in the area. A Hanna multi-parameter probe HI98194 was used to collect data on temperature (°C), conductivity (µS/cm), pH, and Total Dissolved Solids (TDS; ppm) (Table 1). Alkalinity (mg/L solution as $CaCO_3$) was estimated using alkalinity strips.

Water samples were collected using a syringe with a 0.45 µm filter. Samples for cation and anion analyses were collected from 60 mL water samples. Additionally, cation samples were acidified with 0.6 mL of 65% HNO_3 to ensure cations would not precipitate out of solution. Cation and anion samples were sent to the Petrology and Mineralogy Raw Materials lab at the Universität Tübingen for analysis where they were analyzed using ion chromatography compact IC Flex and Compact IC Plus from Metrohm.

Diatom samples were collected from standing water, plants, sediments, and rocks, according to the recommendations of Kelly et al. (2001) [33]. Standing water samples were collected by retrieving 20 mL of surface water, although this did not yield enough diatoms and is therefore not considered further in this paper. Multiple macrophytes located in direct sunlight were selected for epiphytic sampling. Sediment samples were scooped from about a meter offshore, with muds (epipelon) and sands/small rocks (episammon) collected separately. Larger rocks (epilithic) were scrubbed with a clean toothbrush. Distilled water was used to clean the toothbrush onto a tray which was then transferred into a sample container. All diatom samples were treated in the field with Lugol's solution.

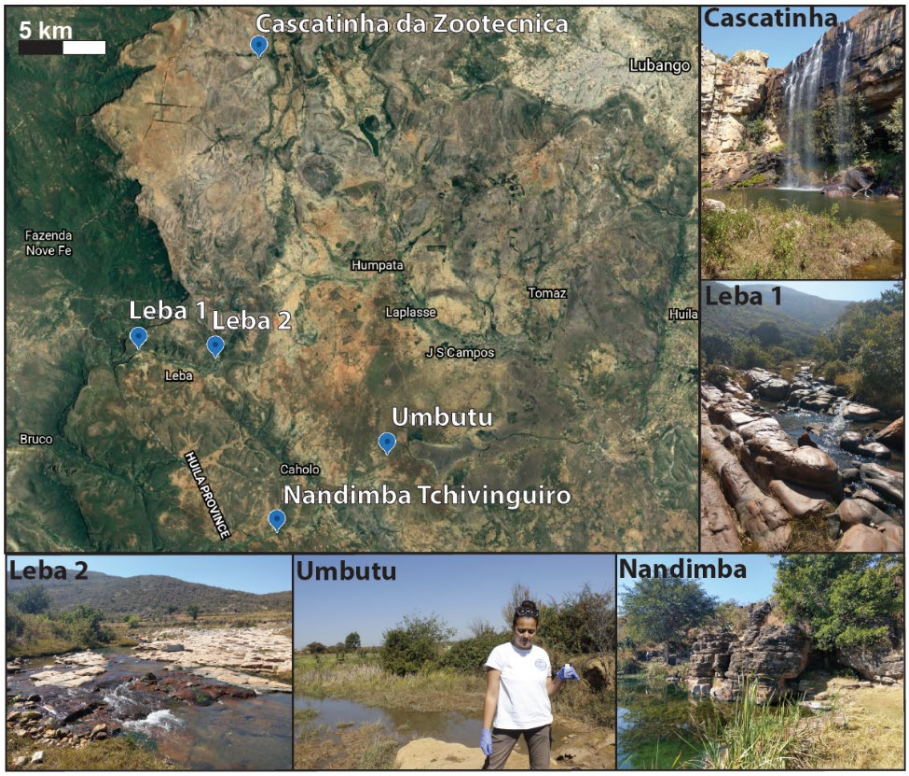

Figure 2. Satellite image from Google Earth of the sampled sites. A field photo from each site is included.

2.3.2. Diatom Preparation and Identification

All samples not already suspended in water were washed with distilled water using a 210 µm sieve. The <210 µm samples were decanted using a centrifuge for five minutes at 2500 revolutions per minute (RPM) to decrease the volume to five mL. Samples were prepared using a modified hot H2O2 method [34]. Each sample was heated at 90 °C with 20 mL of 30% H2O2 until the majority had evaporated (four to five hours) to remove the organics. A few drops of 10% HCl (to remove carbonates) and a Lycopodium spore (to measure concentration for use in future studies) were added to sit for about 24 h. Samples were transferred to 15 mL centrifuge tubes using distilled water and centrifuged for five minutes at 2500 RPM and decanted—a process that was repeated four times to wash off remaining acids. Once this process was finished, one drop of ammonium hydroxide was added to separate the aggregates and remove clays. The sample was centrifuged and decanted a final time at 2500 RPM for five minutes. The sample was adjusted with an appropriate amount of deionized water (given the anticipated concentration of the sample) and added to the coverslip to dry in a dust-free shelf for 24 h. Once the coverslip was dry, Naphrax was used to adhere the cover slip to a glass slide and

heated at 125 °C until the Naphrax was cured (about 20 min). Prepared and unprepared samples are located at the University of Tübingen.

Diatom Preparation and Identification

All samples not already suspended in water were washed with distilled water using a 210 µm sieve. The <210 µm samples were decanted using a centrifuge for five minutes at 2500 revolutions per minute (RPM) to decrease the volume to five mL. Samples were prepared using a modified hot H_2O_2 method [34]. Each sample was heated at 90 °C with 20 mL of 30% H_2O_2 until the majority had evaporated (four to five hours) to remove the organics. A few drops of 10% HCl (to remove carbonates) and a Lycopodium spore (to measure concentration for use in future studies) were added to sit for about 24 h. Samples were transferred to 15 mL centrifuge tubes using distilled water and centrifuged for five minutes at 2500 RPM and decanted—a process that was repeated four times to wash off remaining acids. Once this process was finished, one drop of ammonium hydroxide was added to separate the aggregates and remove clays. The sample was centrifuged and decanted a final time at 2500 RPM for five minutes. The sample was adjusted with an appropriate amount of deionized water (given the anticipated concentration of the sample) and added to the coverslip to dry in a dust-free shelf for 24 h. Once the coverslip was dry, Naphrax was used to adhere the cover slip to a glass slide and heated at 125 °C until the Naphrax was cured (about 20 min). Prepared and unprepared samples are located at the University of Tübingen.

When possible, at least 400 diatom valves were counted on an Olympus BX50 light microscope at 1000× magnification with a 700D Canon Camera attached to take photos of taxa (S1). The presence of extremely small taxa (<5 µm) indicates samples were not biased towards larger taxa during sample preparation. All planktonic and some epilithic samples could not be included because there were too few specimens in the sample. Identification was conducted using Gasse (1986), Cocquyt (1998), Taylor et al. (2007a), and Spaulding et al. (2020) [35–38]. A valve was counted as one if more than 50% of the valve was visible and identifiable. In all cases, specimens were identified to the highest taxonomic level as accurately as possible (Table 2; S2). Light microscope identification was supplemented with Scanning Electron Microscope photos taken at the Microfossils Laboratory in the Department of Geosciences of the Eberhard Karls Universität Tübingen with a

Table 1. Collected and calculated physical and chemical parameters of the sites including water temperature (Temp.), pH, conductivity (Cond.), alkalinity (Alk.), Total Dissolved Solids (TDS), and major cations and anions. Measurements with an asterisk (*) were calculated using Geochemist Workbench.

Sites	Lat. (° S)	Long. (° E)	Elevation (m)	Water Body Type			Water Type	Temp. (°C)	pH	Cond. (µS/cm)	* Alk. (mg/L sol'n as $CaCO_3$)	TDS (ppm)
Cascatinha da Zootécnica 1	14.9166	13.3114	1670	Waterfall Pool			Na-Cl	14.22	8.26	17	1	8
Nandimba Tchivinguiro 1	15.1675	13.3207	1677	Cold Spring			$Mg\text{-}HCO_3$	22.12	7.35	186	147	186
Umbutu 1	15.1263	13.3815	1806	Cold Spring			$Mg/Ca\text{-}HCO_3$	22.18	7.16	1035	47	520
Leba 1	15.0704	13.2240	1689	River			$Ca/Mg\text{-}HCO_3$	14.84	7.92	95	16	40
Leba 2	15.0749	13.2868	1730	River			$Na/Ca\text{-}HCO_3/Cl$	17.80	7.75	34	2	13
Sites	**Li^+ (mg/L)**	**Na^+ (mg/L)**	**K^+ (mg/L)**	**Ca^{2+} (mg/L)**	**Mg^{2+} (mg/L)**	**Sr^{2+} (mg/L)**	*** HCO_3^- (mg/L)**	**F^- (mg/L)**	**Cl^- (mg/L)**	**Br^- (mg/L)**	**NO_3^- (mg/L)**	**PO_4^{3-} (mg/L)**	**SO_4^{2-} (mg/L)**	**I^- (mg/L)**
Cascatinha da Zootécnica 1	0.00	0.60	0.25	0.11	0.06	0.00	0.83	0.01	0.64	0.01	0.16	0.01	0.06	0.01
Nandimba Tchivinguiro 1	0.00	2.20	1.40	28.00	19.00	0.00	176.20	0.22	4.20	0.03	0.89	0.06	0.71	0.01
Umbutu 1	0.00	1.30	0.90	9.20	5.60	0.00	57.47	0.08	[illegible]	0.01	0.89	0.20	0.34	0.06
Leba 1	0.01	2.10	0.48	3.10	1.50	0.07	19.64	0.02		0.00	0.01	0.01	0.53	0.01
Leba 2	0.00	0.87	0.51	0.35	0.13	0.00	1.96	0.01	[illegible]10	0.00	0.49	0.01	0.34	0.01

Phenom XL Scanning Electron Microscope (Figures 3 and 4). The electron source is a Cerium Hexaborit (CeB6) cathode. Samples were coated with 70 nm gold and analyzed with a Back Scatter Detector (BSD) with 15 kV acceleration voltage.

2.3.3. Analytical Methods

Hydrochemistry of the water bodies was analyzed using Geochemist Workbench (GWB). Given the remote location of this work, well-constrained alkalinity and HCO_3^- measurements were not possible. Alkalinity strips were used to estimate alkalinity in the field and reflect the trends calculated by GWB. GWB was used balance the ions using HCO_3^-. Given the abundance of Ca^{2+} in the bedrock, such assumptions are likely valid and provide reasonable results that allow for better analysis of the data [39]. Water body type was determined according to USGS water quality standards where a dominant ion represents 50% of total ions measured in mEq/L [40]. If no ion represented 50%, the top two ions were used in descending order.

Correspondence analysis was used to determine the relationship between hydrochemistry and the composition of the diatom assemblage [41,42]. Angolan taxa were grouped by hydrochemical preferences based on data from Gasse (1986), Gasse et al. (1995), Sonneman et al. (2000), Taylor et al. (2007a), and Spaulding et al. (2020) [13,35,37,38,43], although many taxa were missing data in all or some categories of interest. Correspondence analysis for each hydrochemical parameter was run on the formed groups and the percentage of the groups at each site to determine whether the groupings can predict the measured and calculated parameters (conductivity, pH, temperature, alkalinity, and cations and anions). Because of the varied nature of the data presented in the literature, regional variability in diatom ecological preferences, and the possibility of misidentification or morphologically similar taxa with different ecological preferences, groupings do not represent specific, quantitative hydrochemical preferences. Rather, the typically quantitative parameters (conductivity, temperature, pH, and alkalinity) are clustered along a gradient (where Group 1 is low and Group 5 is high) based on observed preferences in the aforementioned literature to show general trends of inferred hydrochemistry based on the observed diatom assemblages (S2). Thus, Chi-square could not be used to confirm the significance of the data, as categorical correspondence cannot account for the quantitative gradient for each parameter. Chi-square was used for categories that can be categorical and were not measured in the field, including pollution and trophic level.

Table 2. A list of all diatom percentages in relation to the total diatoms in each community of each water body. Percentages of taxa with an abundance of at least 2% within a habitat at a water body were used. Epilithic refers to diatoms on rock, epipelic are diatoms in muds, epiphytic are diatoms on plants, and episammic are diatoms on sands. Planktonic samples did not yield enough diatoms to reach the 400-valve minimum and are therefore not included in this study. Planktonic counts can be found in S2.

Site	Sample Type	*Achnanthidium exiguum*	*Achnanthidium macrocephalum*	*Achnanthidium minutissimum*	*Achnanthidium saprophilum*	*Adlafia* spp.	*Amphora pediculus*	*Brachysira neoexilis*	*Cymbella affinis*	*Encyonema neogracile*	*Eunotia* cf. *minor*	*Eunotia pectinalis* var. *undulata*	*Eunotia monodon*	*Eunotia* spp.	*Fragilaria capucina*	*Fragilaria* spp.	*Frustulia crassinervia*	*Gessleria* sp 1 and *Sellaphora* cf. *atomoides*	*Gomphonema acuminatum*	*Gomphonema gracile sl*	*Gomphonema parvulum*
Cascatinha da Zootécnica 1	Epithilthic		12.9		9.7	3.2							9.7			6.5					3.2
	Epipelic		11.6	0.2	2.9	4.3		3.4	0.2	10.9	6.3	4.8	15.6	0.2		0.8	0.9			2.7	2.3
	Epiphytic		15.1	2.1		9.9		7.7	1.0	5.4	11.6	3.1	11.8							7.2	4.8
Nandimba Tchivinguiro 1	Epilithic	0.2		12.1	0.7	3.6	0.9	1.3	1.3	1.1	0.2	0.2		0.9				0.2		0.9	3.4
	Epipelic	0.2		2.2			0.4		0.8		1.1			0.8				4.2		0.2	0.3
	Epiphytic			12.7	5.3		2.0		0.6		5.9							2.9		0.2	6.4
	Episammic	0.1		2.8														26.1			
Umbutu 1	Epithilthic	0.5		24.2	1.9	23.0		3.4									3.4				24.0
	Epipelic	2.6		20.8	2.6	1.8		5.1	2.8				0.3	0.5		4.6	0.5		7.2		10.5
	Epiphytic	0.5		10.6	2.7	6.9		9.4	0.7		0.2	0.2							6.7		18.2
Leba 1	Epilithic	0.8	2.5	33.2	1.7	5.9			0.4	0.4	0.8				4.2					2.1	3.8
	Epipelic	0.9		29.9	1.3	11.2		0.2	0.2	0.2	1.5	1.5	0.2	0.2	1.9	0.4			0.7		2.1
	Epiphytic	0.9		40.3		14.6			1.1	0.5			0.5		0.9	1.8				0.9	2.3
	Episammic	3.8		26.4		6.4		0.4	2.0	0.2	0.4	0.4	1.1	0.4	0.4	2.2	0.2			0.2	2.9
Leba 2	Epilithic		11.4	2.6		4.0			0.4		4.4	0.7	2.6								19.3
	Epipelic		15.6	2.0	1.6	0.4		1.4		0.8	2.8		0.8	2.2			0.4				1.8
	Epiphytic	0.2	8.0	0.5		9.0		7.1		3.1	6.1	0.2	6.8	7.1		5.7				0.2	2.6
	Episammic		25.4	8.8		14.0		3.6	0.5	0.2	1.2	1.7	6.7	2.6		2.6				1.0	2.1

Site	Sample Type	*Gomphonema pseudosphaerophorum*	*Gomphonema venusta*	*Gomphonema* spp.	*Grunowia solgensis*	*Navicula cryptocephala*	*Navicula cryptotenella*	*Navicula angusta*	*Navicula erifuga*	*Navicula radiosa*	*Nitzschia* cf. *zeamonii*	*Nitzschia amphibia*	*Nitzschia* cf. *frustulum*	*Nitzschia* cf. *palea*	*Pinnularia diceros*	*Platessa hustedtii*	*Punctastriata* cf. *mimetica*	*Sellaphora* cf. *nigri*	*Sellaphora pupula*	*Sellaphora* cf. *saugerresii* and *Gessleria* sp 2	*Ulnaria* cf. *biceps*	*Ulnaria* cf. *contracta*	*Ulnaria* cf. *unlabiseriata*
Cascatinha da Zootécnica 1	Epithilthic		9.7		6.5	19.4	6.5						6.5	0.2	0.2								0.2
	Epipelic	1.9		3.6		21.5	0.5	2.5					0.2		0.2								
	Epiphytic			2.9	0.2	8.5		0.2					0.2										
Nandimba Tchivinguiro 1	Epilithic		0.2		2.9	2.9	0.2		39.8			14.6	3.6	0.4		1.3	1.1						
	Epipelic			0.6	3.9	3.7						47.4	7.6	7.7		6.6	3.4	0.9	1.5	3.5	0.1	2.5	0.2
	Epiphytic	1.6			1.2	2.1		1.2			2.5	31.4	2.7	3.5		11.1	1.0		0.6	0.2	3.2		0.5
	Episammon	0.1			23.3			1.8			0.7	12.2	12.2	0.9		1.8	0.3	5.1		9.5			
Umbutu 1	Epithilthic			0.5	1.7	11.3				0.2		2.9			0.7	0.2			1.7		0.5		0.3
	Epipelic			4.7		6.4	2.2			11.8		0.5	1.3	2.6	1.0				10.3		0.4	0.2	0.4
	Epiphytic													2.0									
Leba 1	Epilithic		0.4							22.3			5.9	0.4	0.4					0.4	12.8		4.8
	Epipelic		1.5				1.7			36.9		0.6									0.1		1.2
	Epiphytic		3.6				0.5			23.9		2.0		0.2							0.8		0.6
	Episammon		5.3		0.2		0.2			40.2									0.4	0.2	1.1	0.7	1.0
Leba 2	Epilithic	2.6		20.0						4.4	17.8		0.4		0.2	0.2					0.7	6.2	0.9
	Epipelic	0.8	0.6			0.8				6.4	49.1								0.2		0.4	8.0	0.5
	Epiphytic	0.9		1.9		1.4	0.2			1.9	17.0			0.2							0.1	17.2	0.2
	Episammon	0.5				0.2	1.7			1.0	15.7	0.2										9.3	0.2

Figure 3 (next page). SEM photographs of some of the most common diatoms found in the water bodies. Each black or white part of the scale bar is 5 µm. Identifications: (**a**) *Achnanthidium exiguum* (Grunow) Czarnecki; (**b**) *Achnanthidium macrocephalum* (Hustedt) Round & Bukhtiyarova; (**c**) *Achnanthidium minitissimum* (Kützing) Czarnecki; (**d**) *Achnanthidium saprophilum* (H.Kobayashi & Mayama) Round & Bukhtiyarova; (**e**) *Grunowia solgensis* (A.Cleve) Aboal; (**f**) *Nitzschia frustulum* (Kützing) Grunow; (**g**) *Sellaphora pupula* (Kützing) Mereschkovsky; (**h**) *Sellaphora* cf. *nigri* (De Notaris) Wetzel & Ector; (**i**) *Geissleria* sp. 2 Lange-Bertalot & Metzeltin; (**j**) *Sellaphora* cf. *saugerresii* (Desmazières) C.E.Wetzel & D.G.Mann; (**k**) *Sellaphora* cf. *atomoides* (Grunow) Wetzel & Van de Vijver; (**l**) *Platessa hustedtii* (Krasske) Lange-Bertalot (raphe and rapheless valve); (**m**) *Amphora pediculus* (Kützing) Grunow; (**n**) *Geissleria* sp. 1 Lange-Bertalot & Metzeltin; (**o**) *Brachysira neoexilis* Lange-Bertalot; (**p**) *Fragilaria capucina* Desmazières; (**q**) *Nitzschia amphibia* Grunow; (**r**) *Nitzschia* cf. *palea* (Kützing) W.Smith; (**s**) *Ulnaria* cf. *unlabiseriata* D.M.Williams & B.Liu; (**t**) *Punctastriata* cf. *mimetica* E.A.Morales; (**u**) *Ulnaria* cf. *biceps* (Kützing) Compère; (**v**) *Ulnaria* cf. *contracta* (Østrup) E.A.Morales & M.L.Vis.

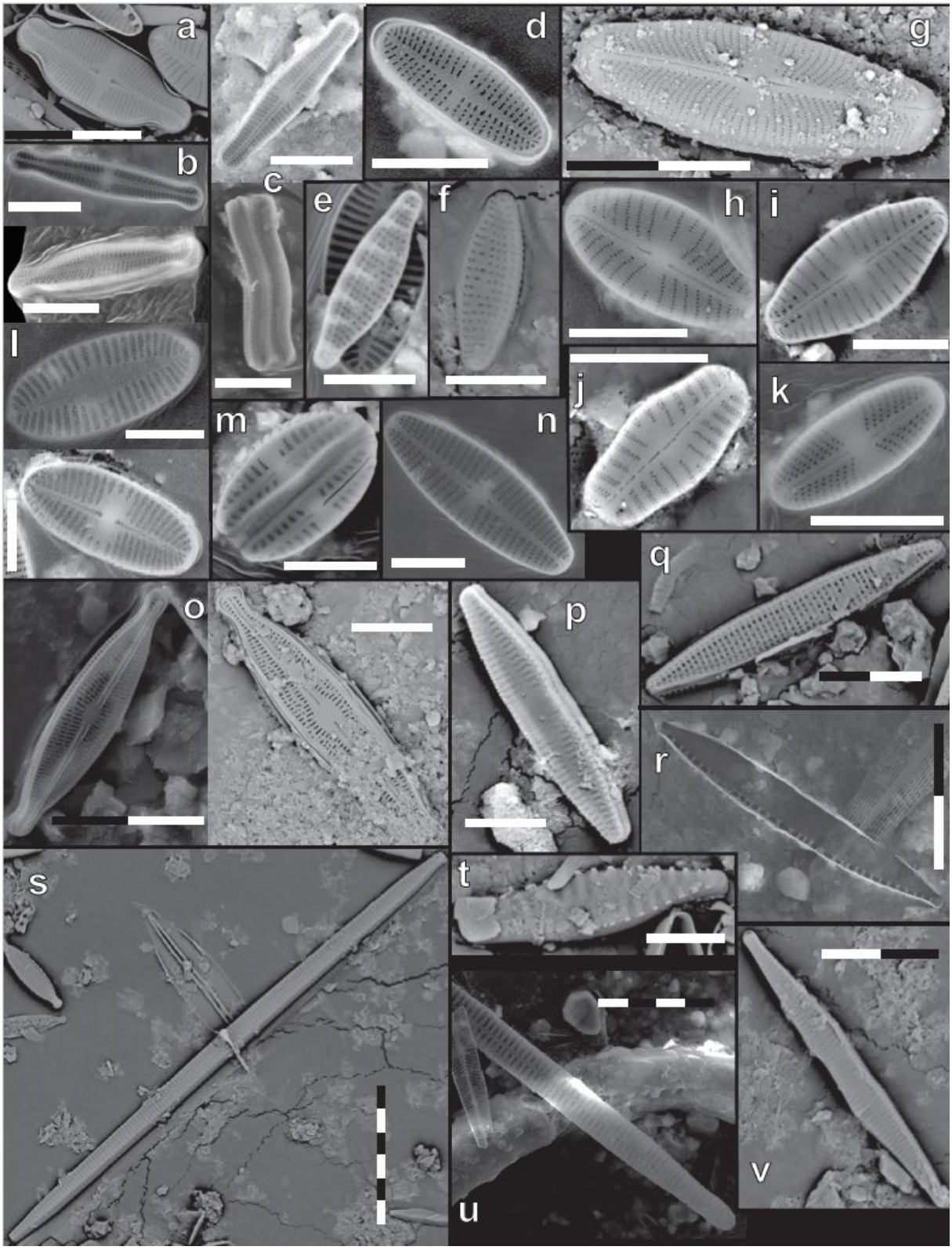
a
b
c
d
e
f
g
h
i
j
k
l
m
n
o
p
q
r
s
t
u
v

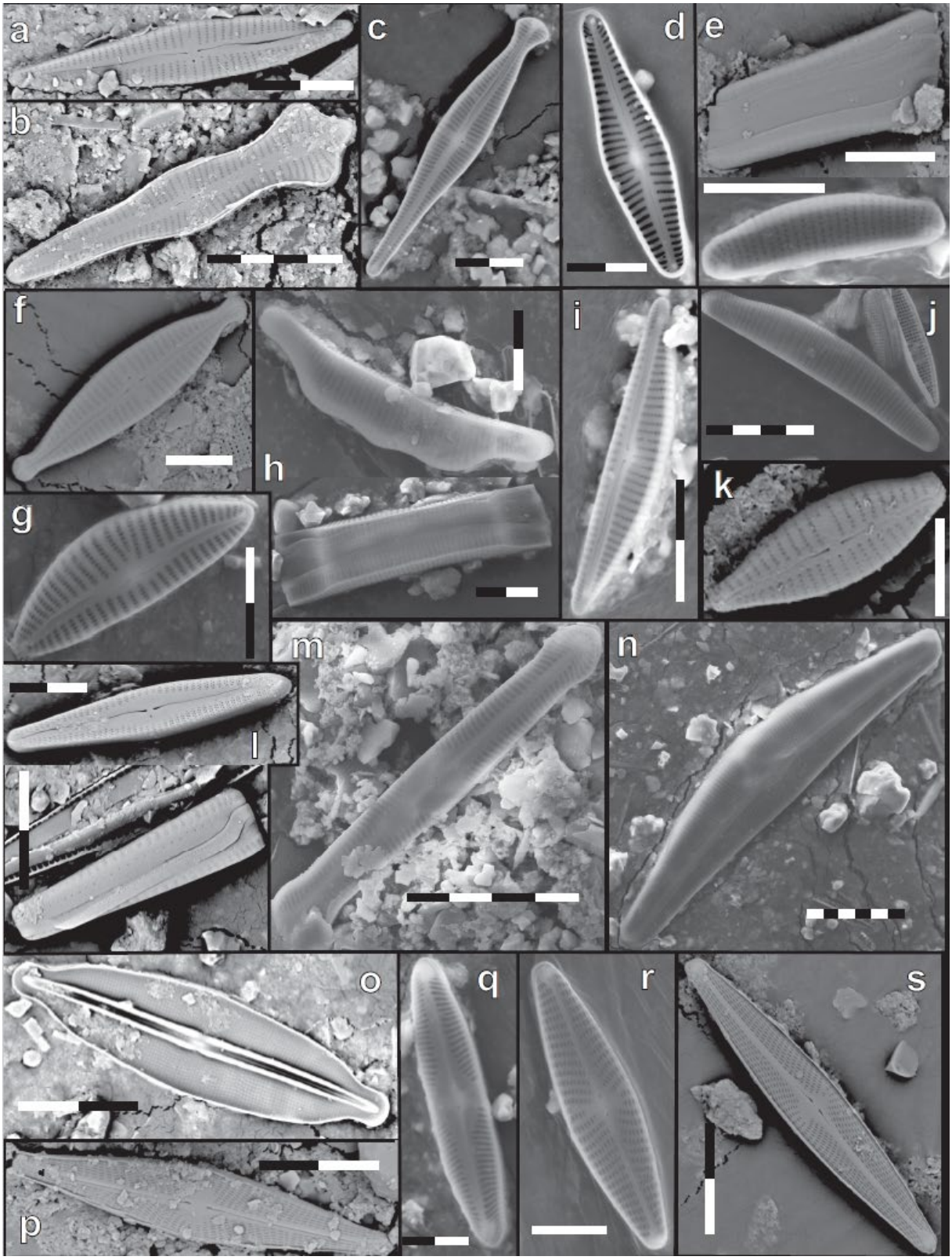
a
b
c
d
e
f
g
h
i
j
k
l
m
n
o
p
q
r
s

Figure 4 (previous page). SEM photographs of some of the most common diatoms found in the water bodies. Each black or white part of the scale bar is 5 μm. Identifications: (**a**) *Gomphonema gracile sl* Ehrenberg; (**b**) *Gomphonema acuminatum* Ehrenberg; (**c**) *Gomphonema pseudosphaerophorum* H.Kobayasi; (**d**) *Gomphonema* cf. *affine* Kützing; (**e**) *Eunotia rhomboidea* Hustedt (girdle and valve view); (**f**) *Gomphonema lagenula* Kützing; (**g**) *Cymbella affinis* Kützing; (**h**) *Eunotia pectinalis* var. *undulata* (Ralfs) Rabenhorst (valve and girdle view); (**i**) *Encyonema neogracile* Krammer; (**j**) *Eunotia* cf. *minor* (Kützing) Grunow; (**k**) *Gomphonema parvulum* (Kützing) Kützing; (**l**) *Gomphonema venusta* Passy, Kociolek & Lowe (valve and girdle view); (**m**) *Pinnularia gibba* (Ehrenberg) Ehrenberg; (**n**) *Cymbella aspera* (Ehrenberg) Cleve; (**o**) *Frustulia crassinervia* (Brébisson ex W.Smith) Lange-Bertalot & Krammer; (**p**) *Navicula* cf. *zanonii* Hustedt; (**q**) *Pinnularia divergens* W.Smith; (**r**) *Navicula cryptotenella* Lange-Bertalot; (**s**) *Navicula radiosa* Kützing.

2.4. RESULTS

2.4.1. Hydrochemical Results

Four water bodies (Umbutu and Nandimba Tchivinguiro, cold springs; Leba, river; and Cascatinha da Zootécnica, waterfall pool) were sampled, with Leba River sampled from two locations along the reach of the river (Figure 2). Located on the Humpata Plateau, all water bodies have relatively high elevation, ranging from Cascatinha da Zootécnica at 1670 m to Umbutu at 1806 m. Conductivity, TDS, and pH vary between Umbutu with the highest conductivity and TDS (1035 μS/cm and 520 ppm, respectively) and lowest pH (7.16) and Cascatinha da Zootécnica with the lowest conductivity and TDS (17 μS/cm and 8 ppm, respectively) and highest pH (8.26) (Table 1; Figure 5). Nearly all sites are of the HCO_3^- type with Umbutu of the Mg/Ca-HCO_3 type, Nandimba Tchivinguiro of the Mg-HCO_3 type, Leba 1 of the Ca/Mg-HCO_3 type, and Leba 2 of the Na/Ca-HCO_3/Cl type. Only Cascatinha da Zootécnica is not of the HCO_3^- type, instead being of the Na-Cl type. Alkalinity ranges from 1 mg/L at Cascatinha da Zootécnica to 147 mg/L at Nandimba Tchivinguiro. Of the cations, Na^+, K^+, Ca^{2+}, and Mg^{2+} all have a concentration greater than 1.00 mg/L in at least one locality (Table 1). Ca^{2+} and Mg^{2+} both have the greatest range, which reflects the dolomitic nature of the Leba Formation. Of the anions, HCO_3^- has the highest molar concentration across the sites except at Cascatinha da Zootécnica where Cl^- (the only other anion to have a concentration greater than 1.00 mg/L) is the dominant anion. NO_3^- and SO_4^{2-} concentrations, common indicators of agricultural and excremental waste pollution, range from 0.01 to 0.89 and 0.06 to 0.71 mg/L, respectively. PO_4^{3-}, a common limiting nutrient for aquatic phytoplankton, ranges across the localities from 0.01 to 0.20 mg/L.

2.4.2. Diatom Assemblage Results

Of the 91 diatom taxa identified, 44 taxa organized into 42 groups (four species, *Geissleria* sp. 1/*Sellaphora* cf. *atomoides* and *Sellaphora* cf. *saugerressi*/*Geissleria* sp. 2 are listed together as they were indistinguishable under the light microscope) are at least 2% abundant within a site's community (epilithic, epiphytic, epipelic, or episammic) (Table 2; Figures 3& 4). The most abundant species in each water body with an abundance of at least 10% in a community are:

- **Cascatinha da Zootécnica**, *Achnanthidium macrocephalum* (Hustedt) Round & Bukhtiyarova (all communities), *Encyonema neogracile* Krammer (epipelic), *Eunotia* cf. *minor* (Kützing) Grunow (epiphytic), *E. rhomboidea* Hustedt (epipelic and epiphytic), and *Navicula cryptocephala* Kützing (epilithic and epipelic)

  Nandimba Tchivinguiro, *Achnanthidium minutissimum* (Kützing) Czarnecki (epilithic and epiphytic), *Grunowia solgensis* (A. Cleve) Aboal (episammic), *Geissleria* sp. 1 and *Sellaphora* cf. *atomoides* (Grunow) Wetzel & Van de Vijver (episammic), *Navicula erifuga* (OF Müller) Bory (epilithic), *Nitzschia amphibia* Grunow (all communities), *N. frustulum* (Kützing) Grunow (episammic), and *Platessa hustedtii* (Krasske) Lange-Bertalot (epiphytic)

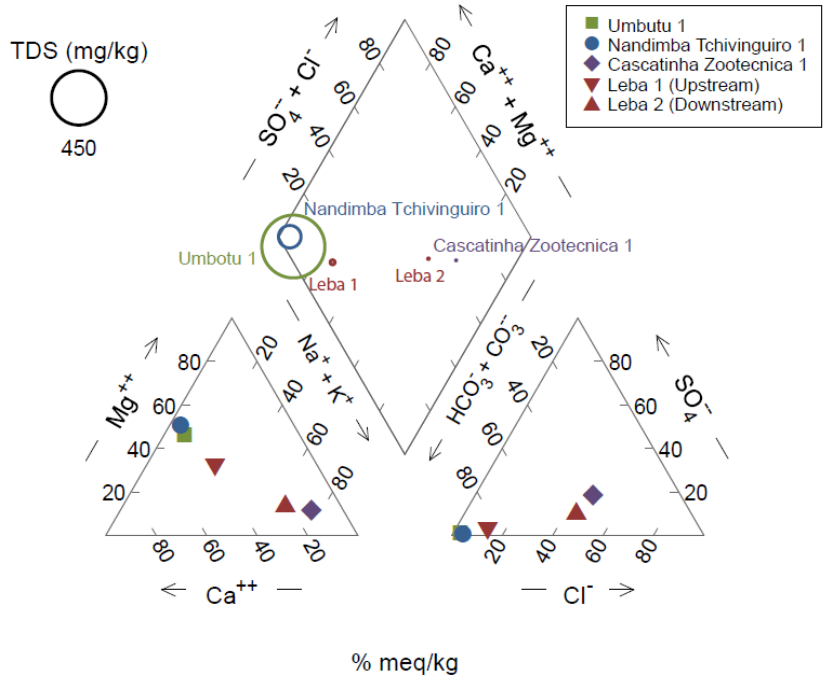

Figure 5 (previous page). Piper diagram of sites made using Geochemist Workbench with total dissolved solids (TDS) represented by the size of the circle in the diamond.

- **Umbutu**, *A. minutissimum* (all communities), *Gomphonema parvulum* (Kützing) Kützing (all communities), *Navicula cryptotenella* Lange-Bertalot (epilithic), and *Sellaphora pupula* (Kützing) Mereschkowsky (epipelic and epiphytic)
- **Leba 1**, *A. minutissimum* (all communities), *Navicula radiosa* Kützing (all communities), and *Ulnaria* cf. *biceps* (Kützing) Lange-Bertalot (epilithic)
- **Leba 2**, *A. macrocephalum* (epililthic, epipelic, and episammic)), *Ulnaria* cf. *contracta* (GS West) (epiphytic), *G. parvulum* (epilithic), and *Navicula* cf. *zanonii* Hustedt (all communities)

Taxa tend to be found in communities related to their life habits (i.e., *Eunotia* tend to be more present on epiphytic samples). It is uncommon for a species to be at least 10% abundant and not found, at least in trace amounts, in the other habitats. Therefore, to remove community bias based on each species' life habits, correspondence analysis was run on lumped communities for each water body rather than separately.

2.5. DISCUSSION

2.5.1. Hydrochemistry

Hydrochemistry is influenced by the source and chemistry of local precipitation, the residence time of water, local vegetation, anthropogenic pollution, and the lithological and hydrological properties of bedrock [40]. Given the proximity of the sites and similar historic annual rainfall records [24,25], differences in precipitation across the sites are likely minimal, meaning it is unlikely that precipitation is the main driver of local hydrochemistry. The residence time of the different water bodies is beyond the scope of this study and would require future sampling, although given the sedimentary nature of the bedrock and the high elevation, residence times are likely short. Because samples were collected during the dry season, local variation in vegetation is limited. Seasonally reduced vegetation and low fertility of local soils (which hinder deep root systems) likely lessen the impact macrophytes have on localized, seasonal fluctuations in water chemistry (such as pH) during the dry season. Therefore, vegetation is anticipated to have a minimal impact on hydrochemistry. To understand pollution, one can focus on high levels of SO_4^{2-} unrelated to lithological chemistry (typically from gypsum), as well as on other measured potential pollutants such as NO_3^-. If local pollution drives hydrochemistry,

we anticipate that sites closer to Lubango, the second most populous city in Angola [44], would cluster together in Figure 5 and have higher concentrations of NO_3^- and SO_4^{2-}, following the assumption that locations with higher populations have higher potential for pollution. Cascatinha da Zootécnica has the largest population, followed by Umbutu and Leba 1 [44]. Livestock can also increase pollution, given the assumption that larger livestock populations have higher pollution potential. Umbutu has the largest population of ruminants per area [45]. Therefore, if Cascatinha da Zootécnica, Umbutu, and Leba 1 plot together on the piper diagram, local pollution may be driving hydrochemistry. In contrast, bedrock would be a driver of hydrochemistry if Leba 1, Umbutu, and Nandimba Tchivinguiro cluster together in Figure 5, given their similar sedimentary bedrock. Cascatinha da Zootécnica, which is also located within the Chela Group but downstream of metaluminous granitoid bedrock, would plot separately. Leba 2 would plot between these clusters because it lies within the same Chela sedimentary group as Leba 1, Umbutu, and Nandimba Tchivinguiro, but is surrounded by mafic sills (Figure 1C).

Based on these predictions, it appears that bedrock has the largest impact on local hydrochemistry (Figure 5). Umbutu and Nandimba Tchivinguiro cluster closely, with Leba 1 nearby, due to similar percentages of HCO_3^-, Ca^{2+}, and Mg^{2+}. Umbutu and Nandimba Tchivinguiro also have large TDS compared to the other water bodies, which are at least an order of magnitude smaller (Table 1). Leba 2 and Cascatinha da Zootécnica plot further away with higher percentages of Cl^-, Na^+, and K^+. Umbutu, Leba 1, Leba 2, and Nandimba Tchivinguiro are all located within the Chela Group, either on the Cangalongue Formation of dolostones, siltstones, and Fe-rich sandstones, the Leba Formation of dolostones, or a combination of the two, given the uncertainty of local bedrock boundaries (Figure 1C,D). Input through the Leba and Cangalongue Formations likely leads to the high concentrations of HCO_3^-. In addition, both Nandimba Tchivinguiro and Umbutu are cold water springs. As waters move through the dolostones of the Leba Formation, high concentrations of HCO_3^-, Ca^{2+}, and Mg^{2+} as well as high conductivity and TDS are expected. In contrast, Leba 1 and 2 likely have a larger input from surface waters. Input from surface runoff or smaller tributaries between Leba 1 and 2 may contribute to their variation and explain why they do not have similar hydrochemistries despite being only 4.6 km apart (Figure 2). In addition, Leba 2′s bedrock is also interspersed with mafic sills and has higher amounts of Na^+ and K^+ compared to other sites within the

Chela Group. Igneous input could explain why Leba 2 lies closest to Cascatinha da Zootécnica, which is influenced by granitoid bedrock, in Figure 5. The high concentrations of Cl^-, Na^+, and K^+, compared to the other locations, could be due to more minerals such as hornblende, melilite, epidote, or biotite compared to the dolostone and siltstone bedrock of the other sites [46].

Although bedrock appears to be most influential on hydrochemistry, anthropogenic pollution may also have a minor influence. At rural locations with no factories, pollution from agriculture as well as excremental waste are more probable than industrial or urban pollutants. Contamination from waste can be evident through high conductivity and TDS as well as high levels of NO_3^- and PO_4^{3-} [1,3]. None of the sites has dangerous levels of NO_3^- or PO_4^{3-}. While some sites have high conductivity and TDS, it is difficult to distinguish between anthropogenic and bedrock input. Given local land-use, agricultural pollution input is likely, such as at Umbutu where local cattle were herded into the spring during sample collection. Umbutu has the highest PO_4^{3-} at 0.6 mg/L, meaning some of this input could be related to waste pollution. In addition, Nandimba Tchivinguiro and Leba 2 are next to agricultural fields where fertilizer and/or manure could be used to aid production, affecting hydrochemistry. Therefore, although waste pollution does not appear to be a problem hydrochemically (aquatic bacteria have not been investigated), it still likely has an impact on the local water bodies based on observations.

2.5.2. Diatoms as Indicators

Of the 44 most abundant taxa, none are taxa that typically prefer saline/brackish waters such as *Craticula*, *Mastogloia*, or *Anomoeoneis* [47]. *Achnanthidium* and *Navicula* are present across all water bodies. *Achnanthidium* is a cosmopolitan and adaptive genus, particularly *A. minutissimum*, which is one of the most frequently occurring freshwater benthic diatoms globally [48]. *Navicula s.l.*, which is represented by a different species in each water body, is a broad genus and occupies a wide range of hydrochemistries [49]. Cascatinha da Zootécnica is the only water body with a large percentage of *Eunotia*, which tend to live in the benthos of acidic, oligotrophic waters with low conductivity [49]. Nandimba Tchivinguiro has an abundance of small taxa, including varieties of *Achnanthidium*, *Geissleria*, *Sellaphora*, and small *Nitzschia* taxa, which tend to indicate highly oxygenated and meso- to eutrophic waters with moderate to high conductivities [49]. A lack of any

Stephanodiscus in the samples (although biased due to the lack of planktonic samples), but an abundance of *Nitzschia* with occasional *Ulnaria*, means that phosphorus is likely the limiting nutrient in these water bodies rather than silicon given the preferred ratios of phosphorus versus silicon for each genus [50,51]. This is also evidenced by the low amount of phosphate that was measured in the field (Table 1).

Assessing diatom assemblages with water chemistry data provides information about which variables control the composition of local assemblages, which can later be used to determine hydrochemistry and pollution based on collected diatoms. It is important to recognize, however, that diatom communities can represent conditions across multiple seasons whereas collected water chemistry data represent a very short time frame. While this does not make analysis impossible, this bias could be the cause of inconsistencies between diatom-inferred chemistry data and measured data. Previous studies show that conductivity, pH, and ionic composition tend to have the strongest correlations with diatom assemblages [12,13]. Unfortunately, besides conductivity, much of the diatom hydrochemical data are scarce. Therefore, exploratory correspondence analysis results will lead to future questions about interactions between diatom assemblages and hydrochemistry on the Humpata Plateau. These results show that conductivity and trophic level are best inferred by the diatom assemblages (those parameters have a large impact on the composition of the communities), although a lack of data or possible errors for the other parameters limit their interpretation.

Conductivity

Conductivity data for diatom taxa are often collected and reported from northern, eastern, and southern Africa [35,37], although statistically robust data are not always collected [12]. In general, water bodies with low conductivity, such as Cascatinha da Zootécnica, tend to have higher abundance of taxa that prefer low conductivity such as *Encyonema neogracile*, *Eunotia* cf. *minor*, and *Eunotia rhomboidea*, whereas water bodies with high conductivity, such as Nandimba Tchivinguiro, tend to have higher abundance of taxa that prefer moderate/high conductivity water such as *Grunowia solgensis*, *Navicula erifuga*, and *Nitzschia* cf. *frustulum* (Table 2). Figure 6 (which reflects the proportions of the groupings from S2 of the counted diatoms from each community) shows that all communities have a substantial proportion of diatoms located in the “low/medium” and/or “medium” conductivity categories. Water

bodies with lower conductivity, including Cascatinha da Zootécnica, Leba 1, and Leba 2, have substantial portions of their diatoms in the “low conductivity” category, with Leba 1′s spread also in the “low/medium” category and Cascatinha da Zootécnica’s and Leba 2′s spread more evenly split between “low”, “low/medium”, and “medium” (except for Cascatinha da Zootécnica’s epilithic community which is spread evenly across all groupings). Nandimba Tchivinguiro’s groupings reflect its higher conductivity with larger proportions of its diatoms in the “medium” and “medium/high conductivity” categories. Umbutu, despite having the highest measured conductivity, has diatoms spread evenly across all four groupings. Nonetheless, at Umbutu, the epipelic, and epiphytic communities have a larger proportion in the “medium/high” category compared to all sites with low conductivity (Cascatinha da Zootécnica, Leba 1, and Leba 2), except for Cascatinha da Zootécnica’s epilithic community (Figure 6). Correspondence analysis shows that Axis 1 is controlled by conductivity, with lower conductivities plotting negatively and higher conductivities plotting positively (Figure 7). While Umbutu does seem to be an outlier in this data, the diatom assemblages do appear to reliably decipher conductivity with Cascatinha da Zootécnica and Leba 2 plotting closest to the “low” grouping, Leba 1 closest to the “low/medium” grouping, and Nandimba Tchivinguiro closest to the “medium/high” grouping (Figure 7).

pH

Correspondence analysis shows diatom assemblages do not accurately infer pH, despite having the most available preference data besides conductivity. pH clusters show the largest proportion of all diatoms in the “medium” pH category, except for Nandimba Tchivinguiro where diatoms are mostly in the “medium/high” category, except for the episammic taxa which are spread across all categories (Figure 6). Given that the pH of the sites ranges from neutral at Umbutu to slightly alkaline at Cascatinha da Zootécnica and that the taxa observed are mostly circumneutral to slightly alkaliphilic in their preference, the large proportion in the “medium” pH group is not surprising. Cascatinha da Zootécnica evenly splits its diatoms between the “low,” “medium,” and “high” pH clusters despite having the highest measured pH. Nonetheless, Cascatinha da Zootécnica does have more diatoms in the “high” category compared to most other communities besides Nandimba Tchivinguiro episammic and Leba 2′s epilithic, epipelic, and episammic communities (Figure 6). Axis 1 of Figure 7 is not exclusively controlled by pH and has less predictive power

compared to Axis 1 in the conductivity biplot. The most obvious inconsistency is the placement of the “high” pH category between the “low” and “low/medium” groupings. This pattern makes sense given that both Cascatinha da Zootécnica and Leba 2 had larger proportions of taxa that prefer “high” pH in the balloon plot but confuses the interpretation of how pH might determine diatom assemblages. These results may be biased by the similar measured pH across the water bodies (Table 1) or by errors in reported pH preferences causing errors in the pH diatom groupings (S2). It is also larger proportions of taxa that prefer “high” pH in the balloon plot but confuses the interpretation of how pH might determine diatom assemblages. These results may be biased by the similar measured pH across the water bodies (Table 1) or by errors in reported pH preferences causing errors in the pH diatom groupings (S2). It is also possible that there could have been equipment failure at Cascatinha da Zootécnica in collecting the appropriate pH measurements, seeing as the rest of the sites plot near reasonable “medium” groups in the biplot (Figure 7).

Temperature

Despite sparse and sometimes unreliable data regarding how diatoms are impacted by temperature [12], diatom assemblages may weakly infer accurate relative water temperatures on the Humpata Plateau. Waters with lower temperatures (Cascatinha da Zootécnica 14.22 °C and Leba 2 17.80 °C) have the majority of their diatoms in the “low/medium” temperature category (Figure 6). The outlier of this trend is Leba 1 which, despite having a recorded temperature of 14.84 °C, has a balloon plot similar to the higher temperature sites (Nandimba Tchivinguiro 22.12 °C and Umbutu 22.18 °C), with the majority of taxa plotting in the “medium” temperature category (besides Nandimba Tchivinguiro epilithic which has its majority in the “medium/high” category). Nonetheless, the warmer waters of Nandimba Tchivinguiro and Umbutu have more taxa in the “medium/high” and “high” categories than the other water bodies showing that temperature may have some predictive power in determining the diatom assemblages (Figure 6). This is less clear on the biplot where the axes are controlled by other variables, given that neither Axis 1 nor Axis 2 align the temperature gradient correctly (Figure 7). Despite this, Nandimba Tchivinguiro and Umbutu plot closest together and Cascatinha da Zootécnica and Leba 2 cluster near the “low/medium” temperature grouping, reflecting the measured patterns (Figure 7). One complication with temperature data, however, is that temperature was only taken on one day at one time at each site even though

Figure 6. Balloon plots, which represent the percentage of the diatoms of each grouping based on the available data for each parameter, at each site divided by community. The organization for the groups is indicated in S2.

Figure 7. Correspondence analysis of the groupings for the different variables at each site. Chi-square values are only relevant for trophic level and pollution because the rest of the data are not purely categorical and/or were measured in the field. Chi-square values for trophic level and pollution are 2,356 and 346, respectively.

temperature of these sites likely changes throughout the day. Therefore, it is difficult to deduce how diatom assemblages and temperature may be related. These results indicate that diatom assemblages cannot infer temperature either due to data collection bias or that diatom assemblages are instead impacted by the influence of temperature on other variables such as ionic composition, pH, and conductivity as a physical parameter [12].

Alkalinity and Ionic Species

Alkalinity may be inferable using the diatom assemblages, although limited preference data hinder interpretations (S2). This is supported by the tails of the data which mimic the calculated trends, such as how Leba 2 and Cascatinha da

Zootécnica (besides Cascatinha da Zootécnica's epilithic community) with low alkalinity are mostly split between "low" to "medium" alkalinity clusters or how Nandimba Tchivinguiro, as the location with the highest alkalinity, has more diatoms in the "medium/high" category compared to nearly all other communities (Figure 6). In contrast, an overrepresentation of taxa that prefer "low/medium" and "medium" alkalinity complicate the ability to see if diatom assemblages can infer alkalinity. The lack of data is evident in the alkalinity biplot where neither Axis 1 nor Axis 2 represent alkalinity (Figure 7). Despite this, the sites are located near to other sites with similar alkalinity calculations, such as Cascatinha da Zootécnica and Leba 2 plotting together, although closest to the "medium" cluster. It is therefore difficult to say much about whether or not alkalinity can be inferred by the diatom communities.

The ionic species mirror the preferred alkalinity, as a measure of HCO_3^- in the system, of diatom taxa. Understanding the ionic data is complicated given the difficulty of organizing taxa with broad ionic preferences and the added complication that data include both optimal cations and anions. For example, while communities of the Ca- and/or Mg-HCO_3 type waters such as Nandimba Tchivinguiro epipelic, Umbutu epipelic and epiphytic, and Leba 1 epiphytic are the only water bodies with taxa in the Ca/Mg-HCO_3 grouping, the Na-HCO_3 grouping includes taxa from each community, which is reasonable considering each water body is either of the Na- or HCO_3-type (Figure 6). The inability to distinguish between the role of cations versus anions in diatom preference groupings therefore hinders interpretation of the correspondence analysis. Axis 1 of the biplot may relate to the presence of Cl^- in the water with the Na+Ca/Mg-HCO_3, Na-Cl and Na-HCO_3, Na-Cl groups plotting more positively on Axis 1 (Figure 7). Axis 2 appears to be related to the presence of Na^{2+} in the water, with the Ca/Mg-HCO_3 grouping plotting far more negatively than the others, although, the conflation of both anions and cations limits the ability to deduce patterns across these data (Figure 7).

Trophic Levels and Pollution

Understanding how assemblages might infer accurate trophic levels and pollution is extremely limited due to sparse preference data and no reference data collected in the field. Despite minimal preference data, trophic levels may be inferred by the diatom assemblages, with a Chi-square value of 2,356. Axis 1, which explains 87.9% of the data's variance, appears to be controlled by trophic level with negative

numbers corresponding to hyper- to eutrophic conditions and positive numbers corresponding to oligo- to mesotrophic conditions (Figure 7). Based on the biplot, Nandimba Tchivinguiro is hyper/eutrophic, Leba 2 is oligo/mesotrophic, and Leba 2, Cascatinha da Zootécnica, and Umbutu are all oligo to eutrophic (Figure 7). In contrast, the sampled water bodies do not cluster closely with pollution categories and have a Chi-Square value of 346, giving the appearance that diatom assemblages may be unable to infer pollution reliably. The biplot does appear to divide the pollution tolerance (although not directly along Axis 1 or 2) with the three groupings plotting in three distinct areas across the biplot (Figure 7). From this plot, we anticipate that Nandimba Tchivinguiro to be most polluted and Cascatinha da Zootécnica or Leba 2 to be least polluted (Figure 7). This may represent a bias in that water chemistry data is only a snapshot of the chemistry when the samples were collected, but that collected diatoms can represent multiple seasons and could have survived through varying degrees of pollution. One method to further explore this outcome includes using diatom indices for pollution and trophic levels [52]. While this could help interpret data, such indices, which are often created in Europe, they have mixed results in their effectiveness for African samples [53–55].

2.6. CONCLUSIONS

This research includes the first description of water chemistry and diatom communities on the Humpata Plateau in southwestern Angola. Water chemistry is most influenced by bedrock composition, although more research must be completed to determine the impact of other variables such as vegetation, residence time, and anthropogenic pollution. Diatom communities across the water bodies were documented and correspondence analysis was used to determine whether diatom communities can infer hydrochemical variables for future water-quality and paleoclimate studies. Diatoms appear to have predictive power for conductivity and trophic level, although sparse data on diatom chemistry preference limits understanding of their ability to infer pH, temperature, alkalinity, ionic species, and pollution.

Diatom counts may be used for diatom indices on pollution or trophic levels to learn more about how diatoms can benefit hydrochemical studies in this region. Such indices, however, are untested in the region (as well as throughout most of Africa) and would need to be explored further before any definitive conclusions can be

made. During the next field season during the wet season, more water and diatom samples will be collected as well as samples from surrounding sediments and bedrock to learn more about the chemistries of these surfaces. Work conducted during the wet season will determine whether these observed patterns are visible at other points during the year. The second field season will provide more insight into bedrock/water interactions, trophic levels, pollution, and evaporation/precipitation budget, particularly related to comparisons between the wet and dry seasons. $\delta^{18}O$ and $\delta^{2}H$ will be used to classify the local meteoric water line. The persistent research in this area will provide more clarity about how diatoms and hydrochemistry data can be used to better understand local waters and pollution to benefit the livelihoods of local communities.

2.7. REFERENCES

1. Lapworth, D.J.; Nkhuwa, D.C.W.; Okotto-Okotto, J.; Pedley, S.; Stuart, M.E.; Tijani, M.N.; Wright, J. Urban Groundwater Quality in Sub-Saharan Africa: Current Status and Implications for Water Security and Public Health. *Hydrogeol. J.* **2017**, *25*, 1093–1116, doi:10.1007/s10040-016-1516-6.

2. Paca, J.M.; Santos, F.M.; Pires, J.C.M.; Leitão, A.; Boaventura, R.A.R. Quality Assessment of Water Intended for Human Consumption from Kwanza, Dande and Bengo Rivers (Angola). *Environ. Pollut.* **2019**, *254*, 113037, doi:10.1016/j.envpol.2019.113037.

3. Silva, M.M.; Gomes, E.M.C.; Isaías, M.; Azevedo, J.M.M.; Zeferino. B. Spatial and Seasonal Variations of Surface and Groundwater Quality in a Fast-Growing City: Lubango, Angola. *Environ. Earth Sci.* **2017**, *76*, 1–17, doi:10.1007/s12665-017-7149-9.

4. WHO. *Guidelines for Drinking-Water Quality*, 4th edn. World Health Organization: Geneva, Switzerland, 2017.

5. Godfrey, S.; Obika, A. Improved Community Participation: Lessons from Water Supply Programmes in Angola. *Commun. Dev. J.* **2004***, 39*, 156–165, doi:10.1093/cdj/39.2.156.

6. Nicholson, S.E.; Funk, C.; Fink. A.H. Rainfall Over the African Continent from the 19th through the 21st Century. *Glob. Planet. Change* **2018**, *165*, 114–127, doi:10.1016/j.gloplacha.2017.12.014.

7. Gasse, F. Hydrological Changes in the African Tropics since the Last Glacial Maximum. *Quat. Sci. Rev.* **2000**, *19*, 189–211, doi:10.1016/S0277-3791(99)00061-X.

8. Battarbee, R.W.; Jones, V.J.; Flower, R.J.; Cameron, N.G.; Bennion, H.; Carvalho, L.; Juggins, S. Diatoms. In *Tracking Environmental Change Using Lake Sediments. Volume 3: Terrestrial, Algal, and Siliceous Indicators;* Smol, J.P., Birks, H.J.B., Last W.M., Eds.; Kluwer Academic Publishers: Dordrecht, The Netherlands, 2001.

9. Fritz, S.C.; Cumming, B.F.; Gasse, F.; Laird. K.R. Diatoms as indicators of hydrologic and climatic change in saline lakes. In *The Diatoms: Applications for the Environmental and Earth Sciences*; Stoermer, E.F., Smol, J.P. Eds.; Cambridge University Press: Cambridge, UK, 2010.

10. Cocquyt, C.; Ndjombo, E.L.; Tsamemba, S.T.; wa Malale, H.N.S. Freshwater Diatoms in the Democratic Republic of the Congo: A Historical Overview of the Research and Publications. *Phytokeys* **2019**, *136*, 107.

11. Birks, B.; Heiri, O.; Eppa, H.; Bjune, A.E. Strengths and Weaknesses of Quantitative Climate Reconstructions Based on Late-Quaternary Biological Proxies. *Quat. Int.* **2012**, DOI: 10.2174/1874213001003020068

12. Juggins, S. Quantitative Reconstructions in Palaeolimnology: New Paradigm Or Sick Science? *Quat. Sci. Rev.* **2013**, *64*, 20–32, doi:10.1016/j.quascirev.2012.12.014.

13. Gasse, F.; Juggins, S.; Khelifa, L.B. Diatom-Based Transfer Functions for Inferring Past Hydrochemical Characteristics of African Lakes. *Palaeogeogr. Palaeoclimatol. Palaeoecol.* **1995**, *117*, 31–54, doi:10.1016/0031-0182(94)00122-O.

14. Vanormelingen, P.; Verleyen, E.; Vyverman, W. The diversity and distribution of diatoms: From cosmopolitanism to narrow endemism. *Biodivers. Conserv.* **2008**, *17*, 393–405, doi:10.1007/s10531-007-9257-4.

15. Soininen, J.; Teittinen, A. Fifteen important questions in the spatial ecology of diatoms. *Freshw. Biol.* **2019**, *64*, 2071–2083, doi:10.1111/fwb.13384.

16. Huntley, B.J.; Russo, V.; Lages, F.; Ferrand, N. *Biodiversity of Angola*; Springer Cham: Basel, Switzerland, 2019, doi:10.1007/978-3-030-03083-4.

17. Lopes, F.C.; Pereira, A.J.; Mantas, V.M.; Mpengo, H.K. Morphostructural Characterization of the Western Edge of the Huila Plateau (SW Angola), Based on Remote Sensing Techniques." *J. Afr. Earth Sci.* **2016**, *117*, 114–123, doi:10.1016/j.jafrearsci.2016.01.007.

18. Lopes, F.C.; Ramos, A.M.; Gomes, C.R.; Ussombo, C.C. The Geoheritage of Lubango-Tundavala Road Traverse in the Serra Da Leba (SW Angola): Outcrops Characterization and Numerical Assessment for Outdoor Educational Activities and Geoconservation Purpose. *J. Afr. Earth Sci.* **2019**, *157*, 103510, doi:10.1016/j.jafrearsci.2019.05.018.

19. Correia, H. Sobre a existência de rochas vulcanoclásticas na Formação da Chela (Região do Planalto da Humpata). *Ciênc. Geol*. **1973**, *1*, 27–32.

20. Correia, H. O Grupo da Chela e Formação da Leba como novas unidades litoestratigráficas resultantes da redefinição da Formação da Chela na região do Planalto da Humpata (Sudoeste de Angola). *Bol. Soc. Geol.* **1976**, *20*, 65–130.

21. Pereira, E.; Tassinari, C.C.G.; Rodrigues, J.F.; Van-Dúnem, M.V. New data on the deposition age of the volcano-sedimentary Chela Group and its Eburnean basement: Implications to post-Eburnean crustal evolution of the SW of Angola. *Comun. Geol.* **2011**, *98*, 29–40.

22. de Matos, D.; Martin, A.C.; Senna-Martinez, J.C.; Pinto, I.; Coelho, A.G.; Ferreira, S.S.; Oosterbeek. L. Review of Archaeological Research in Angola. *Afr. Archaeol. Rev.* **2021**, doi:10.1007/s10437-020-09420-8.

23. Pombo, S.; de Oliveira, R.P. Evaluation of Extreme Precipitation Estimates from TRMM in Angola. *J. Hydrol.* **2015**, *523*, 663–679, doi:10.1016/j.jhydrol.2015.02.014.

24. SASSCAL WeatherNet-Monthly Values. Available online: www.sasscalweathernet.org/weatherstat_monthly_AO_we.php (accessed on 10 October 2020).

25. CCKP. 2021. Climate change knowledge portal. Available online: https://climateknowledgeportal.worldbank.org/download-data (accessed on 14 April 2021).

26. Tyson, P.D.; Preston-Whyte, R.A. *The Weather and Climate of Southern Africa*; Oxford University Press Southern Africa: Cape Town, South Africa, 2000.

27. Tyson, P.D. *Climatic Change and Variability in Southern Africa*; Oxford University Press: Cape Town, South Africa, 1986.

28. Chase, B.M.; Niedermeyer, E.M.; Boom, A.; Carr, A.S.; Chevalier, M.; He, F.; Meadows, M.E.; Ogle, N.; Reimer, P.J. Orbital Controls on Namib Desert Hydroclimate Over the Past 50,000 Years. *Geology* **2019**, *47*, 867–871, doi:10.1130/G46334.1.

29. Meissner, R. Interaction and existing constraints in international river Basins. In *International Waters in Southern Africa*; Mikiyasu Nakayama, Ed.; United Nations University Press: Tokyo, Japan, 2003; pp. 249–273.

30. Heyns, P. Water Resource Management in Southern Africa. In *International Waters in Southern Africa*; Mikiyasu Nakayama, Ed.; United Nations University Press: Tokyo, Japan, 2003, pp. 5–37.

31. Lindenmaier, F.; Miller, R.; Fenner, J.; Christelis, G.; Dill, H.G.; Himmelsbach, T.; Kaufhold, S.; Lohe, C.; Quinger, M.; Schildknecht, F.; et al. Structure and Genesis of the Cubango Megafan in Northern Namibia: Implications for its Hydrogeology. *Hydrogeol. J.* **2014**, *22*, 1307–1328, doi:10.1007/s10040-014-1141-1.

32. Wellington, J.H. The Kunene River and the Etosha Plain. *South. Afr. Geogr. J.* **1938**, *20*, 21–32, doi:10.1080/03736245.1938.105591186.

33. Kelly, M.G.; Adams, C.; Graves, A.C.; Jamieson, J.; Krokowski, J.; Lycett, E.B.; Murray-Bligh, J.; Prichard, S.; Wilkins, C. *The Trophic Diatom Index: A User's Manual*; Environmental Agency: Bristol, UK, 2001.

34. Battarbee, R.W. Diatom Analysis. In *Handbook of Holocene Palaeoecology & Palaeohydrology*, Berglund, B.E., Ed.; The Blackburn Press: Caldwell, NJ, USA, 1986, 527–570.

35. Gasse, F. East African Diatoms: Taxonomy, Ecological Distribution. *Bibl. Diatomol.* **1986**, *11*, 201.

36. Cocquyt, C. Diatoms from the Northern Basin of Lake Tanganyika. *Bibl. Diatomol.* **1998**, *39*, 1–274.

37. Taylor, J.C.; Harding, W.R.; Archibald, C.G.M. *An. Illustrated Guide to Some Common Diatom Species from South. Africa*. Water Research Commission: Pretoria, South Africa, 2007.

38. Spaulding, S.A.; Bishop, I.W.; Edlund, M.B.; Lee, S.; Furey, P.; Jovanovska, E.; Potapova, M. *Diatoms of North. America*. https://diatoms.org/species. (first accessed on 26 August 2019)

39. Eby, G. Chapter 6: Carbon Chemistry. In *Principles of Environmental Geochemistry*; Waveland Press, Inc., Long Grove, Illinois USA 2016; pp. 129–161.

40. Bartos, T.T.; Ogle. K.M. Water Quality and Environmental Isotopic Analyses of Ground-Water Samples Collected from the Wasatch and Fort Union Formations in Areas of Coalbed Methane Development—Implications to Recharge and Ground-Water Flow, Eastern Powder River Basin, Wyoming. Available online: https://pubs.usgs.gov/wri/wri024045/htms/report2.htm (accessed on 10 December 2020).

41. Benzecri, J.-P. *Correspondence Analysis Handbook*; Marcel Dekker Inc: New York, NY, USA, 1992.

42. Kassambara, A. 2017. *Practical Guide to Principal Component Methods in R*. Available online: http://www.sthda.com/english/articles/31-principal-component-methods-in-r-practical-guide/ (first accessed on 15 February 2021).

43. Sonneman, J.A.; Sincock, A.; Fluin, J.; Reid, M.; Newall, P.; Tibby, J.; Gell, P. *An. Illustrated Guide to Common Stream Diatom Species from Temperate Australia*. Cooperative Research Centre for Freshwater Ecology Identification Guide No 33, Adalaide University: Adalaide, Australia, 2000.

44. WorldPop. 2018. (www.worldpop.org-School of Geography and Environmental Science, University of Southampton; Department of Geography and Geosciences, University of Louisville; Departement de Geographie, Universite de Namur) and Center for International Earth Science Information Network (CIESIN), Columbia University. Global High Resolution Population Denominators Project-Funded by The Bill and Melinda Gates Foundation (OPP1134076). Available online: https://dx.doi.org/10.5258/SOTON/WP00660, (accessed on 16 March 2021).

45. Conchedda, G.; Cinardi, G.; Steinfeld. H. 2015. Africa Ruminants Tropical Livestock Units (TLU). Available online: http://www.fao.org/geonetwork/srv/en/metadata.show?id=52752&currTab=simple (accessed on 16 March 2021).

46. USGS. Metaluminous Granite. Available online: https://mrdata.usgs.gov/catalog/term-simple.php?term=4.4.2.2&thcode=4 (accessed on 16 December 2020).

47. Owen, R.B.; Potts, R.; Behrensmeyer, A.K.; Ditchfield. P. Diatomaceous Sediments and Environmental Change in the Pleistocene Olorgesailie Formation, Southern Kenya Rift Valley. *Palaeogeogr. Palaeoclimatol. Palaeoecol.* **2008**, *269*, 17–37, doi:10.1016/j.palaeo.2008.06.021.

48. Potapova, M.; Hamilton, P.B. Morphological and Ecological Variation within the Achnanthidium Minutissimum (Bacillariophyceae) Species Complex. *J. Phycol.* **2007**, *43*, 561–575, doi:10.1111/j.1529-8817.2007.00332.x.

49. Taylor, J.C.; Cocquyt, C. Diatoms from the Congo and Zambezi Basins – Methodologies and Identification of the Genera. *Afr. J. Aquat. Sci.* **2019**, doi:10.2989/16085914.2019.1628702.

50. Kilham, P.; Kilham, S.S.; Hecky, R.E. Hypothesized Resource Relationships among African Planktonic Diatoms. *Limnol. Oceanogr.* **1986**, *31*, 1169–1181, doi:10.4319/lo.1986.31.6.1169.

51. Descy, J.-P.; Sarmento, H. Microorganisms of the East African Great Lakes and their Response to Environmental Changes. *Freshw. Rev.* **2008**, *1*, 59–73, doi:10.1608/FRJ-1.1.4.

52. Abassi, T.; Abassi, S.A. *Water Quality Indices*; Elsevier: Amsterdam, The Netherlands, 2012.

53. Bellinger, B.J.; Cocquyt, C.; O'Reilly, C.M. Benthic Diatoms as Indicators of Eutrophication in Tropical Streams. *Hydrobiologia* **2006**, *573*, 75–87, doi:10.1007/s10750-006-0262-5.

54. Taylor, J.C.; van Vuuren, M.S. J.; Pieterse, A.J.H. The Application and Testing of Diatom-Based Indices in the Vaal and Wilge Rivers, South Africa. *Water, S.A.* **2007**, *33*, doi:10.4314/wsa.v33i1.47871.

55. Dalu, T.; Bere, T.; Froneman, P.W. Assessment of Water Quality Based on Diatom Indices in a Small Temperate River System, Kowie River, South Africa. *Water, S.A*. **2016**, *42*, 183, doi:10.4314/wsa.v42i2.02.

2.8. SUPPLEMENTAL DATA

S1: Supplementary Diatom Plates for identification of taxa.

S2: Tab1: Raw diatom count across the water bodies including the number of phytoliths and Lycopodium spores. **Tab2:** Diatom ecological groupings based on Gasse (1986), Gasse et al. (1995), Sonneman et al. (2000), Taylor et al. (2007a), and Spaulding et al. (2020).

CHAPTER 3: Hydroclimate Cycles over 35,000 years as Lake Nakuru, Kenya[2]

3.1. INTRODUCTION

Over several decades, scientists have attempted to understand how the tropics respond to changes in global climate and the hydrological cycle. These studies indicate that the African Humid Period (AHP; 15-5 ka) was the result of precessional forcing (Kutzbach & Street-Perrott, 1985; Garcin et al., 2009; Foerster et al., 2012; Junginger & Trauth, 2013; Junginger et al., 2014), but the controls on other climatological changes through the Pleistocene are not as well understood (Singarayer & Burrough, 2015; Lupien et al., 2022). Knowledge during the Last Glacial Maximum (LGM; 26.5-19 ka) and the lead up to the AHP are far more limited, although records show that globally the LGM was dry (Barker et al, 2004; Gasse, 2000; Gasse, 2008). While decreased insolation resulting in decreased latitudinal location in the mean annual position of the ITCZ (Kutzbach & Street-Perrott, 1985; Braconnot et al., 2008) and expansion of the Northern Hemisphere continental ice sheet (Arbuszewski et al., 2013; Broecker & Putname, 2013) would reduce Eastern African rainfall, these mechanisms cannot accommodate southeastern African LGM records (Tierney et al., 2008; Stager et al., 2011; Truc et al., 2013). Low amplitude precessional variability of the LGM decreases insolation's control on Eastern African climate resulting in other forcing mechanisms increasing in importance (Tjallingii et al., 2008; Kuechler et al., 2013; Singarayer & Burrough, 2015). Controls like SST of the Indian Ocean (Tierney et al., 2008), Walker Circulation weakening the El Niño Southern Oscillation (ENSO) system (Tian & Jiang, 2020), or a reduction of meltwater suppressing Atlantic Meridional Overturning Circulation (such as during a Heinrich event) (Otto-Bliesner et al., 2014) have been proposed as controls to reduce rainfall in Eastern Africa, but limited Eastern African records muffle clarity on

[2] This work is currently *in prep.* ROBAKIEWICZ, E.; BERGNER, A.; ROSCA, C.; KÜBLER, S.; SCHÖTTLE, V.; MINGRAM, J.; TRAUTH, M.H.; & JUNGINGER, A., *in prep*, Hydroclimate Cycles over 35,000 years as Lake Nakuru, Kenya: *Quaternary Science Reviews.*

the LGM's impact on the Eastern African tropics. Ultimately to understand how African hydroclimate responded to changes across the last glacial period equatorial records across this time period are vital.

As a closed basin at one of the highest points of East African Rift System (EARS) only 40 km south of the Equator, Lake Nakuru is a valuable site to study past rainfall patterns across the EARS. As a lake with one of the highest primary productivity rates in the world (Livingstone & Melack, 1984; Vareschi & Jacobs, 1985; Ballot et al., 2004), Lake Nakuru has been the focus of many studies related to Late Pleistocene paleolimnological and paleoclimatological change (Leakey, 1931; Nilsson, 1931; Nilsson, 1940; Gregory, 1968; Washbourn-Kamau, 1971; Butzer et al., 1972; Cohen et al., 1983; Hastenrath & Kutzbach, 1983; Cohen & Nielsen, 1986; Dühnforth et al., 2006). Early observations of paleoshorelines, lake deposits, and modern decadal-scale lake level changes (Nilsson, 1931; Flint, 1959a; McCall, 1967) indicated that as a closed basin with flat basin floor morphology and steep slopes, Lake Nakuru responds sensitively to changes in precipitation (Nilsson, 1931; Flint, 1959b; Trauth et al. 2010; Olaka et al., 2010). The Nakuru record was instrumental in understanding African climate change through time based on Leakey's (1931) and Nilsson's (1931) glacial "Great Pluvial" or "Gamblian" hypothesis which dominated paleoanthropological and archaeological interpretations for decades (e.g., Leakey et al. ,1943; Leakey, 1950; Cole, 1963; Robson, 1967) but has since been discredited as summarized by Kingston & Hill (2005). Given the vast abundance of archaeological material in the region observed from the first European explorations (Gregory, 1921), an interest in the relationship between past climates and hominin evolution and archaeology drove and continues to drive research across the EARS (Ambrose, 1984; Ambrose & Sikes, 1991; deMenocal, 1995; Potts, 1998; Maslin & Trauth, 2009; Trauth et al., 2010; Griffith, 2020; Foerster et al., 2022).

As understanding of the record progressed, "Gamblian" stratigraphic correlation became outdated (Flint, 1959a) as scientists were better able to calculate elevation

and absolute dates of paleoshorelines, gaining an understanding of past lake levels at Lake Nakuru and other soda lakes across the EARS (Washbourn-Kamau, 1971; Butzer et al., 1972). The near universal wet AHP in the central and northern part of the EARS became apparent through shoreline data that indicated a peak in lake levels ~11 ka[3] (Washbourn-Kamau, 1971; Butzer et al., 1972). Micropaleontological evidence (including ostracods and diatoms) from cores taken in 1969 from Lakes Nakuru, Elmenteita, and Naivasha indicated a potential peak in lake levels >24 ka, low lake levels until ~15.5 ka, and a huge increase in lake levels ~11.5 ka (Fig. 1) (Cohen et al., 1983; Cohen & Nielsen, 1986; Richardson & Dussinger, 1986). The calculated lake levels from paleoshorelines indicated that Paleolake Nakuru, which had been 180 m higher than present day (Washbourn-Kamau, 1971; Dühnforth et al., 2006), responded to precipitation change of ~65% during the ~11.5 ka highstand based on Butzer et al.'s (1972) and Richardson & Richardson's (1972) estimations. Additional paleoprecipitation models indicated Lake Nakuru's sensitivity to increased moisture, with estimations greater than the Naivasha Basin only ~60 km away: ~35% or 300 mm more per year over the Nakuru-Elmenteita basin, but ~15% over Naivasha (Hastenrath & Kutzbach, 1983); ~45% over Nakuru but 20 to 25% over Naivasha (Bergner et al., 2003; Dühnforth et al., 2006); although further, unpublished studies have indicated that modified parameters may bring both basins to ~23% increase (Kniess, 2006; Junginger & Trauth, 2013). Despite decades of studies, changes at Lake Nakuru before the AHP are unclear, requiring further evaluation to understand how local environments change in response to global climate.

While Lake Nakuru has been studied as a data point for the AHP, its climate record is valuable to understand more about climate mechanisms, change, and variability across the last glacial, including the LGM. In this study, new findings from ~11.5 m of 17-m cores taken by the Lake Naivasha Coring Project (LNCP) in 2004

[3] All ages from studies before 1998 in this paper are calibrated using the RCarbon package in R (Crema & Bevan, 2021) with INTCAL20 (Reimer et al., 2020).

highlight variability in Eastern African hydroclimate before the AHP (Fig. 2). Using a multi-proxy record from lithological, micropaleontological, and geochemical data, this paper presents high-resolution lake depth and hydroclimatic change from the past 35 kyr at Lake Nakuru. With such high-resolution data, we aim to answer: **(1)** how variable is the chemistry, depth, and rate of change of Lake Nakuru at the end of the Pleistocene? and **(2)** which aspects of global climate is Lake Nakuru responding to over the past 35 ka? Through a review of other Eastern African lake records, we aim to better understand hydroclimate variability from ~35 ka until the AHP. By better understanding Lake Nakuru's changing depth and productivity over the last 35 kyr, we provide an important overview into environmental changes and cycles across Late Pleistocene-Holocene climatological phases.

3.2. GEOLOGICAL AND CLIMATOLOGICAL SETTING

3.2.1. Geological Setting

Lake Nakuru (00°22'S, 36°05'E) is located at the highest part of the Gregory Rift, the Eastern Branch of the EARS, at about 1,760 m above sea level in the northwestern corner of the Nakuru-Elmenteita basin (Fig. 3). The EARS began warping in the Miocene, although the Nakuru-Elmenteita basin was not impacted by faulting activity until ~7 Ma, with activity increasing across the Pliocene and into the Pleistocene (McCall, 1967; Baker & Wohlenberg, 1971; Strecker et al., 1990; Kanda, 2010). By the mid-Pleistocene, Menengai, Lake Nakuru's closest volcano, had formed, creating the basin's northern boundary and separating it from the Baringo-Bogoria basin (McCall, 1967; Leat, 1984). Eburru, a dissected volcanic massif, separates the Nakuru-Elmenteita basin from the Naivasha basin in the south (McCall, 1967). The Nakuru-Elmenteita basin lies between Kinangop-Bahati platform to the east and the Mau Escarpment to the west (McCall, 1967). The study site lies below a late Pleistocene trachytic hill called Sirrkon Hill (Fig. 3). The volcanic material of the Nakuru-Elmenteita Basin consists of peralkaline or metaluminous trachyte or sodium- and carbonate-rich pantellerite which, in addition to semi-arid

conditions, leads to the alkaline nature of modern-day Lake Nakuru (Table 1; Baker & Wohlenberg, 1971; Leat, 1984). Exposed rocks in the basin consist of either volcanics (including lavas, ashes, tuffs, and pumices) or sediments (including alluvial/colluvial sands and silts; diatomites and diatomaceous silts; and pebble beds) (Conti et al., 2021), highlighting previous phases in which the basin was far wetter. Given the high elevation of Lake Nakuru which limits outside input into the basin, local geology has an incredibly strong control on the hydrochemistry of the lake.

3.2.2. Climatological Setting

Lake Nakuru has a closed drainage system that covers 1,800 km^2 with no surface outflow, meaning that outflow is mostly controlled by evaporation and subsurface seepage (McCall, 1967; Milbrink, 1977; Odada et al., 2006; Jirsa et al., 2013). As a closed system, the water budget is controlled almost exclusively by local climate, with inflow controlled by precipitation and local ephemeral rivers (Odada et al., 2006; Kimaru et al., 2019). In contrast to other lakes within the EARS, Lake Nakuru does not have modern groundwater inflow from hot springs through local faults (Odada et al., 2006; Jirsa et al., 2013). With most of the inflow and outflow controlled by the ratio between precipitation and evaporation, Nakuru is an amplifier lake – a lake that responds sensitively to small changes in climate (Olaka et al., 2010). This is evident over the past 100 years of recorded lake levels which show high variability that includes a fall from the 1920s to 1950s, a rise between 1961-1962, a fall from 1973-1974, a fall from 1993-1997 (Washbourn-Kamau, 1971; Odada et al., 2006; Kimaru et al., 2019), and current increased intensity in flooding (2009-2020) likely linked to modern anthropogenic climate (Fig. 4; RCMRD, 2021).

The amount of rainfall in Equatorial Eastern Africa is a result of a climatologically complex system with major convergence zones, oceans, and rifts that create complicated weather patterns through time (Nicholson, 1996). Important zones of convergence controlled by insolation include the Intertropical Convergence Zone

(ITCZ; which influences the location of the wet tropical rainbelt) and the Congo Air Boundary (CAB) which draw in moisture. While the CAB does not heavily influence rainfall in the Nakuru-Elmenteita basin today, changing solar insolation on a scale of thousands of years has resulted in the CAB's north-eastward expansion (Junginger et al., 2014). Sea surface temperatures (SST) contribute a strong control over moisture conditions in Equatorial Eastern Africa as well (Nicholson, 2017; Hirons & Turner, 2018). During positive Indian Ocean Dipole years, SST warm in the western Indian Ocean and cool in the eastern Indian Ocean, weakening Walker Circulation and increasing Eastern African rainfall (Marchant et al., 2007; Hirons & Turner, 2018; Lüdecke et al., 2021). SST in the Pacific Ocean impact Eastern African rainfall through ENSO where warm SST in the eastern Pacific and cool SST in the western Pacific yield heavier rainfall over Eastern Africa, particularly during the short rains (Nicholson, 1996; Ntale & Gan, 2004; Nicholson, 2017). SST also impact the strength of the West African and Indian monsoons, which create dry conditions over Eastern Africa in-season, but wetter conditions off-season (Nicholson, 1996; Nicholson, 2017). Lastly, topography across the EARS causes local variation in rainfall as local highlands can block moist airflow (Nicholson, 1996). Beyond these factors, variability may also be dependent on North Atlantic Oscillation, Atlantic Multidecadal Oscillation, and volcanic activity, although these factors are less important or less understood (Lüdecke et al., 2021).

Today, Lake Nakuru lies in a semi-arid environment where annual rainfall varies between 700 and 900 mm/year, with annual evaporation ~1,800 mm/year (Odada et al., 2006; Jirsa et al., 2013). The lake receives rainfall over two rainy seasons – the long rains from April to August and the short rains from October to November (Nicholson, 2017). Currently, the surface area of Lake Nakuru varies between 36 and 65 km^2, with an average depth between 0.5 and 3.5 m (Jirsa et al., 2013; RCMRD, 2021). Because of its shallow depth, Lake Nakuru is only temporarily thermally stratified in the middle of the day, with winds mixing the lake in the afternoon,

resulting in high primary productivity and the largest population of lesser flamingos in the world (Vareschi & Jacobs, 1985). As a result of local peralkaline trachytes and high evaporation, the lake is highly alkaline and saline of the Na-HCO_3-type (Table 1).

3.3. MATERIAL AND METHODS

3.3.1. Core Collection and Composite

Cores NAK-X and NAK-Y were collected by the LNCP in 2004 ~15 m apart in overlapping sections with a Usinger Coring System. The coring site is located on the eastern shore of Lake Nakuru in Kenya (-0.345925, 36.115342; Fig. 3) and was above water during collection. Sixteen meters were collected for NAK-X and 17 m for NAK-Y, although this study focuses on a ~11.5 m composite section (NAK) representing the first ~7 m of NAK-X and the overlapping 10.5 m of ~NAK-Y. The cores were transported to and split at the Geoforschungszentrum Potsdam (GFZ) in Germany and are currently located at Eberhard Karls Universität Tübingen. The NAK core composite was created using LacCore CoreWall programs based on original photographs, X-Ray Fluorescence (XRF) data, magnetic susceptibility (MagSus), and recent core photo scans. Data was then spliced and converted into the composite using CoreWall and Feldman.

3.3.2. Chronology

Organic samples, including paleoroots and charcoal, were collected from NAK-Y and NAK-X for radiocarbon dating and tephra samples for $^{40}Ar/^{39}Ar$ dating (Table 2). Radiocarbon samples were prepared through wet sieving with distilled water. The >250-µm fraction was then screened for charcoal which was picked and sent to Beta analytics, Kiel, and ETH Zürich dating laboratories. Tephra samples were sent to the Berkeley Geochronology Center for $^{40}Ar/^{39}Ar$ dating. A total of eight radiocarbon ages and two $^{40}Ar/^{39}Ar$ ages have been successful, although only one of the tephras was not reworked.

A Bayesian age model was created using the BACON package in R (Blaauw & Christen, 2011). Hiatuses were included in areas with visible pedogenesis (3.44 and 6.13 m) and at the large gap at 7.78 m. Slumps were used in areas with thick *in-situ* tephras (2.88-2.90 and 5.07-5.16 m) which are deposited rapidly and do not represent the usual deposition rate (Lowe, 2011). Reworked tephras were not considered slumps as their deposition reflects normal depositional rates. The inputted, non-calibrated ages are listed in Table 2.

3.3.3. Geochemical Analyses

Magnetic Susceptibility

MagSus was measured for NAK-X and NAK-Y using an automatic Bartington® point sensor with 1 mm point separation and 4 mm spatial resolution at the GFZ. Only 10 m of NAK-X and 9 m of NAK-Y were measured, as metal liners were used beginning at NAK-X8 and NAK-Y7. MagSus data is included in Suppl. 1. MagSus data was smoothed using a Triangular Moving Average (filter=10) using the Zoo Package (Zeileis & Grothendieck, 2005) and plotted using the Rioja Package (Juggins, 2022) in R.

X-Ray Fluorescence

µ-XRF scanning was performed at the Max-Planck Institute for Chemistry in Mainz in 2021. The cores were scanned with a nondestructive µ-XRF scanner from Avaatech using a rhodium tube and protocol from Richter et al. (2006). Elements were scanned along 1-mm intervals at 10 kV for Mg, Al, Si, P, S, Cl, Ar, K, Ca, Ti, V, Cr, Mn, Fe, Co, Ni, Cu, Ba, Coherence, and Incoherence and at 30 kV for K, Ca, Sc, Ti, V, Cr, Mn, Fe, Co, Ni, Cu, Zn, Ga, As, Br, Rb, Sr, Y, Zr, Mo, Coherence, Incoherence, Pb, and U (Suppl. 1). Gaps and inconsistencies in the data were noted and removed using CoreWall. Smoothing using a Triangular Moving Average (filter=10) was conducted with the Zoo Package (Zeileis & Grothendieck, 2005) and plotted using the Rioja Package (Juggins, 2022) in R.

Total Carbon, Nitrogen, and Organic Carbon

NAK-Y was sampled at ~10-cm resolution for Total Carbon (TC), Total Nitrogen (TN), and Total Organic Carbon (TOC) analysis. Samples were run two or three times and the mean, standard deviation, and relative standard deviation were calculated on runs within one order of magnitude from each other (Suppl. 2).

3.3.4. Diatom Sampling and Counting

Diatom samples (N = 216) were collected across the 11.5 m NAK composite approximately every ~5 cm. Samples were prepared using the Battarbee (1986) hot H_2O_2 method. Dry samples, weighed to approximately 0.1 grams, were treated with 30% H_2O_2 to remove organic matter and 10% HCl to remove carbonates. The samples were then centrifuged at 2,500 RPM for 5 minutes and repeatedly decanted. After decanting a third time, a drop of ammonia solution (30–33% NH_3) was added to disaggregate sediments and colonial diatoms. The samples were then centrifuged and decanted twice more. Upon completion, *Lycopodium* microspores (Batch 3862; 9666 spores) were added to the solution and dissolved to quantify diatom concentration:

$$Diatom\ Concentration = \frac{(\#\ of\ Microspheres\ Introduced * \#\ of\ Counted\ Diatoms)}{(1 + \#\ of\ Microspheres\ Counted)}$$

Slides were prepared by pipetting one drop of the prepared samples onto a clean coverslip which sat in a dry air ventilator for 24 hours. Coverslips were then adhered to slides using Naphrax and placed on a 125°C hot plate for 20 minutes until the Naphrax solidified. All counts were conducted using an Olympus BX50 light microscope at 1000x magnification with a 700D Canon Camera. Samples were also observed using a Phenom XL Scanning Electron Microscope at the Microfossils Laboratory in the Department of Geosciences of Universität Tübingen. The electron source was a Cerium Hexaborit (CeB6) cathode. Samples were coated with 70 nm gold and analyzed with a Back Scatter Detector with 15 kV acceleration voltage. Diatom taxa identification is based on Gasse (1986),

Cocquyt (1998), Taylor et al. (2007), Taylor & Cocquyt (2016), the US Diatom Database (Spaulding et al., 2022), and Cocquyt & Verschuren (2023).

A minimum of 300 diatom valves were counted per slide. If one species was dominant, a minimum of 100 non-dominant valves were counted. Raw diatom counts are available in Suppl. 3. For analysis, percentages of each taxon relative to the total number of counted valves per sample were calculated. Stratigraphic zones based off of the diatom assemblages were calculated using constrained hierarchical clustering with Bray-Curtis dissimilarity within the Rioja Package in R (Juggins, 2022).

3.3.5. Statistical Methods

Principal Component Analysis

Principal Component Analysis (PCA) was conducted on the XRF data to understand the trends across the cores. PCA is used to break down dimensionality and show more interpretable data (Jolliffe & Cadima, 2016). Elements not included in the PCA had medians below 50 counts per second (cps) including Mg, P, V, Cr, Cu, Ba, Sc, Ga, As, Br, and Ar. Other elements removed from the PCA include Cl, which indicated whether NAK-X or NAK-Y were used in the NAK splice, and Mn and Zn, which were flat along the core. For elements with XRF data from both the 10 kV and 30 kV runs, 10 kV results were used as they resulted in higher eigenvalues for the PCA.

Transfer Function

Ecological interpretations are based on modern assemblage data from the East African Diatom Base within the European Diatom Database Index and can be used to interpret hydrochemical parameters throughout the core using the weighted averaging method (ter Braak & Looman, 1986; Gasse et al., 1995). The modern African training set includes each taxon's optimum (the statistically derived value of an environmental parameter where each taxon reaches its maximum) and tolerance (the given range of each environmental parameter for each taxon) for each

environmental parameter based on regression analysis. With these data, past environmental parameters for Nakuru are estimated using the total sum of the relative percentage of each fossil taxon, weighted by its optimum, and standardized to the total percentage of the diatom assemblage used in the transfer function (Chalié & Gasse, 2002). Statistical analyses were conducted in R and all stratigraphic plots were made with the package Rioja (Juggins, 2022). Based on Gasse et. al (1995), conductivity and pH were reconstructed.

Other Diatom Proxies

To better understand changes in the paleocommunities and system dynamics of Lake Nakuru, other diatom proxies were calculated. Species richness was calculated using the Vegan Package in R (Oksanen et al., 2022). A mixing proxy was calculated using *Aulacoseira*/(*Cyclostephanos* + *Stephanodiscus* + 1) (A/(C+S)), where an increase indicates greater mixing with a strong nutrient flux and high Si:P ratio in the euphotic zone (Gasse, 2002). Aerophilic and brackish taxa, based on Gasse (1986) and Taylor et al. (2007), were also plotted to show relative changes across the assemblages. Habitat classifications are included in Suppl. 3. Lastly, an index was created to highlight increasing freshness, *Thalassiosira faurii*/(*T. faurii* + *T. rudolfi*) (*T.* Index). Historically, *T. faurii* and *T. rudolfi* were highlighted as having the same salinity preferences (Gasse et al., 1995), but further studies have shown that past analyses of *T. faurii* overstated its salinity preference (Roubeix et al., 2014). In addition, workers have recognized that *T. faurii* and *T. rudolfi* may represent a species complex (Hasle, 1978; Brindle et al., 2018), indicating that this ratio between deeper water, lower salinity preference *T. faurii* and shallower water, higher salinity preference *T. rudolfi* should indicate depth and/or freshness for these *Thalassiosira*-rich through NAK. All diatom plots were made with the Rioja Package in R (Juggins, 2022).

3.4. RESULTS

3.4.1. Composite Lithology and Correlation

In general, the sediment cores are dominated by finely laminated silts and clays/muds of different colors and laminae thicknesses (<1-10 mm) with occasional fine sandy sections and three *in-situ* ash/tuff layers at 2.90, 5.11, and below 11.52 m (Fig. 2). The upper ~0.6 m of the NAK composite are densely rooted, dark-brown, organic-rich pedogenic muds. Below ~0.6 m, banded brown clays are interspersed with mm-thick white layers. After a reworked lapilli/sand layer from 1.49-1.54 m, the banded brown clays continue with a small 1-cm fault offset at a 60° angle to the horizontal plane until ~2.15 m. The white, diatom-rich bands become denser between 2.4 and 2.6 m. These layers, after being interrupted by an *in-situ* ash layer from 2.88-2.91 m, grade into coarser sands at ~3.09 m. These light gray, slightly greenish sands end at 3.44 m, where a sharp contact between the sands and mixed clays with plant remnants indicate pedogenesis and short-term desiccation. The clays after 3.44 m were green immediately after coring but have since turned brown. The green clays are well-laminated with white, diatom-rich layers up to a couple mm thick. Since core opening in 2004, yellow-orange sulfur aggregates have formed within the green clays. A thick yellowish-gray tephra from 5.07-5.16 m breaks up this section, with two dark layers at 5.49 and 5.65 m, which may be ~1-mm-thick ashes. Reworked sand-sized volcaniclastics from 6.06 to 6.13 m terminate this zone and were dated to 36.5 ± 1.9 ka (Table 2). Beneath this section are hard, brown, non-laminated clays with vertical lines that indicate pedogenesis and, likely, a hiatus. At ~7.30 m, unlaminated brown clays transition into softer, unlaminated, green clays. We indicate a hiatus from 7.78-8.00 m due to known core loss and an unclear lithological change, although it is unknown how much sediment was lost. Below this gap, clays are mostly unlaminated, soft, sticky, and brown. Alteration of this section has resulted in oxidized sediments after ~9.6 m. At 11.14 m, the brown clays become soft and green with potentially biologically-mediated nodules at the top of the section.

At 11.52 m until the end of the core, the sediments consist of volcaniclastics, the top 8 cm of which were bulk dated to 38.9 ± 1.1 ka (Table 2). The similar age to the Menengai Tuff (35.62 ± 0.26 ka), which originated 12 km north of the coring site and has been observed across numerous lakes across the EARS (Blegen et al., 2016), indicates these deposits likely represent the same period of volcanic activity, although this interpretation requires further exploration.

Uncertainties in correlation occur in parts of the composite core. The unlaminated pedogenic muds from the top of the cores have few clear sedimentological features and low MagSus, causing complications in correlating NAK-X1 and NAK-Y1. The relationship between the cores is clearer between 1.54-6.13 m. NAK-X5I and NAK-Y5I&II were correlated using MagSus and XRF data, but the correlation between NAK-X5II and NAK-Y5II is unclear. Due to limited sedimentological features, no MagSus data, post-collection oxygenation, and increased sedimentation for NAK-X than NAK-Y, correlation below this point was not possible. NAK-Y consists of several meters of tuffs after NAK-Y7II which are not visible in the NAK-X record until NAK-X9I. It is hypothesized that below ~7 m NAK-X shifted and was not cored completely vertically given ~1.5 m more of brown clay at NAK-X before the deposition of the Menengai Tuff. Therefore, after the large hiatus and beginning at 8 m, only NAK-Y samples were used for this study.

3.4.2. Age model

Initial runs of the age model indicated that the first two carbon dates do not fit well with standard accumulation rates. It is believed that the first age (NAK-AJ-17; located at 0.75 m, 0.93 ± 40 ka) was likely moved through bioturbation from roots evident at the top of the core (Table 2). The second age (NAK-AJ-02; located at 1.25 m, 6.2 ± 60 ka) is near the end of the AHP but indicates an unrealistically slow accumulation rate. It is therefore believed that there is a substantial hiatus or erosional event where several to tens of cm of sediment, representing several hundreds to thousands of years, were lost. It is unclear what may have caused this, but the drill

site located near to Sirrkon Hill which is >150 m high indicates that a mass wasting event is possible.

Six radiocarbon dates and the Menengai Tuff were used for the age model (Fig. 5A; Table 2). The presence of potentially large hiatuses at 6.13 and 7.78 m isolate a dated charcoal at 7.01 m and the Tuff at 11.52 m. Because of this, there is low certainty in the age model nearby. The age model presented therefore only includes 1.5-6 m where there are multiple ages and only a short-term hiatus (~150 years). The accumulation rate stays fairly even at ~20 yr/cm from ~20-14 ka. The fastest rates throughout the section (~12 yr/cm) occur between ~14-13 ka and the slowest rates (~35-40 yr/cm) between ~15.5-15 (the hiatus) and ~13-12 ka (Fig. 5B).

3.4.3. Geochemical Analyses

TC, TN, TOC, TOC/N

TC, TOC, and TN are highest in the upper 3 m of NAK (Fig. 6). The ranges and averages from the top 3 m for TC are 0.3-5.6% and 3.7%; for TN, 0.0-0.3% and 0.2%; and for TOC, 0.2-5.2% and 2.8%, respectively. For the rest of the core, they are 0.1-1.7% and 0.4% for TC; 0.0-0.2% and 0.1% for TN; and 0.1-1.1% and 0.4% for TOC. The only other increase is located at the bottom of the core at ~11.14 m at the soft, green clays with nodules. TOC/N across the core ranges between 3.36-21.4% with an average of 11.2% not including a large peak of 55.5% at 10.85 m.

Smoothed Magnetic Susceptibility and XRF Results

MagSus stays low for the upper ~5.6 m of the composite (range: 0.4-800; median: 87), with a deviation between ~2.8-3.35 m (Fig. 7). MagSus begins to steadily increase at ~5.6 m after which the average MagSus is ~1,000. The pedogenic hard, brown clay has a MagSus range between 270-2,100. There is then a drastic drop in MagSus after ~7.3 m at the soft green clays (19-200; 56). After the large hiatus, MagSus is high (1,000-2,100; 1,600) for the unlaminated brown clays.

The smoothed XRF elements included in the PCA are featured in Figure 7. Lithogenic elements, including Al (range: 63-720 cps; median: 300 cps), Si (880-

7,700; 3,800 cps), Ti (150-1,300; 630 cps), Fe (3,150-40,100; 10,900 cps), Co (34-480; 210 cps), Rb (81-500; 260 cps), Y (74-600; 230 cps), Zr (380-3,400; 1,300 cps), and U (39-160; 80 cps), show that the majority of input into the system can be traced to local igneous source rocks. Potassium (520-5,100; 2,100 cps), which generally decreases from the bottom to the top of the composite, while likely lithogenic, is enhanced in some areas and muted in others, indicating that it likely includes authigenic components as well. Calcium (110-13,000; 1,000 cps) does not vary across the core except with an increase from ~1.50-3.10 m. Nickel (72-240; 130 cps) varies subtly but appears to increase around the green clays. Similarly, incoherence/coherence (inc/coh) (1.5-1.6; 2.5) increases in the green clays, but also in the top ~3.10 m of the core. Sulfur (0-2,700; 330 cps) is incredibly stable below 8 m and has two larger deviations above ~1.15 m and between ~4.6-6.0 m. Strontium (20-720; 110 cps) stays fairly flat across the record but is more variable above ~4.1 m. Molybdenum (0-1, 710; 65 cps) is unvarying across the section except in areas with thick white laminations such as from ~0.75-1.1 and ~4.75-5.75 m. Lead (9-130; 53 cps) varies across the core with no clear trend. Below ~9.6 m, the oxidation of the sediments results in post-
depositional fluctuations in the XRF record and therefore should be interpreted with caution.

PCA

Dimension 1 (Dim1) of the XRF PCA represents 32.3% of the data with Ti, Al, Rb, Zr, K, Co, Si, Fe, and Y exerting significant, positive control (Fig. 8A). This variability represents the amount of weathering of igneous source rocks, given that elements often have lithogenic sources and that reworked clastic samples plot positively along Dim1 and more laminated sediments such as the brown banded clays plot more negatively. Dimension 1 therefore represents a balance between the igneous source rock and the physical and chemical weathering of those sediments, indicating a relationship with precipitation where increased precipitation results in increased

weathering. Dimension 2 (Dim2) represents 21.5% of the data with Ni, inc/coh, Sr, Ca, S, U, and Si controlling it positively and only K significantly controlling it negatively. The lithologies of the composite core control Dim2, with brown banded clay plotting the most positively, unlaminated brown clays plotting the most negatively, and pedogenic muds, green clays, sands, tephras, and reworked clastics all slightly positive but closer to zero. Dimension 2 is therefore likely related to the amount of organic matter in the sediments which seems to also relate to the amount of water within the basin since K can be deposited authigenically. This indicates that biogenic elements are depositing more readily during wetter phases at Nakuru. The PCA loadings are highly variable (Fig. 9) with Dim1 generally greater than 0 above ~1.5 m and between ~3.35-4.4, ~4.7-7.25, ~8.0-8.8, ~9.4-10.2, and ~10.5-11.2 m and Dim2 is only consistently above 0 above ~5.8 m and below ~11.3 m.

The correlation matrix shows how strongly correlated the lithogenic elements (Y, Si, Al, Ti, Rb, Zr, K, Fe, and Co) are (Fig. 8B). Some of these elements, Ti, Fe, Rb, Co, and especially K, negatively correlate with biogenic elements like Ca, Sr, inc/coh, and Ni. This indicates that deposition of less-weathered sediments often results in a decrease in biogenic deposition whereas deposition of more-weathered sediments often results in higher biogenic deposition, highlighting a relationship between weathering, likely related to rainfall, and biological productivity within this lake system.

XRF Ratios

The ratios selected for further analysis include Ca/Mg, Fe/Mn, Si/Zr, Sr/Ti, and K/Ti (Fig. 9). Ca/Mg is highest in the top ~4.1 m of the core, with the largest peaks from ~1.45-3 m, indicating increases in primary productivity in the upper part of the core (Naeher et al., 2013; Davies et al., 2015). Fe/Mn indicates anoxic conditions (Davies et al., 2015) in the upper ~1.15 m and from ~7.25-7.78 m of the composite. Si/Zr is incredibly variable, although it indicates that diatom productivity (Burnett et al., 2011) may have been higher in the top ~6.25m compared to the bottom of the

core. Sr/Ti indicates that cyanobacteria production (Kylander et al., 2011) was highest between ~1.45-4.7 m. Lastly, Ti/K, which indicates increased illitization of clays and likely decreased precipitation (Foerster et al., 2018), peaks between ~3.05-4.95, ~5.55-7.3, and <8.0 m except for a decrease between ~11.1-11.25m.

3.4.4. Diatom Results

Diatoms often increase in abundance with other diatoms common in their habitats (Fig. 6). Benthic taxa including *Encyonema muelleri* (Hustedt) Mann, *Epithemia adnata* (Kützing) Brébisson, *E. gibberula* (Ehrenberg) Kützing, *Nitzschia fonticola* (Grunow) Grunow, *N. palea* (Kützing) Smith, *N. palea* var. *debilis* (Kützing) Grunow, *Pantocsekiella ocellata* (Pantocsek) Kiss & Ács, and *Pseudostaurosira brevistriata* (Grunow) Williams & Round are most abundant between ~1-2.7, ~5.5-7.25, and ~8.0-11.15 m. Other taxa such as *Aulacoseira granulata* (Ehrenberg) Simonsen, which is planktonic, and the light centric species, whose taxonomic designation is unknown, also follow the patterns of the benthic taxa. Both *Thalassiosira faurii* (Gasse) Hasle and *Thalassiosira rudolfi* (Bachmann) Hasle, as planktonic taxa, share fairly similar patterns and are most abundant from ~0.8-3.55, ~4.7-5.5, and ~7.3-7.78, with *T. rudolfi* also abundant below 11.15 m. The largest deviation along the core occurs between ~3.55-4.6 m where *Stephanocyclus meneghinianus* (Kützing) Skabichevskij, a littoral, planktonic species, becomes incredibly abundant. Eight zones based on the total diatom assemblage were created using Bray-Curtis dissimilarity and mostly follow lithological changes in the core. The boundaries occur at 0.8, 3.55, 4.8, 5.5, 7.3, 8 (the large hiatus), and 11.14 m.

Diatom concentration is lowest at the bottom of the core and highest in the banded brown clays, although in general concentration is variable across the core (Fig. 6). Species richness waivers between ~10 and 40, with the largest decreases concurrent with increases in *Thalassiosira rudolfi*. The calculated conductivity (range: 193-6,380 µS/cm) is nearly always above 1,000 µS/cm with peaks >3,000 µS/cm between ~3-5.5, ~7.25-7.78, and ~11-11.5 m (Fig. 9). The pH (7.3 to 9.4) follows a

similar trend, but with a longer alkaline phase between ~0.75-5.5 m. The mixing proxy, A/(C+S), is lowest at the green clays. The *T.* Index, which indicates freshening conditions, gradually increases over time with two jumps at ~5.5 and ~2.75 m. The abundance of aerophilic taxa is low with increases at ~2.9-3.75 m and ~8.0-10.7 m. The abundance of brackish taxa tends to increase in zones with an increase in benthic taxa, especially between ~5.5-7.25 and ~8.0-11.15 m.

3.5. DISCUSSION

3.5.1. Lake Nakuru's Unique Proxies

The deposition, chemistry, and productivity of lakes are determined by their vertical and horizontal morphology, altitude, energy input/output, physical input/output, local climate, long-term climate, and biotic influences (Talling, 2001). To best understand environmental change through lake sediments, we must understand how these variables relate to one another and impact different proxies. Often, shallow, tropical lakes like Nakuru have chemical responses that are "ecologically dominant," meaning that lake biota greatly impact its geochemical signature and deposition (Talling, 2001). Lake Nakuru's high primary productivity, as well as other unique variables, such as its closed basin system, highly alkaline source rocks, amplified response to climate change, high elevation, minimal riverine input, etc. (Fazi et al., 2018), control its sedimentological, biological, and chemical changes, highlighting the necessity of careful examination using multiple high-resolution proxies.

Anoxic/Oxic Deposition at Paleolake Nakuru

The sedimentological facies deposited at NAK indicate distinct phases of anoxic and oxic depositional conditions. The green clays across the core indicate deposition during anoxic conditions, evident through its green color (IUSS Working Group, 2014) and increase in Fe/Mn (Fig. 9). The change from the green of the freshly sliced cores to the current brown color (Fig. 2) indicates oxygenation after opening, reminiscent of the green rust clay mineral, fougerite, which forms in anoxic, highly

productive waterbodies and, when in contact with oxygen, alters to ferrihydrite, lepidocrocite, and goethite (Trolard et al., 2007). Anoxic conditions in lakes can be caused by exceedingly high biological productivity, such as from an increase in nutrients (Lung'ayia et al., 2001; Ndebele-Murisa et al., 2010; Brothers et al., 2014); deep water that creates anoxic bottom waters (Pilskaln & Johnson, 1991; Owen & Crossley, 1992; Hecky et al., 1994); a decrease in mixing such as through decreased wind or a change in wind direction (MacIntyre, 2012); or a decrease in temperature/density gradients (De Cort et al., 2013; Kragh et al., 2020). Other evidence of anoxia within the green clays includes a decrease in lithogenic elements (Fig. 7) and Dim1 (Fig. 9), indicating a decrease in clastic deposition potentially related to deeper lake conditions and/or more heavily weathered input. In the green clays, inc/coh, an indicator for organic matter and productivity (Burnett et al., 2011; Davies et al., 2015), increases, representing anoxic sediments either as a result of increased productivity or preservation (Mahamat Ahmat et al. 2017). Within the diatomaceous laminated green clays, which have an extrapolated accumulation rate of ~20 yr/cm, inc/coh, Mo, and S are elevated but potentially related to seasonal lake mixing and temporary anoxic conditions like those observed at other lakes in Eastern Africa (Pilskaln & Johnson, 1991; Owen & Crossley, 1992) and typical in eutrophic soft water lakes with seasonal algal communities (Brauer, 2004). The cause of layering is unknown and dependent on the lake itself given that tropical lakes result in different layering regimes such as (a) increased mixing during the dry season due to wind strength (Hare & Carter, 1984), (b) increased mixing during the wet season due to increased external hydrological input (Egborge, 1979), (c) permanently deep water anoxia resulting in dark layers from sediment input in the rainy season and light layers from diatom input during the dry, windy season (Pilskaln, 2004), or (d) a completely different system all together.

Across the rest of the core, sediments were oxygenated. The brown clays are interpreted as shallower, oxygenated layers, based on high lithogenic/igneous

components with low biogenic components (Fig. 7) and pedogenesis between ~6.05 and 7.25 m. The sands between ~3.09 and 3.44 m indicate high-energy deposition such as from an alluvial fan, river, or shoreline. The location of the sands above the pedogenic laminated green clays indicates a rapid rather than gradual change in depositional energy. These sands, dated to ~15 ka (Table 2), are interpreted as the beginning the AHP. After 15 ka between 3.09 and 1.5 cm, the slight decrease and lack of variability of lithogenic/igneous elements and Dim1 indicate an increase in chemical over physical weathering. The laminated brown muds above this section indicate oxygenated sediments undergoing cyclic rainfall and/or changes in paleoproductivity. In addition, above 3.09 m, inc/coh; Ca and Sr (Fig. 7); and TOC/N, TOC, and TN (Fig. 6) all increase, indicating increased primary productivity and/or preservation. The reworked volcaniclastics at 1.49-1.54 m deposited after 12.8 ka indicate the potential for high-energy events to bring larger clasts into the system. With a 6.2 ka charcoal at 1.25 m and the steep slope adjacent to the coring site, it is believed that a mass-wasting event occurred after 12.8 and before 6.2 ka, as explained in section 4.2, removing a substantial portion of Nakuru's AHP sediments. The sediments located above 1.25 m have been reworked by roots and represent slower deposition.

Reevaluation of Thalassiosira rudolfi *as Paleodepth Indicator for Lake Nakuru*

Diatoms and other micropaleontological proxies like ostracods as conductivity and pH indicators are used within closed basins to represent changing depths, yet the results from this study indicate that this interpretation may not be valid for NAK. *Thalassiosira rudolfi* is a well-documented high alkalinity preference taxon whose increase in closed basins has been used to indicate shallowing conditions (Halfman et al., 1992; Gasse et al., 1995; Owen et al., 2014; Muiruri et al., 2021). Lithological, geochemical, and other diatom proxies within NAK do not support this interpretation, however. The *T. rudolfi*-rich, anoxic green sediments (>11.14, 8-7.3; and 5.45-4.75 m) are unlikely to represent shallowing conditions. While shallow lakes can be

anoxic, it is uncommon for these conditions to last more than several days to months (Brothers et al., 2014; Kragh et al., 2020), let alone centuries. Increased *T. rudolfi* phases are also accompanied by decreased species richness with other high alkalinity indicator taxa, like *Stephanocyclus meneghinianus, Anomoeoneis sphaerophora* Pfitzer*, Mastogloia elliptica* (Agardh) Cleve*,* and *Nitzschia frustulum* (Kützing) Grunow*,* or shallow water taxa, like *Epithemia adnata* and *E. gibberula,* relatively absent (Fig. 6). Instead, the well-oxygenated brown clays have increased species richness and littoral and brackish taxa (Fig. 6; Fig. 9). Evidence of pedogenesis within the brown clays from ~6 to 7.25 m also indicates shallowing of the system when *T. rudolfi* is less abundant. Other proxies, including a decrease in lithogenic/igneous elements (Fig. 7) and K/Ti (Fig. 9) indicate that *T. rudolfi* phases are likely not shallowing. Instead, we propose five hypotheses of what might cause the variation between the low-diversity *T. rudolfi* and the high diversity, benthic layers below 4.75 m: **Hyp1)** changes in groundwater flow; **Hyp2)** changes in mixing; **Hyp3) c**hanges in nutrient loading; **Hyp4)** changes in depth; and **Hyp5)** changes in the closedness of the lake system.

Hyp1 Changes in groundwater could come from increased hydrothermal activity or groundwater connections between Naivasha and Nakuru-Elmenteita (Dühnforth et al., 2006; Olaka et al., 2010) that could be controlled by climatic, volcanic, or tectonic variables. These changes could impact the hydrochemistry, mixing, nutrient loading, and/or depth of Lake Nakuru. **Hyp2** Changes in mixing could occur due to changes in wind strength, depth, temperature, and/or seasonality. Given limited evidence of large tectonic processes changing basin shape over the last 36 kyr (McCall, 1967), these variables are likely controlled by climate. **Hyp3** Changes in nutrient loading at Lake Nakuru would come from either increased rainfall or volcanic activity such as hydrothermal or volcanic ash input. **Hyp4** Changes in depth are likely controlled by rainfall, either through direct precipitation/surface flow or groundwater flow. **Hyp5** Changes in whether Lake Nakuru is an opened or closed basin relate to Nakuru's

connection with Elmenteita or Menengai which have been hypothesized, and proven in the case of Elmenteita, by many previous workers (Washbourn-Kamau, 1971; Cohen & Nielsen, 1986; Richardson & Dussinger 1986; Dühnforth et al., 2006). Such changes between Lake Magadi and Natron have been observed to impact the diatom record (Gasse et al., 1997). A connection between Lake Nakuru with Elmenteita would only occur if Nakuru was ~80 m deep and with Menengai if Nakuru was ~186 m deep. Such scenarios are unlikely given nearby evidence of pedogenesis on short timescales.

It is currently unclear which of the hypotheses would have created anoxic conditions and increased *T. rudolfi* visible in NAK. Changes in groundwater (Hyp1) cannot currently be constrained with our proxies but would influence other variables (Hyp2-4). The decreased diversity within the *T. rudolfi* layers might indicate increased depth (Hyp4) and/or reduced mixing (Hyp2), as diversity tends to increase closer to shore with heavier mixing (Stevenson & Stoermer, 1981; Moos et al., 2005; Cantonati et al., 2009; Laird et al., 2010; Hayashi, 2011; Laird et al., 2011). Decreased mixing (Hyp2) is supported by A/(C+S) which decreases within the *T. rudolfi*-rich sections (Fig. 9). The high diversity sections below ~4.75 m have increased benthic (Fig. 6) and brackish taxa (Fig. 9), indicating that these phases may have been shallower (Hyp4), more alkaline, and/or better mixed (Hyp2) than *T. rudolfi*-rich layers. Potential deepening (Hyp4) of the *T. rudolfi* layers is also supported by a decrease in K/Ti (Fig. 9) and inc/coh (Fig. 7) since tropical lakes often increase in primary productivity during the wet seasons (Zébazé Togouet et al., 2007). If the *T. rudolfi* layers are controlled by nutrient loading (Hyp3), those controls could be climatic (resulting in deepening/mixing conditions as outlined above) or volcanic. Increased chemical weathering and erosion of volcanic source rock into Lake Nakuru due to increased precipitation could result in increased nutrients and algal blooms. Periods of higher volcanic activity have also resulted in algal blooms in both modern and ancient contexts (Kurenkov, 1966; Yuretich, 1982; Thevenon et al.,

2002; Duggen et al., 2010; Yuan et al., 2019). The pulses of *T. rudolfi* occur after the Menengai Tuff, around the tephra layer at ~5.05 m, and near the core loss at 8 m (Fig. 6). Two ignimbrites/ash-flows from Menengai erupted between ~29 ka to 8.5 ka, with the second likely older than 12.85 ka (Leat, 1984; Leat, 1991), although the dates of these sequences are heavily debated (Riedl et al., 2020). As one of the youngest volcanoes within the EARS (Blegen et al., 2016; Riedl et al., 2020), Menengai could be responsible for ash deposits resulting in diatom blooms, although such impacts are often short-term. Given the impact of many of these hypotheses on one another, it is anticipated that the increased *T. rudolfi* is likely a combination of these hypotheses.

3.5.2. 35 ka of Hydroclimate Change at Lake Nakuru

From ~35.6-12.7 ka, Nakuru was always at least a slightly alkaline lake (pH >8), even during deeper conditions (Fig. 9). General trends throughout the core indicate freshening, deepening (*T.* Index; Fig. 9), and an increase in organic matter (Dim2; Fig. 9) leading into the AHP.

Zone 8 – Anoxic Conditions – ~35.6 ka, 11.5-11.14 m

At Lake Nakuru, Zone 8 (~35.6 ka, 11.5-11.14 m) represents deposition of the Menengai Tuff followed by an anoxic, low diversity, *T. rudolfi* phase, indicating deeper waters and/or increased stratification. TN in this phase is higher than the rest of the core until ~3 m (Fig. 6), potentially representing increased nutrient input. Because of the known volcanic input, it is unclear whether depth or productivity caused anoxia, although productivity from the Tuff would be short-term, potentially visible as a peak in Dim2 input at ~11.4 m. Therefore, increased precipitation likely contributes as well, as evident by Dim1 being less than 1 (Fig. 9). The Fe-, Co-, and Pb-rich nodules at the top of this section (Fig. 7) indicate that the lake may have desiccated after this phase, meaning that if this phase was wetter, it was not hundreds of meters deep. Other records in Africa demonstrate a wet phase ~35 ka, but with poor age constraints, including Lakes Turkana >40 ka (Butzer et al., 1972),

Elmenteita 33.5 ± 2 ka (Cohen & Nielsen, 1986), Mweru Wantipa (Cheshi) <38.5 ± 3.4 ka (Stager, 1988), and Malawi >38 ka (Finney et al., 1996). Chew Bahir, which is incredible well-dated (Foerster et al., 2012; Trauth et al. 2018), exhibits a wet phase from ~37 to 35 ka, with the last wetness pulse located ~35 ka (Fig. 10) (Foerster et al., 2012). At Lake Tanganyika, ~37 ka there is an increase in biogenic silica and Rb/K which indicates a change in source, potentially related to an increase in precipitation (Burnett et al., 2011), also evident in the δD record which decreases by 30 ka (Tierney et al., 2008). Lake Chala exhibits a high lake phase from ~60 to 22 ka, far longer than the record seen at Lake Nakuru
(Moernaut et al., 2010).

Zone 7 – Shallow/Land Surface, Oxygenated Conditions – <35.6 - >24 ka, 11.14-8 m

Zone 7 (<35.6 **-** >24 ka, 11.14-8 m) is interpreted as a dry, well-mixed zone after a phase of desiccation. In addition to the nodules representing desiccation in Zone 8, TOC/N increases to 55.5 at the beginning of Zone 7, whereas the range otherwise is 3-20 (Fig. 9). TOC/N in sediments from 4-10 indicate mostly algal input and >20 mostly vascular land plant input (Meyers, 1994), meaning that TOC/N of 55.5 might indicate a fully dry land surface. The elevated lithogenic and igneous elements support this (Fig. 7). In addition, the input of aerophilic taxa from 11.14-8 m implies a shallow lake with periods of aerial exposure. Across Zone 7, the taxa imply shallow waters with benthic taxa such as *Epithemia adnata*, *E. gibberula, Nitzschia fonticola*, and *Pseudostaurosira brevistriata*, ranging from 29-57% with a median 44% (Fig. 6). The only common planktonic diatom, *T. rudolfi,* illustrates that the waters were slightly alkaline, with a calculated conductivity of 1,400 µS/cm and a pH of 8.5 (Fig. 9). Dim2 shows that this zone has very little organic material (Fig. 9), evident also in the PCA Biplot (Fig. 8A). Very few lacustrine records exist during this phase, likely a result of dry conditions. Available records from Chew Bahir show drying post-35 ka with only brief peaks in humidity (Foerster et al., 2012) and from Lake Tanganyika drying ~31 ka (Fig. 10).

Zone 6 – Wet, anoxic conditions – >24 ka, 8-7.3 m

Zone 6 (>24 ka, 8-7.3 m) returns to soft green clays dominated by *T. rudolfi*. Core loss before this zone means that there is uncertainty whether there was volcanic activity, especially since the timing of volcanic periods at Menengai is not well constrained 29-8.5 ka (Riedl et al., 2020; Conti et al., 2021). While *T. rudolfi* is the dominant taxa, this phase includes more *T. faurii* compared to lower in the record (Fig. 9), showing that conditions may have been slightly wetter, supported by decreased Dim 1 and K/Ti (Fig. 9). Earlier Lake Nakuru records may also show this wet anoxic phase (Fig. 1) (Cohen et al., 1983; Richardson & Dussinger, 1986). While developing an ostracod transfer function, Cohen et al. (1983) compared the outcomes of the ostracod record with the earlier analyzed diatom record and found a depth peak >24 ka that was not observed by the diatom record (Fig. 1). If these two zones match up, this finding supports not only deeper conditions within Zone 6, but also the limitations of a diatom-based transfer function at Lake Nakuru. Other highstands have been observed at Lakes Chad >26 ka, Nakuru >25 ka, and Albert ~32-29 ka (Butzer et al., 1972; Harvey, 1976). Multiple wet phases are visible at Chew Bahir ~27-26 and ~25-24 ka (Foerster et al., 2012) and at Lake Tanganyika ~27 ka and ~25 ka (Tierney et al., 2008).

Zone 5 – Shallow/Land Surface with Pedogenesis/Hiatus – ~23.9-18.7 ka, 7.3-5.45m

Zone 5 (~23.9-18.7 ka, 7.3-5.45 m) includes two lithologies: a hard, brown paleosol and laminated green clays (Fig. 2). In general, this zone is associated with similar variables to Zone 7 (low organic matter, increased K/Al, many benthics) until the laminated green clays. At the beginning of Zone 5 (~24 ka), Lake Nakuru was dry with evidence for desiccation before 20 ka based on lithological change and pedogenesis. Around ~20 ka, there is a change in depositional energy that reworked volcaniclastics from the Menengai Tuff (Table 2). After this, alternating anoxic and diatom-rich layers indicate a stable water body with cyclic depositional patterns (Fig. 11). The transition into green clays is accompanied by an increase in biogenic

elements and organic matter and a decrease in K/Ti and lithogenic elements (Fig. 7; Fig. 9). Diatom assemblages from the brown clays into the laminated green clays decrease in high alkalinity-preference taxa like *Epithemia gibberula* and *Thalassiosira rudolfi* and increase in freshwater, benthic taxa like *Nitzschia fonticola*, *Nitzschia palea* series, and *Pantosekiella oscellata*, indicating slightly fresher waters. Therefore, while the brown paleosol likely indicates the dry conditions of the LGM (Porter & Zhisheng, 1995; Gasse, 2000), the switch to the laminated green clays signals a ~1.5 kyr transitional phase ~20 ka with increased organic matter, anoxic conditions, and humidity (Fig. 9; Fig. 11).

Zone 4 – Wetter, Anoxic Conditions – ~18.7-17.5 ka, 5.45-4.75 m

Between Zones 5 and 4, there is an increase in the *T.* Index that signals that this high *T. rudolfi* phase in Zone 4 (~18.7-17.5 ka, 5.45-4.75 m) is the result of increased depth, despite being associated with a thick tephra. The tephra creates a brief burst of anoxia (Fe/Mn) that cannot account for the ~1.2 kyr of anoxia observed in this phase from the S, Mo, and Fe/Mn records (Fig. 9; Fig. 11). The decreased benthic taxa; increased planktonic taxa, including a spike in the deep freshwater-preference taxa *Aulacoseira granulata;* increased Dim1 (Fig. 9); and decreased K/Ti (Fig. 11) support this conclusion. This *T. rudolfi*, low diversity phase is laminated, indicating non-disturbed cyclicity. This wet phase from 18.7-17.5 ka at Lake Nakuru matches up incredibly well with a wet phase at Lake Masoko from 18.7 to 17.2 ka (Barker et al., 2003) and Chew Bahir after ~19 ka until the Younger Dryas (Fig. 10; Foerster et al., 2012). Other records also show potential increased humidity as well, although these records are not as well time-constrained including at Lakes Rukwa (Barker et al., 2002), Tanganyika (Burnett et al., 2011), and Albert (Harvey, 1976; Beuning et al., 1997). Lake Tanganyika appears to have a complicated record at this stage, but a combination of increased biogenic silica and Rb/K may indicate increased precipitation during this timeframe (Burnett et al., 2011) with a slight increase in δD (Tienery et al., 2008). No wet phase is visible at Lake Chala (Verschuren et al., 2009).

Zone 3 – Highly Alkaline Lake Phase – ~17.5-15.4 ka, 4.8-3.55 m

Zone 3 (~17.5-15.4 ka, 4.8-3.55 m) is a layer of laminated soft green clays with roots, indicating desiccation and a short hiatus at the top. This phase is almost exclusively *Stephanocyclus meneghinianus* (Fig. 11), resulting in a conductivity of 4,600 µS/cm and pH of 8.8: the highest across the entire core (Fig. 9). Such saline water could be chemically stratified as evidenced at Nasikie Engida in the South Kenya Rift where high salinity results in strong chemical stratification, preventing wind-induced disturbance in waters only 1–2 m deep (Renaut et al., 2021). Primary productivity increases after 16.5 ka, including that of diatoms (Si/Zr and diatom concentration) and cyanobacteria (Sr/Ti) (Fig. 11) which tend to prefer shallower, highly alkaline waters (Grant et al., 2006). At ~15.9 ka, several planktonic-rich layers indicate a short-term deepening (Fig. 11). This is followed by a decrease in diatom productivity and inc/coh as well as an increase cyanobacteria productivity, leading to a desiccation around 15.2 ka which matches a similar desiccation at Lake Victoria (Stager et al., 2002), a pause in increasing humid conditions at Chew Bahir (Foerster et al., 2012), and a dip in δD at Lake Tanganyika (Tierney et al., 2008).

Zone 2 – Gradual Wetter Conditions – ~15.4-<6 ka with Large Hiatus, 3.55-0.8 m

Zone 2 (~15.4- <6 ka, 3.55-0.8 m) represents a variety of sediments including sands, tephras, and brown clays with white diatom layers and high organic content (Fig. 11). This section is interpreted as the AHP given the age of ~15 ka at 3.41 m and indicated by the lower conductivity and pH of 1,200 µS/cm and 8.5, respectively. The AHP is evident in nearly all the lakes across the EARS, particularly after the Younger Dryas 12.9-11.7 ka, at Lakes Turkana, Elmenteita, Nakuru, Naivasha, Magadi, Rukwa, Chad (Butzer et al., 1972; Cohen & Nielsen, 1986); Lake Chesi (Stager, 1988); Chew Bahir (Foerster et al., 2012); Paleolake Suguta (Garcin et al., 2009); Lake Albert (Harvey, 1976); Lake Chala (Verschuren et al., 2009) and Lake Masoko (Barker et al., 2003; Garcin et al., 2007). At Lake Nakuru, this phase

contains the most diverse diatom record which may be a result of increased resolution due to a higher accumulation rate after 14 ka (~12 yr/cm) (Fig. 5B).

Zone 2a – Variable Wet Conditions – ~15.4-13.7 ka, 3.55-2.6 m

Zone 2a (~15.4-13.7 ka, 3.55-2.6 m) includes sands, a tephra, and banded brown clays. The sands are interpreted as the beginning of the AHP but seem to bias the XRF and diatom data. This is evident in the low diatom concentration and increase in aerophilic taxa in this section, suggesting potential dissolution and mixing (Fig. 6). Because of this, the high percentage of *T. rudolfi* in this section is not interpreted like earlier anoxic sections, particularly with the lack of evidence for anoxia and the high species richness (Fig. 6), but rather taphonomic bias (Ryves et al., 2001; Flower & Ryves, 2009). Despite this bias, there is a gradual shift in this subzone from *T. rudolfi* to freshwater *Aulacoseira* taxa, indicating wetter conditions (Fig. 11). With the shift to the banded brown clays, proxies signal wetter conditions, including a decrease in Dim1 and K/Ti, and increased productivity, including an increase in Dim2, Ca/Mg, and Sr/Ti (Fig. 9), which is also evident in the PCA Biplot (Fig. 8). The tephra at 2.88-2.91 m with an extrapolated date of ~14.1 ka does not appear to create the anoxic conditions that may be visible earlier in NAK.

Zone 2b – Stable, Wet Conditions – ~13.7-12.7 ka, 2.6-1.65 m

Zone 2b (~13.7-12.7 ka, 2.6-1.65 m) appears more stable than the earlier phase of the AHP (Fig. 11). This subzone indicates high productivity and organic matter (Ca/Mg, Sr/Ti, and Dim2; Fig. 6) with heavily weathered sediments depositing into the basin (Dim1; Fig. 9). The *T.* Index indicates deeper conditions than earlier in the zone (Fig. 9). These stable wet conditions may correlate with an increase in *Aulacoseira granulata* var. *angustissima* (Müller) Simonsen and *Thalassiosira* ~15.5 to 13.5 ka from Richardson & Dussinger (1986). It is believed that this demonstrates that between the two cores, Richardson & Dussinger may represent a deeper part of the lake with less mixing.

Zone 2c – Deep Lake but No Record – ~12.7-Unknown ka, 1.65-0.8 m

Zone 2c (~12.7-Unknown ka, 1.65-0.8 m) is dominated by *Thalassiosira faurii* (Fig. 6), but the timeframe of this section is not well constrained with a date of ~6 ka at 1.25 m implying a mass-wasting event between~12.7 and 6 ka. The lack of *Stephanodiscus*, like that observed by Richardson & Richardson (1972) at ~11.5 ka, also indicates erosion since *Stephanodiscus* represents substantially fresher and deeper waters than those observed from the diatom communities from NAK. An alternative hypothesis could be the depth differences between the locations, although the sites are only located ~2 km apart at similar elevations, making this drastic difference unlikely (Fig. 3B). Either way, the lack of *Stephanodiscus* demonstrates that Lake Nakuru does not rapidly deepen at the start of the AHP like other records at Lake Tanganyika (Tierney et al., 2008) and Chew Bahir (Foerster et al., 2012), but rather gradually deepens after the Younger Dryas, reflecting Nakuru's unique record in documenting moisture availability given that other lakes likely received overflow waters from other basins.

Zone 1 – Post AHP Heavily Bioturbated – 0-0.8 m

Zone 1 (0-0.8 m) represents modern deposition where bioturbation is likely. This zone consists mostly of *Pantocsekiella oscellata*, *Pseudostaurosira brevistriata*, *Aulacoseira muzzanensis* (Meister) Krammer, and *Cyclostephanos dubius* (Hustedt) Round, the latter two which were not evident across the rest of the core (Fig. 6). This zone was calculated as the freshest, with a conductivity of ~700 and a pH of 7.7, which is very different from modern conditions (Table 1), indicating substantial mixing.

3.5.3. Towards Understanding Lake Nakuru's Variable Record

The increase in *T. rudolfi* in anoxic zones indicates either increased volcanic activity, rainfall, or a combination of both. While it is believed that the availability of fresh, volcanic materials may be a contributing factor to primary productivity during these phases, it is believed that these layers most likely represent an increase in

rainfall causing anoxic conditions in a deeper lake setting given that volcanic-induced increases in primary productivity would be short lived. With this assumption, we attempt to determine what might cause this recurring depth-induced anoxia.

While much of our understanding of Eastern Africa is based on a low-latitude response to precessional forcing (Kutzbach & Street-Perrott, 1985; Garcin et al., 2006; Foerster et al., 2012; Junginger et al., 2014), other forcing mechanisms are clearly important to EARS hydroclimate. Lake Nakuru's periodic wet phases may highlight the importance of SST and the teleconnection between high and low latitudes on Eastern African rainfall over the past 35 ka on a centennial scale, particularly the Dansgaard-Oeschger and Heinrich cycles (Holmgren et al., 2003; Trauth et al., 2018; Schaebitz et al., 2021). Through the last glacial, 30 short warming/cooling events have been observed in Greenland's ice cores (Fig. 10; Huber et al., 2006). A Dansgaard-Oeschger (DO) event, or Greenland Stadial (Dansgaard et al., 1969; Dansgaard et al., 1993), results in an 8-15°C increase over decades (Kindler et al., 2014). Temperatures then gradually cool until there is a rapid drop back to glacial temperatures called Heinrich (H) events, or Greenland Interstadials (Heinrich, 1988). H events result in decreases in SST and salinity, with large calving events occurring over 6-8 kyr (Bond et al., 1992; Cimatoribus et al., 2013). Not all DO events are followed by H events, making their relationship unclear, although modeling results show that H events are potentially driven by ice sheet dynamics, whereas DO events are driven by ocean dynamics (Mann et al., 2021). The importance and relationship of ocean (Vettoretti & Peltier, 2016), ice sheet, and atmospheric (Dima et al., 2018; Erhardt et al., 2019), including volcanic (Lohmann & Svensson, 2022), dynamics is still unclear. Regardless, within the geological record these phases are globally, temporally synchronous (Adolphi et al., 2018), as evident in the similarities between the Greenland Ice Sheet and Arabian Sea records (Fig. 10).

DO and H events impact global temperatures and moisture flux by impacting SST in the North Atlantic, ultimately impacting Atlantic meridional overturning circulation strength (Deplazes et al., 2014; Cheng et al., 2016), which has larger impacts on the hydroclimate of the tropics, particularly related to ITCZ and monsoon strength (Sachs & Lehman, 1999). The clearest evidence come from marine (e.g., Ivanochko et al., 2005; Itambi et al., 2009; Deplazes et al., 2013; Deplazes et al., 2014) and speleothem records (e.g., Wang et al., 2001; Holmgren et al., 2003; Fleitmann et al., 2009; Cheng et al., 2013; Cheng, Sinha et al., 2013; Cheng et al., 2016; Budsky et al., 2019). Along the Indo-Arabian peninsula, warmer SST during DO phases result in rainfall in Eastern Africa similar to ENSO, whereas during H events, freshwater input to the North Atlantic causes a decrease/shutdown of the Atlantic meridional overturning circulation, resulting in drier conditions (Deplazes et al., 2014). Data from tropical lakes are lacking, particularly those with high enough resolution and strong enough age models to note millennial-scale changes (Voelker, 2002). This appears to be supported by proxies in Eastern Africa that show that H events result in drier conditions than DO events (Stager et al., 2011; Foerster et al., 2012; Trauth et al. 2018). Despite weak age control across the EARS, except for Chew Bahir (Trauth et al., 2018), the synchroneity of events across the EARS (Fig. 10) hints at these events' strength.

The Chew Bahir, Lake Tanganyika, the Burundi Highlands, Lake Masoko, and Lake Rutundu records follow precession over the past 25 ka (Fig. 10). Because Nakuru's record is incomplete during the Holocene, this trend is difficult to detect, although Dim1 and K/Ti indicate wetter conditions towards the present. At Lake Nakuru, longer-scale climate change is visible including in Zone 7 which matches with the LGM 26.5-19 ka (Clark et al., 2009) and Zone 2a with the Bølling–Allerød (B-A) interstadial 14.7-12.9 ka (Gasse, 2000). All compared records have increasing or stable aridity over the LGM and a bump in humidity at the B-A (Fig. 10). On millennial DO and H scales, Chew Bahir, which has the highest resolution, is

incredibly variable and mirrors changes in the Arabian Sea and North Greenland ice sheet, with dry H events and wet DO events except at DO4 and DO2. At Nakuru, LGM dry conditions last until ~18.7 ka, followed by wetter conditions, which decline before H1 ~16.7 ka (Hemming, 2004), followed by increased humidity again at the B-A (Fig. 10). While not as drastic, this trend is visible at Lakes Tanganyika, Masoko, Rutundu, and the Burundi Highlands. Tanganyika, especially, shows a decrease in humidity at H1 whereas a gap in the record at Masoko also indicates drier conditions. Fitting Nakuru's record to the rest of the DO and H events is difficult given the limited age model, but the placement of the stratigraphic record with two tie points at 23.9 and 35.6 ka suggests how the Nakuru record might fit into the larger EARS context. The peak in K/Ti ~35 ka, likely representing DO7, is visible at Chew Bahir and the Burundi Highlands. DO7 is only a small peak at Lake Masoko, like NAK's Dim1 record. The other potential DO peaks at NAK at ~10.4 and ~9.7 m are subtler but could represent DO6 and 5 which are also muted at Chew Bahir. Lake Tanganyika has a wet phase during this time, although low resolution complicates its connections with DO events. Missing parts of Lake Masoko's record also make its interpretation here unclear although it enters a more humid phase after DO6. The anoxic NAK phase right before ~23.9 ka does not match with a DO event, but could match up with the peak at ~25 ka in the Arabian Sea, ~26 and ~25 ka at Lake Tanganyika, and two wet bursts after ~25 ka in the Burundi Highlands. An alternative hypothesis is that this anoxia phase is DO3 which was wetter at Chew Bahir, but not at the other records. Overall, to analyze the relationship between DO and H events with lakes across the EARS requires high-resolution data with strong age models. If these phases are universal and indicate DO and H phases, it highlights the strength high latitude SST may have on rainfall across Eastern Africa.

3.6. CONCLUSIONS

As a closed basin at one of the highest points of the EARS, Lake Nakuru shows significant changes in lake level with only minimum changes in precipitation. Past

research has utilized Lake Nakuru's record to explain rift-wide climatic changes, like the AHP, but studying Lake Nakuru at high-resolution provides insights into a unique record with incredible sensitivity and minimal external input. This study found through lithological, diatom, TN, TC, TOC, and XRF data from NAK that correlating temporal changes in conductivity and pH from diatom transfer functions with depth does not properly represent the dynamic hydroclimate for 35 ka. Instead, over the past 35 ka, anoxic clays with low species richness and abundant *Thalassiosira rudolfi* (a high conductivity/pH preference taxa) reflect highly productive and/or deeper waters with limited mixing, potentially reflecting changes in SST related to DO events during the Late Pleistocene. The record found a wet phase ~35.6 ka corresponding with DO7, a dry phase of unknown length from <35.6 ka until a desiccation phase 3.14 m later, a wet phase before H2 ~23.9 ka, a dry phase that coincides with the LGM from ~23.9-18.7 ka, a wet phase from ~18.7-17.5 ka, a dry phase from ~17.5-15.4 ka corresponding with H1, and a wet phase representing the AHP where conditions are more variable ~15.4 ka, become stable from ~13.7-12.7 ka, until the record is lost after ~12.7 ka. Similar DO signals at Chew Bahir highlight potential teleconnections between high-latitude SST and African rainfall during this time across the EARS.

While this record's archaeological significance cannot currently be explored with the lack of the age model in the lower parts of the core, this record will be relevant to the numerous archaeological records across the Nakuru-Elmenteita and Naivasha Basins. Of relevance are questions related to the asynchronous transition from the Middle Stone Age to the Late Stone Age across equatorial Eastern Africa (Blegen et al., 2017; Van Baelen et al., 2019) as well as better understanding potential relationships between Ambrose's (1984) Eburran phases with potential changes in environments during the Holocene. Sites within these basins that can benefit from this record include, but are not limited to, Enkapune Ya Muto (Ambrose, 1998), Marmonet Drift (Ambrose, 2002; Slater, 2016), and Prolonged Drift (Merrick, 1975).

3.7. FIGURES

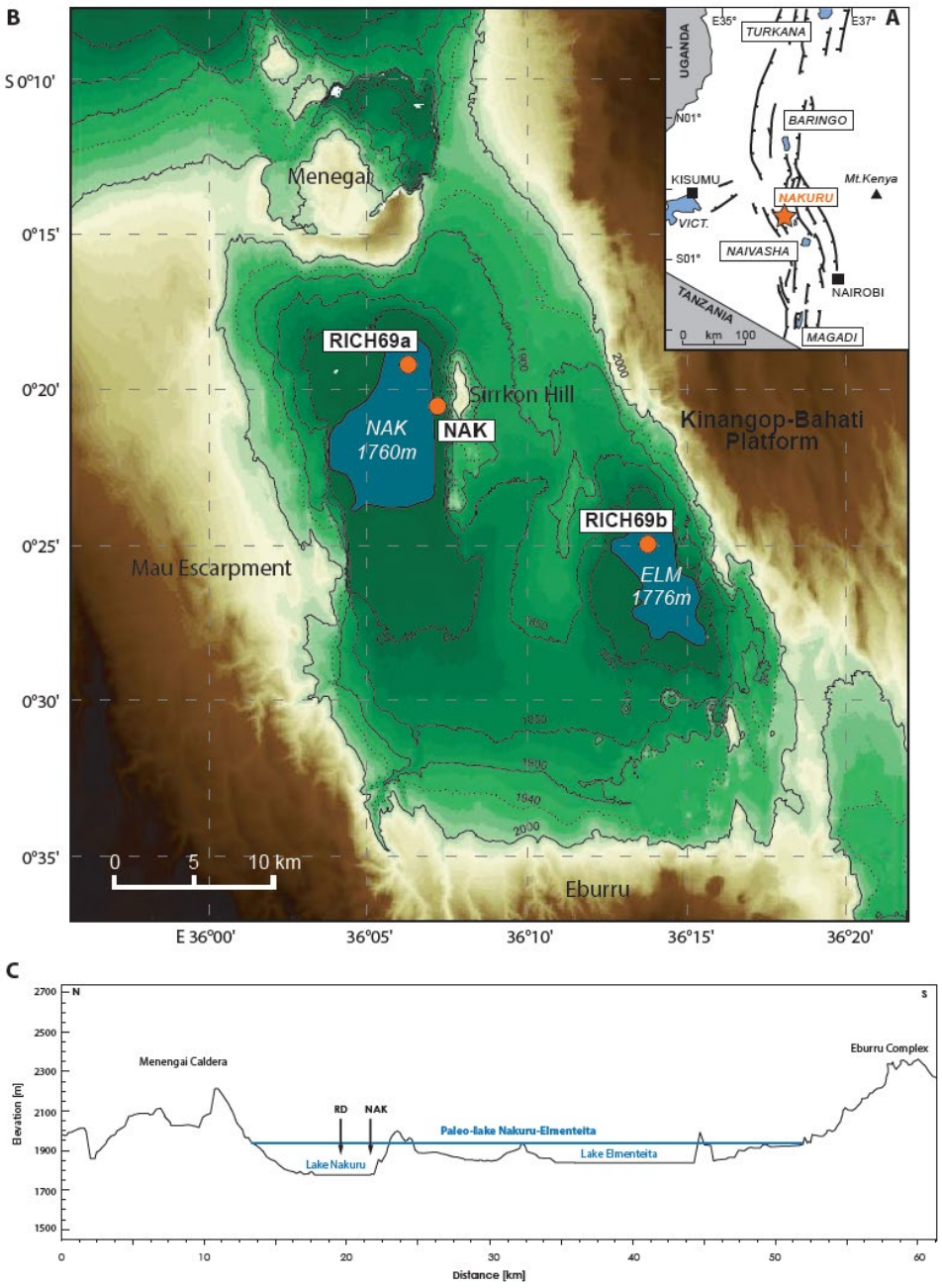

Figure 1 (previous page): A) Map of the Kenyan Eastern Branch of the East African Rift System with other basins labeled and Nakuru starred and highlighted. **B)** Topographic map of the Nakuru-Elmenteita Basin with the modern levels of the lakes shown. Topographic levels at 50-m intervals with the African Humid Period highstand at 1940 meters above sea level (Washbourn-Kamau, 1972). NAK is the core from this study. RICH69 are the cores studied by Cohen & Nielson (1986) and Richard & Dussinger (1986). **C)** Cross section across the Nakuru-Elmenteita Basin with the highstand from the African Humid Period highlighted and the two Nakuru cores from Richardson & Dussinger (1986) and this study labeled.

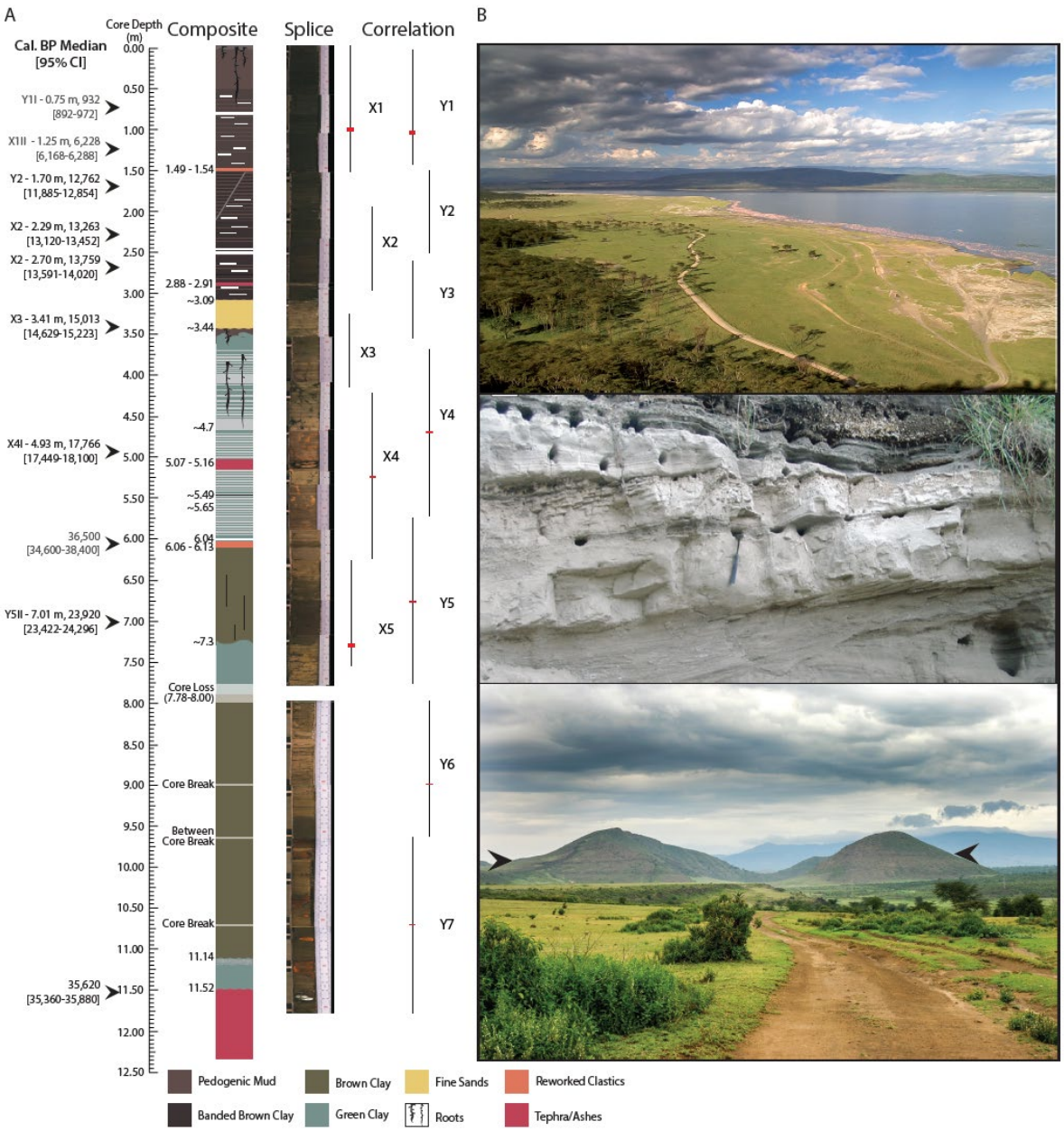

Figure 2: A) Stratigraphic column of the composite core (NAK) with the approximate composite depth of features included. A photographic splice of the cores used for the composite taken in 2019 is included. The location of the two cores in relation to one another is also included. All successful calibrated ages are included, with ages not included in the age model in a gray rather than black. **B)** Field photos of Nakuru from 2004, included an overhead image, a close up of lake sediments around the basin, and paleoshorelines of former highstands from the basin floor marked with arrows.

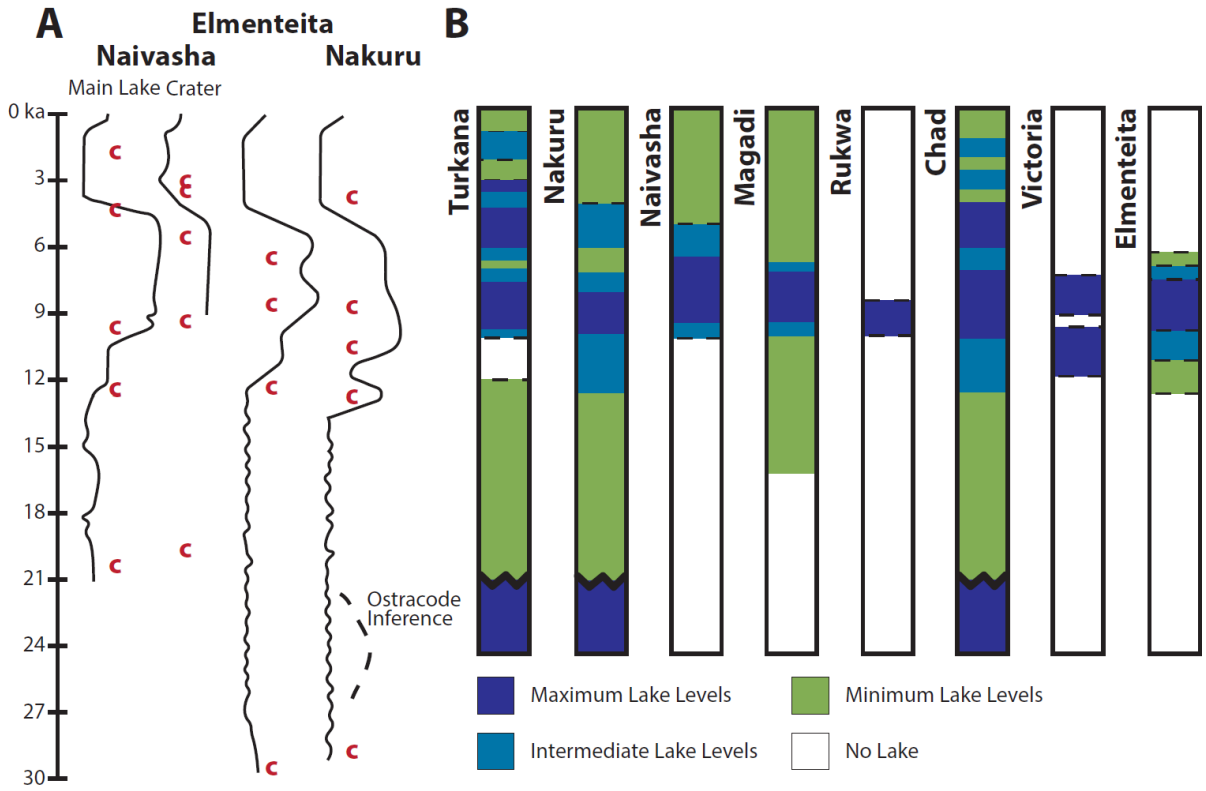

Figure 3: A) Updated figure from Richardson & Dussinger (1986) on the lake levels across Nakuru, Elmenteita, and Naivasha based on diatom data. Nakuru also has additional ostracod data as the dashed line from Cohen et al. (1983). Locations of uncalibrated radiocarbon dates are marked with the red C's. **B)** Updated figure from Cohen & Nielson (1986). The wiggled line represents a period older than 20 kyr uncalBP. Dashed borders represent uncertain timing in the data.

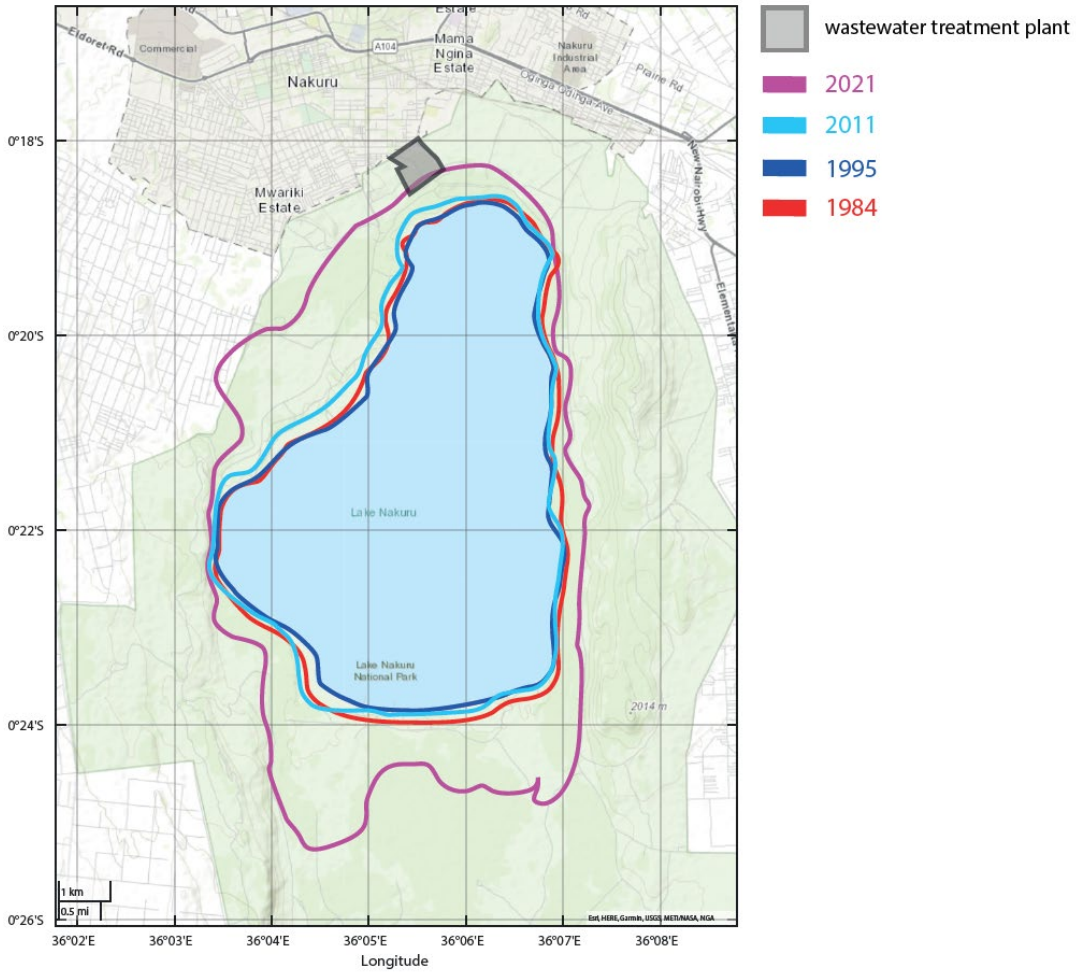

Figure 4: Lake-level changes at Lake Nakuru over the past 40 years. Map generated using "geoscatter" function in MATLAB® and shoreline information from Copernicus satellite data (Google Earth Pro, 2021).

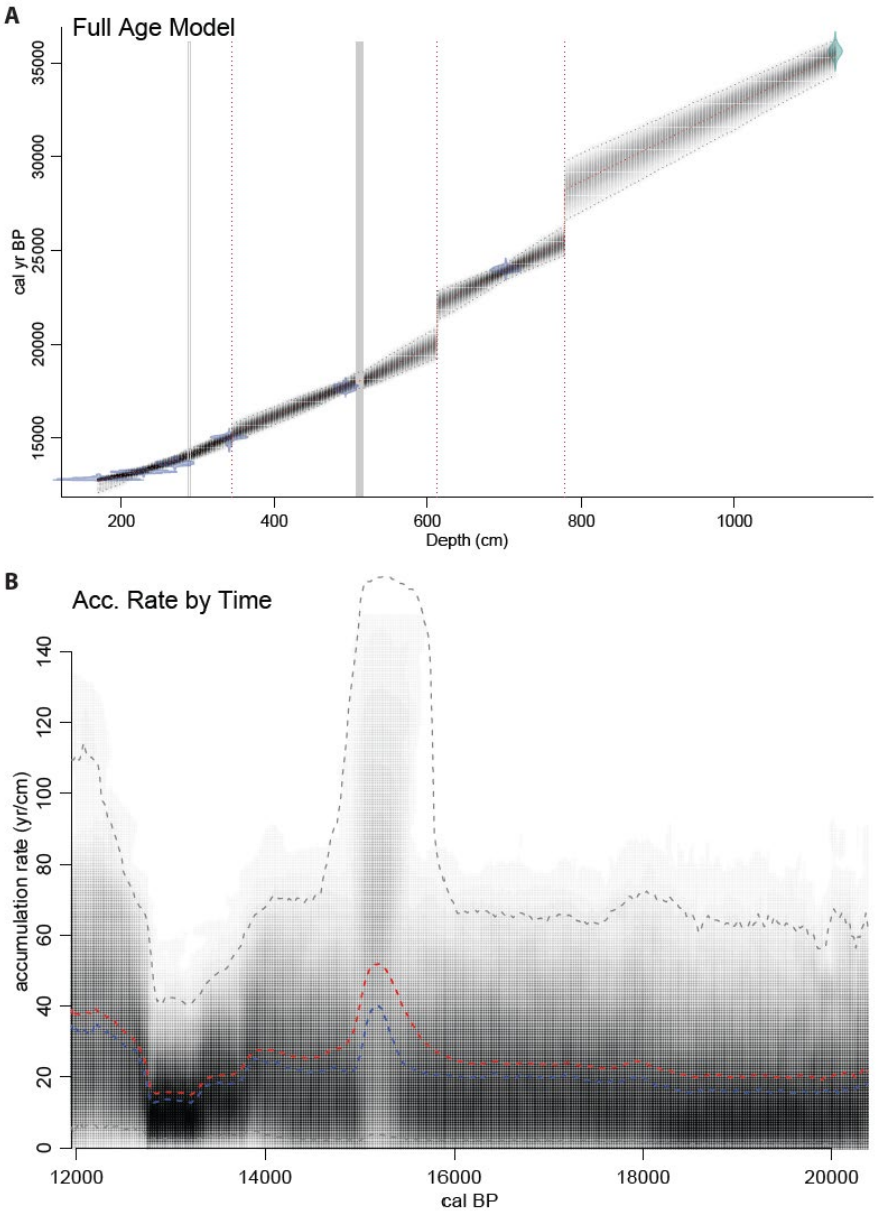

Figure 5: A) Complete age model for NAK starting at the first measured age at 170 cm. Slumps occur between 288-290 and 507-516 cm. Hiatuses occur at 344, 613, and 778 cm. **B)** Accumulation rate by time for the only part of the age model that was used for this study from 150 to 613 cm. A ghost plot shows the average (blue), median (red), and 95% confidence intervals (gray dotted lines).

Figure 6 (next page): Organic proxies against NAK core with ages. TOC/N is highlighted so that the blue color represents periods of mostly phytoplankton input, whereas green indicates mostly terrestrial input based on Meyers (1994). The mean TOC and TN are in black with 95% confidence intervals in gray. Diatom concentration calculated as described in methods. The diatom taxa that reached ≥10% in at least one sample are then included and organized by habitat with green as littoral (shoreline), light blue as littoral planktonic, and dark blue as planktonic. Diatoms with unknown habitats are in gray. Species richness is also included. The various zones are included created using hierarchical clustering with Bray-Curtis dissimilarity with all of the diatom counts.

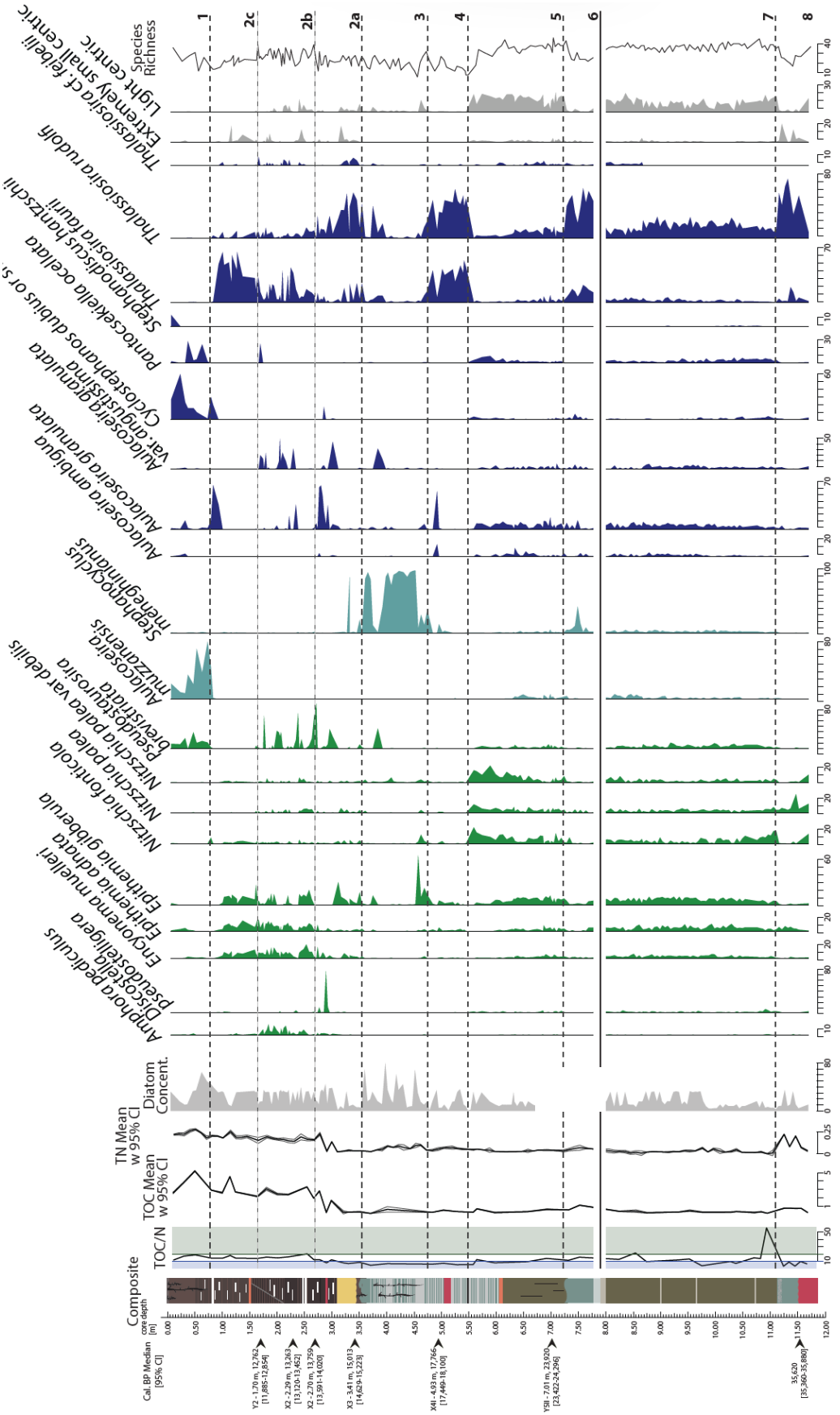
Species Richness
Light centric
Extremely small centric
Thalassiosira cf. fjelbellii
Thalassiosira rudolfi
Thalassiosira faurii
Thalassiosira lacustris
Stephanodiscus hantzschii
Stephanodiscus cf. parvus
Cyclostephanos dubius
Aulacoseira granulata var. angustissima
Aulacoseira granulata
Aulacoseira ambigua
Stephanocyclus meneghiniana
Aulacoseira muzzanensis
Aulacoseira ambigua
Pseudostaurosira brevistriata
Nitzschia palea
Nitzschia fonticola
Epithemia gibberula
Epithemia adnata
Encyonema muelleri
Pseudostaurosira pseudoconstruens
Amphora pediculus
Diatom Concent.
TN Mean w 95% CI
TOC Mean w 95% CI
TOC/N
Composite
core depth [m]
Cal. BP Median [95% CI]
1
2c
2b
2a
3
4
5
6
7
8
Y2 - 1.70 m, 12,762 [11,885–12,854]
X2 - 2.29 m, 13,263 [13,120–13,452]
X2 - 2.70 m, 13,759 [13,591–14,020]
X3 - 3.41 m, 15,013 [14,629–15,223]
X41 - 4.93 m, 17,766 [17,449–18,100]
Y5II - 7.01 m, 23,920 [23,422–24,296]
35,620 [35,360–35,880]

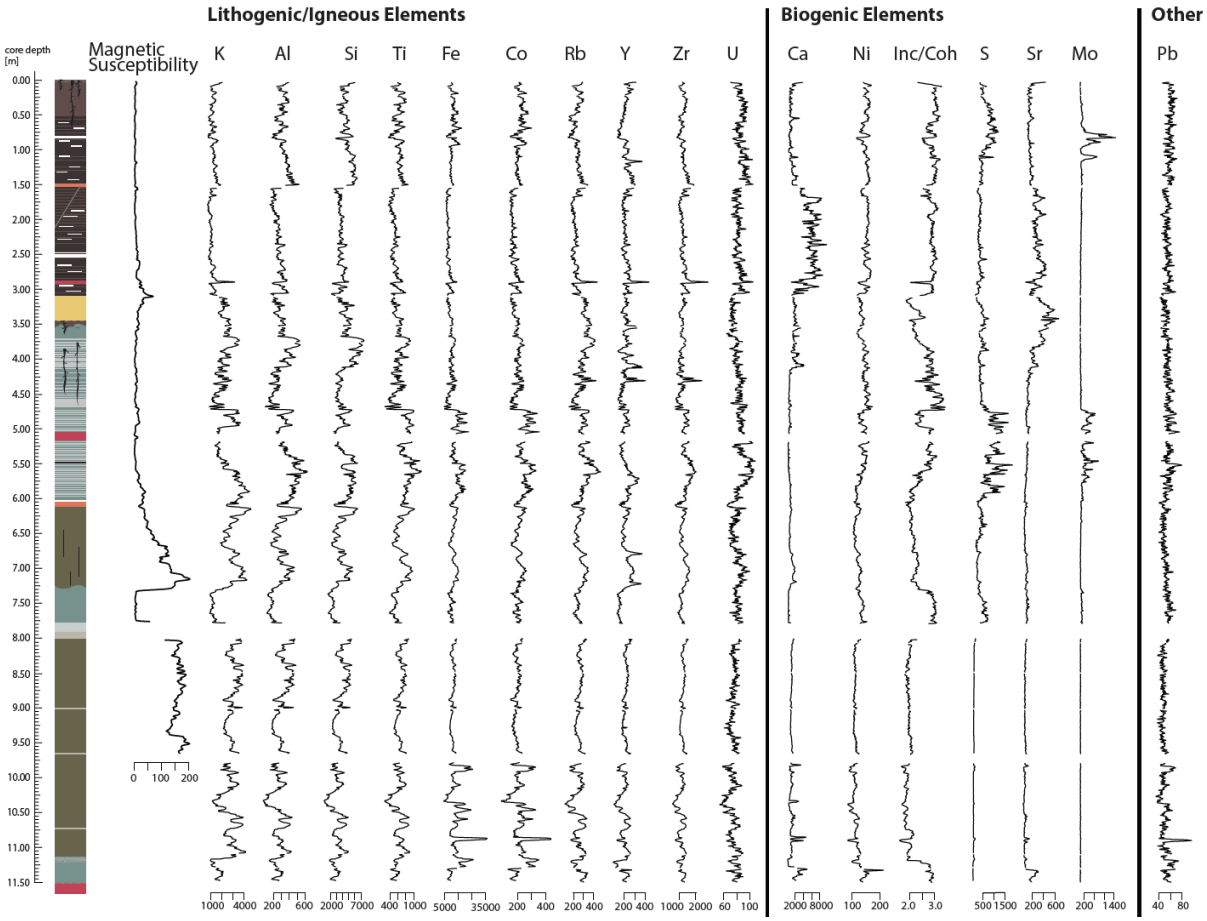

Figure 7: NAK with smoothed magnetic susceptibility and XRF data in counts per second (cps). Elements included in this figure were also included in the PCA.

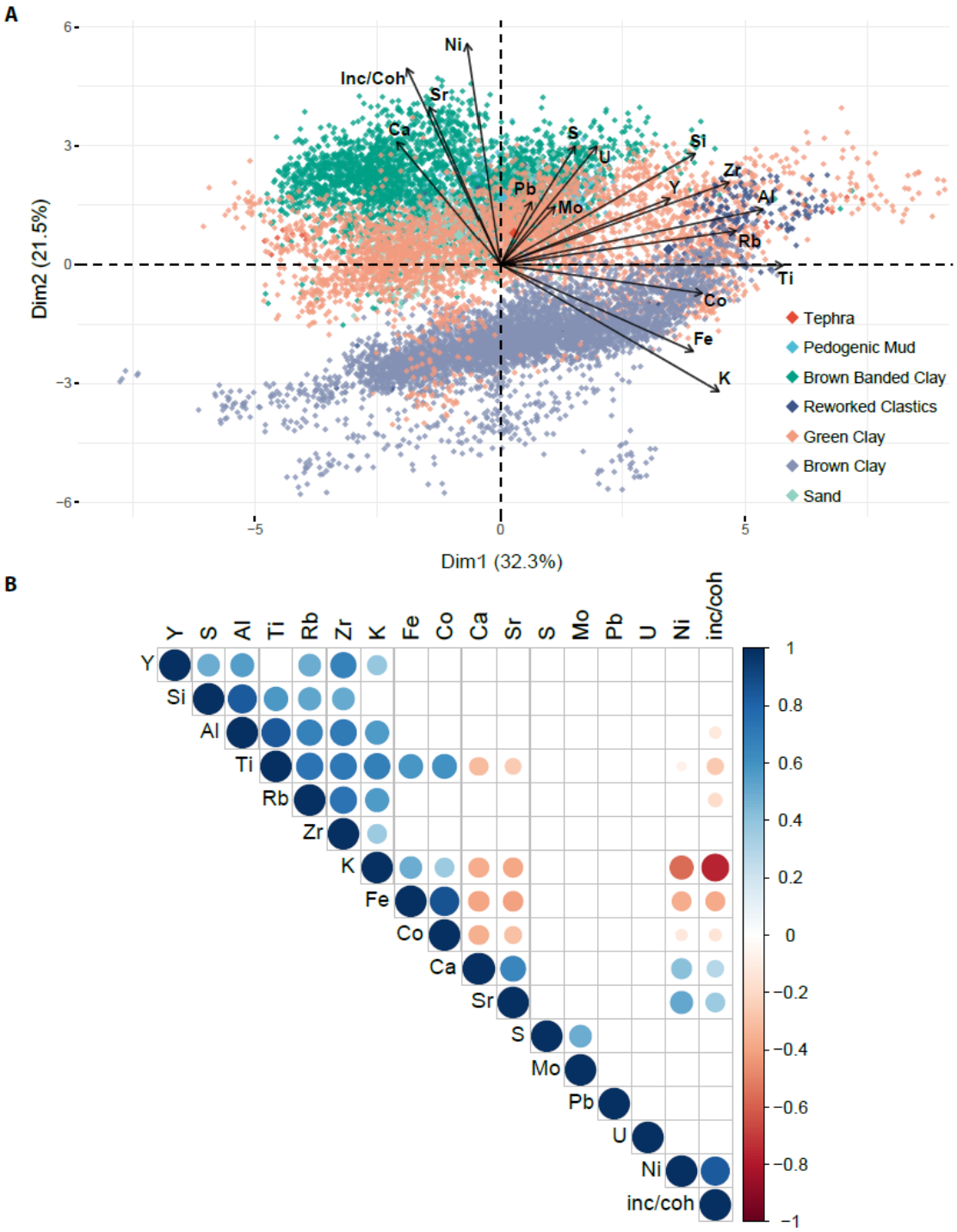

Figure 8: A) Biplot of XRF PCA colored by the lithologies. Dim1 appears to be a precipitation proxy where positive values represent less weathered volcanic sediments. Dim2 appears to represent amount of organic matter in the sediments. **B)** Correlation Matrix of the different elements included in the PCA colored by significant positive or negative correlation.

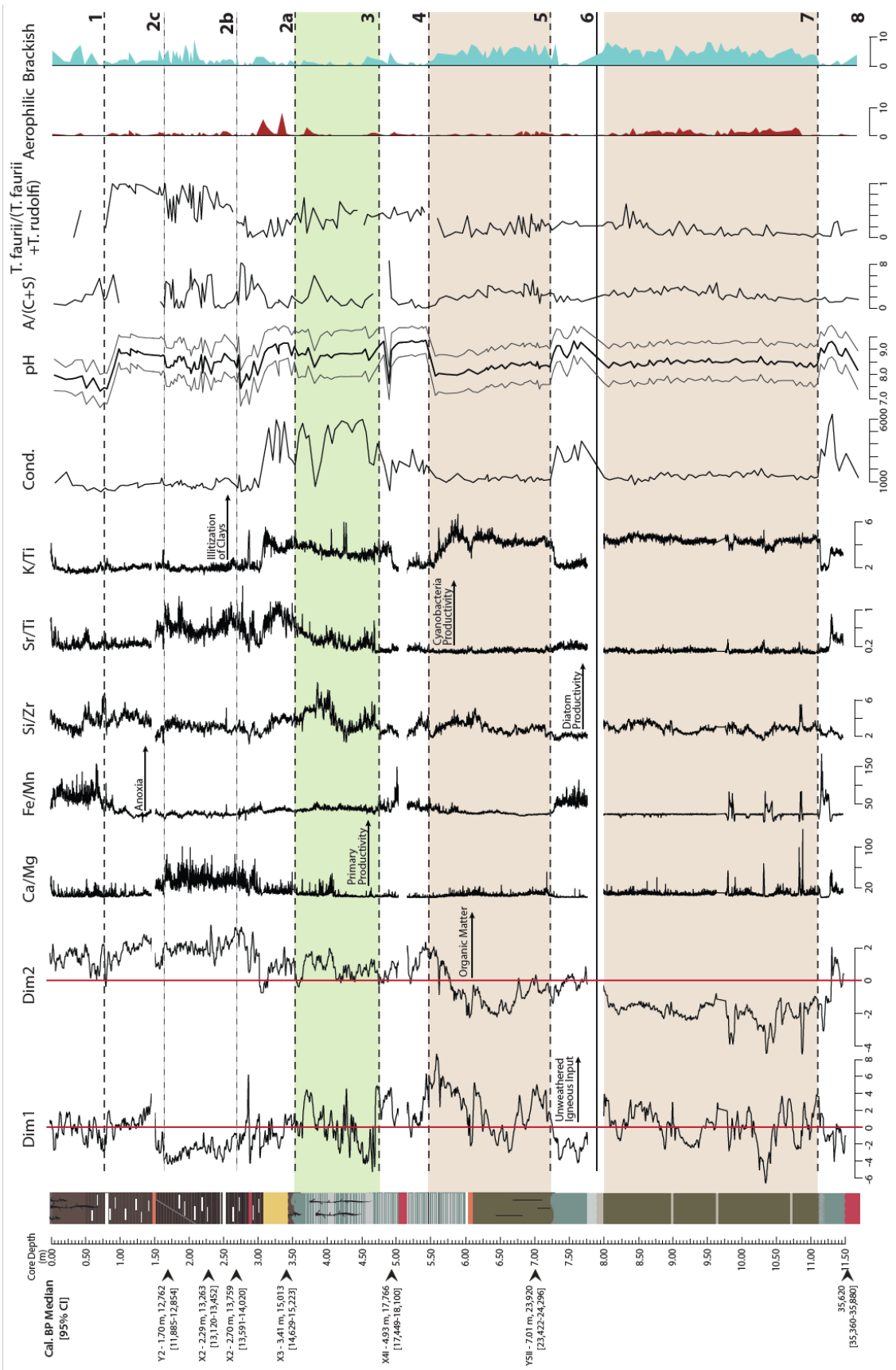
1
2c
2b
2a
3
4
5
6
7
8
Brackish
Aerophilic
T. faurii/(T. faurii +T. rudolfi)
A/(C+S)
pH
Cond.
K/Ti
Sr/Ti
Si/Zr
Fe/Mn
Ca/Mg
Dim2
Dim1
Illitization of Clays
Anoxia
Primary Productivity
Organic Matter
Cyanobacteria Productivity
Diatom Productivity
Unweathered Igneous Input
Core Depth (m)
Cal. BP Median [95% CI]
Y2 - 1.70 m, 12,762 [11,885-12,854]
X2 - 2.29 m, 13,263 [13,120-13,452]
X2 - 2.70 m, 13,759 [13,591-14,020]
X3 - 3.41 m, 15,013 [14,629-15,223]
X4I - 4.93 m, 17,766 [17,449-18,100]
YSII - 7.01 m, 23,920 [23,422-24,296]
35,620 [35,360-35,880]

Figure 9 (previous page): NAK with ages alongside the smoothed PCA loadings of Dim 1 and 2; important XRF ratios; and diatom proxy interpretations. The diatom proxies include the conductivity and pH results from the transfer function by Gasse et al. (1995); a mixing proxy (A/(C+S)) from Gasse et al. (2002); a fresh, deep water proxy (T. faurii/(T. faurii + T. rudolfi)) from this study; and aerophilic and brackish taxa based on Gasse (1986) and Taylor et al. (2007) included in Suppl. 3. The diatom zones outlined in the discussion are highlighted with brown zones indicating shallow conditions and the green zone indicating highlighly alkaline conditions.

Figure 10 (next page): Comparison of lake records across the EARS adapted from Foerster et al. (2012). These are compared with the precession cycle, Dansgaard-Oeschger (DO) events (blue), and Heinrich (H) events (tan). Precession data is from Berger & Loutre (1991). NGRIP data highlights the DO cycles which are numbered (North Greenland Ice Core Project Members, 2004) using δ18O data. The Arabian Sea record from core RC27-14 is from Altabet et al. (2002) using δ15N as a proxy for denitrification and productivity in the Gulf of Oman. The Lake Tanganyika record is from δD of leaf wax to record precipitation variability from Tierney et al. (2008) with a reversed scale. Chew Bahir K record is from Foerster et al. (2012), with a reversed scale. The Lake Masoko record from Barker et al. (2003) uses DCA Axis 1 which was a precipitation-evaporation proxy for water depth using diatom data. The Burundi Highlands record is a precipitation change estimate in mm/yr from pollen records from Bonnefille & Chalie (2000) with the average in black. The δD left wax record from Garelick et al. (2021) from Lake Rukundu on Mount Kenya with a reversed scale is used as a local comparison. The dark line represents the leaf wax data corrected for vegetation and global ice volume whereas the lighter gray line is only corrected for vegetation. Lastly, K/Ti and Dim1, both reversed precipitation proxies, from Lake Nakuru from this study. The top portion uses the calculated age model. The bottom of the record aligns the two dates from this section as tie points to the other records, but is plotted by depth of the core between.

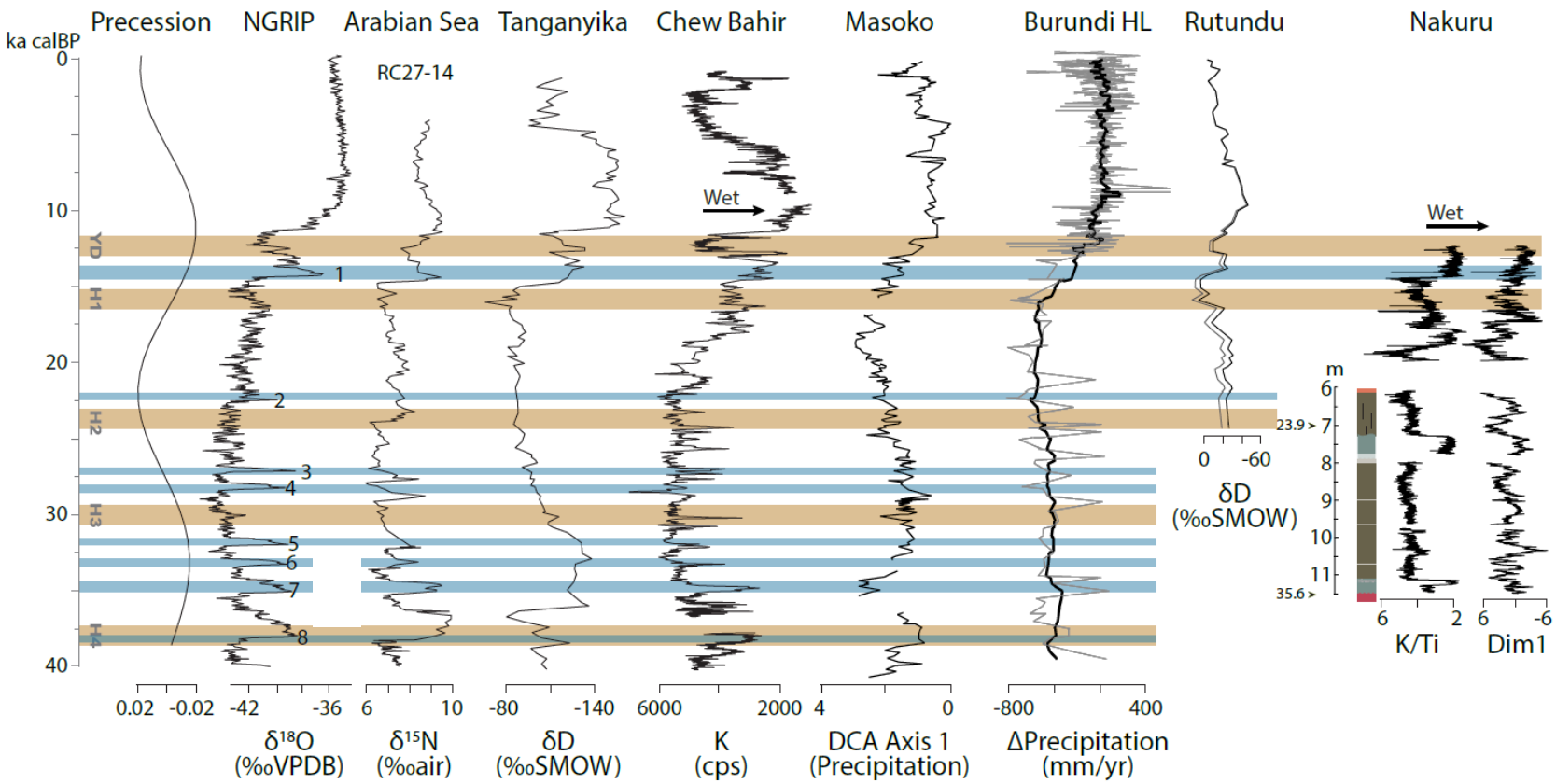
Precession
NGRIP
Arabian Sea
RC27-14
Tanganyika
Chew Bahir
Masoko
Burundi HL
Rutundu
Nakuru
ka calBP
0
10
20
30
40
YD
H1
H2
H3
H4
1
2
3
4
5
6
7
8
Wet
Wet
0.02 -0.02
-42 -36
δ18O (‰VPDB)
6 10
δ15N (‰air)
-80 -140
δD (‰SMOW)
6000 2000
K (cps)
4 0
DCA Axis 1 (Precipitation)
-800 400
ΔPrecipitation (mm/yr)
0 -60
δD (‰SMOW)
m
6
7
8
9
10
11
23.9
35.6
6 2
K/Ti
6 -6
Dim1

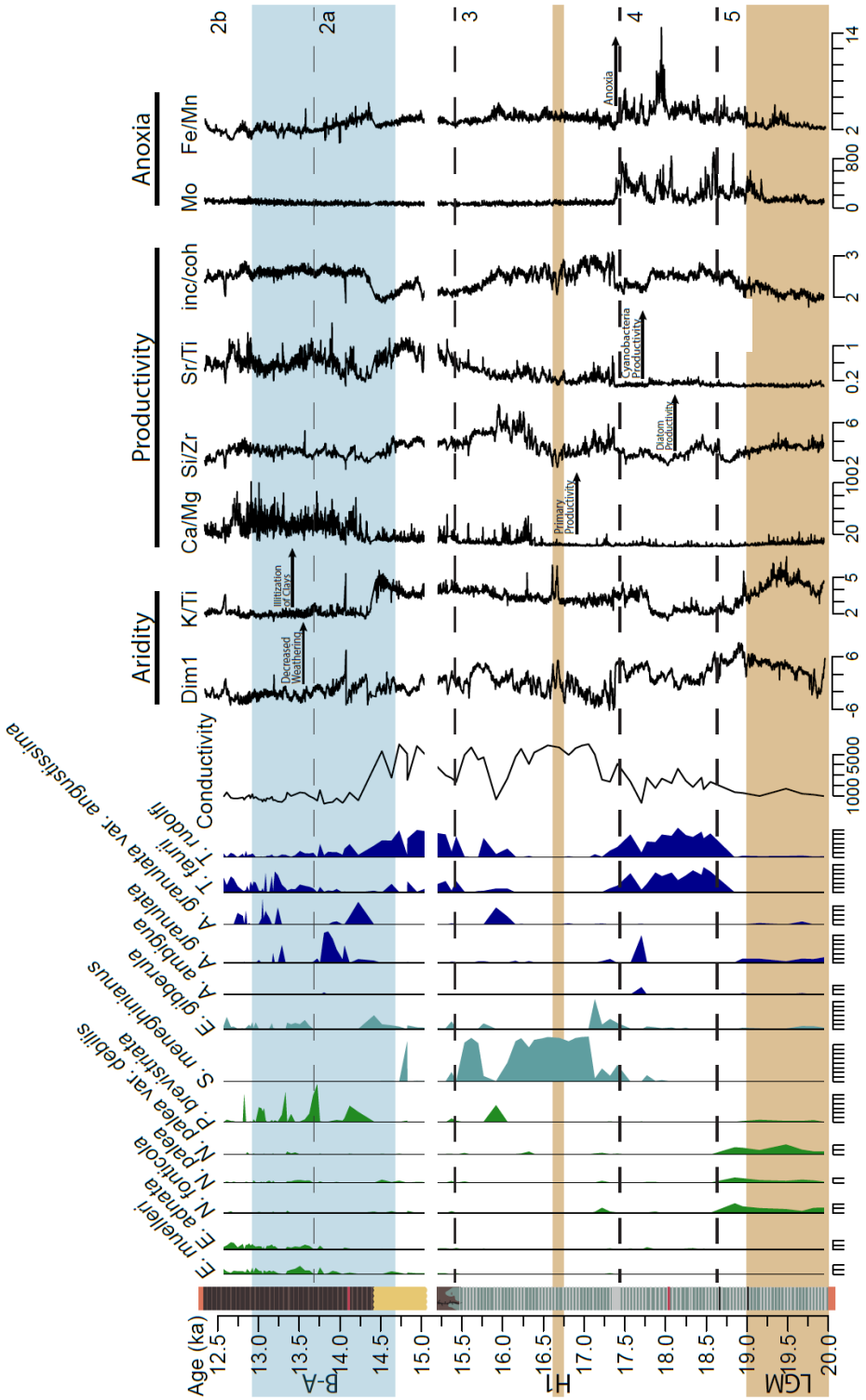

Figure 11: Important parameters along the age model for NAK including diatom taxa that represent >10% in one sample, calculated conductivity, aridity indices (Dim1 and K/Ti), productivity indices (Ca/Mg, Si/Zr, Sr/Ti, and inc/coh), and anoxia indices (Mo and Fe/Mn). Global climate phases are highlighted with anticipated dry phases (Last Glacial Maximum, LGM and Heinrich 1, H1) and the anticipated wet phase in blue (Bølling–Allerød interstadial, B-A).

3.8. TABLES

Table 1: Measured parameters of Nakuru from Jirsa et al. (2013) and Hecky & Kilham (1973). All cations and compounds are measured in mg/L. The Jirsa et al. data reported is the median value. This data was collected during a drought. All other cations measured by Jirsa et al. were <1: Mn 0.021, Fe 0.052, Zn 0.011, As 0.043, Sr 0.033, Mo 0.723, Ba 0.055.

Source	Year	Temp. °C	Cond. (µS/cm)	pH	Na	K	Ca	Mg	SO_4	Cl	HCO_3+CO_3	SiO_2	Si	PO_4	F	NO_3
Hecky & Kilham 1973	1969		10,010	9.8	3,300	237		0.9	62	1,020	121.6*	208		13.6	129	
Jirsa et al 2013	2008-2009	24.8	38,300	10.1	13,560	447	3.6	0.06	444	5,080	22,220		105.1		740	23.6

*Measured in meq/L

Table 2: Samples used to date the Nakuru cores. Table includes the sample name, the core location, the composite location, the sample type, the uncalibrated ages and their errors, the calibrated median ages and their errors using RCarbon (Crema & Brevan, 2021), and the calibrated median ages and their errors from within the age model (Blaauw & Christen, 2011).

Sample Name	Core Sample	NAK Location (m)	Sample Type	Uncal. Age	Error (95% CI)	Cal. Median	Cal. Error (95% CI)	Cal. Median (AM)	Cal. Error (AM) (95% CI)
NAK-AJ-17	Y1I 68-72	0.75	Charcoal	1020	±30	932	±40	931	-19, +41
NAK-AJ-02	X1II 18-23	1.25	Charcoal	5400	±30	6228	±60	6227	-49, +61
BER_PDM NAK-10	Y2 15-20	1.70	Charcoal	10925	±45	12822	±134	12762	-877, +92
NAK-AJ-03	X2 28-33	2.29	Charcoal	11340	±60	13225	±95	13263	-143, +189
BER_PDM NAK-03	X2 68-73	2.70	Charcoal	11844	±78	13692	±305	13759	-168, +261
BER_PDM NAK-07	X3 8-10	3.41	Charcoal	12660	±50	15091	±166	15013	-384, +210
BER_PDM NAK-08	X4I 63-71	4.93	Paleoroot	14545	±55	17763	±236	17766	-317, +334
T111205_1		6.06	Ash	36500	±1900				
BER_PDM NAK-15	Y5II 19-24	7.01	Unknown	20020	±80	24024	±203	23920	-498, +376
T111206_2		11.54	Tephra	38900	±1100				
Menengai Tuff		11.54	Tephra	35620	±620				

*The date used for the tephra at the bottom of the section for the age model is from (Blegen et al., 2016) as our deposits are likely the Menengai Tuff and this date is more constrained than the sample taken from NAK.

3.9. REFERENCES

Adolphi, F., C. B. Ramsey, T. Erhardt, R. L. Edwards, H. Cheng, C. S. M. Turney, A. Cooper, et al. 2018. "Connecting the Greenland Ice-Core and U/Th Timescales Via Cosmogenic Radionuclides: Testing the Synchroneity of Dansgaard–Oeschger Events." *Climate of the Past* 14 (11): 1755-1781. doi:10.5194/cp-14-1755-2018.

Altabet, M.A., Higginson, M.J., Murray, D.W., 2002. The effect of millennial-scale changes in Arabian Sea denitrification on atmospheric CO2. *Nature* 415, 159-162.

Ambrose, S. H. and N. E. Sikes. 1991. "Soil Carbon Isotope Evidence for Holocene Habitat Change in the Kenya Rift Valley." *Science* 253 (5026): 1402-1405.

Ambrose, S. H. 1984. *Holocene Environments and Human Adaptations in the Central Rift Valley, Kenya.* PhD Thesis. University of California, Berkeley.

———.1998. "Chronology of the Later Stone Age and Food Production in East Africa." *Journal of Archaeological Science* 25 (4): 377-392.

———.2002. "Small Things Remembered: Origins of Early Microlithic Industries in Sub-Saharan Africa." *Archeological Papers of the American Anthropological Association* 12 (1): 9-29. doi:10.1525/ap3a.2002.12.1.9.

Arbuszewski, J. A., P. B. deMenocal, C. Cléroux, L. Bradtmiller, and A. Mix. 2013. "Meridional Shifts of the Atlantic Intertropical Convergence Zone since the Last Glacial Maximum." *Nature Geoscience* 6 (11): 959-962. doi:10.1038/ngeo1961.

Baker, B. H. and J. Wohlenberg. 1971. "Structure and Evolution of the Kenya Rift Valley." *Nature (London)* 229 (5286): 538-542. doi:10.1038/229538a0.

Ballot, A., L. Krienitz, K. Kotut, C. Wiegand, J. S. Metcalf, G. A. Codd, and S. Pflugmacher. 2004. "Cyanobacteria and Cyanobacterial Toxins in Three Alkaline Rift Valley Lakes of Kenya—Lakes Bogoria, Nakuru and Elmenteita." *Journal of Plankton Research* 26 (8): 925-935. doi:10.1093/plankt/fbh084.

Barker, P. A., M. R. Talbot, F. Street-Perrott, F. Marret, J. Scourse, and E. O. Odada. 2004. "Late Quaternary Climatic Variability in Intertropical Africa." In *Past Climate Variability through Europe and Africa*, edited by R. W. Battarbee, F. Gasse and C. E. Stickley, 117-138. Dordrecht: Springer Netherlands.

Barker, P., R. Telford, F. Gasse, and F. Thevenon. 2002. "Late Pleistocene and Holocene Palaeohydrology of Lake Rukwa, Tanzania, Inferred from Diatom Analysis." *Palaeogeography, Palaeoclimatology, Palaeoecology* 187 (3): 295-305. doi:10.1016/S0031-0182(02)00482-0.

Barker, P., D. Williamson, F. Gasse, and E. Gibert. 2003. "Climatic and Volcanic Forcing Revealed in a 50,000-Year Diatom Record from Lake Massoko, Tanzania." *Quaternary Research* 60 (3): 368-376. doi:10.1016/j.yqres.2003.07.001.

Battarbee, R. W. 1986. "Diatom Analysis." In *Handbook of Holocene Palaeoecology & Palaeohydrology*, edited by B. E. Berglund, 527-570.

Battarbee, R. W., S. Juggins, F. Gasse, N. J. Anderson, H. Bennion, N. G. Cameron, D. B. Ryves, C. Pailles, F. Chalie, and R. Telford. 2001. "European Diatom Database (EDDI). an Information System for Palaeoenvironmental Reconstruction." *ECRC Research Report* (81): 1-94.

Bergner, A. G. N., M. H. Trauth, and B. Bookhagen. 2003. "Paleoprecipitation Estimates for the Lake Naivasha Basin (Kenya) during the Last 175 K.Y. using a Lake-Balance Model." *Global and Planetary Change* 36 (1): 117-136. doi:10.1016/S0921-8181(02)00178-9.

Beuning, K. R. M., M. R. Talbot, and K. Kelts. 1997. "A Revised 30,000-Year Paleoclimatic and Paleohydrologic History of Lake Albert, East Africa." *Palaeogeography, Palaeoclimatology, Palaeoecology* 136 (1-4): 259-279. doi:10.1016/S0031-0182(97)00034-5.

Blaauw, M. and J. A. Christen. 2011. "Flexible Paleoclimate Age-Depth Models using an Autoregressive Gamma Process." *Bayesian Analysis* 6 (3): 457-474. doi:10.1214/ba/1339616472.

Blegen, N., F. H. Brown, B. R. Jicha, K. M. Binetti, J. T. Faith, J. V. Ferraro, P. N. Gathogo, J. L. Richardson, and C. A. Tryon. 2016. "The Menengai Tuff: A 36 Ka Widespread Tephra and its Chronological Relevance to Late Pleistocene Human Evolution in East Africa." *Quaternary Science Reviews* 152: 152-168. doi:10.1016/j.quascirev.2016.09.020.

Blegen, N., T. Faith, A. Mant-Melville, D. J. Peppe, and C. A. Tryon. 2017. "The Middle Stone Age After 50,000 Years Ago: New Evidence from the Late Pleistocene Sediments of the Eastern Lake Victoria Basin, Western Kenya." *PaleoAnthropology* 2017: 139-169.

Bond, G., H. Heinrich, W. Broecker, L. Labeyrie, J. McManus, J. Andrews, S. Huon, et al. 1992. "Evidence for Massive Discharges of Icebergs into the North Atlantic Ocean during the Last Glacial Period." *Nature (London)* 360 (6401): 245-249. doi:10.1038/360245a0.

Bonnefille, R. and F. Chalié. 2000. "Pollen-Inferred Precipitation Time-Series from Equatorial Mountains, Africa, the Last 40 Kyr BP." *Global and Planetary Change* 26 (1): 25-50. doi:10.1016/S0921-8181(00)00032-1.

Braconnot, P., C. Marzin, L. Grégoire, E. Mosquet, and O. Marti. 2008. "Monsoon Response to Changes in Earth's Orbital Parameters: Comparisons between Simulations of the Eemian and of the Holocene." *Climate of the Past* 4 (4): 281-294. doi:10.5194/cp-4-281-2008.

Brauer, A. 2004. "Annually Laminated Lake Sediments and their Palaeoclimatic Relevance." *The Climate in Historical Times: Towards a Synthesis of Holocene Proxy Data and Climate Models*: 109-127.

Brindle, M., J. Mohan, C. Beck, and J. R. Stone. 2018. "Three Novel Species of Bacillariophyta (Diatoms) in the Genera Surirella and Thalassiosira from Pleistocene Paleolake Lorenyang (~2 - 1.6 Ma) Turkana Basin, Kenya." *Phytotaxa* 371 (3): 230. doi:10.11646/phytotaxa.371.3.6.

Broecker, W. S. and A. E. Putname. 2013. "Hydrologic Impacts of Past Shifts of Earth's Thermal Equator Offer Insight into those to be Produced by Fossil Fuel CO2." *PNAS* 110 (42): 16710-16715. doi:10.1073/pnas.1301855110.

Brothers, S., J. Köhler, K. Attermeyer, H. P. Grossart, T. Mehner, N. Meyer, K. Scharnweber, and S. Hilt. 2014. "A Feedback Loop Links Brownification and Anoxia in a Temperate, Shallow Lake." *Limnology and Oceanography* 59 (4): 1388-1398. doi:10.4319/lo.2014.59.4.1388.

Budsky, A., J. A. Wassenburg, R. Mertz-Kraus, C. Spötl, K. P. Jochum, L. Gibert, and D. Scholz. 2019. "Western Mediterranean Climate Response to Dansgaard/Oeschger Events: New Insights from Speleothem Records." *Geophysical Research Letters* 46 (15): 9042-9053. doi:10.1029/2019GL084009.

Burnett, A. P., M. J. Soreghan, C. A. Scholz, and E. T. Brown. 2011. "Tropical East African Climate Change and its Relation to Global Climate: A Record from Lake Tanganyika, Tropical East Africa, Over the Past 90+ Kyr." *Palaeogeography, Palaeoclimatology, Palaeoecology* 303 (1): 155-167. doi:10.1016/j.palaeo.2010.02.011.

Butzer, K. W., G. L. Isaac, J. L. Richardson, and C. Washbourn-Kamau. 1972. "Radiocarbon Dating of East African Lake Levels." *Science* 175 (4026): 1069-1076.

Cantonati, M., S. Scola, N. Angeli, G. Guella, and R. Frassanito. 2009. "Environmental Controls of Epilithic Diatom Depth-Distribution in an Oligotrophic Lake Characterized by Marked Water-Level Fluctuations." *European Journal of Phycology* 44 (1): 15-29. doi:10.1080/09670260802079335.

Chalié, F. and F. Gasse. 2002. "Late Glacial–Holocene Diatom Record of Water Chemistry and Lake Level Change from the Tropical East African Rift Lake Abiyata (Ethiopia)." *Palaeogeography, Palaeoclimatology, Palaeoecology* 187 (3): 259-283. doi:10.1016/S0031-0182(02)00480-7.

Cheng, H., R. L. Edwards, A. Sinha, C. Spötl, L. Yi, S. Chen, M. Kelly, et al. 2016. "The Asian Monsoon Over the Past 640,000 Years and Ice Age Terminations." *Nature (London)* 534 (7609): 640-646. doi:10.1038/nature18591.

Cheng, H., R. L. Edwards, C.-C. Shen, V. J. Polyak, Y. Asmerom, J. Woodhead, J. Hellstrom, et al. 2013. "Improvements in 230Th Dating, 230Th and 234U Half-Life Values, and U–Th Isotopic Measurements by Multi-Collector Inductively Coupled Plasma Mass Spectrometry." *Earth and Planetary Science Letters* 371-372: 82-91. doi:10.1016/j.epsl.2013.04.006.

Cheng, H., A. Sinha, F. W. Cruz, X. Wang, R. L. Edwards, F. M. D'Horta, C. C. Ribas, M. Vuille, L. D. Stott, and A. S. Auler. 2013. "Climate Change Patterns in Amazonia and Biodiversity." *Nature Communications* 4 (1): 1411. doi:10.1038/ncomms2415.

Cimatoribus, A. A., S. S. Drijfhout, V. Livina, and G. van der Schrier. 2013. "Dansgaard–Oeschger Events: Bifurcation Points in the Climate System." *Climate of the Past* 9 (1): 323-333. doi:10.5194/cp-9-323-2013.

Clark, P. U., A. S. Dyke, J. D. Shakun, A. E. Carlson, J. Clark, B. Wohlfarth, J. X. Mitrovica, S. W. Hostetler, and A. M. McCabe. 2009. "The Last Glacial Maximum." *Science* 325 (5941): 710-714. doi:10.1126/science.1172873.

Cocquyt, C. 1998. *Diatoms from the Northern Basin of Lake Tanganyika*. Berlin: J. Cramer.

Cocquyt, C. and D. Verschuren. 2023. "Checklist of the Diatoms from Lake Naivasha, Kenya, with some Historical Notes." *PhytoKeys* 224 (1): 101-174. doi:10.3897/phytokeys.224.98168.

Cohen, A. S., R. Dussinger, and J. Richardson. 1983. "Lacustrine Paleochemical Interpretations Based on Eastern and Southern African Ostracodes." *Palaeogeography, Palaeoclimatology, Palaeoecology* 43 (1): 129-151. doi:10.1016/0031-0182(83)90051-2.

Cohen, A. S. and C. Nielsen. 1986. "Ostracodes as Indicators of Paleohydrochemistry in Lakes; a Late Quaternary Example from Lake Elmenteita, Kenya." *Palaios* 1 (6): 601-609. doi:10.2307/3514710.

Cole, S. 1963. *The Prehistory of East Africa*. New York: Macmillan.

Conti, P., M. Pistis, S. Bernardinetti, A. Barbagli, A. Zirulia, L. Serri, T. Colonna, E. Guastaldi, and G. Ghiglieri. 2021. "Tectonic Setting of the Kenya Rift in the Nakuru Area, Based on Geophysical Prospecting." *Geosciences (Basel)* 11 (2): 80. doi:10.3390/geosciences11020080.

Crema E. R. & Bevan, A. 2021. “Inference from large sets of radiocarbon dates: software and methods.” *Radiocarbon* 63, 23-39. https://dx.doi.org/10.1017/RDC.2020.95.

Dansgaard, W., S. J. Johnsen, H. B. Clausen, D. Dahl-Jensen, N. S. Gundestrup, C. U. Hammer, C. S. Hvidberg, et al. 1993. "Evidence for General Instability of Past Climate from a 250-Kyr Ice-Core Record." *Nature (London)* 364 (6434): 218-220. doi:10.1038/364218a0.

Dansgaard, W., S. J. Johnsen, J. Møller, and C. C. Langway. 1969. "One Thousand Centuries of Climatic Record from Camp Century on the Greenland Ice Sheet." *Science* 166 (3903): 377-381. doi:10.1126/science.166.3903.377.

Davies, S. J., H. F. Lamb, and S. J. Roberts. 2015. "Micro-XRF Core Scanning in Palaeolimnology: Recent Developments." In *Micro-XRF Studies of Sediment Cores*, edited by I. W. Croudace and R. G. Rothwell. Vol. 17, 189-226: Springer.

De Cort, G., I. Bessems, E. Keppens, F. Mees, B. Cumming, and D. Verschuren. 2013. "Late-Holocene and Recent Hydroclimatic Variability in the Central Kenya Rift Valley: The Sediment Record of Hypersaline Lakes Bogoria, Nakuru and Elementeita." *Palaeogeography, Palaeoclimatology, Palaeoecology* 388: 69-80. doi:10.1016/j.palaeo.2013.07.029.

deMenocal, P. B. 1995. "Plio-Pleistocene African Climate." *Science* 270 (5233): 53-59. doi:10.1126/science.270.5233.53.

Deplazes, G., A. Lückge, L. C. Peterson, A. Timmermann, Y. Hamann, K. A. Hughen, U. Röhl, et al. 2013. "Links between Tropical Rainfall and North Atlantic Climate during the Last Glacial Period." *Nature Geoscience* 6 (3): 213-217. doi:10.1038/ngeo1712.

Deplazes, G., A. Lückge, J.-B. W. Stuut, J. Pätzold, H. Kuhlmann, D. Husson, M. Fant, and G. H. Haug. 2014. "Weakening and Strengthening of the Indian Monsoon during Heinrich Events and Dansgaard-Oeschger Oscillations." *Paleoceanography* 29 (2): 99-114. doi:10.1002/2013PA002509.

Dima, M., G. Lohmann, and G. Knorr. 2018. "North Atlantic Versus Global Control on Dansgaard-Oeschger Events." *Geophysical Research Letters* 45 (23): 12,991-12,998. doi:10.1029/2018GL080035.

Duggen, S., N. Olgun, P. Croot, L. Hoffmann, H. Dietze, P. Delmelle, and C. Teschner. 2010. "The Role of Airborne Volcanic Ash for the Surface Ocean Biogeochemical Iron-Cycle: A Review." *Biogeosciences* 7 (3): 827-844. doi:10.5194/bg-7-827-2010.

Dühnforth, M., An. G. N. Bergner, and M. H. Trauth. 2006. "Early Holocene Water Budget of the Nakuru-Elmenteita Basin, Central Kenya Rift." *Journal of Paleolimnology* 36 (3): 281-294. doi:10.1007/s10933-006-9003-z.

Egborge, A. B. M. 1979. "The Effect of Impoundment on the Water Chemistry of Lake Asejire, Nigeria." *Freshwater Biology* 9 (5): 403-412. doi:10.1111/j.1365-2427.1979.tb01525.x.

Erhardt, T., E. Capron, S. O. Rasmussen, S. Schüpbach, M. Bigler, F. Adolphi, and H. Fischer. 2019. "Decadal-Scale Progression of the Onset of Dansgaard–Oeschger Warming Events." *Climate of the Past* 15 (2): 811-825. doi:10.5194/cp-15-811-2019.

Fazi, S., A. Butturini, F. Tassi, S. Amalfitano, S. Venturi, E. Vazquez, M. Clokie, S. W. Wanjala, N. Pacini, and D. M. Harper. 2018. "Biogeochemistry and Biodiversity in a Network of Saline–alkaline Lakes: Implications of Ecohydrological Connectivity in the Kenyan Rift Valley." *Ecohydrology & Hydrobiology* 18 (2): 96-106. doi:10.1016/j.ecohyd.2017.09.003.

Finney, B. P., C. A. Scholz, T. C. Johnson, and S. Trumbore. 1996. "Late Quaternary Lake-Level Changes of Lake Malawi." *The Limnology, Climatology and Paleoclimatology of the East African Lakes*, edited by T. C. Johnson, E. O. Odada, and K. T. Whittaker, Gordon and Breach Science Publishers: 495-508.

Fleitmann, D., H. Cheng, S. Badertscher, R. L. Edwards, M. Mudelsee, O. M. Göktürk, A. Fankhauser, et al. 2009. "Timing and Climatic Impact of Greenland Interstadials Recorded in Stalagmites from Northern Turkey." *Geophysical Research Letters* 36 (19): L19707-n/a. doi:10.1029/2009GL040050.

Flint, R. F. 1959a. "On the Basis of Pleistocene Correlation in East Africa." *Geological Magazine* 96 (4): 265-284. doi:10.1017/S0016756800060751.

———. 1959b. "Pleistocene Climates in Eastern and Southern Africa." *Bulletin of the Geological Society of America* 70 (3): 343-373. doi:10.1130/0016-7606(1959)70.

Flower, R. J. and D. B. Ryves. 2009. "Diatom Preservation: Differential Preservation of Sedimentary Diatoms in Two Saline Lakes." *Acta Botanica Croatica* 68 (2): 381-399.

Foerster, V., A. Asrat, C. B. Ramsey, E. T. Brown, M. S. Chapot, A. Deino, W. Duesing, M. Grove, A. Hahn, and A. Junginger. 2022. "Pleistocene Climate Variability in Eastern Africa Influenced Hominin Evolution." *Nature Geoscience* 15 (10): 805-811.

Foerster, V., D. M. Deocampo, A. Asrat, C. Günter, A. Junginger, K. H. Krämer, N. A. Stroncik, and M. H. Trauth. 2018. "Towards an Understanding of Climate Proxy Formation in the Chew Bahir Basin, Southern Ethiopian Rift." *Palaeogeography, Palaeoclimatology, Palaeoecology* 501: 111-123. doi:10.1016/j.palaeo.2018.04.009.

Foerster, V., A. Junginger, O. Langkamp, T. Gebru, A. Asrat, M. Umer, H. F. Lamb, et al. 2012. "Climatic Change Recorded in the Sediments of the Chew Bahir Basin, Southern Ethiopia, during the Last 45,000 Years." *Quaternary International* 274: 25-37. doi:10.1016/j.quaint.2012.06.028.

Garcin, Y., A. Junginger, D. Melnick, D. O. Olago, M. R. Strecker, and M. H. Trauth. 2009. "Late Pleistocene–Holocene Rise and Collapse of Lake Suguta, Northern Kenya Rift." *Quaternary Science Reviews* 28 (9): 911-925. doi:10.1016/j.quascirev.2008.12.006.

Garcin, Y., A. Vincens, D. Williamson, G. Buchet, and J. Guiot. 2007. "Abrupt Resumption of the African Monsoon at the Younger Dryas—Holocene Climatic Transition." *Quaternary Science Reviews* 26 (5): 690-704. doi:10.1016/j.quascirev.2006.10.014.

Garcin, Y., A. Vincens, D. Williamson, J. Guiot, and G. Buchet. 2006. "Wet Phases in Tropical Southern Africa during the Last Glacial Period." *Geophysical Research Letters* 33 (7): L07703-n/a. doi:10.1029/2005GL025531.

Garelick, S., J. M. Russell, S. Dee, D. Verschuren, and D. O. Olago. 2021. "Atmospheric Controls on Precipitation Isotopes and Hydroclimate in High-Elevation Regions in Eastern Africa since the Last Glacial Maximum." *Earth and Planetary Science Letters* 567: 116984. doi:10.1016/j.epsl.2021.116984.

Gasse, F., S. Juggins, and L. B. Khelifa. 1995. "Diatom-Based Transfer Functions for Inferring Past Hydrochemical Characteristics of African Lakes." *Palaeogeography, Palaeoclimatology, Palaeoecology* 117 (1): 31-54. doi:10.1016/0031-0182(94)00122-O.

Gasse, F. 1986. *East African Diatoms: Taxonomy, Ecological Distribution*. Berlin: J. Cramer.

———. 2000. "Hydrological Changes in the African Tropics since the Last Glacial Maximum." *Quaternary Science Reviews* 19 (1): 189-211. doi:10.1016/S0277-3791(99)00061-X.

Gasse, F., P. Barker, P. A. Gell, S. C. Fritz, and F. Chalie. 1997. "Diatom-Inferred Salinity in Palaeolakes: An Indirect Tracer of Climate Change." *Quaternary Science Reviews* 16 (6): 547-563. doi:10.1016/S0277-3791(96)00081-9.

Gasse, F., P. Barker, and T. C. Johnson. 2002. "A 24,000 Yr Diatom Record from the Northern Basin of Lake Malawi." *The East African Great Lakes: Limnology, Palaeolimnology and Biodiversity*: 393-414.

Gasse, F., F. Chalié, A. Vincens, M. A. J. Williams, and D. Williamson. 2008. "Climatic Patterns in Equatorial and Southern Africa from 30,000 to 10,000 Years Ago Reconstructed from Terrestrial and Near-Shore Proxy Data." *Quaternary Science Reviews* 27 (25): 2316-2340. doi:10.1016/j.quascirev.2008.08.027.

Google Earth Pro, 2021. 7.3.3.7699. Lake Nakuru, Kenya. Lat -0.352807°, Lon 36.104994°, Eye alt 1757 m. Image Landsat/Copernicus. Accessed May 13, 2021.

Grant, W., C. Gerday, and N. Glansdorff. 2006. "Alkaline Environments and Biodiversity." In *Extremophiles Volume III*, 21-39: EOLSS publishers.

Gregory, J. W. 1968. *The Great Rift Valley: Being the Narrative of a Journey to Mount Kenya and Lake Baringo, with some Account of the Geology, Natural History, Anthropology and Future Prospects of British East Africa*. 1st ed. London: Cass.

Gregory, J. W. 1921. *The Rift Valleys and Geology of East Africa; an Account of the Origin & History of the Rift Valleys of East Africa & their Relation to the Contemporary Earth-Movements which Transformed the Geography of the World. with some Account of the Prehistoric Stone Implements, Soils, Water Supply, & Mineral Resources of the Kenya Colony*. England: Seely, Service & Co. Limited.

Griffith, Peter. 2020. *Late Quaternary Palaeoenvironments and Middle-Late Stone Age Habitat Preferences in the Nakuru-Naivasha Basin, Kenya: Phytolith-Based Evidence from the Site of Prospect Farm*. PhD Thesis. Darwin College.

Halfman, J. D., D. F. Jacobson, C. M. Cannella, K. A. Haberyan, and B. P. Finney. 1992. "Fossil Diatoms and the Mid to Late Holocene Paleolimnology of Lake Turkana, Kenya: A Reconnaissance Study." *Journal of Paleolimnology* 7 (1): 23-35. doi:10.1007/BF00197029.

Hare, L. and J. C. H. Carter. 1984. "Diel and Seasonal Physico-Chemical Fluctuations in a Small Natural West African Lake." *Freshwater Biology* 14 (6): 597-610. doi:10.1111/j.1365-2427.1984.tb00179.x.

Harvey, T. J. 1976. *The Paleolimnology of Lake Mobutu Sese Seko, Uganda-Zaire: The Last 28,000 Years.* Duke University.

Hasle, G. R. 1978. "Some Freshwater and Brackish Water Species of the Diatom Genus *Thalassiosira* Cleve." *Phycologia (Oxford)* 17 (3): 263-292. doi:10.2216/i0031-8884-17-3-263.1.

Hastenrath, S. and J. E. Kutzbach. 1983. "Paleoclimatic Estimates from Water and Energy Budgets of East African Lakes." *Quaternary Research* 19 (2): 141-153. doi:10.1016/0033-5894(83)90001-7.

Hayashi, T. 2011. "Monospecific Planktonic Diatom Assemblages in the Paleo-Kathmandu Lake during the Middle Brunhes Chron: Implications for the Paradox of the Plankton." *Palaeogeography, Palaeoclimatology, Palaeoecology* 300 (1-4): 46-58. doi:10.1016/j.palaeo.2010.12.007.

Hecky, R. E., F. W. B. Bugenyi, P. Ochumba, J. F. Talling, R. Mugidde, M. Gophen, and L. Kaufman. 1994. "Deoxygenation of the Deep Water of Lake Victoria, East Africa." *Limnology and Oceanography* 39 (6): 1476-1481. doi:10.4319/lo.1994.39.6.1476.

Heinrich, H. 1988. "Origin and Consequences of Cyclic Ice Rafting in the Northeast Atlantic Ocean during the Past 130,000 Years." *Quaternary Research* 29 (2): 142-152. doi:10.1016/0033-5894(88)90057-9.

Hemming, S. R. 2004. "Heinrich Events: Massive Late Pleistocene Detritus Layers of the North Atlantic and their Global Climate Imprint." *Reviews of Geophysics (1985)* 42 (1): RG1005-n/a. doi:10.1029/2003RG000128.

Hirons, L. and A. Turner. 2018. "The Impact of Indian Ocean Mean-State Biases in Climate Models on the Representation of the East African Short Rains." *Journal of Climate* 31 (16): 6611-6631. doi:10.1175/JCLI-D-17-0804.1.

Holmgren, K., J. Lee-Thorp, G. R. J. Cooper, K. Lundblad, T. C. Partridge, L. Scott, R. Sithaldeen, A. S. Talma, and P. D. Tyson. 2003. "Persistent Millennial-Scale Climatic Variability Over the Past 25,000 Years in Southern Africa." *Quaternary Science Reviews* 22 (21): 2311-2326. doi:10.1016/S0277-3791(03)00204-X.

Huber, C., M. Leuenberger, R. Spahni, J. Flückiger, J. Schwander, T. F. Stocker, S. Johnsen, A. Landais, and J. Jouzel. 2006. "Isotope Calibrated Greenland Temperature Record Over Marine Isotope Stage 3 and its Relation to CH 4." *Earth and Planetary Science Letters* 243 (3): 504-519. doi:10.1016/j.epsl.2006.01.002.

Itambi, A. C., T. von Dobeneck, S. Mulitza, T. Bickert, and D. Heslop. 2009. "Millennial-Scale Northwest African Droughts Related to Heinrich Events and Dansgaard-Oeschger Cycles: Evidence in Marine Sediments from Offshore Senegal." *Paleoceanography* 24 (1): PA1205-n/a. doi:10.1029/2007PA001570.

IUSS Working Group. 2014. "World Reference Base for Soil Resources 2014. International Soil Classification System for Naming Soils and Creating Legends for Soil Maps."

Ivanochko, T. S., R. S. Ganeshram, G.-J. A. Brummer, G. Ganssen, S. J. A. Jung, S. G. Moreton, and D. Kroon. 2005. "Variations in Tropical Convection as an Amplifier of Global Climate Change at the Millennial Scale." *Earth and Planetary Science Letters* 235 (1): 302-314. doi:10.1016/j.epsl.2005.04.002.

Jirsa, F., M. Gruber, A. Stojanovic, S. O. Omondi, D. Mader, W. Körner, and M. Schagerl. 2013. "Major and Trace Element Geochemistry of Lake Bogoria and Lake Nakuru, Kenya, during Extreme Draught." *Chemie Der Erde* 73 (3): 275-282. doi:10.1016/j.chemer.2012.09.001.

Jolliffe, I. T. and J. Cadima. 2016. "Principal Component Analysis: A Review and Recent Developments." *Philosophical Transactions of the Royal Society of London. Series A: Mathematical, Physical, and Engineering Sciences* 374 (2065): 20150202. doi:10.1098/rsta.2015.0202.

Juggins, S. 2022. *Rioja: Analysis of Quaternary Science Data*. Vol. R package version 1.0-5.

Junginger, A., S. Roller, L. A. Olaka, and M. H. Trauth. 2014. "The Effects of Solar Irradiation Changes on the Migration of the Congo Air Boundary and Water Levels of Paleo-Lake Suguta, Northern Kenya Rift, during the African Humid Period (15–5 Ka BP)." *Palaeogeography, Palaeoclimatology, Palaeoecology* 396: 1-16. doi:10.1016/j.palaeo.2013.12.007.

Junginger, A. and M. H. Trauth. 2013. "Hydrological Constraints of Paleo-Lake Suguta in the Northern Kenya Rift during the African Humid Period (15–5 Ka BP)." *Global and Planetary Change* 111: 174-188. doi:10.1016/j.gloplacha.2013.09.005.

Kanda, I. K. 2010. "Aquifer Stratigraphy and Hydrogeochemistry of the Lake Nakuru Basin, Central Kenya Rift." Unpublished Dissertation. University of Nairobi.

Kimaru, A. N., J. M. Gathenya, and C. K. Cheruiyot. 2019. "The Temporal Variability of Rainfall and Streamflow into Lake Nakuru, Kenya, Assessed using SWAT and Hydrometeorological Indices." *Hydrology* 6 (4): 88. doi:10.3390/hydrology6040088.

Kindler, P., M. Guillevic, M. Baumgartner, J. Schwander, A. Landais, and M. Leuenberger. 2014. "Temperature Reconstruction from 10 to 120 Kyr B2k from the NGRIP Ice Core." *Climate of the Past* 10 (2): 887-902. doi:10.5194/cp-10-887-2014.

Kingston, John D. and Andrew Hill. 2005. "When it Rains it Pours: Legends and Realities of the East African Pluvials." In *Interpreting the Past*, 189-205: Brill.

Kniess, U. 2006. "Hydrologische Modellierung Im Zentralen Kenya-Rift." Unpublished Diploma Thesis. University of Potsdam.

Kragh, T., K. T. Martinsen, E. Kristensen, and K. Sand-Jensen. 2020. "From Drought to Flood: Sudden Carbon Inflow Causes Whole-Lake Anoxia and Massive Fish Kill in a Large Shallow Lake." *The Science of the Total Environment* 739: 140072. doi:10.1016/j.scitotenv.2020.140072.

Kuechler, R. R., E. Schefuß, B. Beckmann, L. Dupont, and G. Wefer. 2013. "NW African Hydrology and Vegetation during the Last Glacial Cycle Reflected in Plant-Wax-Specific Hydrogen and Carbon Isotopes." *Quaternary Science Reviews* 82: 56-67. doi:10.1016/j.quascirev.2013.10.013.

Kurenkov, I. I. 1966. "The Influence of Volcanic Ashfall on Biological Processes in a Lake." *Limnology and Oceanography* 11 (3): 426-429. doi:10.4319/lo.1966.11.3.0426.

Kutzbach, J. E. and F. Street-Perrott. 1985. "Milankovitch Forcing of Fluctuations in the Level of Tropical Lakes from 18 to 0 Kyr BP." *Nature (London)* 317 (6033): 130-134. doi:10.1038/317130a0.

Kylander, M. E., L. Ampel, B. Wohlfarth, and D. Veres. 2011. "High-Resolution X-Ray Fluorescence Core Scanning Analysis of Les Echets (France) Sedimentary Sequence: New Insights from Chemical Proxies." *Journal of Quaternary Science* 26 (1): 109-117. doi:10.1002/jqs.1438.

Laird, K. R., M. V. Kingsbury, and B. F. Cumming. 2010. "Diatom Habitats, Species Diversity and Water-Depth Inference Models Across Surface-Sediment Transects in Worth Lake, Northwest Ontario, Canada." *Journal of Paleolimnology* 44 (4): 1009-1024. doi:10.1007/s10933-010-9470-0.

Laird, K. R., M. V. Kingsbury, C. F. M. Lewis, and B. F. Cumming. 2011. "Diatom-Inferred Depth Models in 8 Canadian Boreal Lakes: Inferred Changes in the Benthic:Planktonic Depth Boundary and Implications for Assessment of Past Droughts." *Quaternary Science Reviews* 30 (9): 1201-1217. doi:10.1016/j.quascirev.2011.02.009.

Leakey, L. S. B. 1931. "East African Lakes." *The Geographical Journal* 77 (6): 497-508. doi:10.2307/1785041.

Leakey, L. S. B. 1950. "The Lower Limit of the Pleistocene in Africa." *Rep.18th Int.Geol.Congr.(London)*: 62-65.

Leakey, M. D., L. S. B. Leakey, P. M. Game, and A. J. H. Goodwin. 1943. "Report on the Excavations at Hyrax Hill, Nakuru, Kenya Colony, 1937–1938." *Transactions of the Royal Society of South Africa* 30 (4): 271-409. doi:10.1080/00359194309519847.

Leat, P. T. 1984. "Geological Evolution of the Trachytic Caldera Volcano Menengai, Kenya Rift Valley." *Journal of the Geological Society* 141 (6): 1057-1069. doi:10.1144/gsjgs.141.6.1057.

Leat, P. T. 1991. "Volcanological Development of the Nakuru Area of the Kenya Rift Valley." *Journal of African Earth Sciences* 13 (3): 483-498. doi:10.1016/0899-5362(91)90111-B.

Livingstone, D. A. and J. M. Melack. 1984. "Some Lakes of Subsaharan Africa.". In *Lakes and Reservoirs*, edited by F. B. Taub, 467-497.

Lohmann, J. and A. Svensson. 2022. "Ice Core Evidence for Major Volcanic Eruptions at the Onset of Dansgaard–Oeschger Warming Events." *Climate of the Past* 18 (9): 2021-2043. doi:10.5194/cp-18-2021-2022.

Lowe, D. J. 2011. "Tephrochronology and its Application: A Review." *Quaternary Geochronology* 6 (2): 107-153. doi:10.1016/j.quageo.2010.08.003.

Lüdecke, H.-J., G. Müller-Plath, M. G. Wallace, and S. Lüning. 2021. "Decadal and Multidecadal Natural Variability of African Rainfall." *Journal of Hydrology* 34: 100795. doi:10.1016/j.ejrh.2021.100795.

Lung'ayia, H., L. Sitoki, and M. Kenyana. 2001. "The Nutrient Enrichment of Lake Victoria (Kenyan Waters)." *Hydrobiologia* 458 (1-3): 75-82. doi:10.1023/A:1013128027773.

Lupien, R. L., J. M. Russell, E. J. Pearson, I. S. Castañeda, A. Asrat, V. Foerster, H. F. Lamb, et al. 2022. "Orbital Controls on Eastern African Hydroclimate in the Pleistocene." *Scientific Reports* 12 (1): 3170. doi:10.1038/s41598-022-06826-z.

MacIntyre, S., R. D. Robarts, C. R. Goldman, and C. Kumagai. 2012. "Climatic Variability, Mixing Dynamics, and Ecological Consequences in the African Great Lakes." In *Climatic Change and Global Warming of Inland Waters*, 311-336. Chichester, UK: John Wiley & Sons, Ltd. doi:10.1002/9781118470596.ch18.

Mahamat Ahmat, A., M. Boussafir, C. Le Milbeau, R. Guégan, T. De Oliveira, and L. Le Forestier. 2017. "Organic Matter and Clay Interaction in a Meromictic Lake: Implications for Source Rock OM Preservation (Lac Pavin, Puy-De-Dôme, France)." *Organic Geochemistry* 109: 47-57. doi:10.1016/j.orggeochem.2017.03.014.

Mann, L. E., A. A. Robel, and C. R. Meyer. 2021. "Synchronization of Heinrich and Dansgaard-Oeschger Events through Ice-Ocean Interactions." *Paleoceanography and Paleoclimatology* 36 (11) doi:10.1029/2021PA004334.

Marchant, R., C. Mumbi, S. Behera, and T. Yamagata. 2007. "The Indian Ocean Dipole the Unsung Driver of Climatic Variability in East Africa." *African Journal of Ecology* 45 (1): 4-16. doi:10.1111/j.1365-2028.2006.00707.x.

Maslin, M. A. and M. H. Trauth. 2009. "Plio-Pleistocene East African Pulsed Climate Variability and its Influence on Early Human Evolution." In *The First Humans – Origin and Early Evolution of the Genus Homo*, 151-158. Dordrecht: Springer Netherlands.

McCall, G. J. H. 1967. *Geology of the Nakuru-Thomson's Falls-Lake Hanningon Area*.

Merrick, Harry Vincent. 1975. *Change in Later Pleistocene Lithic Industries in Eastern Africa.* PhD Thesis. University of California, Berkeley.

Meyers, P. A. 1994. "Preservation of Elemental and Isotopic Source Identification of Sedimentary Organic Matter." *Chemical Geology* 114 (3): 289-302. doi:10.1016/0009-2541(94)90059-0.

Milbrink, G. 1977. "On the Limnology of Two Alkaline Lakes (Nakuru and Naivasha) in the East Rift Valley System in Kenya." *Internationale Revue Der Gesamten Hydrobiologie* 62 (1): 1-17. doi:10.1002/iroh.1977.3510620101.

Moernaut, J., D. Verschuren, F. Charlet, I. Kristen, M. Fagot, and M. De Batist. 2010. "The Seismic-Stratigraphic Record of Lake-Level Fluctuations in Lake Challa: Hydrological Stability and Change in Equatorial East Africa Over the Last 140kyr." *Earth and Planetary Science Letters* 290 (1-2): 214-223. doi:10.1016/j.epsl.2009.12.023.

Moos, M. T., K. R. Laird, and Brian F. Cumming. 2005. "Diatom Assemblages and Water Depth in Lake 239 (Experimental Lakes Area, Ontario): Implications for Paleoclimatic Studies." *Journal of Paleolimnology* 34 (2): 217-227. doi:10.1007/s10933-005-2382-8.

Muiruri, V., R. B. Owen, R. Potts, A. L. Deino, A. K. Behrensmeyer, S. Riedl, N. Rabideaux, et al. 2021. "Quaternary Diatoms and Palaeoenvironments of the Koora Plain, Southern Kenya Rift." *Quaternary Science Reviews* 267: 107106. doi:10.1016/j.quascirev.2021.107106.

Naeher, S., A. Gilli, R. P. North, Y. Hamann, and C. J. Schubert. 2013. "Tracing Bottom Water Oxygenation with Sedimentary Mn/Fe Ratios in Lake Zurich, Switzerland." *Chemical Geology* 352: 125-133. doi:10.1016/j.chemgeo.2013.06.006.

Ndebele-Murisa, M., C. F. Musil, and L. Raitt. 2010. "A Review of Phytoplankton Dynamics in Tropical African Lakes: Review Article." *South African Journal of Science* 106 (1): 13-18.

Nicholson, S. E. 2017. "Climate and Climatic Variability of Rainfall Over Eastern Africa." *Reviews of Geophysics (1985)* 55 (3): 590-635. doi:10.1002/2016RG000544.

———. 1996. "A Review of Climate Dynamics and Climate Variability in Eastern Africa." Johnson, Thomas C.; Odada, Eric O.(Eds.) and Whittaker, Katherine T., The Limnology, Climatology and Paleoclimatology of the East African Lakes., Amsterdam, Gordon and Breach Science Publishers: 25-56.

Nilsson, E. 1940. "Ancient Changes of Climate in British East Africa and Abyssinia: A Study of Ancient Lakes and Glaciers." *Geografiska Annaler* 22 (1-2): 1-79. doi:10.1080/20014422.1940.11880682.

———. 1931. "Quaternary Glaciations and Pluvial Lakes in British East Africa." *Geografiska Annaler* 13: 249-349. doi:10.2307/519647.

North Greenland Ice Core Project members. 2004. High-resolution record of northern hemisphere climate extending into the last interglacial period. *Nature* 431, 147-151.

Ntale, H. K. and T. Y. Gan. 2004. "East African Rainfall Anomaly Patterns in Association with El Niño/Southern Oscillation." *Journal of Hydrologic Engineering* 9 (4): 257-268. doi:10.1061/(ASCE)1084-0699(2004)9:4(257).

Odada, E. O., J. Raini, and R. Ndetei. 2006*. Lake Nakuru: Experience and Lessons Learned Brief*.

Oksanen, J., F. G. Blanchet, M. Friendly, R. Kindt, P. Legendre, D. McGlinn, P. R. Minchin, R. B. O'Hara, G. L. Simpson, and P. Solymos. 2022. *Vegan: Community Ecology Package.* R Package Version 2.5-7.2020.

Olaka, L., E. Odada, M. Trauth, and D. Olago. 2010. "The Sensitivity of East African Rift Lakes to Climate Fluctuations." *Journal of Paleolimnology* 44 (2): 629-644. doi:10.1007/s10933-010-9442-4.

Otto-Bliesner, B., J. M. Russell, P. U. Clark, Z. Liu, J. T. Overpeck, B. Konecky, P. deMenocal, S. E. Nicholson, F. He, and Z. Lu. 2014. "Coherent Changes of Southeastern Equatorial and Northern African Rainfall during the Last Deglaciation." *Science* 346 (6214): 1223-1227. doi:10.1126/science.1259531.

Owen, R. B. and R. Crossley. 1992. "Spatial and Temporal Distribution of Diatoms in Sediments of Lake Malawi, Central Africa, and Ecological Implications." *Journal of Paleolimnology* 7 (1): 55-71. doi:10.1007/BF00197031.

Owen, R. B., R. W. Renaut, A. K. Behrensmeyer, and R. Potts. 2014. "Quaternary Geochemical Stratigraphy of the Kedong–Olorgesailie Section of the Southern Kenya Rift Valley." *Palaeogeography, Palaeoclimatology, Palaeoecology* 396: 194-212. doi:10.1016/j.palaeo.2014.01.011.

Pilskaln, C. H. 2004. "Seasonal and Interannual Particle Export in an African Rift Valley Lake: A 5-Yr Record from Lake Malawi, Southern East Africa." *Limnology and Oceanography* 49 (4): 964-977. doi:10.4319/lo.2004.49.4.0964.

Pilskaln, C. H. and T. C. Johnson. 1991. "Seasonal Signals in Lake Malawi Sediments." *Limnology and Oceanography* 36 (3): 544-557. doi:10.4319/lo.1991.36.3.0544.

Porter, S. C. and A. Zhisheng. 1995. "Correlation between Climate Events in the North Atlantic and China during the Last Glaciation." *Nature (London)* 375 (6529): 305-308. doi:10.1038/375305a0.

Potts, R. 1998. "Environmental Hypotheses of Hominin Evolution." *American Journal of Physical Anthropology* 107 (27): 93-136. doi:10.1002/(SICI)1096-8644(1998)107:27+3.0.CO;2-X.

RCMRD. 2021. *The Rising Water Level and Expansion of the Rift Valley Lakes from Space*. Nairobi, Kenya.

Reimer, P. J., W. E. N. Austin, E. Bard, A. Bayliss, P. G. Blackwell, C. B. Ramsey, M. Butzin, et al. 2020. "The IntCal20 Northern Hemisphere Radiocarbon Age Calibration Curve (0–55 Cal kBP)." *Radiocarbon* 62 (4): 725-757. doi:10.1017/RDC.2020.41.

Richardson, J. L. and R. A. Dussinger. 1986. "Paleolimnology of Mid-Elevation Lakes in the Kenya Rift Valley." *Hydrobiologia* 143 (1): 167-174. doi:10.1007/BF00026659.

Richardson, J. L. and A. E. Richardson. 1972. "History of an African Rift Lake and its Climatic Implications." *Ecological Monographs* 42 (4): 499-534.

Richter, T. O., S. van der Gaast, B. Koster, A. Vaars, R. Gieles, H. C. de Stigter, H. de Haas, and T. C. E. van Weering. 2006. "The Avaatech XRF Core Scanner: Technical Description and Applications to NE Atlantic Sediments." In *New Techniques in Sediment Core Analysis*, edited by R. G. Rothwell, 1-2: Geological Society of London.

Riedl, S., D. Melnick, G. K. Mibei, L. Njue, and M. R. Strecker. 2020. "Continental Rifting at Magmatic Centres; Structural Implications from Late Quaternary Menengai Caldera, Central Kenya Rift." *Journal of the Geological Society* 177 (1): 153-169. doi:10.1144/jgs2019-021.

Robson, G. E. 1967. "The Caves of Sof Omar." *The Geographical Journal* 133 (3): 344-349. doi:10.2307/1793545.

Roubeix, V., F. Chalié, and F. Gasse. 2014. "The diatomThalassiosira Faurii(Gasse) Hasle in the Ziway–Shala Lakes (Ethiopia) and Implications for Paleoclimatic Reconstructions: Case Study of the Glacial–Holocene Transition in East Africa." *Palaeogeography, Palaeoclimatology, Palaeoecology* 402: 104-112. doi:10.1016/j.palaeo.2014.03.014.

Ryves, D. B., S. Juggins, S. C. Fritz, and R. W. Battarbee. 2001. "Experimental Diatom Dissolution and the Quantification of Microfossil Preservation in Sediments." *Palaeogeography, Palaeoclimatology, Palaeoecology* 172 (1): 99-113. doi:10.1016/S0031-0182(01)00273-5.

Sachs, J. P. and S. J. Lehman. 1999. "Subtropical North Atlantic Temperatures 60,000 to 30,000 Years Ago." *Science* 286 (5440): 756-759. doi:10.1126/science.286.5440.756.

Schaebitz, F., A. Asrat, H. F. Lamb, A. S. Cohen, V. Foerster, W. Duesing, S. Kaboth-Bahr, et al. 2021. "Hydroclimate Changes in Eastern Africa Over the Past 200,000 Years may have Influenced Early Human Dispersal." *Communications Earth & Environment* 2 (1). doi:10.1038/s43247-021-00195-7.

Singarayer, J. S. and S. L. Burrough. 2015. "Interhemispheric Dynamics of the African Rainbelt during the Late Quaternary." *Quaternary Science Reviews* 124: 48-67. doi:10.1016/j.quascirev.2015.06.021.

Slater, Philip Aaron. 2016. *Change in Lithic Technological Organization Strategies during the Middle and Later Stone Ages in East Africa*. PhD Thesis. University of Illinois.

Spaulding, S. A., Bishop, I. W., Edlund, M. B., Lee, S., Furey, P., Jovanovska, E. and Potapova, M. "Diatoms of North America." https://diatoms.org/species.

Stager, J. C. 1988. "Environmental Changes at Lake Cheshi, Zambia since 40,000 Years B.P." *Quaternary Research* 29 (1): 54-65. doi:10.1016/0033-5894(88)90071-3.

Stager, J. C., Paul A. Mayewski, and L. D. Meeker. 2002. "Cooling Cycles, Heinrich Event 1, and the Desiccation of Lake Victoria." *Palaeogeography, Palaeoclimatology, Palaeoecology* 183 (1-2): 169-178. doi:10.1016/S0031-0182(01)00468-0.

Stager, J. C., D. B. Ryves, B. M. Chase, and F. S. R. Pausata. 2011. "Catastrophic Drought in the Afro-Asian Monsoon Region during Heinrich Event 1." *Science*. doi:10.1126/science.1198322.

Stevenson, R. J. and E. F. Stoermer. 1981. "Quantitative Differences between Benthic Algal Communities Along a Depth Gradient in Lake Michigan." *Journal of Phycology* 17 (1): 29-36. doi:10.1111/j.1529-8817.1981.tb00815.x.

Strecker, M. R., P. M. Blisniuk, and G. H. Eisbacher. 1990. "Rotation of Extension Direction in the Central Kenya Rift." *Geology (Boulder)* 18 (4): 299-302. doi:10.1130/0091-7613(1990)0182.3.CO;2.

Talling, J. F. 2001. "Environmental Controls on the Functioning of Shallow Tropical Lakes." *Hydrobiologia* 458 (1-3): 1-8. doi:10.1023/A:1013121522321.

Taylor, J. C. and C. Cocquyt. 2016. *Diatoms from the Congo and Zambezi Basins – Methodologies and Identification of the Genera*. Vol. 44 Informa UK Limited. doi:10.2989/16085914.2019.1628702.

Taylor, J. C., W. R. Harding, and C. G. M. Archibald. 2007. *An Illustrated Guide to some Common Diatom Species from South Africa*. Pretoria, South Africa: Water Research Commission.

ter Braak, C. and C. Looman. 1986. "Weighted Averaging, Logistic Regression and the Gaussian Response Model." *Vegetatio* 65 (1): 3-11. doi:10.1007/BF00032121.

Thevenon, F., D. Williamson, and M. Taieb. 2002. "A 22 Kyr BP Sedimentological Record of Lake Rukwa (8°S, SW Tanzania): Environmental, Chronostratigraphic and Climatic Implications." *Palaeogeography, Palaeoclimatology, Palaeoecology* 187 (3): 285-294. doi:10.1016/S0031-0182(02)00481-9.

Tian, Z. and D. Jiang. 2020. "Weakening and Eastward Shift of the Tropical Pacific Walker Circulation during the Last Glacial Maximum." *Boreas* 49 (1): 200-210. doi:10.1111/bor.12417.

Tierney, J. E., J. M. Russell, Y. Huang, J. S. Sinninghe Damsté, E. C. Hopmans, and A. S. Cohen. 2008. "Northern Hemisphere Controls on Tropical Southeast African Climate during the Past 60,000 Years." *Science (New York, N.Y.)* 322 (5899): 252. doi:10.1126/science.1160485.

Tjallingii, R., M. Claussen, J. B. W. Stuut, J. Fohlmeister, A. Jahn, T. Bickert, F. Lamy, and U. Röhl. 2008. "Coherent High- and Low-Latitude Control of the Northwest African Hydrological Balance." *Nature Geoscience* 1 (10): 670-675. doi:10.1038/ngeo289.

Trauth, M. H., V. Foerster, A. Junginger, A. Asrat, H. F. Lamb, and F. Schaebitz. 2018. "Abrupt Or Gradual? Change Point Analysis of the Late Pleistocene–Holocene Climate Record from Chew Bahir, Southern Ethiopia." *Quaternary Research* 90 (2): 321-330. doi:10.1017/qua.2018.30.

Trauth, M. H., M. A. Maslin, A. L. Deino, A. Junginger, M. Lesoloyia, E. O. Odada, D. O. Olago, L. A. Olaka, M. R. Strecker, and R. Tiedemann. 2010. "Human Evolution in a Variable Environment: The Amplifier Lakes of Eastern Africa." *Quaternary Science Reviews* 29 (23): 2981-2988. doi:10.1016/j.quascirev.2010.07.007.

Trolard, F., G. Bourrié, M. Abdelmoula, P. Refait, and F. Feder. 2007. "Fougerite, a New Mineral of the Pyroaurite-Iowaite Group; Description and Crystal Structure." *Clays and Clay Minerals* 55 (3): 323-334. doi:10.1346/CCMN.2007.0550308.

Truc, L., M. Chevalier, C. Favier, R. Cheddadi, M. E. Meadows, L. Scott, A. S. Carr, G. F. Smith, and B.M. Chase. 2013. "Quantification of Climate Change for the Last 20,000 years from Wonderkrater, South Africa: Implications for the Long-Term Dynamics of the Intertropical Convergence Zone." *Palaeogeography, Palaeoclimatology, Palaeoecology* 386: 575-587. doi:10.1016/j.palaeo.2013.06.024.

Vareschi, E. and J. Jacobs. 1985. "The Ecology of Lake Nakuru. VI. Synopsis of Production and Energy Flow." *Oecologia* 65 (3): 412-424. doi:10.1007/BF00378917.

Verschuren, D., J. S. Sinninghe Damsté, J. Moernaut, I. Kristen, M. Blaauw, M. Fagot, H. G. Haug, et al. 2009. "Half-Precessional Dynamics of Monsoon Rainfall Near the East African Equator." *Nature (London)* 462 (7273): 637-641. doi:10.1038/nature08520.

Vettoretti, G. and W. R. Peltier. 2016. "Thermohaline Instability and the Formation of Glacial North Atlantic Super Polynyas at the Onset of Dansgaard-Oeschger Warming Events." *Geophysical Research Letters* 43 (10): 5336-5344. doi:10.1002/2016GL068891.

Voelker, A. H. L. 2002. "Global Distribution of Centennial-Scale Records for Marine Isotope Stage (MIS) 3: A Database." *Quaternary Science Reviews* 21 (10): 1185-1212. doi:10.1016/S0277-3791(01)00139-1.

Wang, Y. J., H. Cheng, R. L. Edwards, Z. S. An, J. Y. Wu, C.-C. Shen, and J. A. Dorale. 2001. "A High-Resolution Absolute-Dated Late Pleistocene Monsoon Record from Hulu Cave, China." *Science* 294 (5550): 2345-2348. doi:10.1126/science.1064618.

Washbourn-Kamau, C. K. 1971. "Late Quaternary Lakes in the Nakuru-Elmenteita Basin, Kenya." *The Geographical Journal* 137 (4): 522-535. doi:10.2307/1797148.

Yuan, W., G. Liu, L. Xu, X. Niu, and C. Li. 2019. "Petrographic and Geochemical Characteristics of Organic-Rich Shale and Tuff of the Upper Triassic Yanchang Formation, Ordos Basin, China; Implications for Lacustrine Fertilization by Volcanic Ash." *Canadian Journal of Earth Sciences* 56 (1): 47-59. doi:10.1139/cjes-2018-0123.

Yuretich, R. F. 1982. "Possible Influences upon Lake Development in the East African Rift Valleys." *The Journal of Geology* 90 (3): 329-337. doi:10.1086/628684.

Zébazé Togouet, S. H., T. Njine, N. Kemka, M. Nola, S. F. Menbohan, W. Koste, C. Boutin, and R. Hochberg. 2007. "Spatio-Temporal Changes in the Abundance of the Populations of the Gastrotrich Community in a Shallow Lake of Tropical Africa." *Limnologica* 37 (4): 311-322. doi:10.1016/j.limno.2007.06.003.

Zeileis, A. and G. Grothendieck. 2005. "Zoo : S3 Infrastructure for Regular and Irregular Time Series." *Journal of Statistical Software* 14 (6). doi:10.18637/jss.v014.i06.

3.10. SUPPLEMENTAL DATA

Suppl. 1: Tab1: Magnetic Susceptibility data organized in the NAK composite. **Tab2:** Raw XRF data in counts per second (cps) for all elements in both 10 kV and 30 kV for the NAK composite.
Suppl. 2: Measured Total Carbon, Total Nitrogen, and Total Organic Carbon for the NAK composite. Calculated TOC/TN is also included.
Suppl. 3: Tab1: Raw diatom counts for NAK composite including the core location. Counts for phytoliths, counting spores, and sponge spicules are also included. **Tab2:** Diatom habitat groups based off of Gasse (1986) and Taylor et al. (2007). Habitat groups: 1=littoral, 2=littoral planktonic, and 3=planktonic. Salinity groups are on a gradient where 1=fresh and 5=marine.

CHAPTER 4: Hydroclimate reconstructions in the Suguta Valley, northern Kenya, during the Early-Middle Pleistocene Transition[4]

4.1. INTRODUCTION

One of the most pronounced global climate changes of the Quaternary, the Early-Middle Pleistocene Transition (EMPT), occurred between 1,200–700 ka. During the EMPT, glacial-interglacial cycles became longer and more intense, changing from 41- to 100-kyr cycles (e.g., Shackleton & Opdyke, 1977; Pisias & Moore, 1981; Mudelsee & Statteger, 1997), possibly a result of long-term cooling trends associated with changing pCO_2 and thickening of Northern Hemisphere ice sheets (e.g., Mudelsee & Schulz, 1997; Maslin & Ridgwell, 2005; Clark et al., 2006; Head et al., 2008; Maslin & Bierley, 2015). This intensification led to abrupt "saw-toothed" glacial-interglacial transitions via two stages (Maslin & Brierley, 2015). The first (900–700 ka) resulted in a significant increase in global ice volume over 41-kyr cycles (Mudelsee & Stattegger, 1997; Maslin & Brierley, 2015), after which (post-700 ka), the climate system became a more complex three-state system with full interglacials, full glacials, and intermediate interglacials over 100-kyr cycles (Paillard, 1998).

Eastern African hydroclimate responds to a combination of tectonic processes (Xue et al., 2019), global temperatures/pCO_2, low-latitude insolation forcing (Clement et al., 2004; Deino et al., 2006; Trauth et al., 2009; Joordens et al., 2011; Yost et al., 2021), tropical sea surface temperatures (Vuille et al., 2005; Tierney et al., 2011; Johnson et al., 2016), and glacial-interglacial cycles (Rossignol-Strick, 1984; Larrasoaña et al., 2003; Kutzbach et al., 2020). The relative strength and importance of each factor through time remains largely unknown and variable (Lupien et al. 2022), resulting in uncertainty over how regional environments responded to the

[4] This work has been accepted. ROBAKIEWICZ, E.; OWEN, R.B.; ROSCA, C.; DEINO, A.; GARCIN, Y.; TRAUTH, M.H.; KÜBLER, S.; & JUNGINGER, A., *accepted*, Hydroclimate reconstructions in the Suguta Valley, northern Kenya, during the Early-Middle Pleistocene Transition: *Palaeogeography, Palaeoclimatology, Palaeoecology.*

EMPT. Fortunately, within the Suguta Valley in the northern Kenya Rift (36.55°E, 2.22°N), flood basalts have capped lacustrine sediments of this age (Dunkley et al., 1993), preserving them and enabling an examination of regional hydroclimate.

This study fills a gap in northern Kenya Rift sedimentological records between 900–700 ka and helps increase understanding of EMPT paleoclimatology and paleoenvironments. Previous studies in the neighboring Turkana Basin indicate that a floodplain dominated, with erosion and/or non-deposition to the northeast and south (Feibel, 2011). Brown & McDougall (2011) noted a paucity of sedimentary evidence between 1,000–800 ka and an absence of ~700–200 ka strata, although studies at neighboring Chew Bahir provide a record back to 620 ka (Duesing et al., 2021; Foerster et al., 2022). Similarly, the southern Baringo Basin indicates a ~1 Myr unconformity between the end of the Chemeron Formation (~1,570 ka (Hill et al., 1986)) and the beginning of the Kapthurin Formation (~610 ka (Deino & McBrearty, 2002)) with many lacustrine phases of the Kapthurin Formation indicating alkaline and saline lakes (Renaut et al., 1999). Here, we present a new hydroclimate dataset from a lacustrine sequence (KSI) deposited between ~931 and 831 ka, coinciding with a paucity of sedimentary evidence at Turkana and other East African Rift System (EARS) basins. This study aims to explore EMPT hydroclimate variability within the Suguta-Turkana Basin and understand its regional impacts.

4.2. GEOLOGICAL AND HYDROCLIMATOLOGICAL SETTING

4.2.1. Geological Setting

The Suguta Valley (northern Kenya Rift) forms part of the eastern branch of the EARS, a 3,000-km-long continental rift initiated during the Miocene by mantle plume activity (F1A; Ebinger & Sleep, 1998; Ebinger et al., 2000; Chorowicz, 2005; Pik et al., 2008; Purcell, 2018). Initial uplift and doming gave way to north-south Plio-Pleistocene rifting (Baker & Wohlenberg, 1971) forming the Suguta Valley due to subsidence along the inner trough by at least ~1.8 Ma, with coeval volcanism separating it from other basins (Morley et al., 1992; Dunkley et al., 1993). In the

north, the Barrier volcanic complex erupted ~1.37 Ma and separates Suguta from Lake Turkana today, although hydrological separation was not achieved until ~221 ka (Dunkley et al., 1993; McDougall et al., 2012), a date which may be pushed back to ~780 ka (F1B; Junginger et al., 2023). To the south, the Korosi volcanic shield did not form until ~380 ka (Dunkley et al., 1993), far later than the timeframe of this study. Consequently, this study reflects changes in a larger Suguta-Turkana-Baringo catchment.

Today, the Suguta Valley is ~80 km long by 17–21 km wide (F1C), with a 12,800 km^2 catchment (~180 km north-south; ~35–70 km east-west) (Dunkley et al., 1993; Garcin et al., 2009; Junginger & Trauth, 2013). The modern Suguta is a NNE-trending half graben with its floor ~1,000–275 m above sea level (asl) (Bosworth & Maurin, 1993; Saneyoshi et al., 2006; Melnick et al., 2012; Junginger et al., 2014). The rift margins are faulted monoclines with a possible border fault to the northeast and hills rising to 750 (west) and 1,100 m asl (east) (Dunkley et al., 1993). Basin subsidence is controlled by extensional faulting overprinted by strike-slip and compressional deformation (Dunkley et al., 1993; Le Gall et al., 2005; Vetel & Le Gall, 2006). The catchment includes Plio-Pleistocene alkaline basalts and trachytes with Precambrian gneisses of the Mozambique Orogenic Belt in the northeast (F1B; Bosworth & Maurin, 1993; Dunkley et al., 1993).

4.2.2. Hydroclimatological Setting

Equatorial Eastern African climate is primarily characterized by changes in precipitation rather than temperature. Rainfall is bimodal, peaking from March–May (long rains) and October–November (short rains) (Nicholson, 1996; 2017). Modern Suguta is the most arid setting in Kenya (Ojany & Ogenoo, 1973), with daily temperatures of 30–50°C; annual precipitation of <300 mm/yr, increasing to 1,000 mm/yr along rift shoulders (Junginger & Trauth, 2013); and evaporation rates of 3,000–4,000 mm/yr (Nyenzi et al., 1981; Garcin et al., 2009). Lake Logipi, in the lowest part of Suguta, varies seasonally in response to inflows from the Suguta

River, smaller ephemeral rivers, springs, and groundwater from Lakes Turkana and Baringo (Dunkley et al., 1993; Junginger & Trauth, 2013). Much of the lake desiccates into salt pans during the dry season, but, at its maximum, can cover 80 km^2 (Castanier et al., 1993). Contrasts between increased precipitation at higher elevations and hyper-arid conditions at lower elevations characterize Paleolake Suguta as an “amplifier lake”, which responds sensitively to even minor climatic changes (Olaka et al., 2010; Trauth et al., 2010).

Today’s hyper-aridity contrasts with the 300-m-deep paleolake that formed 15–5 ka during the African Humid Period (AHP) (Garcin et al., 2009; Junginger & Trauth, 2013; Junginger et al., 2014). During the AHP, precipitation is estimated to have been only 20–30% higher than today (Borchardt & Trauth, 2012; Junginger & Trauth, 2013), yet Paleolake Suguta was 75 times deeper (Garcin et al., 2009). Towards the end of the AHP, the water level of Paleolake Suguta dropped by 240 m 8.5–7.3 ka, underlining its climate sensitivity (Garcin et al., 2009).

Truckle (1976) and Dunkley et al. (1993) described Pleistocene and Holocene fluvio-lacustrine deposits as the ‘Suguta Beds’. Early to Middle Pleistocene lacustrine sediments in southern and western Suguta, between the Namarunu and Emuruangogolak volcanoes, document past humid conditions (Truckle, 1976; Casanova et al., 1988; Sturchio et al., 1993; Trauth et al., 2007). The 41-m section, Kamuge-Suguta I (KSI), northwest of Emuruangogolak, is one of the best exposed Pleistocene lacustrine sequences in the area (F1C). KSI is located along the eastern banks of the Suguta River near its confluence with the Kamuge River (1.640098°N, 36.294669°E, 362 m asl). The sediments, mostly clays, silts, and diatomites, are intercalated with carbonates and tephras and document hydroclimatic changes during part of the EMPT (F2).

4.3. MATERIALS AND METHODS

4.3.1. Sample Collection, Stratigraphy and Grain Sizes

Sediments were collected in 2007 from a 41-m section sampled at 50-cm intervals with additional samples taken where carbonates were present, yielding 93 samples. Grain sizes were described in the field with fine-grained lithologies also analyzed on a Malvern MasterSizer 2000 at Eberhard Karls Universität Tübingen. Preparation followed Meyer et al. (2020) with replicate analyses (5x) to calculate 90% confidence intervals. MasterSizer results reflect both clastic grains and biogenic diatoms – a common occurrence in African sediments (Meyer et al., 2020) – limiting its interpretability. Because of these complications, the MasterSizer's results were supplemented with qualitative observations to generate the KSI stratigraphic column.

4.3.2. Chronology

Three tuff samples from KSI were dated by the $^{40}Ar/^{39}Ar$ method, consisting of coarse ash from Plinian fallout and reworked lapilli tuffs. Samples were processed at the Berkeley Geochronology Center (BGC). Feldspar phenocrysts were separated using conventional techniques including disaggregation using a ceramic mortar and pestle, sieving, dilute HF and distilled water rinses, and hand-picking under a binocular microscope to obtain a finished product of clean grains as free of inclusions as possible.

The final mineral separates were irradiated in the Cd-lined CLICIT position of the Oregon State University TRIGA reactor for two hours (BGC irradiation #375). This irradiation employed sanidine phenocrysts from the Alder Creek Rhyolite of California (orbitally referenced age=1.1848±0.0006 Ma; Niespolo et al., 2017) as the neutron fluence monitor mineral. Standards and unknowns were co-irradiated in circular concentric rings in wells in an aluminum disk with both unknowns on the same disk. The appropriate neutron fluence factor (the '*J*' parameter of $^{40}Ar/^{39}Ar$ dating calculations; McDougall & Harrison, 1999) for the sample positions was calculated from a planar fit of the standard calibrations, with median 1σ errors

derived by Monte Carlo simulation in the predicted *J* value of ~0.4%. Reactor-induced isotopic production ratios for these irradiations were: $(^{36}Ar/^{37}Ar)_{Ca}$=3.65±0.02 × 10^{-4}, $(^{38}Ar/^{37}Ar)_{Ca}$=1.96±0.08 × 10^{-5}, $(^{39}Ar/^{37}Ar)_{Ca}$=6.95±0.09 × 10^{-4}, $(^{37}Ar/^{39}Ar)_{K}$=3.24±0.16 × 10^{-4}, $(^{38}Ar/^{39}Ar)_{K}$=1.220±0.003 × 10^{-2}, $(^{40}Ar/^{39}Ar)_{K}$ = 3.5±0.9 × 10^{-4}. Atmospheric $^{40}Ar/^{36}Ar$=298.56±0.31 (Lee et al., 2006) and decay constants follow (Min et al., 2000).

The irradiated sanidine phenocrysts were then analyzed at the BGC using the single-crystal $^{40}Ar/^{39}Ar$ total-fusion (SCTF) technique. With this approach, individual grains are heated rapidly to fusion and degassed in <10 seconds under ultra-high vacuum. After several minutes of gas purification, argon measurements are carried out using an automated extraction line feeding a single-collector MAP-215 mass spectrometer, using analog multiplier signal measurement.

Age distributions obtained from a suite of SCTF analyses are often complicated by anomalous or imprecise results, originating from such sources as detrital contamination, excess ^{40}Ar trapped in primary phenocrysts, subtle alteration, potassium-poor composition, or analytical failure. Any analyses of the latter type are eliminated first. Secondly, plagioclase grains (Ca/K >2 as determined by the $^{40}Ar/^{39}Ar$ measurement process) are omitted from further treatment as they exhibit much greater analytical uncertainty than the anorthoclase or sanidine phenocrysts that dominate these samples. Thirdly, we omit analyses with anomalously high analytical uncertainty, likely from incomplete fusion, fusion of non-feldspathic grains, or very small grain size (i.e., less than a few hundred microns). Fourthly, we identify distinctly older grains (xenocrysts) using a gap-finding technique (Deino et al., 2019[a,b]), with the sensitivity set to a gap score of seven, to identify most old outliers easily identified by a human observer, yet with little impact on the primary age distribution. Finally, we may arbitrarily eliminate an older mode of a clearly multimodal distribution that was not identified by the gap-finding routine due to proximity to the primary mode. Ultimately, the $^{40}Ar/^{39}Ar$ result is reported as the weighted-mean age of the

accepted analyses, with ± 1s modified standard error, computed as the standard error expanded by the root of the mean square weighted deviation (MSWD), if MSWD >1.

We also analyzed the argon systematics using 'inverse isochron' regressions ($^{36}Ar/^{40}Ar$ *vs*. $^{39}Ar/^{40}Ar$) calculated from the accepted grain analyses. The age and error estimates derived from the isochron regressions are then compared to analytical weighted means.

4.3.3. Diatom Sample Preparation and Counting

About 0.1 g of sample was added to 20 ml of 30% H_2O_2 and heated to 90°C to remove organics (Battarbee, 1986). 10% HCl (to remove carbonates) and a *Lycopodium* microspore (to measure concentrations) were then added, with samples rinsed in DI water and centrifuged to remove remaining acids. Ammonia solution (30–33% NH_3) was added to separate aggregates and remove clays before a final rinsing in DI water. Samples were added to coverslips and dried for 24 hours. Naphrax was used to adhere cover slips to glass slides and heated at 125°C until cured.

When possible, at least 400 diatom valves were counted on a Fisher B2-Series light microscope at 1000× magnification. If one species was dominant, a minimum of 100 non-dominant valves were counted. Identification was conducted using Spaulding et al. (2022), Gasse (1986), Cocquyt (1998), and Taylor et al. (2007). A valve was counted if >50% of the valve was visible and identifiable. In all cases, specimens were identified to the lowest taxonomic level possible. Identifications were confirmed on a Phenom XL Scanning Electron Microscope with a Cerium Hexaborit (CeB6) cathode at the Universität Tübingen. Samples were coated with 70 nm gold and analyzed at 15 kV acceleration voltage.

4.3.4. Diatom Analysis

Diatom concentrations were calculated using *Lycopodium* spores (Batch-050220211; 18,400 spores).

$$DiatomConcentration = \frac{(\#ofMicrospheresIntroduced * \#ofCountedDiatoms)}{(1 + \#ofMicrospheresCounted)}$$

An adapted Planktonic Diatom Index (PDI) was used to characterize deep lakes (Deino et al., 2006; Kingston et al., 2007) where deep lake conditions occur when PDI≥10.

$$PDI = \sqrt{\frac{\%ofPlanktonicDiatoms}{(\%ofLittoralPlanktonic + \%ofLittoralDiatoms)}}$$

Ecological interpretations are based on modern assemblage data from the East African Diatom Database within the European Diatom Database Index (EDDI) (Battarbee et al., 2001). Hydrochemical parameters (conductivity and pH) were determined using weighted averaging (ter Braak & Looman, 1986; Gasse et al., 1995). The modern African training set includes each taxon's optimum and tolerance for each environmental parameter. Paleoenvironmental parameters are estimated using the total sum of the relative percentage of each fossil taxon, weighted by its optimum, and standardized to the total percentage of the diatom assemblage used in the transfer function (Chalié & Gasse, 2002). Weighted tolerances were then added to create a range for the calculated parameter. Statistical analyses were conducted in R and are accessible in GitLab. Stratigraphic plots were made using the R package Rioja (Juggins, 2022).

4.3.4. XRF and PCA

Bulk samples selected for major oxide- (SiO_2, Al_2O_3, Fe_2O_3, CaO, MgO, K_2O, Na_2O, TiO_2, MnO, P_2O_5) and trace element (Ca, Cr, Ga, Nb, Ni, Rb, Sr, V, Y, Zn, Zr) analyses via X-Ray Fluorescence (XRF) were pulverized and mixed with 7.5 g MERCK spectromelt A12, followed by gradual melting up to 1200°C to fused beads using an Oxiflux system. Measurements were carried out on a Bruker AXS S4 Pioneer XRF device (Rh-tube, 4 kW) at the Universität Potsdam.

The oxide for each sample was normalized by dividing each oxide's percentage by the total percentages without Loss on Ignition (LOI) and multiplying by 100.

Samples were then converted to elemental weight percentages and parts per million (ppm).

$$Weight\%ofElement = NormWeight\%ofOxide * \left(\frac{\#ofCationsinOxide * AtomicMassofCation}{AtomicMassofOxide}\right)$$

The Chemical Index of Alteration (CIA) (Nesbitt & Young, 1982) was calculated to indicate the degree of weathering of source rocks to the sediments. Numbers closer to 100 indicate more heavily weathered deposits and/or slower erosion rates (Owen et al., 2014; 2018). To use this index, XRF data was converted into molar proportions:

$$MolarProportionoftheOxide = \left(\frac{NormalizedWeightPercentageofOxide}{MolarMassofOxide}\right)$$

The CIA was then calculated using:

$$CIA = \frac{Al_2O_3}{(Al_2O_3 + CaO^* + Na_2O + K_2O)} * 100$$

CaO* (inorganic CaO) was estimated by subtracting the molar proportions of P_2O_5 from CaO (McLennan, 1993). If the estimated CaO* was greater than Na_2O, the molar proportion of Na_2O was used, as Ca weathers more readily than Na. Carbonate features were not used in this analysis as they do not reflect the valley's weathering regime.

Principal Component Analysis (PCA) was run for XRF data to reduce dimensionality and interpret elemental relationships and possible transport mechanisms (Jolliffe & Cadima, 2016). Known tephra layers were not included as they do not represent the same depositional regimes as other sediments. PCA was run in R and the code is accessible on GitLab.

4.4. RESULTS

4.4.1. Stratigraphy and Grain Sizes

The KSI sediments include laminated clays, diatomites, silts, fine to coarse sands, carbonates, and tephras (F2; S1). From 0–9 m, the KSI section consists

mainly of laminated silty diatomites with laminated silty diatomaceous clays from ~5–6 m (F2). Carbonate concretions are present at 0.2 m and a black, massive carbonate layer occurs at 2.2 m. Carbonates also occur at 9.2 and 10.25 m and are separated by silty, carbonate-rich clay. The former is black with mm-sized nodules, whereas the latter is gray and irregular with paleoroot fillings. Laminated silts dominate 10.5–12.5 m, above which are beds of fluvial coarse sands. A dated tephra (SUG07-KS-01; T1) is present at 14.8 m, with silt above and sandy silt below, both of which contain yellow pumice. Grain size decreases from coarse sands to silts and laminated clays from 13–17.9 m. Carbonate content increases from 16–17.9 m, where another black, massive carbonate with mudcracks marks a transition to fewer carbonates and more fine-grained sediments. Diatoms are less abundant within the clays from 18–21 m. Laminated clayey diatomites and pure diatomites continue to 27.5 m, with bedded carbonate concretions (<20 cm) at 25.3 m. Abundant diatoms disappear above 27.5 m. Above 27.5 m, KSI is coarser grained with numerous tephra horizons interbedded in laminated clayey silts, silts, and silty sands. Alternating pumiceous sand, angular volcanic clasts, bones, burrows, and calcite coatings dominate from 28.5–30.5 m. A 20-cm-thick tephra with yellow pumice at 32 m (SUG07-KS-05; T1) is overlain by a 70-cm-thick sand. Carbonate-rich sediments, starting at 33.4 m, include calcareous paleoroots (F2). The overlying sediments are “baked” carbonate clay with silty components, evidenced by clumped aggregates and discoloration. Sand at ~35.5 m is overlain by clayey and silty deposits with several orange tephra horizons at 41 m (SUG07-KS-2a; T1), which have been weathered due to surface exposure and heat-altered by the overlying basalt.

4.4.2. Chronology and Sedimentation Rates Estimates

A total of 76 grains were analyzed from three samples (S2): of these, 25 were retained in the calculation of representative mean ages. The majority of analyses were rejected due to anomalously old ages by the gap-finding procedure (42),

reflecting the high degree of detrital contamination present in most samples. An additional four were rejected based on plagioclase composition.

The oldest sample (SUG07/KS-1, reworked pumice) shows a simple, quasi-gaussian symmetrical distribution with just one anomalously old analysis out of 17 (F3A; T1). This sample also exhibits a MSWD (1.2) close to the expectation of 1, indicating that the analytical errors account for the observed dispersion. These straightforward characteristics suggest that the weighted-mean age of 885±5 ka should provide accurate timing for the eruption that was the source of these lapilli.

The next-oldest sample (SUG07/KS-5, reworked fine pumice and detrital matrix) exhibits 21 analyses registered as anomalously old by the gap-finding technique, leaving nine analyses as a primary mode candidate. However, this remaining distribution contains two well-defined modes with a high MSWD (8.6), indicating the presence of geological dispersion. Here, the older mode was eliminated on the principal that it may represent xenocrysts not identified by the gap-finding technique, due to the relatively close age proximity to the youngest mode. In fact, the older mode is very similar in age and Ca/K composition to SUG07/KS-1 and may represent incorporation of tephra from that earlier eruption during fluvial transport. After elimination, the remaining five grains give a weighted-mean age of 830±5 ka with a MSWD=1.5.

The youngest sample (SUG07/KS-2a) was obtained from Plinian fallout ash immediately below the capping mafic lava of the Kamuge-Suguta confluence area. It apparently represents a partially silicic precursor eruptive phase before lava effusion. Most of the 29 grains analyzed were omitted as older contaminants or plagioclase, leaving four K-feldspar grains forming a distinct primary mode with a weighted-mean age of 448±22 ka.

The isochron evaluations of the accepted analyses (F3B; T1) yield ages that are within error of the weighted means and $^{40}Ar/^{36}Ar$ compositions that are indistinguishable from atmosphere (298.56±0.31; Lee et al., 2006). The isochron age

errors for samples SUG07/KS-1 and SUG07/KS-4 are equal to or slightly better than the analytical mean errors, however, due to the narrow range of $^{39}Ar/^{40}Ar$ composition and relatively high uncertainty in $^{36}Ar/^{40}Ar$, the isochron regression for sample SUG07/KS-2a yields an error that is about four times that of the weighted mean. This is a shortcoming of the isochron approach with this particular data set; hence is rejected. For the sake of consistency, the weighted-mean analytical ages and errors are the preferred dating result for all samples.

Given these dates, the ~17.5 m of sediment from 14.8–32.25 m represent deposition over ~54 ka, although a potential hiatus exists at 25.3 m. A mean sedimentation rate of ~32.3 cm/kyr (0.3 mm/yr) is estimated, consistent with other estimated diatomite deposition rates across Eastern Africa (c.f. Trauth, 2014) ranging from 10 cm/kyr in the southern Kenya Rift (Owen et al., 2012) to 80–200 cm/kyr at Olorgesailie (Isaac & Isaac, 1977; Potts et al., 1999). Extrapolation to the base of the section suggests an age of ~931 ka, although several hiatuses indicate an older age. The relatively young age of SUG07/KS-2a suggests at least one large hiatus between 32.5 and 40 m, although multiple breaks in deposition are possible (F2).

4.4.3. Diatom Analysis

Diatoms are most abundant in the lower 27.5 m with gaps at 10–12.5, 16–16.5, 18, and 19.5–21 m (F4; S3). Freshwater, planktonic diatoms are most abundant, particularly *Aulacoseira agassizii* (Ostenfeld) Simonsen*, A. distans* (Ehrenberg) Simonsen, *A. granulata* (Ehrenberg) Simonsen, and *A. granulata* var. *angustissima* (Müller) Simonsen (F4; Gasse, 1980; Owen et al., 2014). Notable exceptions occur at 17 and 17.5 m where >99% of counted taxa are *Stephanocyclus meneghinianus* (Kützing) Kulikovskiy, Genkal & Kociolek (formerly *Cyclotella meneghiniana* Kützing), a periphytic indicator of mildly to strongly saline conditions in littoral and planktonic settings (Owen et al., 2014). Shallow water taxa are most abundant from 23.5–27 m, where they peak up to 76%. Epiphytic taxa include *Cocconeis placentula* Ehrenberg and *Caloneis bacillum* (Grunow) Cleve, with

the latter associated with flowing water. *Hantzschia amphioxys* (Ehrenberg) Grunow and *Luticola mutica* (Kützing) DG Mann are often found in damp soil or swamps. Other freshwater to mildly saline epiphytes and benthic taxa include *Nitzschia amphibia* Grunow*, Epithemia gibberula* (Ehrenberg) Kützing*, E. sorex* Kützing*, Achnanthidium exiguum* (Grunow) Czarnecki*, Sellaphora pupula* (Kützing) Mereschkovsky, and *Staurosira construens* Ehrenberg. Collectively, these taxa indicate fresh, shallow, or swampy conditions perhaps with nearby inflowing streams from 23.5–27 m (Owen et al., 2014). Highly saline indicators are absent throughout KSI, indicating that saline phases were not extreme, not preserved, or developed too quickly to be visible at 50-cm intervals.

Of the 82 taxa, 52 are reported within the EDDI (S3). The percentage of taxa missing in the transfer functions ranges from 0–36%, averaging to 9.4%. The missing data can be attributed to an irregular *Aulacoseira granulata* morphotype (Plates 17/18/19) also recorded by Gasse (1975), *Epithemia hirundiformis* Müller, and *Nitzschia radicula* Hustedt. *Stephanodiscus neoastraea* Håkansson & Hickel is also not in the database, although modern studies show that the ecology is similar to *Stephanodiscus astraea* (Ehrenberg) Grunow (Genkal, 2009). Consequently, these data were used. Absence of data clearly limits the precision of the transfer functions, although comparison with other diatom proxies such as PDI and supplemental XRF data support their inferences. Conductivity is a proxy for the precipitation-evaporation balance of a lake system and is linked with changes in the hydrological budget and climate, whereas pH provides additional evidence of changes in hydrochemistry (Battarbee, 1986; Gasse et al., 1995). Both conductivity and pH remain consistent through the section except at 17 and 17.5 m where they are estimated at ~6,030 µS/cm and 8.85, respectively, due to the abundance of *Stephanocyclus meneghinianus* (F4; S3). The range for other parts of the section are considerably fresher at ~150–870 µS/cm and 7.14–7.91, respectively. PDI≥10 indicates a deep paleolake (Kingston et al., 2007), occurring at 17.8, 18.5, and 23 m.

4.4.4. XRF Analysis and PCA

SiO_2 is the most abundant oxide in the KSI sediments and constitutes 55–65% (median=59.0%) of the total oxides, except within carbonates (F5; S4). This reflects opaline silica in diatoms and the strongly silica-oversaturated peralkaline volcanics of the eastern Emuruagiring Plateau and the panterellitic Lower Trachytes of Emuruangogolak (Dunkley et al., 1993). TiO_2 (0.19–2.6%, median=1.3%), Fe_2O_3 (2.9–13.2%, 9.3%), Al_2O_3 (3.0–18.9%, 15.9%), K_2O (0.4–4.0%, 2.9%), Zr (190–920 ppm, 660 ppm), Zn (40–207 ppm, 164 ppm), and Rb (21–140 ppm, 115 ppm) show similar trends to SiO_2, with respect to the main excursion reflecting igneous sources. In contrast, CaO (0.3–71.3%. 1.7%), MnO (0.08–12.5%, 0.18%), Ba (104–6750 ppm, 373 ppm), Sr (111–1790 ppm, 210 ppm), and LOI (2–37.7%, 9.2%) show similar trends with low values except within carbonates and carbonate-rich sediments, reflecting authigenic and/or biogenic influences. P_2O_5 (0.07–22.5%, 0.28%) is only abundant in carbonates associated with clayey and silty diatomites, reflecting its biogenic nature and potential adsorption within clays. MgO (0.6–5.6%, 1.7%) and Na_2O (1.3–16.6%, 5.0%) do not follow the trends of other oxides, indicating additional controls, such as potential changes in the catchment area or fluvial regime, and their potential for authigenic precipitation during more arid phases.

Carbonates were evident in peaks across all oxide and trace element plots (F5) and dominated the PCA, with Dimension 1 (Dim1) representing 54.6% of the XRF data trends (S5). Calcareous features, indicated by elevated LOI (F5), were removed to detrend the data and focus on sediment input. Chromium, Ga, Nb, Ni, V, and Y were not used for analysis as they were detected at low levels, although they tended to reflect deposition from igneous, particularly basaltic source rocks. With the removal of tephras, carbonates, and less relevant trace elements, Dim1 (38.9%) is significantly controlled by lithogenic elements (Zr, Zn, Al, and Rb in the negative direction), with biogenic/authigenic elements (Sr, Ca, and P) plotting positively (F6; S5). Dim1 is interpreted as a wetness proxy, where an increase in

biogenic/authigenic elements is linked to drier conditions when shallow, nutrient-rich oxygenated waters result in increased biological activity and authigenic precipitation. In contrast, increases in lithogenic elements reflect wetter conditions, when more non-soluble cations are brought into the system as clastics. Dimension 2 (Dim2; 21.4%) is controlled positively by Ti, K, Ba, Fe, and Al and negatively by Mg (with Ca contributing an additional ~5%) (F6; S5). Positive Dim2 values therefore represent more neutral and wetter settings with negative values indicating saline, alkaline, and drier conditions.

Ti/Ca and K/Al reflect changes in deposition within the alkaline basaltic and trachytic igneous system (F6; S5). Titanium is an abundant and stable lithogenic element used as a proxy for erosion and transport of silts and fine sands, as it is brought into the system through wind or water transport (Davies et al., 2015). Calcium is a water-soluble element that can be biogenic or lithogenic and allogenic or authigenic, therefore representing sediment input, local precipitation, and/or biological activity. By comparing Ca with Ti, which is not affected by diagenetic overprinting or biological processes (Fitzpatrick & Chittleborough, 2002; Mannella et al., 2019), Ca from igneous sources is removed, leaving biogenic/authigenic Ca depositing over drier phases. Aluminum is an abundant and stable element that is transported through clastic grains, particularly clays. Potassium is water-soluble and abundant in igneous rocks, particularly in trachytes and authigenic clays. When K/Al increases, it reflects a change in clay mineralogy where K fixes during the illitization of smectites in higher pH systems related to drier conditions (Foerster et al., 2018). Both ratios indicate wetter phases from 0–9 and 18–27.5 m and drier phases from 9.2–17.9 and 28–41 m (F6).

The mean CIA through the section is 49.1 (F6). CIA was used to create four zones with constrained hierarchical cluster analysis using Bray-Curtis dissimilarity (CONISS) to create separate rather than overlapping zones within stratigraphic sequence. Four zones were selected rather than the three zones recommended the

broken stick model based on visible changes in the lithology as well as the absence of diatoms. Regardless, the distance of the zones is ~2.25 (S5) and results in boundaries between 8–8.5, 18–18.5, and 29–29.5 m. Because these boundaries were created without carbonate features, they were updated to match changes in lithology, resulting in Phase 1 from 0–9, Phase 2 from 9.2–17.9, Phase 3 from 18–27.5, and Phase 4 from 28–41 m (F7; S4). The mean CIA for Phases 1, 2, 3, and 4 are 44.1, 41.4, 58.9, and 48.4, respectively (F6; S4).

4.5. DISCUSSION

4.5.1. Morphological and Volcanic History

The morphology of the Suguta catchment during KSI's deposition differed significantly from today, with local volcanoes erupting throughout the Pleistocene and Holocene as rifting widened and deepened the formerly shallow basin (Dunkley et al., 1993). Tephras most likely come from Emuruangogolak or Namarunu despite their ability to travel long distances (>5,000 km) within short timeframes (minutes to days) (Lowe, 2011), as most nearby Kenya Rift volcanoes are younger than KSI (Dunkley et al., 1993). The trachytic shield of Emuruangogolak began forming 900±100 ka and continued to develop until 500±100 ka (Weaver, 1977; Dunkley et al., 1993), with dated Emuruangogolak eruptions at 864±7 ka (Dunkley et al., 1993). At Namarunu, two eruptions took place during KSI's deposition at 871±5 and 840±5 ka (Dunkley et al., 1993). The massive capping basalt at KSI likely flowed from Emuruangogolak during a 185±11 ka eruption. Older local basalts (4–2.33 Ma) from Namarunu (Dunkley et al., 1993) may have contributed to KSI's sedimentary basaltic influx.

4.5.2. Lithological Deposition

Dunkley et al. (1993) observed that the capping basalt, 25 m southwest of KSI, overlies poorly stratified and cross-stratified sands cut by large channels. These sands indicate nearby fluvial conditions, which may have eroded several hiatuses at KSI, thus explaining the large age gap in the upper sequence. Older sands at KSI

support Truckle's (1976 & 1977) suggestion that Paleolake Suguta, despite being laterally extensive, was at least periodically shallow. Rapid lateral facies variations might reflect delta/fan switching (sedimentary control) and/or lake level variations (a climatic control). The latter scenario would imply rapid changes from deep water (laminated diatomites) to shallower lakes with alluvial fans and deltas.

Clays likely also indicate phases of fluvial deposition, with mixed lithologies and graded bedding likely representing direct riverine deposition, and interbedded clays and silt to fine sands representing flood plains. Fluvial clays may have also been transported into deeper lake waters as hypopycnal or hyperpycnal flows where they would have become interbedded with diatomites on a seasonal or longer-term basis. Today, cm-scale clastic laminae related to seasonal Omo River flooding into Lake Turkana are a modern example of laminated clays being preserved in fully oxygenated water tens of meters deep (Cohen, 1984). Other clays may represent authigenic clays which are well-documented across Eastern Africa such as at Chew Bahir (Foerster et al., 2018), although further studies of the mineral composition are necessary to distinguish between authigenic and allogenic clays.

4.5.3. Biological Deposition

O'Sullivan (1983) recognized four types of laminations in lakes: ferrogenic, calcareous, biogenic, and clastic. He noted that a flat basin morphometry (reduced slumping and lateral creep) and periodicity in sediment supply are important. In addition, deep waters prevent wind-induced lake floor reworking and favor anoxic bottom conditions and organic preservation with suppression of infauna, preserving laminae. This is the case at Lake Malawi where mm-scale *Aulacoseira-Stephanodiscus-Nitzschia* laminae are common (Owen & Crossley, 1992; Pilskaln & Johnson, 1991). In some circumstances, however, shallow, highly saline lakes can preserve lamination due to infauna inhibition. Strong chemical stratification can also prevent wind-induced disturbance in waters 1–2 m deep, as is the case at Nasikie Engida in the South Kenya Rift (Renaut et al., 2021). Therefore, while deep lakes

can preserve laminated diatomites, evidence across Eastern Africa indicates that shallower lakes can preserve laminae as well.

Three diatomite facies are distinguished in KSI: **a)** finely laminated diatomites (mm-thick); **b)** laminated clayey diatomites (<1 cm); and **c)** laminated silty diatomites (1–2 cm) (F2). Facies 1 and 2 often have a higher concentration of diatoms than Facies 3. **a)** The finely laminated diatom layers at 23.5–25 m indicate deep water with high percentages of *Aulacoseira granulata,* that is favored by deep, silica-rich waters and high wind turbulence, and long, thin benthic taxa, that can be transported into deeper waters, including *Ulnaria acus* (Kützing) Aboal and *Nitzschia radicula* (Gasse, 1986). **b)** The laminated clayey diatomites host variable communities, including shallow- and deep-water taxa, suggesting mixed flora from different settings. The inclusion of *Aulacoseira* (*A. ambigua* (Grunow) Simonsen, *A. granulata* var. *angustissima*) that occur in shallow to moderate water, also indicates deposition from variable lake depths. **c)** Laminated silty diatomites only occur in the lower sequence. Parts of the laminated sequence where benthic taxa are common may reflect shallowing events with subsequent floral mixing during deposition or sampling. Littoral and/or fluvial taxa can also be introduced from nearby rivers (Barker et al., 1991).

Five carbonate types are present at KSI: **a)** yellow, disk-like layered concretions <20 cm in diameter; **b)** flat, irregular, gray, and coarse-grained carbonates; **c)** dark (almost black) hard layers with mm-scale nodules; **d)** carbonate-rich clays and silts; and **e)** soil carbonates (F2). Such a variety in fluvio-lacustrine deposits is common in Eastern Africa, with the Plio-Pleistocene fluvio-lacustrine sediments and carbonate layers of Olduvai basin providing prime examples (Hay, 1976; Cerling & Hay, 1986; Bennett et al., 2012; Liutkus et al., 2005; Ashley et al., 2014, Stanistreet et al., 2020). **a)** The disk-like concretions occur twice in the record, close to lithological changes towards coarser sediments. Stanistreet et al. (2020) and Bennett et al. (2012) describe similar carbonates as accretional nodules just below erosional surfaces,

reflecting secondary growth. Erosional features were not observed at KSI but are not excluded given the lithological changes. If hiatuses exist, then they were short-lived, as there are no well-developed soils (Stanistreet et al., 2020). **b)** Flat, gray, coarse-grained carbonates occur in silty clays and sands and are interpreted as algal mats in shallow, stagnant waters, representing primary carbonate. **c)** Dark, thin (<5 cm) carbonate layers in clays, silts, and clayey carbonates indicate shallow, alkaline waters, resulting in the precipitation of primary carbonates. **d)** Calcareous clays are secondary, likely forming when Paleolake Suguta dried, given that similar carbonate (and gypsum) crusts are observed today (Dunkley et al., 1993). **e)** Secondary soil carbonates form after desiccation and indicate hiatuses.

4.5.4. Paleoenvironmental Reconstructions

Phase 1 (0–9 m, >885 ka): Freshwater Lake

The mostly laminated silts and diatomites from 0–9 m indicate deposition in a freshwater lake with variable water depth. High Ti/Ca and low K/Al ratios reflect silty clastic inputs during shallow phases, with a mean CIA of 44.1, suggesting low to moderate weathering in the catchment (F7). Carbonate concretions at 0.2 m indicate a hiatus. Abundant planktonic taxa, including *Aulacoseira ambigua, A. granulata, A. muzzanensis,* and *Stephanodiscus* cf. *minutulus* (Kützing) Cleve & Möller (F2), imply both shallow and deeper lakes during Phase 1. From 2–4 m, littoral taxa (*Epithemia*, *Gomphonema, Nitzschia* spp.*)* constitute 11.3–29.0% of the assemblage, indicating a shallower stage. A black, primary carbonate at 2.2 m supports this conclusion. Increased *A. ambigua* percentages across the rest of the phase suggests that waters were of intermediate depth, with PDI<10 across the section. The transfer functions indicate an average conductivity of only ~310 µS/cm and pH of 7.36 (F7), implying an open lake and wet climate. Phase 1 ends with a black, precipitated carbonate at 9.2 m, increased LOI, and a disappearance of diatoms, representing potential desiccation.

Phase 2 (9.2–17.9 m, ~885 ka): Fluvial and Flood Plains with Temporary Standing Water

Sediments at 9.2–17.9 m are more variable than the rest of the sequence, with silty clay to coarse sands indicating river settings and flood plains with episodic lakes (F7). An increase in biogenic/authigenic input, reduced Ti/Ca and enhanced K/Al ratios, and decreased CIA (41.2), also suggest a drier climate with less weathering compared to Phase 1. SUG07/KS-1 at 14.7 m is dated to 885±5 ka (T1), with potential hiatuses at 10.2 and 13 m. Non-diatomaceous laminated silts and clays (9–13 m) suggest a flood plain begins this phase. Carbonate crusts with high LOI and rhizoliths indicate land surfaces, possibly with highly alkaline ephemeral waters with algal mats. The lack of diatoms could reflect high pH waters that prevented diatom growth and/or competitive exclusion or post-mortem dissolution (Barker et al., 1994; Ryves et al., 2013). Sands (13–14.2 m) suggest fluvial conditions followed, with a possible erosion surface at 13 m. Diatoms (*Aulacoseira* spp., *Epithemia hirundiformis*) at 14.2–15.5 m indicate a freshwater lake. Diatoms are absent at 16–17 m reflecting either short-term desiccation or highly alkaline conditions, supported by the presence of carbonates and calcareous silty clays. Diatoms at 17–17.5 m are dominated by *Stephanocyclus meneghinianus* with low diversity, suggesting a highly alkaline lake (average conductivity and pH of ~5,970 µS/cm and 8.85, respectively; F4; F7). Black carbonate at 17.9 m suggests alkaline conditions and potential desiccation.

Transition from Phase 2 to Phase 3

The Phase 2 to 3 diatom transition indicates major changes within a short stratigraphic interval that deviate from KSI's generally freshwater *Aulacoseira*-dominated communities. At 17 and 17.5 m, assemblages are >98% *Stephanocyclus meneghinianus*, a mostly shallow and saline water indicator (F4) (Gasse, 1986; Owen et al., 2014). In contrast, at 17.8 m, *Stephanodiscus neoastraea* (>97%) indicates a major shift to fresher, deeper water, also evidenced

by the transfer functions and PDI. Diatoms disappear at 17.9 (a black carbonate) and 18 m (carbonate-rich layered clays and silts), ultimately returning at 18.5 m with >99% *S. neoastraea*. The most significant change across Dim2 also occurs here with negative values at ~16–19 m, reflecting increased carbonate precipitation (F7), which is also evident in increased MgO from 10–17 m (F5). With a sedimentation rate of 32.3 cm/kyr, it is unlikely that this major change is the result of a long-term hiatus between these points. In addition, there is no sedimentological evidence for a substantial hiatus, with mudcracks within the black carbonate representing temporarily dry conditions. Paleolake Suguta therefore changed from a shallow, saline, and even desiccated lake into a deeper, freshwater lake over hundreds of years, mirroring rapid responses to changing climate during the AHP (Bergner et al., 2009; Olaka et al., 2010; Trauth et al., 2010; Garcin et al., 2012; Junginger & Trauth, 2013; Junginger et al., 2014). Limiting nutrients might also partly explain the unusual increase in *S. neoastraea* and could reflect changes in source water, depth, mixing, or seasonality given its abundance in low Si:P environments (Kilham et al., 1986). None of these hypotheses are mutually exclusive and can all be partially linked to depth variations. It is conceivable that this is not the only part of the sequence that changed rapidly, but at 50-cm resolution, such events may have been missed.

Phase 3 (18–27.5 m, >831 ka, <885 ka): Highly Fluctuating Lacustrine Conditions

Laminated clays, silts, and diatomites dominate 18–27.5 m, indicating a variable lacustrine phase (F7). Increased clastics and Ti/Ca, decreased K/Al, and abundant *Aulacoseira* similarly reflect a paleolake. The CIA average of 58.9 indicates more heavily weathered source rocks compared to the rest of the outcrop. Major increases and decreases in water levels over millennia are indicated by rapid transitions from shallow, alkaline diatoms (17.5 m) to freshwater taxa (17.8 m) and the development of mudcracks (17.9 m) as discussed in 5.4.3. Diatoms are absent at 18 m, but give way to deep, freshwater taxa at 18.5 m. At 19 m, a low concentration of diatoms indicates a shift to shallower conditions with the return of littoral and littoral-

planktonic assemblages, supported by a slight increase in K/Al and less stratified clays and clayey silts. *Ulnaria ulna* (Kützing) Compère makes up 12.4% of the assemblage at 19 m and could signal swampy conditions, although this taxon can be reworked into the plankton (Gasse, 1986; Owen & Renaut, 2000). Diatoms are absent at 19.5–21 m, which has high CIA and Ti/Ca. The laminated silts and clays are interpreted as a shallow, alkaline swamp in which the diatom frustules may have dissolved. At 21.5–23 m, the assemblage is dominated by *A. granulata*, indicating deeper water (F4). Diatoms are scarce at 22.5 m but *A. granulata* are dominant (55/75 counted valves), which is interpreted as due to diagenesis rather than desiccation based on the lack of other clear evidence for desiccation. Finely laminated diatomaceous layers at 23.5–25 m indicate deep water, although increased *A. granulata* var. *angustissima* may reflect shallower influences. These deposits are also associated with long, thin littoral taxa (*Ulnaria*, *Nitzschia*) (Gasse, 1986). Owen and Renaut (2000) reported mixed *Aulacoseira*-*Synedra* (*Ulnaria*) from similar mm-scale laminated Miocene diatomites in the Tugen Hills as deep-water floras, noting that the diatoms might represent a seasonal succession controlled by Si:P ratios (Kilham et al., 1986). The presence of carbonate concretions at 25.3 m indicates a potential hiatus, although the diatom assemblages between 25–27 m have similarly high percentages of *A. granulata* with increasing *A. granulata* var. *angustissima*. At 27.5 m, *A. granulata* dominates again before diatoms disappear permanently.

Phase 4 (28–41 m, ~831, >448 ka): Fluvial and Flood Plain Deposition

Non-diatomaceous laminated silts, carbonates, sands, sandy calcareous tephra, and tephra layers from 28–41 m indicate rivers and flood plains during this phase (F7). The shift to biogenic/authigenic deposition, decrease in Ti/Ca, and gradual increase in K/Al support this suggestion. Diatoms are scarce throughout this phase, with the area perhaps flooding occasionally, such as at 33 m where 26/35 diatoms are *Aulacoseira*. This is supported by a nearly 1-m-thick marker horizon of pumice

and riverine sands in a carbonate matrix with bones (fish, turtle, crocodile, antelope). Increased volcanic activity is indicated by elevated Cr, Ni, Mg, V, Fe, and Ti which are at their highest concentrations in the KSI record (F5; S4). The large timeframe between 831±5 ka (32.25 m) and 448±22 ka (41.5 m) indicates either a decrease in sedimentation rate and/or one or more hiatuses, potentially at 33.4, 35.5, 40.5, and 41 m.

4.5.5. Regional Comparison and Relation to the EMPT

Earlier reviews of Eastern African Pleistocene environments around the EMPT note that freshwater lakes existed between 1,100–900 ka during a humid period extending between southern Arabia (Nicholson et al., 2020), the Afar Basin in northern Ethiopia (Gasse, 1990; Trauth et al., 2005; 2007), and the Olorgesailie Basin in southern Kenya (F8; Owen et al., 2009; Trauth et al., 2009; Trauth et al., 2015). The EMPT represents the change from 41- to 100-kyr glacial cycles and increasing long-term global ice volume by ~50 m sea-level-equivalent from 1,200-700 ka (Pisias & Moore, 1981; Clark et al., 2006; Maslin & Brierley, 2015). Across the EMPT, sea surface temperatures in the North Atlantic and tropical ocean upwelling regions decreased, particularly from 920–880 ka, leading to an intensification of the East Asian winter monsoon and arid phases in Asia and Africa (Clark et al., 2006; Sun et al., 2006; Head et al., 2008; Lee et al., 2020). In addition, there is evidence for an increase in North Atlantic Deep-Water formation (Martin-Garcia et al., 2018), a reduction of North Atlantic thermohaline circulation (Clark et al., 2006; Head et al., 2008), and an increase in Walker circulation (McClymont & Rosell-Melé, 2005), particularly around 900 ka. These global changes, that expanded grassland biomes during intensification of glacial cycles and colder climates, resulted in mass migration of mammals globally (Azzaroli et al., 1988; Vrba, 1996; Head & Gibbard, 2005; van Kolfschoten & Markova, 2005; Martinez-Navarro & Rabinovich, 2011), including members of our genus *Homo* (Head & Gibbard, 2005; deMenocal, 2004;). Global changes during the EMPT are highlighted in F8.

Regional comparison of paleoenvironmental change along the Gregory Rift between ~931–831 ka is difficult given the lack of well-constrained age models and paleolake records (F8). Recent core records from the Koora Basin shed light on the EMPT with three hydroclimatic phases evident from diatoms (Muiruri et al., 2021a). Phase 1 (~1000–860 ka) was characterized by shallow fresh lakes with two desiccation episodes. The paleolakes then deepened during Phase 2 (~860–780 ka) and remained high. Phase 3 (780–700 ka) shows greater variability with shallow and deep lakes that periodically dried out. At Lake Magadi, located within 20 kilometers from the Koora Basin, pollen are not preserved between 940–750 ka, but earlier floras suggest stable drier climates with more varied conditions after ~750 ka (Muiruri et al., 2021b). Olorgesailie, located just north of Koora and Magadi, was dominated by terrestrial sediments through much of the EMPT (with a lake only developing at ~980 ka), but with two wetter intervals during Phase 3 that match the later wetter conditions at Koora and Magadi (Potts et al., 2018).

The KSI deposits represent two lacustrine intervals with variable lake levels that are suggestive of broadly wetter conditions. The first developed by >931 ka with the second after 885 ka and ceasing before 831 ka, spanning the major Phase 1 to 2 transition at Koora. The first lake expansion does not match well with Phase 1 low levels at Koora. However, the second may reflect the major Koora deepening at 860 ka, which peaked at about the same time at MIS21g (Muiruri et al., 2021a). Regardless, such variability highlights the intense changes that occurred globally around 900 ka (F8). Other parts of the EMPT are less comparable, possibly because of the impact of local tectonics, volcanism, autocyclic sedimentation, variability between chronological models (Muiruri et al. 2021a), and heightened environmental changes associated with the EMPT. Indeed, Potts et al. (2020) noted difficulties in their attempts to correlate between Koora lake levels and global climate, especially before 500 ka.

Detailed comparisons are even more difficult elsewhere. At Olduvai Gorge, Bed III claystones and sandstones (1.15–0.70 Ma) indicate rivers and shallow waters during the early EMPT (F8) (Stanistreet et al., 2020). At Munyu wa Gicheru, multiple lacustrine phases (1.96–1.65 Ma) led into terrestrial conditions at 1.65–0.724 Ma (Owen et al. 2014). Further north of Munya wa Gicheru, at Kariandusi in the Elmenteita-Nakuru Basin, a 31-m-thick diatomite (~0.987 Ma–post-0.946 Ma) documents a deep, freshwater lake. This large paleolake ceased with the development of cross-bedded sands and relatively thin diatomites (Trauth et al., 2007). Floodplains dominated the Turkana Basin during the EMPT, with erosion removing ~1–0.8 Ma records at Koobi Fora (Brown & McDougall, 2011). With no hydrological separation evident during KSI's deposition (McDougall et al., 2012), the KSI section could represent a southern extension of a Suguta/Turkana megalake with the lack of evidence for Paleolake Turkana related to burial below the modern lake and erosion of marginal areas.

Overall the differences between the basins with records across the EMPT highlight the local variability across the region. This indicates that regional-scale reconstructions linking climate and hominin evolution minimize the complexities of the relationships, given that each basin shows a unique record. Regardless, during this time period, the paleoanthropological and archaeological records are poor in part because of few records across this time. Evidence of periods of freshwater lakes at Paleolake Suguta highlight that this may be an important area to study potential hominin activity during the EMPT.

4.6. CONCLUSIONS

Reviews of EMPT records in Eastern Africa show, like global climate records, that lake dynamics across the EARS varied through space and time. KSI provides insights into changes of Paleolake Suguta between >931–831 ka. Dates of 885±5 and 831±5 ka in the middle of the outcrop, allowed reconstruction of lake dynamics across the later EMPT. The KSI record indicates two wetter and two drier intervals.

Shallow, intermediate, and deep freshwater lakes developed by at least ~931 ka with drier conditions setting in before 885 ka. The second lacustrine interval was characterized by variable freshwater, shallow to deep, paleolakes, and a closed-basin lake with higher salinities. These paleolakes appear to have changed from one state to another over a scale of hundreds of years leading to the development of a drier flood plain some time before 831 ka.

The Suguta record documents how variable EMPT humid phases were at a fine scale, reflecting the profound global climatic changes during this time. Comparisons with core records from the southern Kenya Rift show generally poor correlations for these detailed phases, likely reflecting the impacts of tectonism, volcanism, and autocyclic sedimentation on local paleoenvironments. However, the onset of deeper lakes at Koora appear to have developed at about the same time as the second lacustrine interval at Suguta and led to major lake expansions in both basins, peaking during oxygen isotope stage 21g, and perhaps reflecting a major inflection in the global climate record.

4.7. FIGURES

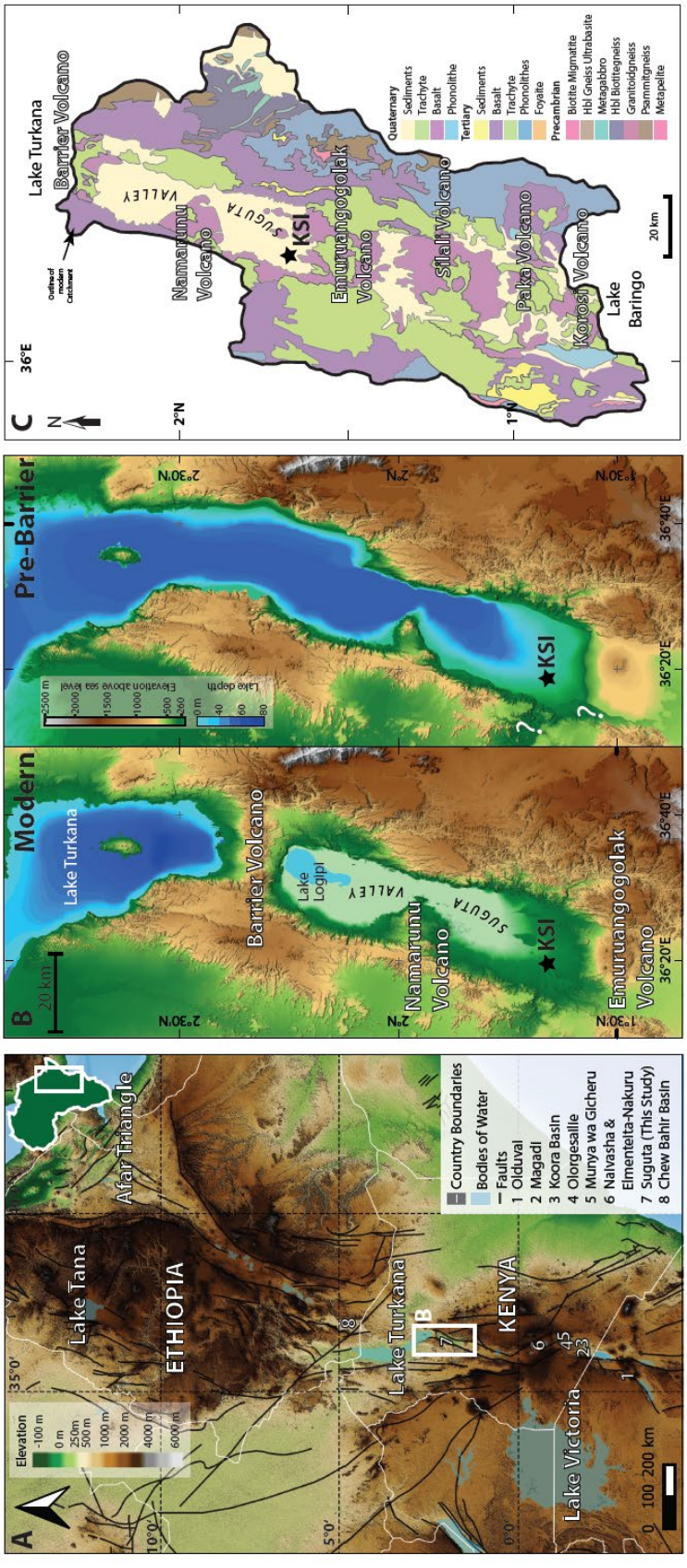
A
Lake Tana
Afar Triangle
ETHIOPIA
Lake Turkana
KENYA
Lake Victoria
Elevation
Country Boundaries
Bodies of Water
Faults
1 Olduvai
2 Magadi
3 Koora Basin
4 Olorgesaille
5 Munya wa Gicheru
6 Nalvasha &
Elmenteita-Nakuru
7 Suguta (This Study)
8 Chew Bahir Basin
0 100 200 km
B
Modern
Lake Turkana
20 km
Barrier Volcano
Lake
Logipi
VALLEY
SUGUTA
Namarunu
Volcano
KSI
Emuruangogolak
Volcano
Pre-Barrier
Elevation above sea level
Lake depth
C
Lake Turkana
Barrier Volcano
Outline of
modern
Catchment
VALLEY
SUGUTA
Namarunu
Volcano
KSI
Emuruangogolak
Volcano
Silali Volcano
Paka Volcano
Korosi Volcano
Lake
Baringo
20 km
Quaternary
Sediments
Trachyte
Basalt
Phonolithe
Tertiary
Sediments
Basalt
Trachyte
Phonolithes
Foyalite
Precambrian
Biotite Migmatite
Hbl Gneiss Ultrabasite
Metagabbro
Hbl Biotitegneiss
Granitoidgneiss
Psammitgneiss
Metapelite

Figure 1 (previous page): (A) Map of the Eastern Branch of the East African Rift System (EARS) including elevation, large bodies of water, and faults. Sites included in this study are also included from south to north: **1** Olduvai (Stanistreet et al., 2020); **2** Lake Magadi (Owen et al., 2018; 2019); **3** Koora Basin (Deino et al., 2019); **4** Olorgesailie (Owen et al., 2014; Potts et al., 2018); **5** Munya wa Gicheru (Owen et al., 2014); **6** Naivasha and Elmenteita-Nakuru (Trauth et al., 2007); and **7** Paleolake Suguta (This Study). The study area is highlighted with a white box. **(B)** Modern versus Pre-Barrier Volcanic Complex topographic maps showing the change between the Suguta and Turkana basins. **(C)** Geological map of the modern Suguta catchment with the African Humid Period (AHP) paleolake maximum highlighted. The studied outcrop, KSI, is starred. Sources for this map include Baker (1963), Dodson (1963), Makinouchi et al. (1984), Ochieng (1988), Van Kekem (1986), Mosley (1993), and Ackermann & Heinrichs (2001).

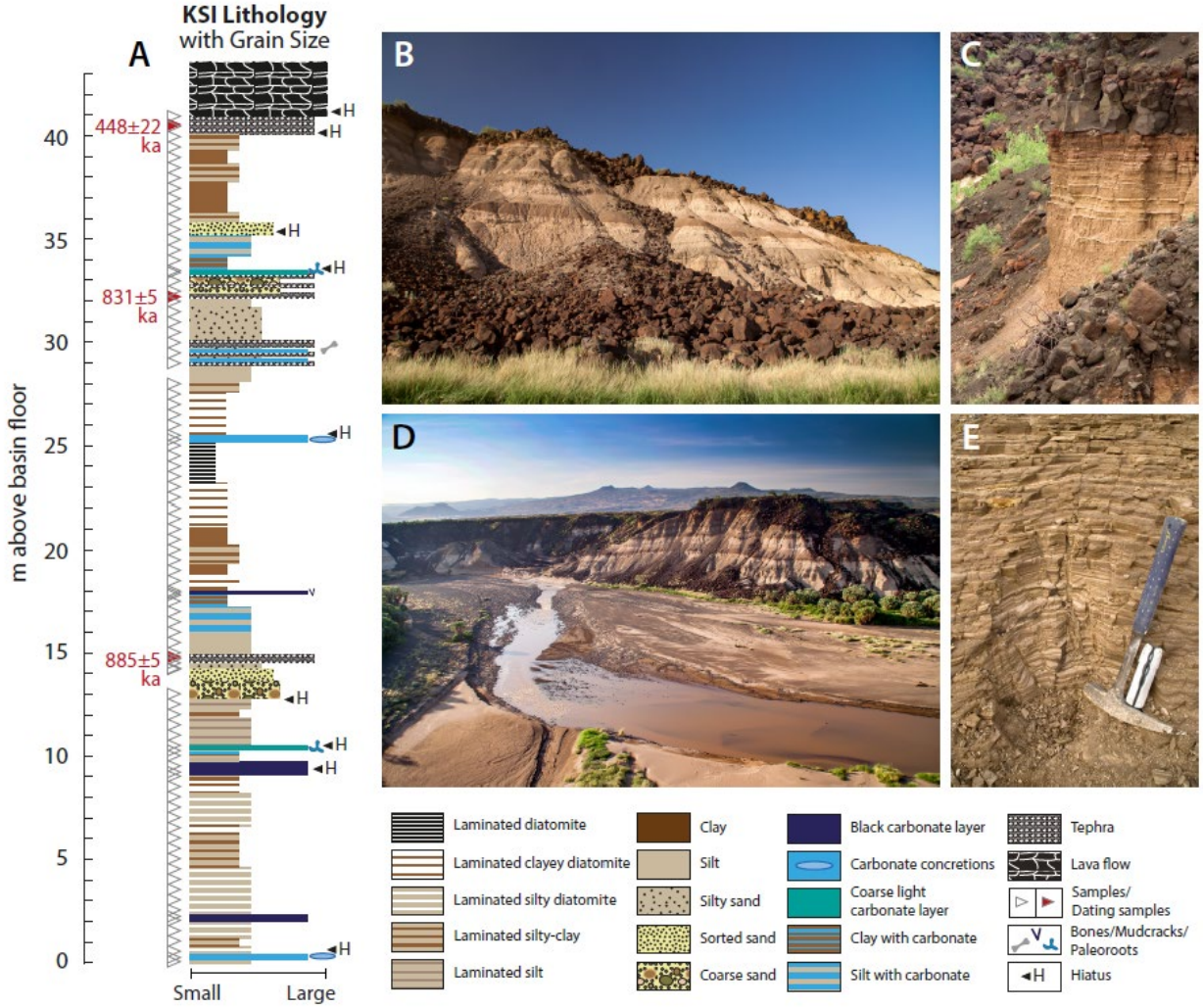

Figure 2: (A) Lithographic column including relative grain sizes, sample locations, and dated units of site Kamuge-Suguta I (KSI). **(B)** KSI from the base of the sequence. **(C)** Close-up of laminated sediments located underneath flood basalts at 41.2 m. **(D)** Aerial photo of KSI and the Suguta River. **(E)** Close-up of laminated diatomites located lower in the section.

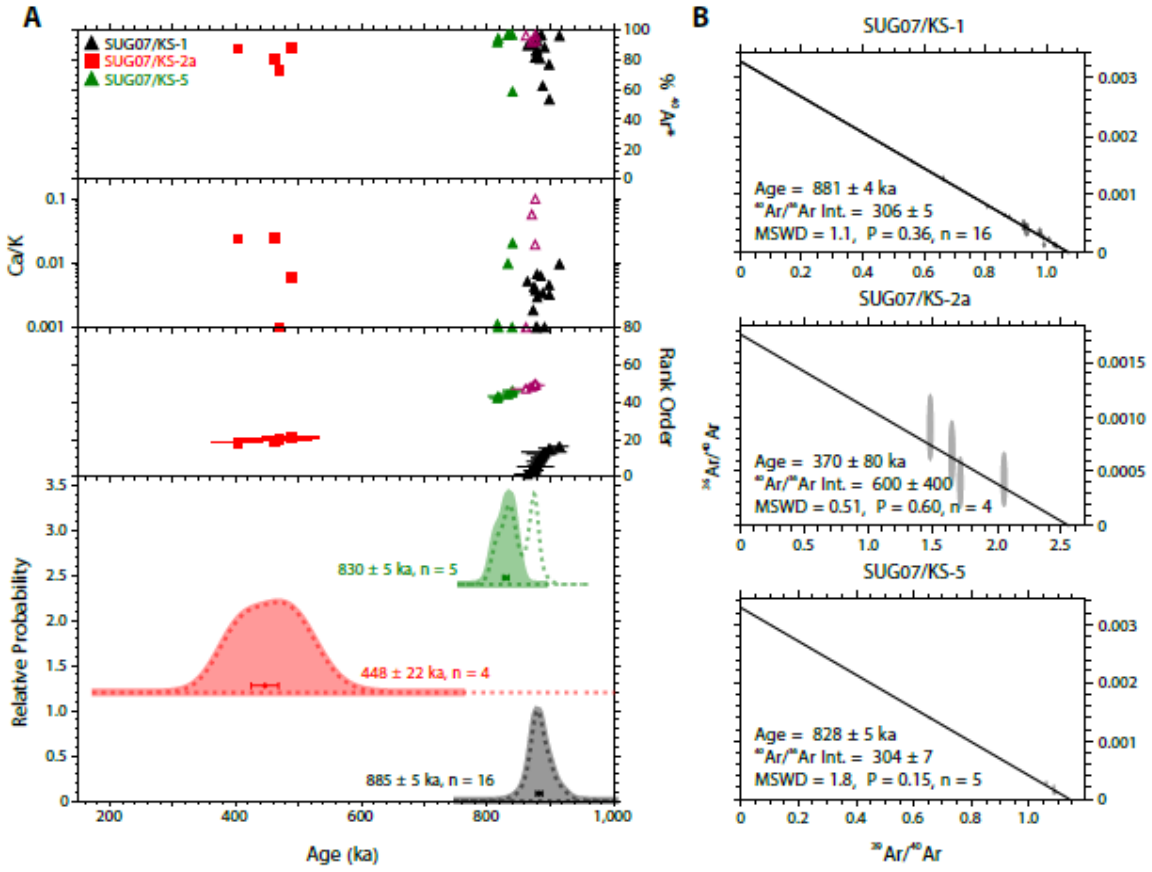

Figure 3: (A) Age-probability spectra of SCTF analyses. Displayed age range is limited to 150 to 1,000 ka; refer to S2 for analyses outside this range (all omitted from the accepted age populations). Dashed line represents age-probability density curve of all analyses for a given sample, whereas filled areas represent accepted analyses. Ages shown in text and as error bars are weighted-means with 1- modified standard error. **(B)** 'Inverse' isochron plots ($^{36}Ar/^{40}Ar$ vs. $^{39}Ar/^{40}Ar$ isotope correlation diagrams) of the accepted SCTF experiments. The isochron age is the x-axis intercept and is shown at 1-. '$^{40}Ar/^{39}Ar$ Int.' refers to 'trapped' non-radiogenic $^{40}Ar/^{36}Ar$ ratio derived from y-axis intercept of the isochron. 'MSWD' refers to 'mean square of weighted deviates,' a measure of the observed scatter about the t line, compared to the expected scatter. 'P' refers to the probability that the observed scatter can be explained by analytical errors alone. 'n' is the number of analyses.

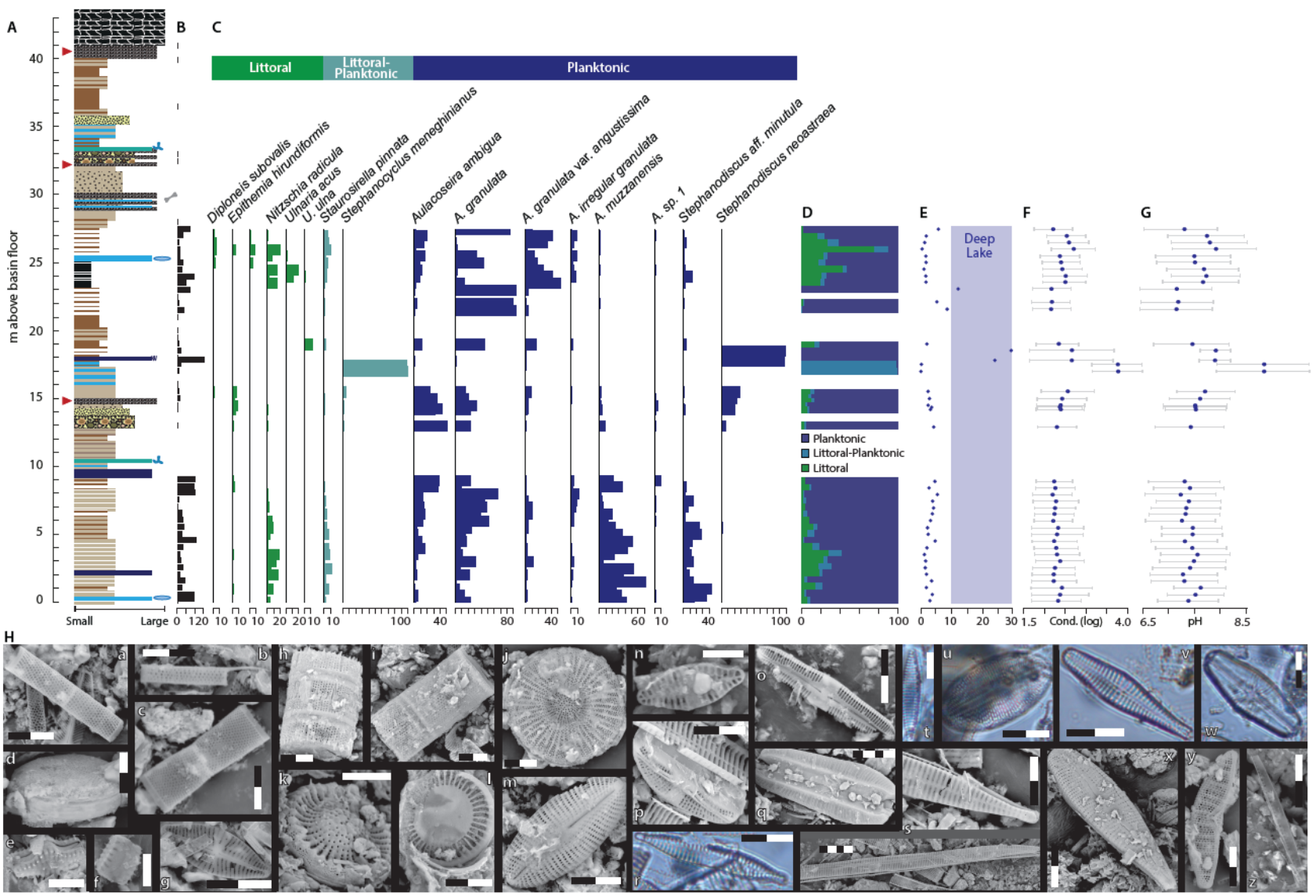
A
B
C
m above basin floor
Small
Large
Littoral
Littoral-Planktonic
Planktonic
Diploneis subovalis
Epithemia hirundiformis
Nitzschia radicula
Ulnaria acus
U. ulna
Staurosirella pinnata
Stephanocyclus meneghinianus
Aulacoseira ambigua
A. granulata
A. granulata var. angustissima
A. irregular granulata
A. muzzanensis
A. sp. 1
Stephanodiscus aff. minutula
Stephanodiscus neoastraea
D
Planktonic
Littoral-Planktonic
Littoral
E
Deep Lake
F
Cond. (log)
G
pH
H

Figure 4 (previous page): (A) KSI lithological column. **(B)** Diatom concentration. **(C)** Diatom species percentages for taxa that make up at least 5% of one sample. Diatom species are organized by littoral, littoral planktonic, and planktonic species. **(D)** Diatom habitat preferences. **(E)** Planktonic Diatom Index (PDI). **(F)** Conductivity based on Gasse et al. (1995) transfer function with the tolerance range. **(G)** pH based on Gasse et al. (1995) transfer function with the tolerance range. **(H)** SEM and light microscope photographs of some of the most common diatoms. Each black or white part of the scale bar is 5 µm. Identifications: **a** *Aulacoseira granulata* (Ehrenberg) Simonsen; **b** *Aulacoseira granulata* var *angustissima* (Müller) Simonsen; **c** *Aulacoseira granulata* var irregular; **d** *Thalassiosira rudolfi* (Bachmann) Hasle; **e** *Staurosira construens* Ehrenberg; **f** *Staurosirella pinnata* (Ehrenberg) Williams & Round; **g** *Geissleria decussis* (Hustedt) Lange-Bertalot; **h** *Aulacoseira agassizi* (Ostenfeld) Simonsen; **i** *Aulacoseira muzzanensis* (Meister) Krammer; **j** *Stephanodiscus neoastraea* Håkansson & Hickel; **k** *Stephanodiscus* cf. *minutulus* (Kützing) Cleve & Möller; **l** *Stephanocyclus meneghinianus* (Kützing) Kulikovskiy, Genkal & Kociolek (formerly *Cyclotella meneghiana* Kützing); **m** *Diploneis subovalis* Cleve; **n** *Planothidium rostratum* (Oestrup) Round & Bukhityarova; **o** *Caloneis bacillum* (Grunow) Cleve; **p** *Amphora copulata* (Kützing) Schoeman & Archibald; **q** *Epithemia hirundiformis* Mueller; **r** *Fragilaria capucina* var *vaucheraie* (Kützing) Lange-Bertalot; **s** *Ulnaria acus* (Kützing) Aboal; ***t*** *Nitzschia cf paleacea* (Grunow) Grunow; **u** *Cocconeis placentula* var *euglypta* (Ehrenberg) Grunow; **v** *Gomphonema* aff. *intricatum* Kützing; **w** *Sellaphora pupula* (Kützing) Mereschkovsky; **x** *Gomphonema* cf. *olivacoides* Foged; **y** *Epithemia adnata* (Kützing) Brébisson; and **z** *Nitzschia* cf. *radicula* Hustedt

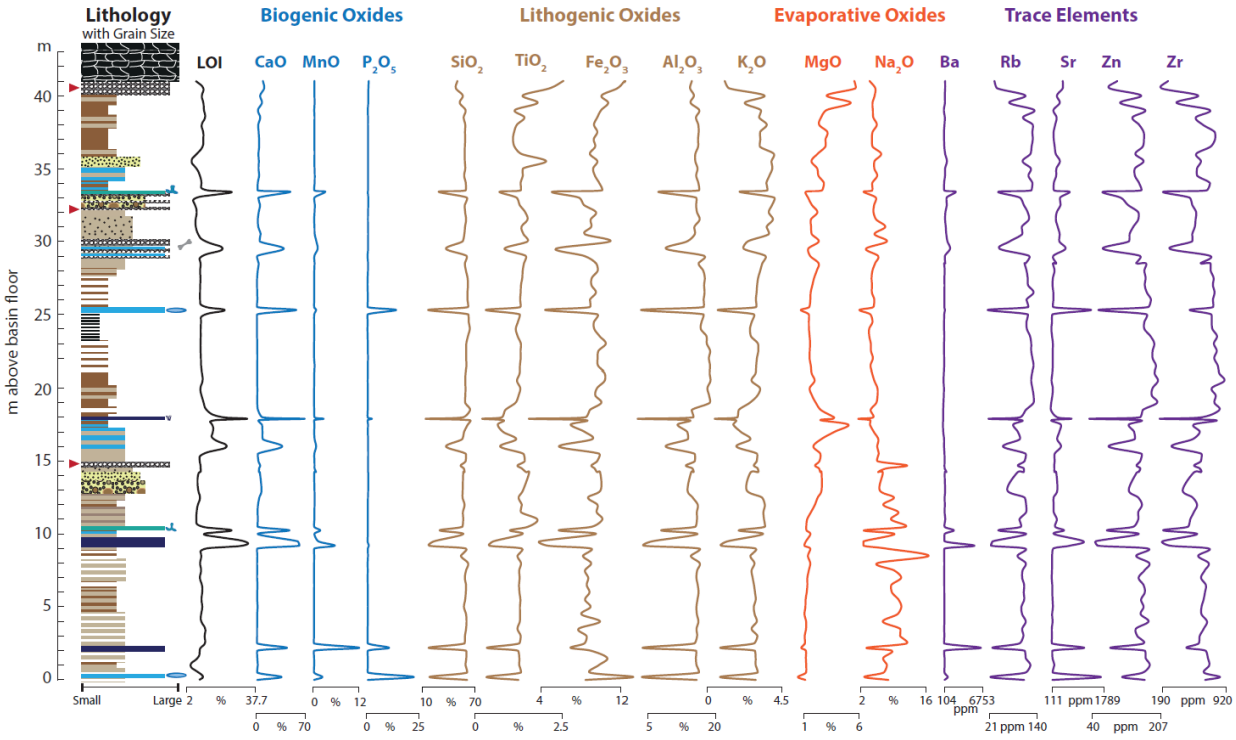

Figure 5: KSI lithographic column with XRF results, including Loss on Ignition (LOI), normalized oxides divided by potential origins, and trace elements Ba, Rb, Sr, Zn, and Zr that were included in the Principal Component Analysis (PCA). Plots were smoothed with exponential smoothing. Major spikes indicate carbonate rich layers across nearly all plots.

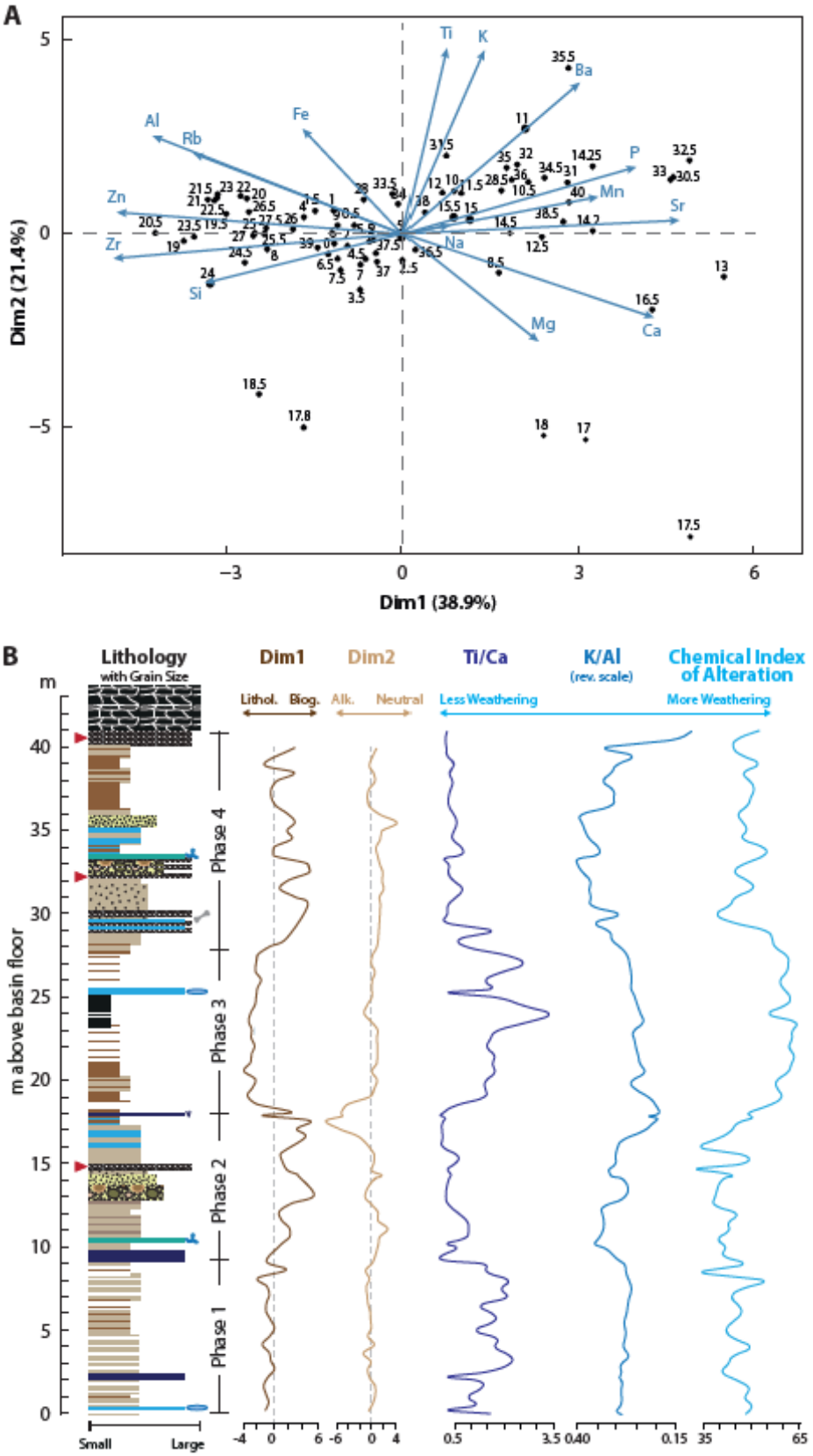
A
Ti
K
Ba
Al
Rb
Fe
P
Zn
Mn
Sr
Zr
Na
Si
Mg
Ca
Dim2 (21.4%)
Dim1 (38.9%)
B
Lithology
with Grain Size
Dim1
Dim2
Ti/Ca
K/Al
(rev. scale)
Chemical Index
of Alteration
Lithol.
Biog.
Alk.
Neutral
Less Weathering
More Weathering
m above basin floor
Phase 1
Phase 2
Phase 3
Phase 4
Small
Large

Figure 6 (previous page): (A) Biplot of the Principal Component Analysis (PCA) of major oxides and trace elements Ba, Cr, Rb, Sr, Zn, and Zr. Dimension 1 (Dim1) represents 38.9% of variability which is interpreted as biogenic/authigenic vs. lithogenic elements. Dimension 2 explains 21.4% and is interpreted as alkaline vs. neutral waters (S5). Elements that are considered having significant control over the dimensions represent higher than average impact on the dimension. **(B)** Lithographic column with Dim1 and Dim2 loadings of the PCA, Ti/Ca, K/Al in the inverse, and the Chemical Index of Alteration (CIA). Plots were smoothed with exponential smoothing.

Figure 7 (next page): Lithogenic column divided into the four phases with important data and interpretations from the multiple proxies in this study, including stratigraphic analysis, PCA (Dim1 and Dim2), CIA (Nesbitt & Young, 1982), XRF ratios (Ti/Ca and K/Al), diatom habitat, PDI (Kingston et al., 2007), transfer function parameters including conductivity in log and pH (Gasse et al., 1995). Data were used to create a paleoenvironmental reconstruction that includes phases of volcanics within KSI.

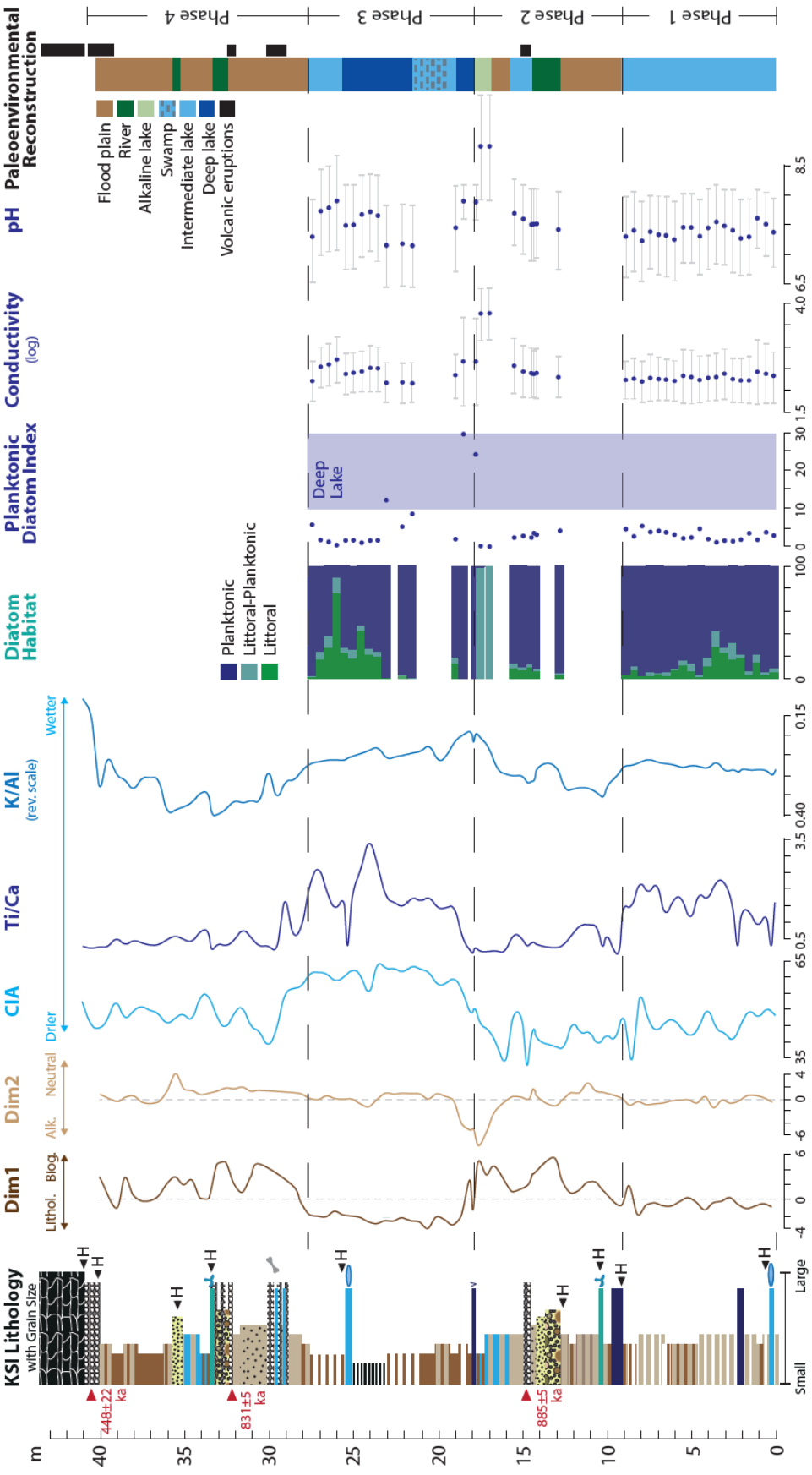
KSI Lithology
with Grain Size
Large
Small
m
40
35
30
25
20
15
10
5
0
448±22 ka
831±5 ka
885±5 ka
Dim1
Litthol.
Biog.
Dim2
Alk.
Neutral
CIA
Drier
Wetter
Ti/Ca
K/Al
(rev. scale)
Diatom Habitat
Planktonic
Littoral-Planktonic
Littoral
Planktonic Diatom Index
Deep Lake
Conductivity
(log)
pH
Paleoenvironmental Reconstruction
Flood plain
River
Alkaline lake
Swamp
Intermediate lake
Deep lake
Volcanic eruptions
Phase 4
Phase 3
Phase 2
Phase 1

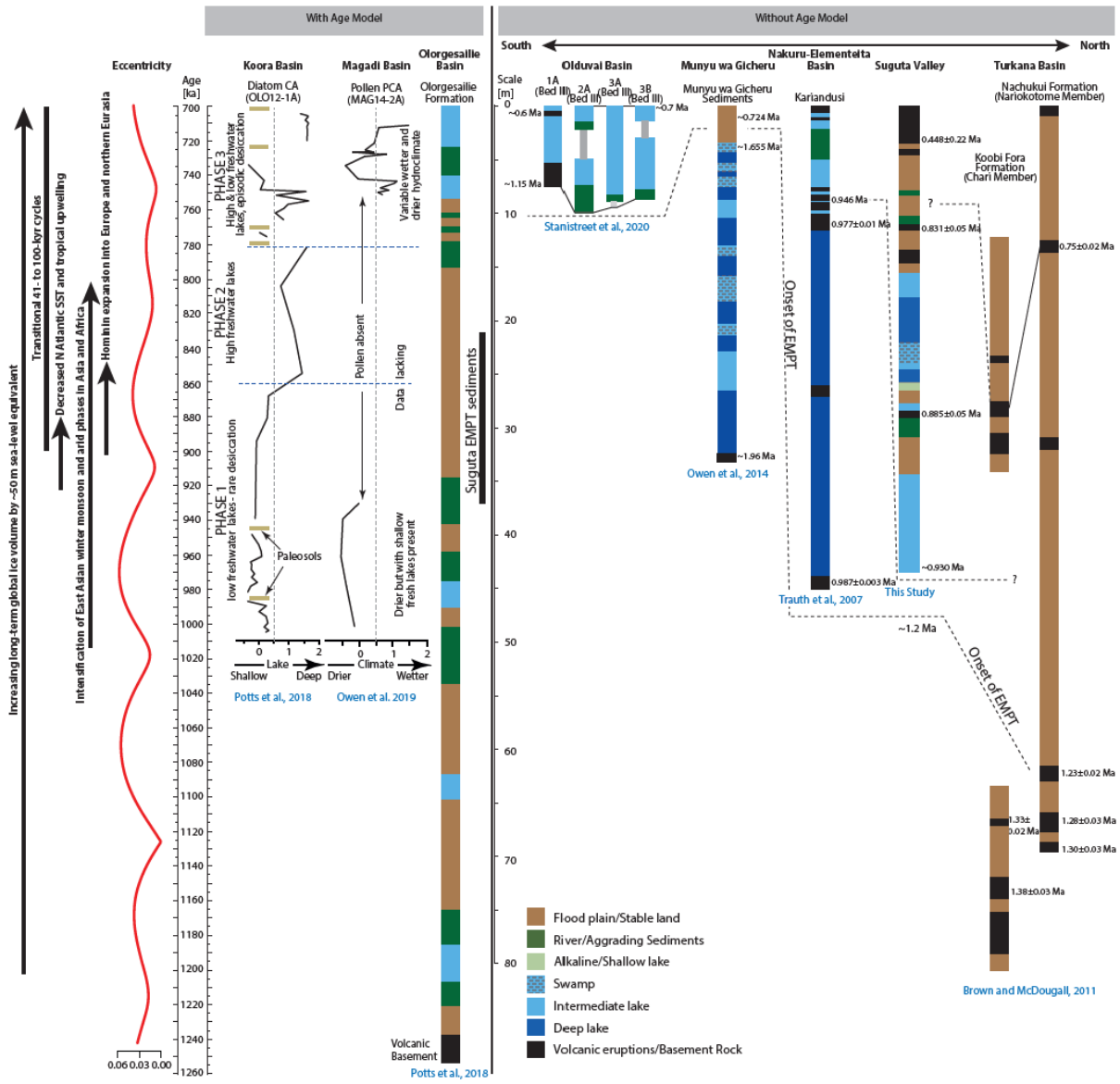

Figure 8: Comparison of records across the Eastern Branch of the EARS that are included in the text separated by those with an age model and those without.

4.8. TABLES

Table 1: Tephra samples with their lithology, location, and data associated with their calculated ages.

Sample	Lab ID	Lithology	Longitude (°E)	Latitude (°N)	n†	MSWD‡	Ca/K§	± Ca/K	Weighted-mean age		Isochron age	
									ka	± 1σ mse¶	ka	± 1σ mse¶
SUG07/KS-1	25130	Reworked lapilli	36.293741	1.640124	16/17	1.2	0.004	0.003	**885**	**5**	881	4
SUG07/KS-2a	25135	Coarse fallout ash	36.293869	1.639776	4/29	1.0	0.02	0.04	**448**	**22**	371	84
SUG07/KS-5	25148	Reworked lapilli and detrital matrix	36.294238	1.639772	5/30	1.5	0.0	0.2	**830**	**5**	828	5

†Number included in weighted-mean over total number of grains.
‡Mean square weighted deviation
§Median Ca/K value
¶Modified standard error = standard error multiplied by root MSWD when MSWD>1.

4.9. REFERENCES

Ackermann, E. and T. Heinrichs. 2001. *Geologie-Ostafrika*. Vol. 1:1000000 Deutsche Forschungsgemeinschaft.

Ashley, G. M., E. J. Beverly, N. E. Sikes, and S. G. Driese. 2014. "Paleosol Diversity in the Olduvai Basin, Tanzania: Effects of Geomorphology, Parent Material, Depositional Environment, and Groundwater on Soil Development." *Quat. Int.* 322-323: 66-77. doi:10.1016/j.quaint.2013.12.047.

Azzaroli, A., C. De Giuli, G. Ficcarelli, and D. Torre. 1988. "Late Pliocene to Early Mid-Pleistocene Mammals in Eurasia: Faunal Succession and Dispersal Events." *Palaeogeography, Palaeoclimatology, Palaeoecology* 66 (1): 77-100. doi:10.1016/0031-0182(88)90082-X.

Baker, B. H. 1963. *Geological Map of the Baragoi Area.* 53rd ed. Vol. 1:125,000 Ministry of Commerce & Industry Mines and Geological Department Kenya.

Baker, B. H. and J. Wohlenberg. 1971. "Structure and Evolution of the Kenya Rift Valley." *Nature (London); Nature* 229 (5286): 538-542. doi:10.1038/229538a0.

Barker, P., F. Gasse, N. Roberts, and M. Taieb. 1991. *Taphonomy and Diagenesis in Diatom Assemblages; a Late Pleistocene Palaeoecological Study from Lake Magadi, Kenya*. Vol. 214.

Barker, P., J.-C. Fontes, and F. Gasse. 1994. "Experimental Dissolution of Diatom Silica in Concentrated Salt Solutions and Implications for Paleoenvironmental Reconstruction." *Limnol. Oceanogr.* 39 (1): 99-110. doi:10.4319/lo.1994.39.1.0099.

Battarbee, R. W. 1986. "Diatom Analysis." In *Handbook of Holocene Palaeoecology & Palaeohydrology*, edited by B. E. Berglund, 527-570.

Battarbee, R. W., S. Juggins, F. Gasse, N. J. Anderson, H. Bennion, N. G. Cameron, D. B. Ryves, C. Pailles, F. Chalie, and R. Telford. 2001. "European Diatom Database (EDDI). an Information System for Palaeoenvironmental Reconstruction." *ECRC Research Report* (81): 1-94.

Bennett, C. E., J. D. Marshall, and I. G. Stanistreet. 2012. "Carbonate Horizons, Paleosols, and Lake Flooding Cycles: Beds I and II of Olduvai Gorge, Tanzania." *J. Hum. Evol.* 63 (2): 328-341.

Bergner, A. G. N., M. R. Strecker, M. H. Trauth, A. Deino, F. Gasse, P. Blisniuk, and M. Dühnforth. 2009. "Tectonic and Climatic Control on Evolution of Rift Lakes in the Central Kenya Rift, East Africa." *Quat. Sci. Rev.* 28 (25): 2804-2816. doi:10.1016/j.quascirev.2009.07.008.

Borchardt, S. and M. H. Trauth. 2012. "Remotely-Sensed Evapotranspiration Estimates for an Improved Hydrological Modeling of the Early Holocene Mega-Lake Suguta, Northern Kenya Rift." *Palaeogeogr. Palaeoclimatol. Palaeoecol.* 361: 14-20.

Bosworth, W. and A. Maurin. 1993. "Structure, Geochronology and Tectonic Significance of the Northern Suguta Valley (Gregory Rift), Kenya." *J. Geol. Soc. London* 150 (4): 751-762. doi:10.1144/gsjgs.150.4.0751.

Brown, F. H. and I. McDougall. 2011. "Geochronology of the Turkana Depression of Northern Kenya and Southern Ethiopia." *Evol. Anthropol.* 20 (6): 217-227. doi:10.1002/evan.20318.

Casanova, J., C. Hillaire-Marcel, N. Page, M. Taieb, and A. Vincens. 1988. "Palaeohydrology and Late Quaternary Stratigraphy of Lacustrine Deposits in the Suguta Rift (Kenya)." *Comptes Rendus De Academie Des Sciences* 307.

Castanier, S., M. Bernet-Rollande, A. Maurin, and J. -P Perthuisot. 1993. "Effects of Microbial Activity on the Hydrochemistry and Sedimentology of Lake Logipi, Kenya." *Hydrobiologia (the Hague)* 267 (1-3): 99-112. doi:10.1007/BF00018793.

Cerling, T. E. and R. L. Hay. 1986. "An Isotopic Study of Paleosol Carbonates from Olduvai Gorge." *Quat. Res.* 25 (1): 63-78.

Chalié, F. and F. Gasse. 2002. "Late Glacial–Holocene Diatom Record of Water Chemistry and Lake Level Change from the Tropical East African Rift Lake Abiyata (Ethiopia)." *Palaeogeogr. Palaeoclimatol. Palaeoecol.* 187 (3): 259-283. doi:10.1016/S0031-0182(02)00480-7.

Chorowicz, J. 2005. "The East African Rift System." *J. African Earth Sci.* 43 (1): 379-410. doi:10.1016/j.jafrearsci.2005.07.019.

Clark, P. U., D. Archer, D. Pollard, J. D. Blum, J. A. Rial, V. Brovkin, A. C. Mix, N. G. Pisias, and M. Roy. 2006. "The Middle Pleistocene Transition: Characteristics, Mechanisms, and Implications for Long-Term Changes in Atmospheric pCO2." *Quat. Sci. Rev.* 25 (23-24): 3150-3184. doi:10.1016/j.quascirev.2006.07.008.

Clement, A. C., A. Hall, and A. J. Broccoli. 2004. "The Importance of Precessional Signals in the Tropical Climate." *Clim. Dyn.* 22 (4): 327-341. doi:10.1007/s00382-003-0375-8.

Cocquyt, Christine. 1998. *Diatoms from the Northern Basin of Lake Tanganyika*. Berlin: J. Cramer.

Cohen, A. S. 1984. "Effect of Zoobenthic Standing Crop on Laminae Preservation in Tropical Lake Sediment, Lake Turkana, East Africa." *J. Paleontol.*: 499-510.

Davies, S. J., H. F. Lamb, and S. J. Roberts. 2015. "Micro-XRF Core Scanning in Palaeolimnology: Recent Developments." In *Micro-XRF Studies of Sediment Cores*, edited by Ian W. Croudace and R. Guy Rothwell. Vol. 17, 189-226: Springer.

Deino, Alan L. and Sally McBrearty. 2002. "40Ar/39Ar Dating of the Kapthurin Formation, Baringo, Kenya." *Journal of Human Evolution* 42 (1-2): 185-210. doi:10.1006/jhev.2001.0517.

Deino, A. L., J. D. Kingston, J. M. Glen, R. K. Edgar, and A. Hill. 2006. "Precessional Forcing of Lacustrine Sedimentation in the Late Cenozoic Chemeron Basin, Central Kenya Rift, and Calibration of the Gauss/Matuyama Boundary." *Earth Planet. Sci. Lett.* 247 (1): 41-60. doi:10.1016/j.epsl.2006.04.009.

Deino, A.L., Dommain, R., Keller, C.B., Potts, R., Behrensmeyer, A.K., Beverly, E.J., King, J., Heil, C.W., Stockhecke, M., Brown, E.T., Moerman, J., and deMenocal, P., 2019a. “Chronostratigraphic model of a high-resolution drill core record of the past million years from the Koora Basin, south Kenya Rift: Overcoming the difficulties of variable sedimentation rate and hiatuses.” *Quat. Sci. Rev.* 215(74), 213--231 https://doi.org/10.1016/j.quascirev.2019.05.009.

Deino, A.L., Sier, M.J., Garello, D., Keller, B., Kingston, J., Scott, J., Dupont-Nivet, G., and Cohen, A., 2019b. “Chronostratigraphy of the Baringo-Tugen-Barsemoi (HSPDP-BTB13-1A) Core – 40Ar/39Ar dating, magnetostratigraphy, tephrostratigraphy, sequence stratigraphy and Bayesian age modeling.” *Palaeogeogr. Palaeoclimatol. Palaeoecol.* Vol. 532: A high resolution, multi-proxy record of Pliocene hominin environments in the Kenya Rift Valley: Analysis of the Baringo-Tugen-Barsemoi (BTB) 109519.

deMenocal, P. B. 2004. "African Climate Change and Faunal Evolution during the Pliocene-Pleistocene." *Earth Planet. Sci. Lett.* 220 (1): 3-24. doi:10.1016/S0012-821X(04)00003-2.

Dodson, R. G. 1963. *Geological Map of the South Horr Area*. 60th ed. Vol. 1:250,000 Ministry of Commerce and Industry Mines and Geological Department of Kenya.

Duesing, W., S. Kaboth-Bahr, A. Asrat, A. S. Cohen, V. Foerster, H. F. Lamb, F. Schaebitz, M. H. Trauth, and F. Viehberg. 2021. "Changes in the Cyclicity and Variability of the Eastern African Paleoclimate Over the Last 620 Kyrs." *Quat. Sci. Rev.* 273: 107219. doi:10.1016/j.quascirev.2021.107219.

Dunkley, P. N., M. Srnith, D. J. Allen, and W. G. Darling. 1993. *The Geothermal Activity and Geology of the Northern Sector of the Kenya Rift Valley*: Natural Environmental Research Council.

Ebinger, C. J. and N. H. Sleep. 1998. "Cenozoic Magmatism Throughout East Africa Resulting from Impact of a Single Plume." *Nature* 395 (6704): 788-791. doi:10.1038/27417.

Ebinger, C. J., T. Yemane, D. J. Harding, S. Tesfaye, S. Kelley, and D. C. Rex. 2000. "Rift Deflection, Migration, and Propagation; Linkage of the Ethiopian and Eastern Rifts, Africa." *Geol. Soc. Am. Bull.* 112 (2): 163-176. doi:10.1130/0016-7606(2000)1122.0.CO;2.

Feibel, C. S. 2011. "A Geological History of the Turkana Basin." *Evol.Anthropol* 20 (6): 206-216. doi:10.1002/evan.20331.

Fitzpatrick, R. W. and D. J. Chittleborough. 2002. "Titanium and Zirconium Minerals." *Soil Mineralogy with Environmental Applications* 7: 667-690.

Fleck, R.J., Sutter, J.F., and Elliot, D.H., 1977. “Interpretation of discordant 40Ar/39Ar age-spectra of Mesozoic tholeiites from Antarctica.” *Geochimica et Cosmochimica Acta* (41) 15–32.

Foerster, V., A. Asrat, C. B. Ramsey, E. T. Brown, M. S. Chapot, A. Deino, W. Duesing, M. Grove, A. Hahn, and A. Junginger. 2022. "Pleistocene Climate Variability in Eastern Africa Influenced Hominin Evolution." *Nat. Geosci.* 15 (10): 805-811.

Foerster, V., D. M. Deocampo, A. Asrat, C. Günter, A. Junginger, K. H. Krämer, N. A. Stroncik, and M. H. Trauth. 2018. "Towards an Understanding of Climate Proxy Formation in the Chew Bahir Basin, Southern Ethiopian Rift." *Palaeogeogr. Palaeoclimatol. Palaeoecol.* 501: 111-123. doi:10.1016/j.palaeo.2018.04.009.

Garcin, Y., A. Junginger, D. Melnick, D. O. Olago, M. R. Strecker, and M. H. Trauth. 2009. "Late Pleistocene–Holocene Rise and Collapse of Lake Suguta, Northern Kenya Rift." *Quat. Sci. Rev.* 28 (9): 911-925. doi:10.1016/j.quascirev.2008.12.006.

Garcin, Y., D. Melnick, M. R. Strecker, D. Olago, and J.-J. Tiercelin. 2012. "East African Mid-Holocene Wet–dry Transition Recorded in Palaeo-Shorelines of Lake Turkana, Northern Kenya Rift." *Earth Planet. Sci. Lett.* 331-332: 322-334. doi:10.1016/j.epsl.2012.03.016.

Gasse, F. 1980. "Les Diatomées Lacustres Plio-Pleistocenes Du Gadeb (Ethiopie): Systématique, Paléoécologique, Biostratigraphie." *Rev. Algol.* (3): 1-249.

———. 1975. "L'Évolution Des Lacs De L'Afar Central (Ethiopie Et T.F.A.I.) Du Plio-Pléistocene À L'Actuel. Reconstitution Des Paléomilieux Lacustres À Partir De L'Étude Des Diatomées." PhD, University of Paris.

Gasse, F., S. Juggins, and L. B. Khelifa. 1995. "Diatom-Based Transfer Functions for Inferring Past Hydrochemical Characteristics of African Lakes." *Palaeogeogr. Palaeoclimatol. Palaeoecol.* 117 (1): 31-54. doi:10.1016/0031-0182(94)00122-O.

Gasse, F. 1990. "Tectonic and Climatic Controls on Lake Distribution and Environments in Afar from Miocene to Present." In *Lacustrine Basin Exploration*, 19-41.

Gasse, F. 1986. *East African Diatoms: Taxonomy, Ecological Distribution*. Berlin: J. Cramer.

Genkal, S. I. 2009. "New Data on the Morphology, Taxonomy, Ecology, and Distribution of Stephanodiscus Agassizensis Håkansson Et Hickel (Bacillariophyta)." *Inland Water Biol.* 2 (2): 113-126. doi:10.1134/S1995082909020035.

Hay, R. L. 1976. *Geology of the Olduvai Gorge: A Study of Sedimentation in a Semiarid Basin* Univ. of California Press.

Head, Martin J. and Philip L. Gibbard. 2005. "Early-Middle Pleistocene Transitions: An Overview and Recommendation for the Defining Boundary." Geological Society Special Publication 247 (1): 1-18. doi:10.1144/GSL.SP.2005.247.01.01.

Head, M. J., B. Pillans, and S. A. Farquhar. 2008. "The Early-Middle Pleistocene Transition: Characterization and Proposed Guide for the Defining Boundary." *Episodes* 31 (2): 255-259. doi:10.18814/epiiugs/2008/v31i2/014.

Hill, A., G. Curtis, and R. Drake. 1986. "Sedimentary Stratigraphy of the Tugen Hills, Baringo, Kenya." *Geological Society Special Publication* 25 (1): 285-295. doi:10.1144/GSL.SP.1986.025.01.23.Isaac, G. L. and B. Isaac. 1977. *Olorgesailie: Archeological Studies of a Middle Pleistocene Lake Basin in Kenya* Univ. of Chicago Press.

Johnson, T. C., J. P. Werne, E. T. Brown, A. Abbott, M. Berke, B. A. Steinman, J. Halbur, S. Contreras, S. Grosshuesch, A. Deino, R. P. Lyons, C. A. Scholz, S. Schouten, and J. S. Sinninghe Damste. 2016. "A Progressively Wetter Climate in Southern East Africa Over the Past 1.3 Million Years." *Nature* 537 (7619): 220-224. doi:10.1038/nature19065.

Jolliffe, I. T. and J. Cadima. 2016. "Principal Component Analysis: A Review and Recent Developments." *Philos. Trans. A Math. Phys. Eng. Sci.* 374 (2065): 20150202. doi:10.1098/rsta.2015.0202.

Joordens, J. C. A., H. B. Vonhof, C. S. Feibel, L. J. Lourens, G. Dupont-Nivet, J. H. J. L. van der Lubbe, M. J. Sier, G. R. Davies, and D. Kroon. 2011. "An Astronomically-Tuned Climate Framework for Hominins in the Turkana Basin." *Earth Planet. Sci. Lett.* 307 (1): 1-8. doi:10.1016/j.epsl.2011.05.005.

Juggins, S. 2022. *Rioja: Analysis of Quaternary Science Data*. Vol. R package version 0.9-26.

Junginger, A., S. Kuebler, C. Rosca, R. B. Owen, A. Deino, M. H. Trauth, and H. Vonhof. 2023. "Mid-Pleistocene Volcano-Tectonic Fragmentation of the Turkana-Suguta Megalake."EGU Vienna April 24-29 2023.

Junginger, A., S. Roller, L. A. Olaka, and M. H. Trauth. 2014. "The Effects of Solar Irradiation Changes on the Migration of the Congo Air Boundary and Water Levels of Paleo-Lake Suguta, Northern Kenya Rift, during the African Humid Period (15–5 Ka BP)." *Palaeogeogr. Palaeoclimatol. Palaeoecol.* 396: 1-16. doi:10.1016/j.palaeo.2013.12.007.

Junginger, A. and M. H. Trauth. 2013. "Hydrological Constraints of Paleo-Lake Suguta in the Northern Kenya Rift during the African Humid Period (15–5 Ka BP)." *Glob. Planet. Change.* 111: 174-188. doi:10.1016/j.gloplacha.2013.09.005.

Kilham, P., S. S. Kilham, and R. E. Hecky. 1986. "Hypothesized Resource Relationships among African Planktonic Diatoms." *Limnol. Oceanogr.* 31 (6): 1169-1181. doi:10.4319/lo.1986.31.6.1169.

Kingston, J. D., A. L. Deino, R. K. Edgar, and A. Hill. 2007. "Astronomically Forced Climate Change in the Kenyan Rift Valley 2.7–2.55 Ma: Implications for the Evolution of Early Hominin Ecosystems." *J. Hum. Evol.* 53 (5): 487-503. doi:10.1016/j.jhevol.2006.12.007.

Kutzbach, J. E., J. Guanb, F. Hea, A. S. Cohen, I. J. Orlandd, and G. Chend. 2020. "African Climate Response to Orbital and Glacial Forcing in 140,000-Y Simulation with Implications for Early Modern Human Environments." *PNAS* 117 (5): 2255-2264. doi:10.1073/pnas.1917673117.

Larrasoaña, J., A. Roberts, E. Rohling, M. Winklhofer, and R. Wehausen. 2003. "Three Million Years of Monsoon Variability Over the Northern Sahara." *Clim. Dyn.* 21 (7): 689-698. doi:10.1007/s00382-003-0355-z.

Le Gall, B., W. Vétel, and C. K. Morley. 2005. "Inversion Tectonics during Continental Rifting: The Turkana Cenozoic Rifted Zone, Northern Kenya." *Tectonics* 24 (2): TC2002-n/a. doi:10.1029/2004TC001637.

Lee, J.-Y., Marti, K., Severinghaus, J.P., Kawamura, K., Yoo, H.-S., Lee, J.B., and Kim, J.S., 2006. “A redetermination of the isotopic abundances of atmospheric Ar.” *Geochimica et Cosmochimica Acta* (70) 4507–4512.

Lee, J., S. Kim, and B.-K. Khim. 2020. "A Paleoproductivity Shift in the Northwestern Bay of Bengal (IODP Site U1445) Across the Mid-Pleistocene Transition in Response to Weakening of the Indian Summer Monsoon." *Palaeogeogr. Palaeoclimatol. Palaeoecol.* 560: 110018. doi:10.1016/j.palaeo.2020.110018.

Liutkus, C. M., J. D. Wright, G. M. Ashley, and N. E. Sikes. 2005. "Paleoenvironmental Interpretation of Lake-Margin Deposits using delta13C and delta18O Results from Early Pleistocene Carbonate Rhizoliths, Olduvai Gorge, Tanzania." *Geol.* 33 (5): 377-380. doi:10.1130/G21132.1.

Lowe, D. J. 2011. "Tephrochronology and its Application: A Review." *Quat. Geochronol.* 6 (2): 107-153. doi:10.1016/j.quageo.2010.08.003.

Lupien, R. L., J. M. Russell, E. J. Pearson, I. S. Castañeda, A. Asrat, V. Foerster, H. F. Lamb, H. M. Roberts, F. Schabitz, M. H. Trauth, C. C. Beck, C. S. Feibel, and A. S. Cohen. 2022. "Orbital Controls on Eastern African Hydroclimate in the Pleistocene." *Sci. Rep.* 12 (1): 3170. doi:10.1038/s41598-022-06826-z.

Makinouchi, T., T. Koyaguchi, T. Matsuda, H. Mitsushio, and S. Ishida. 1984. "Geology of the Nachola Area and the Samburu Hills, West of Baragoi, Northern Kenya." *African Study Monographs. Supplementary Issue*. 2: 15-44.

Mannella, G., B. Giaccio, G. Zanchetta, E. Regattieri, E. M. Niespolo, A. Pereira, P. R. Renne, S. Nomade, N. Leicher, and N. Perchiazzi. 2019. "Palaeoenvironmental and Palaeohydrological Variability of Mountain Areas in the Central Mediterranean Region: A 190 Ka-Long Chronicle from the Independently Dated Fucino Palaeolake Record (Central Italy)." *Quat. Sci. Rev.* 210: 190-210.

Martin-Garcia, G., F. J. Sierro, J. A. Flores, and F. Abrantes. 2018. "Change in the North Atlantic Circulation Associated with the Mid-Pleistocene Transition." *Clim. Past.* 14 (11): 1639-1651. doi:10.5194/cp-14-1639-2018.

Maslin, M. A. and C. M. Brierley. 2015. "The Role of Orbital Forcing in the Early Middle Pleistocene Transition." *Quat. Int.*389: 47-55. doi:10.1016/j.quaint.2015.01.047.

Maslin, M. A. and A. J. Ridgwell. 2005. "Mid-Pleistocene Revolution and the 'eccentricity Myth'." *Geol. Soc. Spec. Publ.* 247 (1): 19-34. doi:10.1144/GSL.SP.2005.247.01.02.

McClymont, E. L. and A. Rosell-Melé. 2005. "Links between the Onset of Modern Walker Circulation and the Mid-Pleistocene Climate Transition." *Geol.* 33 (5): 389-392. doi:10.1130/G21292.1.

McDougall, I., and Harrison, T.M., 1999. *Geochronology and thermochronology by the 40Ar/39Ar method.* Oxford University Press on Demand. Oxford, New York.

McDougall, I., F. H. Brown, P. M. Vasconcelos, B. E. Cohen, D. S. Thiede, and M. J. Buchanan. 2012. "New Single Crystal 40Ar/39Ar Ages Improve Time Scale for Deposition of the Omo Group, Omo-Turkana Basin, East Africa." *J. Geol. Soc. London* 169 (2): 213-226. doi:10.1144/0016-76492010-188.

McLennan, S. M. 1993. "Weathering and Global Denudation." *J. Geol.* 101 (2): 295-303. doi:10.1086/648222.

Melnick, D., Y. Garcin, J. Quinteros, M. R. Strecker, D. Olago, and J.-J. Tiercelin. 2012. "Steady Rifting in Northern Kenya Inferred from Deformed Holocene Lake Shorelines of the Suguta and Turkana Basins." *Earth Planet. Sci. Lett.* 331-332: 335-346. doi:10.1016/j.epsl.2012.03.007.

Melson, W. G. and R. Potts. 2002. "Origin of Reddened and Melted Zones in Pleistocene Sediments of the Olorgesailie Basin, Southern Kenya Rift." *J. Archaeol. Sci.* 29 (3): 307-316. doi:10.1006/jasc.2001.0695.

Meyer, I., M. Van Daele, N. Tanghe, M. De Batist, and D. Verschuren. 2020. "Reconstructing East African Monsoon Variability from Grain-Size Distributions: End-Member Modeling and Source Attribution of Diatom-Rich Sediments from Lake Chala." *Quat. Sci. Rev.* 247: 106574. doi:10.1016/j.quascirev.2020.106574.

Min, K.W., Mundil, R., Renne, P.R., and Ludwig, K.R., 2000. „A test for systematic errors in Ar-40/Ar-39 geochronology through comparison with U/Pb analysis of a 1.1-Ga rhyolite." *Geochim. Cosmochim. Acta* 64 (1) 73–98.

Morley, C. K., W. A. Wescott, D. M. Stone, R. M. Harper, S. T. Wigger, and F. M. Karanja. 1992. "Tectonic Evolution of the Northern Kenyan Rift." *J. Geol. Soc. London* 149 (3): 333-348. doi:10.1144/gsjgs.149.3.0333.

Mosley, P. N. 1993. "Geological Evolution of the Late Proterozoic "Mozambique Belt" of Kenya." *Tectonophysics* 221 (2): 223-250.

Mudelsee, M. and K. Stattegger. 1997. "Exploring the Structure of the Mid-Pleistocene Revolution with Advanced Methods of Time-Series Analysis." *Geologische Rundschau* 86 (2): 499-511. doi:10.1007/s005310050157.

Mudelsee, M. and M. Schulz. 1997. "The Mid-Pleistocene Climate Transition: Onset of 100 Ka Cycle Lags Ice Volume Build-Up by 280 Ka." *Earth Planet. Sci. Lett.* 151 (1): 117-123. doi:10.1016/S0012-821X(97)00114-3.

Muiruri, Veronica, R. B. Owen, Richard Potts, Alan L. Deino, Anna K. Behrensmeyer, Simon Riedl, Nathan Rabideaux, T. K. Lowenstein, K. Leet, M. Sier, A. Cohen, D. Deocampo, C. J. Campisano, A. Billingsley, and A. Mbuthia. 2021a. "Quaternary Diatoms and Palaeoenvironments of the Koora Plain, Southern Kenya Rift." *Quat. Sci. Rev.* 267: 107106. doi:10.1016/j.quascirev.2021.107106.

Muiruri, V. M., R. B. Owen, T. K. Lowenstein, R. W. Renaut, R. Marchant, S. M. Rucina, A. Cohen, A. L. Deino, M. J. Sier, S. Luo, K. Leet, C. Campisano, N. M. Rabideaux, D. Deocampo, C.-C. Shen, A. Mbuthia, B. C. Davis, W. Aldossari, and C. Wang. 2021b. "A Million Year Vegetation History and Palaeoenvironmental Record from the Lake Magadi Basin, Kenya Rift Valley." *Palaeogeogr. Palaeoclimatol. Palaeoecol.* 567: 110247. doi:10.1016/j.palaeo.2021.110247.

Nesbitt, H. W. and G. M. Young. 1982. "Early Proterozoic Climates and Plate Motions Inferred from Major Element Chemistry of Lutites." *Nature* 299 (5885): 715-717. doi:10.1038/299715a0.

Nicholson, S. L., A. W. G. Pike, R. Hosfield, N. Roberts, D. Sahy, J. Woodhead, H. Cheng, R. L. Edwards, S. Affolter, M. Leuenberger, S. J. Burns, A. Matter, and D. Fleitmann. 2020. "Pluvial Periods in Southern Arabia Over the Last 1.1 Million-Years." *Quat. Sci. Rev.* 229: 106112. doi:10.1016/j.quascirev.2019.106112.

Nicholson, S. E. 2017. "Climate and Climatic Variability of Rainfall Over Eastern Africa." *Rev. Geophys. (1985)* 55 (3): 590-635. doi:10.1002/2016RG000544.

———. 1996. "A Review of Climate Dynamics and Climate Variability in Eastern Africa." Johnson, Thomas C.; Odada, Eric O.(Eds.) and Whittaker, Katherine T., *The Limnology, Climatology and Paleoclimatology of the East African Lakes.,* Amsterdam, Gordon and Breach Science Publishers: 25-56.

Niespolo, E.M., Rutte, D., Deino, A.L., and Renne, P.R., 2017. “Intercalibration and age of the Alder Creek sanidine Ar-40/Ar-39 standard.” *Quat. Geochronol.* (39) 205–213.

Nyenzi, B. S., P. M. R. Kiangi, and N. N. P. Rao. 1981. "Evaporation Values in East Africa." *Archives for Meteorology, Geophysics, and Bioclimatology Series B* 29 (1-2): 37-55. doi:10.1007/BF02278189.

Ochieng, J. O. 1988. *Geology of the Loiyangalani Area*. Vol. 1:250,000.

Ojany, F. and R. Ogendo. 1973. *Kenya; A Study in Physical and Human Geography*. Nairobi, Kenya: Longman Publishers.

Olaka, L., E. Odada, M. Trauth, and D. Olago. 2010. "The Sensitivity of East African Rift Lakes to Climate Fluctuations." *J. Paleolimnol.* 44 (2): 629-644. doi:10.1007/s10933-010-9442-4.

O'Sullivan, P. E. 1983. "Annually-Laminated Lake Sediments and the Study of Quaternary Environmental Changes — a Review." *Quat. Sci. Rev.* 1 (4): 245-313. doi:10.1016/0277-3791(83)90008-2.

Owen, R. B. and R. Crossley. 1992. "Spatial and Temporal Distribution of Diatoms in Sediments of Lake Malawi, Central Africa, and Ecological Implications." *J. Paleolimnol.* 7 (1). doi:10.1007/BF00197031.

Owen, R. B., R. K. L. Lee, and R. Renaut. 2012. "Early Pleistocene Lacustrine Sedimentation and Diatom Stratigraphy at Munya Wa Gicheru, Southern Kenya Rift Valley." *Palaeogeogr. Palaeoclimatol. Palaeoecol.* 331-332: 60-74. doi:10.1016/j.palaeo.2012.02.033.

Owen, R. B., V. Muiruri, T. Lowenstein, R. Renaut, N. Rabideaux, S. Luo, A. Deino, M. J. Sier, G. Dupont-Nivet, E. P. McNulty, K. Leet, A. Cohen, C. Campisano, D. Deocampo, C.-C. Shen, A. Billingsley, and A. Mbuthia. 2018. „Progressive Aridification in East Africa Over the Last Half Million Years and Implications for Human Evolution.” *PNAS.* 115 (44): 11174-11179. doi:10.1073/pnas.1801357115.

Owen, R. B., R. W. Renaut, A. K. Behrensmeyer, and R. Potts. 2014. "Quaternary Geochemical Stratigraphy of the Kedong–Olorgesailie Section of the Southern Kenya Rift Valley." *Palaeogeogr. Palaeoclimatol. Palaeoecol.* 396: 194-212. doi:10.1016/j.palaeo.2014.01.011.

Owen, R. Bernhart and R. W. Renaut. 2000. "Miocene and Pliocene Diatomaceous Lacustrine Sediments of the Tugen Hils, Baringo District, Central Kenya Rift." In *Lake Basins through Space and Time*, edited by E. H. Gierlowski-Kordesch and K. R. Kelts, 465-472: AAPG Studies in Geology.

Owen, R. B., R. W. Renaut, T. K. Lowenstein, and A. Brasier. 2018. "Spatial and Temporal Geochemical Variability in Lacustrine Sedimentation in the East African Rift System: Evidence from the Kenya Rift and Regional Analyses." *Sedimentology* 65 (5): 1697-1730. doi:10.1111/sed.12443.

Paillard, D. 1998. "The Timing of Pleistocene Glaciations from a Simple Multiple-State Climate Model." *Nature* 391 (6665): 378-381.

Pik, R., B. Marty, J. Carignan, G. Yirgu, and T. Ayalew. 2008. "Timing of East African Rift Development in Southern Ethiopia; Implication for Mantle Plume Activity and Evolution of Topography." *Geology* 36 (2): 167-170. doi:10.1130/G24233A.1.

Pilskaln, C. H. and T. C. Johnson. 1991. "Seasonal Signals in Lake Malawi Sediments." *Limnol. Oceanogr.* 36 (3): 544-557. doi:10.4319/lo.1991.36.3.0544.

Pisias, N. G. and T. C. Moore. 1981. "The Evolution of Pleistocene Climate: A Time Series Approach." *Earth Planet. Sci. Lett.* 52 (2): 450-458. doi:10.1016/0012-821X(81)90197-7.

Potts, R., A. K. Behrensmeyer, and P. Ditchfield. 1999. "Paleolandscape Variation and Early Pleistocene Hominid Activities: Members 1 and 7, Olorgesailie Formation, Kenya." *J. Hum. Evol.* 37 (5): 747-788. doi:10.1006/jhev.1999.0344.

Potts, R., A. K. Behrensmeyer, J. T. Faith, C. A. Tryon, A. S. Brooks, J. E. Yellen, A. L. Deino, R. Kinyanjui, J. B. Clark, C. M. Haradon, N. E. Levin, H. J. M. Meijer, E. G. Veatch, R. B. Owen, and R. W. Renaut. 2018. "Environmental Dynamics during the Onset of the Middle Stone Age in Eastern Africa." *Science.* 360 (6384): 86. doi:10.1126/science.aao2200.

Potts, R., R. Dommain, J. W. Moerman, A. K. Behrensmeyer, A. L. Deino, S. Riedl, E. J. Beverly, E. T. Brown, D. Deocampo, R. Kinyanjui, R. Lupien, R. B. Owen, N. Rabideaux, J. R. Russell, M. Stockhecke, P. deMenocal, J. T. Faith, Y. Garcin, A. Noren, J. J. Scott, D. Wastern, J. Bright, J. B. Clark, A. S. Cohen, C. B. Keller, J. King, N. E. Levin, K. B. Shannon, V. Muiruri, R. W. Renaut, S. M. Rucina, and K. Uno. 2020. "Increased Ecological Resource Variability during a Critical Transition in Hominin Evolution." *Sci. Adv.* 6 (43): eabc8975. doi:10.1126/sciadv.abc8975.

Purcell, P. G. 2018. "Re-Imagining and Re-Imaging the Development of the East African Rift." *Pet. Geosci.* 24 (1): 21-40. doi:10.1144/petgeo2017-036.

Renaut, R. W., J. Ego, J. J. Tiercelin, C. Le Turdu, and R. B. Owen. 1999. "Saline, Alkaline Palaeolakes of the Tugen Hills-Kerio Valley Region, Kenya Rift Valley." *Late Cenozoic Environments and Hominid Evolution: A Tribute to Bill Bishop.Geological Society, London*: 41-58.

Renaut, R. W., R. B. Owen, T. K. Lowenstein, G. De Cort, E. Mcnulty, J. J. Scott, and A. Mbuthia. 2021. "The Role of Hydrothermal Fluids in Sedimentation in Saline Alkaline Lakes: Evidence from Nasikie Engida, Kenya Rift Valley." *Sedimentology* 68 (1): 108-134.

Rossignol-Strick, M. 1985. "Mediterranean Quaternary Sapropels, an Immediate Response of the African Monsoon to Variation of Insolation." *Palaeogeogr. Palaeoclimatol. Palaeoecol.* 49 (3): 237-263. doi:10.1016/0031-0182(85)90056-2.

Ryves, D. B., N. J. Anderson, R. J. Flower, and B. Rippey. 2013. "Diatom Taphonomy and Silica Cycling in Two Freshwater Lakes and their Implications for Inferring Past Lake Productivity." *J. Paleolimnol.* 49 (3): 411-430. doi:10.1007/s10933-013-9694-x.

Saneyoshi, M., K. Nakayama, T. Sakai, Y. Sawada, and H. Ishida. 2006. "Half Graben Filling Processes in the Early Phase of Continental Rifting: The Miocene Namurungule Formation of the Kenya Rift." *Sediment. Geol.* 186 (1): 111-131. doi:10.1016/j.sedgeo.2005.11.012.

Shackleton, N. J. and N. D. Opdyke. 1977. "Oxygen-Isotope and Paleomagnetic Stratigraphy of Pacific Core V28-239 Late Pliocene to Latest Pleistocene." *Deep Sea Research* 24 (4): 449-464. doi:10.1016/0146-6291(77)90420-9.

Spaulding, S. A., Bishop, I. W., Edlund, M. B., Lee, S., Furey, P., Jovanovska, E. and Potapova, M. 2022. "Diatoms of North America." https://diatoms.org/species.

Stanistreet, I. G., C. Doyle, T. Hughes, E. D. Rushworth, H. Stollhofen, N. Toth, K. Schick, and J. K. Njau. 2020. "Changing Depocentre Environments of Palaeolake Olduvai and Carbonates as Marker Horizons for Hiatuses and Lake-Level Extremes." *Palaeogeogr. Palaeoclimatol. Palaeoecol.* 560: 110032. doi:10.1016/j.palaeo.2020.110032.

Sturchio, N. C., P. N. Dunkley, and M. Smith. 1993. "Climate-Driven Variations in Geothermal Activity in the Northern Kenya Rift Valley." *Nature* 362 (6417): 233-234. doi:10.1038/362233a0.

Sun, Y., S. C. Clemens, Z. An, and Z. Yu. 2006. "Astronomical Timescale and Palaeoclimatic Implication of Stacked 3.6-Myr Monsoon Records from the Chinese Loess Plateau." *Quat. Sci. Rev.* 25 (1): 33-48. doi:10.1016/j.quascirev.2005.07.005.

Taylor, J. C., W. R. Harding, and C. G. M. Archibald. 2007. *An Illustrated Guide to some Common Diatom Species from South Africa*. Pretoria, South Africa: Water Research Commission.

ter Braak, C. and C. Looman. 1986. "Weighted Averaging, Logistic Regression and the Gaussian Response Model." *Vegetation* 65 (1): 3-11. doi:10.1007/BF00032121.

Tierney, J. E., S. C. Lewis, B. I. Cook, A. N. Legrande, and G. A. Schmidt. 2011. "Model, Proxy and Isotopic Perspectives on the East African Humid Period." *Earth Planet. Sci. Lett.* 307 (1): 103-112. doi:10.1016/j.epsl.2011.04.038.

Trauth, M. H., J. C. Larrasoana, and M. Mudelsee. 2009. *"*Trends, Rhythms and Events in Plio-Pleistocene African Climate." Vol. 11. Katlenburg-Lindau: Katlenburg-Lindau, Germany: Copernicus GmbH on behalf of the European Geosciences Union (EGU).

Trauth, M. H. 2014. "A New Probabilistic Technique to Build an Age Model for Complex Stratigraphic Sequences." *Quat. Geochronol.* 22: 65-71. doi:10.1016/j.quageo.2014.03.001.

Trauth, M. H., A. G. N. Bergner, V. Foerster, A. Junginger, M. A. Maslin, and F. Schaebitz. 2015. "Episodes of Environmental Stability Versus Instability in Late Cenozoic Lake Records of Eastern Africa." *J. Hum. Evol.* 87: 21-31. doi:10.1016/j.jhevol.2015.03.011.

Trauth, M. H., M. A. Maslin, A. L. Deino, A. Junginger, M. Lesoloyia, E. O. Odada, D. O. Olago, L. A. Olaka, M. R. Strecker, and R. Tiedemann. 2010. "Human Evolution in a Variable Environment: The Amplifier Lakes of Eastern Africa." *Quat. Sci. Rev.* 29 (23): 2981-2988. doi:10.1016/j.quascirev.2010.07.007.

Trauth, M. H., M. A. Maslin, A. L. Deino, M. R. Strecker, A. G. N. Bergner, and M. Dühnforth. 2007. "High- and Low-Latitude Forcing of Plio-Pleistocene East African Climate and Human Evolution." *J. Hum. Evol.* 53 (5): 475-486. doi:10.1016/j.jhevol.2006.12.009.

Trauth, M. H., M. A. Maslin, A. Deino, and M. R. Strecker. 2005. "Late Cenozoic Moisture History of East Africa." *Science* 309 (5743): 2051-2053. doi:10.1126/science.1112964.

Truckle, P. H. 1976. "Geology and Late Cainozoic Lake Sediments of the Suguta Trough, Kenya." *Nature* 263 (5576): 380-383. doi:10.1038/263380a0.

Truckle, P. H. 1977. *The Geology of the Area to the South of Lokori, South Turkana, Kenya* University of Leicester (United Kingdom).

Van Kekem, A. J. 1986. *Reconnaissance Soil Map of the Mount Kulala-Marsabit Area*. 12th ed. Vol. 1:250,000 Kenya Soil Survey, Ministry of Agriculture, and UNESCO Integrated Project of Arid Lands (IPAL).

van Kolfschoten, T. and A. K. Markova. 2005. "Response of the European Mammalian Fauna to the Mid-Pleistocene Transition." *Geological Society Special Publication* 247 (1): 221-229. doi:10.1144/GSL.SP.2005.247.01.12.

Vetel, W. and B. Le Gall. 2006. "Dynamics of Prolonged Continental Extension in Magmatic Rifts: The Turkana Rift Case Study (North Kenya)." *Geol. Soc. Spec. Publ.* 259 (1): 209-233. doi:10.1144/GSL.SP.2006.259.01.17.

Vrba, E. 1996. "The Fossil Record of African Antelopes (Mammalia, Bovidae) in Relation to Human Evolution and Paleoclimate." *Paleoclimate and Evolution, with Emphasis on Human Origins*: 385-424.

Vuille, M., M. Werner, R. S. Bradley, R. Y. Chan, and F. Keimig. 2005. "Stable Isotopes in East African Precipitation Record Indian Ocean Zonal Mode." *Geophys.Res.Lett.* 32 (21): L21705-n/a. doi:10.1029/2005GL023876.

Weaver, S. D. 1977. "The Quaternary Caldera Volcano Emuruangogolak, Kenya Rift, and the Petrology of a Bimodal Ferrobasalt-Pantelleritic Trachyte Association." *Bull. Volcanol.* 40 (4): 209-230. doi:10.1007/BF02597564.

Xue, L., N. D. Gani, and M. G. Abdelsalam. 2019. "Drainage Incision, Tectonic Uplift, Magmatic Activity, and Paleo-Environmental Changes in the Kenya Rift, East African Rift System: A Morpho-Tectonic Analysis." *Geomorphology* 345: 106839. doi:10.1016/j.geomorph.2019.106839.

Yost, C. L., R. L. Lupien, C. Beck, C. S. Feibel, S. R. Archer, and A. S. Cohen. 2021. "Orbital Influence on Precipitation, Fire, and Grass Community Composition from 1.87 to 1.38 Ma in the Turkana Basin, Kenya." *Front. Earth Sci.* 9. doi:10.3389/feart.2021.568646.

4.10. SUPPLEMENTAL DATA

S1: Grain size categories for the KSI profile with whether or not laminated diatoms were present. The following sheets are the results from the MasterSizer.

S2: Table of the 76 grains analyzed from the three samples with information regarding their usefulness in the dating process.

S3: Tab1: Diatom counts across the entire KSI section. Included are the number of *Lycopodium* spores, sponge spicules, and phytoliths from each sample. **Tab2:** Transfer function data for the diatoms taken from Gasse et al. (1995). Habitats are divided into numerical groups – 1 littoral, 2 littoral planktonic, and 3 planktonic. **Tab3:** Resulting data from the transfer function including the weighted averages, minimums, and maximums for conductivity and pH as well as the cation and anion ratios which were not used in this study (Gasse et al., 1995).

S4: The XRF and CIA data in many forms, including the raw weight percent oxide, normalized weight percent oxide, cations in molar proportion and ppm, and the CIA.

S5: PCA analytics for the unused (with carbonates and all trave elements) and used PCAs. Analytics include a scree plot, PCA, biplot, correlations, contributions, correlation matrix, contribution for 5 dimensions, and loadings for 5 dimensions. CONISS analytics including a broken stick model and a dendogram with the clusters highlighted.

CHAPTER 5: CONCLUSIONS

Taken together, these projects highlight climate variability not just across Africa, but across lakes in their responses to changes in global climates and local hydroclimates. In relation to the preliminary questions posed in Chapter 1, **(a)** these projects highlight the importance of thorough analysis of the lithological, geochemical, and biological parameters that can impact lakes and deposited sediments given that geochemical and micropaleontological lake proxies are unique between different lakes. **(b)** Understanding the time scales and rates of environmental change depends on the resolution at which we study lake systems and the specific climatological phenomena and geologic time we are studying. **(c)** Because of this, while we understand a lot of the general trends and mechanisms of global climate impacting African environments on astronomical timescales, as we study these systems at higher resolution we can see that there are shorter term mechanisms that impact environments at finer scales. **(d)** And while these works were unable to connect hominin evolution and innovation with study sites, the variability visible in these records highlight the need to study environments at timescales appropriate to questions related to the paleoanthropological and archaeological data present.

5.1. FUTURE WORK

5.1.1. Paleolake Suguta, Kenya

The work presented in Chapter 2 found that during the Early Middle-Pleistocene Transition there was substantial variability in depth at Paleolake Suguta from full desiccation to deep waters over a ~100 kyr period. To better understand the rate of change, more samples and an age model are required. Given that sampling was only at ~50-cm intervals, higher resolution will provide a greater understanding of the rates of hydroclimatological change across this timeframe. An age model will be constructed using dated tephras from across the Suguta Valley. Through optical and geochemical correlation of tephras across the basin, we will determine the ages of tephras from the studied outcrop and create an age model, providing constraints on rates in and out of lake phases determined from this study. With a stronger age model, I will also study laminated diatomites across the Suguta Basin to determine whether there is any cyclic hydrological change of the paleolake. Preliminary studies indicate that there is stratigraphic cyclicity between three main taxa: *Cyclostephanos*

dubius (Hustedt) Round, *Nitzschia subrostellata* Hustedt, and *Ulnaria ulna* (Nitzsch) Compère. These three taxa occur in cycles of 6 and 12 layers (Fig. 1). With an age model, I will be able to determine what these cycles may represent and provide insights into seasonality at Paleolake Suguta in the Middle Pleistocene.

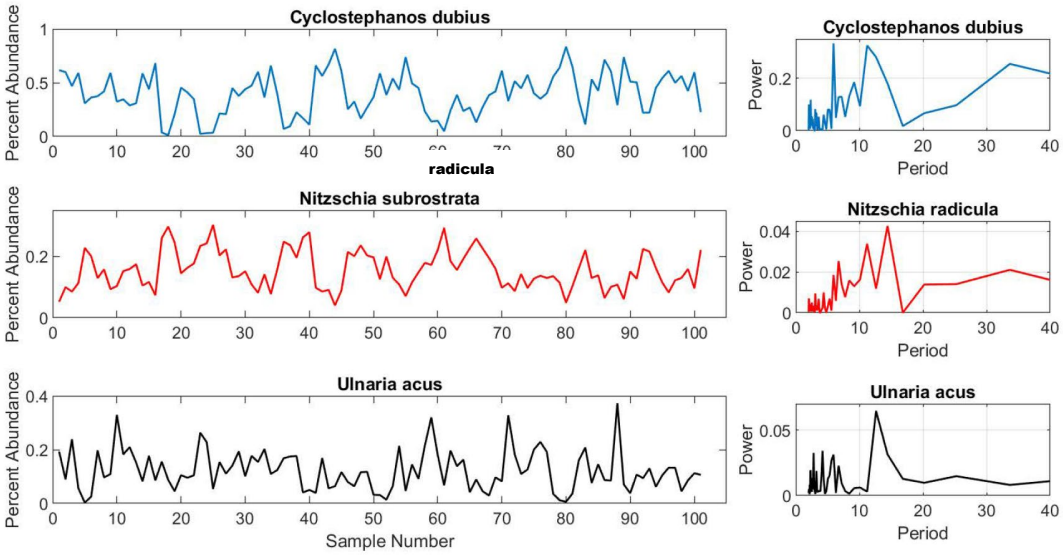

Figure 1: The percent abundance and periodicity of the three main taxa (*Cyclostephanos dubius, Nitzschia radicula*, and *Ulnaria acus*) found along laminated diatomites within the Suguta Basin.

5.1.2. Lake Nakuru, Kenya

The work at Lake Nakuru, Kenya presented in Chapter 3 highlights the importance using multiple proxies to reconstruct paleolake changes. The limnological changes observed at Lake Nakuru are a result of volcanic input, climate change, or a combination of the two. If the changes are climatological, anoxic, *Thalassiosira rudolfi*-phases might indicate increased deepening and/or stratification related to Dansgaard-Oeschger and Heinrich cycles. To determine whether anoxic layers are climatologically controlled, better constraints on sediment deposition into the lake to understand lithological deposition could make it possible to distinguish volcanic versus erosional input. In addition, more ages can better constrain deeper parts of the core, allowing for a core-long age model to compare changes with those observed across the East African Rift System over the past 35 ka.

5.1.3. Humpata Plateau, Angola

The preliminary project on the Humpata Plateau in Angola in the 4th Chapter of this dissertation is the start of many projects exploring proxies and environmental change in the region. Future projects include: (1) an in-depth analysis of potentially

endemic taxa of the region; (2) a continued analysis of the relationship between diatom taxa and hydrochemistry from the second field season; and (3) various analyses of short cores (~30 cm) from the region. From projects 1 and 2, we will gain a sense of how diatom communities change in the modern environment to better extrapolate changes from the short core records. With a better understanding of diatom community responses to environmental change, we then hope to begin short-term reconstructions to determine historic environmental changes to begin learning more about the millennial-scale hydroclimatic controls impacting water bodies on the Humpata Plateau. As we continue to learn more about climates and environments in this region, we aim to work with local students at our partnering university, Mandume ya Ndemufayo University in Lubango, to train students on monitoring environments and water bodies in the region.

5.2. BROADER IMPACTS

Overall, this dissertation provides an overview into how shifts in climate can cause variability in lake levels and chemistry. Future work from these sites will continue to advance understanding of different lake systems around the world while also aiming to keep local populations engaged and informed about how environmental change over the next centuries will impact local water systems. By understanding modern changes in hydrochemistry, we can better prepare communities who need water for their society but are incredibly vulnerable to modern climate change. By reconstructing paleolake dynamics, we can provide insight into variable environments, especially in response to changes in global climate. These changes impact flora and fauna, from diatoms to humans and our hominin ancestors. By understanding limnological variability in the past, we can understand how hominins may have migrated throughout the landscape or why there may have been transitions in past cultures. By understanding past and present limnological systems, we can better understand the planet, our history, and the climatological future.